Formation And Stabilization Of Inverse Emulsion Polymers.

Visioli, Donna Lynn

FORMATION AND STABILIZATION OF INVERSE EMULSION POLYMERS

Lehigh University

PH.D. 1984

FORMATION AND STABILIZATION OF INVERSE EMULSION POLYMERS

BY

DONNA LYNN VISIOLI

A Dissertation

Presented to the Graduate Committee

of Lehigh University

in Candidacy for the Degree of

Doctor of Philosophy

in

Polymer Science and Engineering

Lehigh University

1984

CERTIFICATE OF APPROVAL

Approved and recommended for acceptance as a dissertation in partial fulfillment of the requirements for the degree of Doctor of Philosophy.

6/14/84
Date

Professor in Charge

Professor in Charge

Accepted 7/27/84
(Date)

Special committee directing the doctoral work of Donna L. Visioli.

M. S. El-Aasser, Chairman

J. W. Vanderhoff, Co-advisor

F. M. Fowkes

A. Klein

W. S. Ropp

DEDICATION

To all my educators, especially my parents.

ACKNOWLEDGMENTS

The author wishes to express sincere gratitude to:

Professors M. S. El-Aasser and J. W. Vanderhoff, who directed this work and provided valuable guidance and encouragement (albeit sometimes from afar);

Professors F. M. Fowkes and A. Klein and Dr. W. Ropp for their interest and helpful discussions and suggestions while serving on the Dissertation Committee;

Professor C. A. Silebi for discussions and suggestions on hydrodynamic chromatography and latex rheology;

Professor Sutton Monro for discussions and suggestions on the statistically designed experiment;

The graduate students and staff of the Emulsion Polymers Institute for their cameraderie and support. Special thanks to Rohitha Jayasuriya, Craig Lack, and Ken Brown for generous assistance with experimental techniques, and to Mrs. Olga Shaffer, who greatly enriched this work by generously sharing her expertise in electron microscopy;

Chemical engineering undergraduate student Dale Grove, who diligently and cheerfully performed the many rheological and chromatographic measurements included in this work;

The Emulsion Polymers Institute for financial support;

The American Association of University Women for financial

support through the award of an American Fellowship;

The Graduate School of Lehigh University for financial support through the award of a Scholarship;

Mrs. Jeanne Loosbrock, who cheerfully typed the draft and final copies of this manuscript;

Her mother, for her unfailing support and love.

TABLE OF CONTENTS

LIST OF TABLES

LIST OF FIGURES

ABSTRACT

Surfactants, initiators, and continuous phases were screened for their utility in preparation of inverse polyacrylamide latexes. Several systems suitable for preparing high molecular weight polymer at rapid reaction rate with little coagulum were defined. Monomer emulsion prepared with block copolymeric surfactants had multicellular droplet morphology; under some conditions, the latexes had the same morphology.

Further analysis of the block copolymeric surfactant Tetronic 1102 showed that these multicelled droplets are reticulated emulsifier particles. Addition of aqueous phase to an organic dispersion of these particles fills the particle's interior cells and also swells the adsorbed emulsifier.

Kinetics and mechanism of inverse emulsion polymerization were studied in a system composed of Tetronic 1102 surfactant, acrylamide monomer, and o-xylene continuous phase. Variables included initiator type (oil-soluble 2,2'-azobis(2,4-dimenthyl valeronitrile) or water-soluble potassium persulfate), initiator concentration, surfactant concentration, and polymerization temperature. With persulfate initiator, initiation occurs by diffusion of radicals (which have probably transferred to emulsifier molecules) into monomer droplets. With azo initiator, initiation occurs primarily in the adsorbed emulsifier layer and to a lesser extent in the

continuous phase. With both initiators, particles grow by coagulation. The latex particles retain the multicellular structure of the monomer emulsion only if the polymerization temperature is below the melting temperature of the surfactant's poly(ethylene oxide) segments. This multicellular structure makes deriving the polymerization mechanism more complex. However, the effects of the recipe variables on the number of particles and the mechanism of radical generation in this system are the same as in the sodium p-vinylbenzene sulfonate system described in the pioneering work on inverse emulsion polymerization, but different from conventional emulsion polymerization, and indicate that the subdivision effect is less important in inverse emulsion polymerization. Hence the unusual features of the mechanism proposed in the present work can not be attributed to the unusual structure of Tetronic 1102 but rather they must be considered characteristic of the inverse emulsion polymerization process.

Significant repulsive electrostatic forces can be generated in inverse latexes, but these forces are not adequate to provide stability against settling. Excellent stability is obtained using a block copolymeric surfactant.

CHAPTER I

Introduction

A. Inverse Emulsion Polymerization

Inverse emulsion polymerization consists of emulsification of a hydrophilic monomer (usually in aqueous solution) in a continuous oil medium using a water-in-oil (w/o) emulsifier and polymerization using either a water-soluble or oil-soluble initiator (1.1,1.2). This process is the inverse of conventional emulsion polymerization in regard to the loci of the hydrophilic and hydrophobic phases: in conventional emulsion polymerization, a hydrophobic monomer (usually neat) is emulsified in a continuous water medium using an oil-in-water (o/w) emulsifier. The process is schematically described in Figure 1.1. A dispersion of polymer particles is produced by both inverse and conventional emulsion polymerization (although, in the case of inverse emulsion polymerization, the particles are usually swollen with water). The same loci of initiation of polymerization are available in both inverse and conventional emulsion polymerization, i.e. the monomer swollen micelles, the absorbed emulsifier layer, the continuous medium, and the monomer droplets. However, since the size of the micelles was found to be of the same order of magnitude as the size of the monomer droplets in an inverse emulsion whereas the micelles are usually two to three orders of magnitude smaller than the droplets in a conventional emulsion (1.1), the difference between monomer droplets and micelles may be largely

Figure 1.1

Schematic Representation of
Emulsion Polymerization

conventional emulsion polymerization

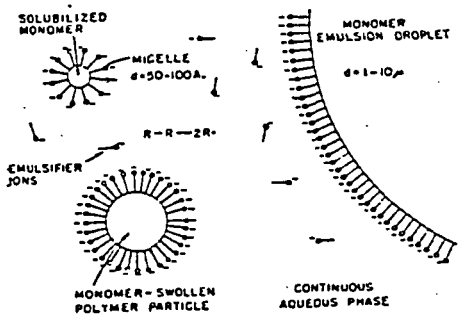

inverse emulsion polymerization

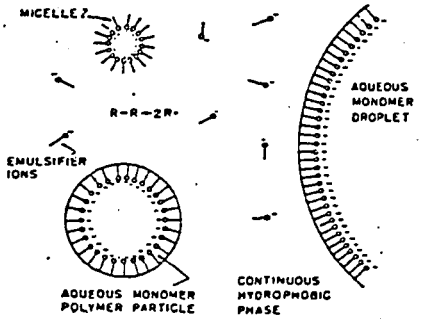

semantic in inverse emulsions. Furthermore, for an emulsifier which is uncrystallizable, the difference between micelles and monomer droplets is largely semantic (1.1). The inverse emulsion polymerization system studied by Vanderhoff et al. (1.1) meets the the criteria of emulsion polymerization: free radicals which are segregated; and the existent free radicals which number within a few orders of magnitude of the number of loci available for segregation. This indicates that classical kinetic and mechanistic analyses of conventional emulsion polymerization can be applied to inverse emulsion polymerization.

The preparation of inverse emulsion polymers was first described by Vanderhoff et al. (1.1,1.2). Typical monomers suitable for this process included sodium p-vinylbenzenesulfonate, sodium vinylbenzylsulfonate, 2-sulfoethyl acrylate, acrylic acid, methacrylic acid, vinylbenzyltrimethylammonium chloride, 2-aminoethylmethacrylate hydrochloride, and acrylamide. Typical initiators included oil-soluble benzoyl peroxide and lauroyl peroxide and water-soluble potassium persulfate or potassium persulfate-sodium bisulfite mixtures. Typical emulsifiers included sorbitan monostearate (Span 60-ICI America), hexadecyl hydrogen phthalate, and a mixture of cetyl and stearyl hydrogen phthalate. Typical oil phases included xylene and perchloroethylene.

In their study of the kinetics and mechanism of inverse emulsion polymerization (using sodium p-vinylbenzene sulfonatemonomer, and o-xylene continuous phase and Span 60 emulsifier), Vanderhoff et al. (1.1) found that the number of particles per unit volume did not

increase with increasing temperature as it generally does in conventional emulsion polymerization. This suggests that the locus of polymerization initiation is not the micelles, as it is in conventional (Smith-Ewart type) emulsion polymerization. Both the low interfacial tension of the emulsions used in this study and electron microscopic study of sodium poly(p-vinyl-benzene sulfonate) emulsified in o-xylene with Span 60 supports the formation of very small droplets, and hence initiation in both monomer droplets and micelles was proposed. This mechanism of initiation is supported by the finding that initiation in monomer droplets can occur in conventional emulsion polymerization if the monomer droplets are small (1.3). Radical generation in conventional emulsion polymerization occurs in the continuous phase, and is followed by radical migration to the micelles. Kinetic analysis of inverse emulsion polymerization showed that, for both oil-soluble benzoyl peroxide and water-soluble potassium persulfate initiators, radicals are generated in or enter the particles pairwise (1.1). Because both of these initiators produce two radicals per molecule, Vanderhoff et al. speculated that in inverse emulsion polymerization, radicals generated in the continuous phase are not effective in initiating polymerization, so polymerization is initiated only by initiator molecules which enter the particles and decompose inside them, regardless of whether the initiator is oil-soluble or water-soluble. The termination reaction is diffusion controlled in both conventional and inverse emulsion polymerization.

Another fundamental study of the kinetics and mechanism of inverse emulsion polymerization has been published by Kurenkov et al. (1.4,1.5) several years after the original study of Vanderhoff et al. Kurenkov et al. studied inverse emulsion polymerization of acrylamide using potassium persulfate initiator in toluene medium with Sentamid S emulsifier. Since Kurenkov et al. did not measure particle size, evaluation of polymerization rate per particle is impossible. This is unfortunate, since theoretical analyses of the mechanism of emulsion polymerization which include measurement of the number of particles as a function of temperature, initiator concentration, and emulsifier concentration cannot be applied to the data of Kurenkov et al.

Qualitatively, then, the conventional and inverse emulsion polymerization processes are basically the reverse of each other. As expected, then, the dependence of polymer solution viscosity on reaction conditions is qualitatively the same: viscosity increases as the initiator concentration decreases, the monomer concentration increases, or the temperature decreases. However, the mechanisms differ in some important ways: the monomer droplets are of the same order of magnitude as the micelles in an inverse emulsion system whereas the droplets are much larger than the micelles in a conventional emulsion polymerization; and initiation occurs in both the droplets and the micelles in an inverse emulsion while it normally occurs in the micelles or in the dispersion medium (homogeneous nucleation) in a conventional emulsion; and initiating radicals must be formed within the particle in inverse

emulsions while they are formed in the continuous phase (or within a particle and subsequently diffuse into the continuous phase) in conventional emulsions.

The kinetics of inverse emulsion polymerization are similar to those of conventional emulsion polymerization: this is not unexpected, since both are radical chain growth processes and thus the rate of polymerization is expected to be proportional to the monomer concentration and to the square root of the initiator concentration multiplied by a factor which expresses the influence of the state of subdivision of the reaction mixture on the polymerization kinetics.

Although only these fundamental studies of inverse emulsion polymerization have appeared in the literature, approximately one hundred patents on preparation and processing of inverse emulsion polymers, inversion of the latex to form a polymer solution, and applications of inverse emulsion polymers have been issued (1.6). These many references to inverse emulsion polymerization in the patent literature underscore its practical advantages and industrial importance. Inverse emulsion polymerization imparts the advantages of conventional emulsion polymerization (i.e., the formation of high molecular weight polymer at rapid rate with efficient heat transfer) to water-soluble monomers. The latex can be inverted by adding excess water and perhaps some oil-in-water emulsifier, which destabilizes the latex and releases the water-swollen polymer particles to the water phase. Since this process

is simply a dilution rather than a dissolution, it proceeds rapidly; in contrast to this facile dilution process, adding dry, powdered hydrophilic polymer to water often forms a viscous layer of hydrated polymer on the outside of the powdered particles and retards further dissolution.

The applications of polymers prepared by inverse emulsion polymerization include flocculation of colloidal dispersions (in applications such as ore processing, sewage treatment, and kraft waste liquor), retention aid in paper making, dewatering of sludges, flocculation of cellulosic fibers, froth flocculation, plugging leaks in tanks and cooling systems, lubricating and cleaning drains, lubricity improver for coatings, and enhanced oil recovery. Polyacrylamide and its copolymers are the polymers most commonly prepared by inverse emulsion polymerization. Polyacrylamide has been shown to be the optimal chemical flooding agent in enhanced oil recovery (1.7). Polyacrylamide is also important in applications such as clarification of sugar juices, films, coatings, adhesives, photographic emulsions, personal care products, surfactants, and thickeners (1.8).

Conventional latexes are stabilized by a combination of electrostatic and steric forces and remain free of stratification or flocculation indefinitely. However, inverse latexes settle within several hours to a few days, forming in some cases a hard sediment which cannot be redispersed by agitation. This difference in stability is due to the difference in stabilization mechanism of water-continuous emulsion compared to oil-continuous emulsions.

Oil-in-water emulsions, like conventional emulsion polymers, are stabilized by electrostatic repulsive forces resulting from the electrostatic double layer formed by emulsifier ions absorbed on the hydrophobic particle surface and counterions from the aqueous phase. However, for a water-in-oil (inverse) emulsion, the electric double layer is very diffuse. The thickness of the double layer of an oil-in-water emulsion is generally 10^{-3} - 10^{-2} um, so electrical interactions occur only at very short distances: that is, the potential energy of the charged particles is zero when they are more than 10^{-2} um apart. For a water-in-oil emulsion, the diffuse double layer is 0.1-1.0 um thick: that is, it is nearly the same order of magnitude as the distance between dispersed particles in the emulsion. Since the particles in this case possess some potential energy, their stability against flocculation is lower.

The mechanism of stabilization of water-in-oil emulsions is a subject of much controversy. Some authors hold the opinion that electrostatic stabilization is not possible in media of low dielectric constant (1.10). However, this view was refused experimentally over thirty years ago (6.3). Other authors, such as Albers and Overbeek, have argued that, although repulsive electrostatic forces are operative in oil-continuous emulsions, these emulsions are stabilized by specific effects due to the structure of the interface (1.9). Although Albers and Overbeek's work is over thirty years old, it is significant in that it is one of the first attempts to relate a colloidal particle's stability

to the structure of the interfacial region.

In their study of the correlation between electrokinetic potential and stability, Albers and Overbeek used several water-in-oil emulsions having stabilizers which they assumed to be ionized somewhat in the oil phase. They show that having a high surface potential is insufficient for stabilizing droplets of radius greater than or equal to one micrometer. They found that the smaller droplet size water-in-benzene emulsions are stabilized by soaps which partially hydrolyze to form products insoluble in either benzene or water. These products accumulate at the interface and stabilize in either of two ways: mechanically; or by forming a rigid continuous layer and thereby interfering with the formation of an electrical double layer in the oil phase. The carbon chain length of the adsorbed emulsifier must be much greater than twenty to sterically stabilize oil-in-water emulsions. In the case of nonionic surfactants, flocculation is not prevented by adsorbed hydrophobic chains of up to 0.2 um. Albers and Overbeek also found that, even at low concentrations of water emulsified in oil, the concentration of the water phase effects stability because of the thickness of the diffuse double layer, as discussed above. Later work, such as that of Higuchi and Misra (6.31-6.33), has shown that emulsion stability is not necessarily related to the specific effects due to the structure of the interface but rather may be related to general thermodynamic effects such as molecular diffusion. These thermodynamic considerations are able to explain phenomena such as poorer stability in light hydrocarbons compared to heavier oils. Theories and experi-

mental findings related to this very controversial area are discussed in detail later in this dissertation.

In both water-in-oil and oil-in-water emulsions, each globule has some potential energy; therefore, after some globules flocculate, the remaining ones act like an expanding spring and accelerate further flocculation. Each globule forced downward is under the cumulative weight of all the globules lying above, causing rapid flocculation which ceases when the remaining bulk concentration of the globules becomes very small. Brownian motion as well as gravity promotes flocculation: flocculated globules are held together (i.e., coagulated) by van der Waal's attractive forces.

B. Free Radical Polymerization of Acrylamide

Acrylamide monomer is a white crystalline solid with a melting point of $84.5 \pm 0.3^{\circ}C$. It is soluble in water and polar organic solvents such as acetone and short-chain alcohols and insoluble in nonpolar solvents such as heptane and carbon tetrachloride (1.10).

Acrylamide can be polymerized by both free radical and by ionic initiators. The product obtained from anionic initiators is a polyamide, poly(β-alanine) (1.11). A wide variety of free radical initiators are suitable for polymerization of acrylamide in bulk or solution, including peroxides, redox systems, γ-radiation, ultrasound waves and, in bulk, heat (1.12). Polymerization can take place in a variety of media, including aqueous solution, inverse suspension, inverse emulsion, precipitate formation, and solid state. Solid state polymerization generally produces low molecular

weight product (1.8). The enthalpy of polymerization of acrylamide is high (19.5 kcal/mole, measured at 74.5°C). It is higher in homogeneous solution than in precipitate forming solvents such as acetone (16.9 kcal/mole), benzene (14.4 kcal/mole), or hexane (13.8 kcal/mole) (1.14). This variation in measured enthalpy of polymerization is attributed both to the differences in heats of interaction of monomer and polymer with the solvent and to possible monomer association in nonpolar solvent (1.14). Such high enthalpy of polymerization makes efficient heat transfer essential in industrial practice.

The kinetics of free radical polymerization of acrylamide in aqueous solution using free radical initiators such as azo compounds, persulfate, and redox initiators has been studied in several papers. With azo initiator, the rate of polymerization shows the classical first-order dependence on monomer concentration and half-order dependence on intiator concentration (1.15). Termination by disproportionation is postulated. In persulfate-initiated polymerization, the order with respect to monomer is higher at low monomer concentration but approaches one as the monomer concentration increases; this is ascribed to recombination of initiator radicals due to a cage effect in solvent (1.16). The cage effect is also operative in azo-initiated systems (1.17). The order with respect to monomer concentration is also nonlinear in the case of polymerization initiated by the persulfate-thiosulfate redox couple (1.18). This nonlinearity is attributed to changes in the rate of initia-

tion throughout the reaction (i.e., nonsteady-state conditions), which is supported by the first order dependence of initial rate on initial monomer concentration and a half-order dependence of initial rate on persulfate concentration.

Free radicals capable of initiating polymerization can also be generated by ionizing radiation. The rate of polymerization shows half-order dependence on the dose rate of ionizing radiation (1.19). The radiation-initiated reaction can be terminated by ferric perchlorate (due to either the ferric ion or ferric hydroxide ion), which indicates the sensitivity of acrylamide polymerizations to contaminants in the system (1.19). Presence of trace amounts of oxygen can also inhibit or retard polymerization (1.20).

Photochemical polymerization of acrylamide at 25°C using either hydrogen peroxide or ferric ion as sensitizer has been used to derive rate constants using the rotating sector method (1.21). The propagation rate constant k_p has a value 1.8×10^4 liter/mole sec and the termination rate constant k_t has the value 1.45×10^7 liter/mole·sec. This value of k_p is unusually high and k_t is unusually low: hence $k_p/k_t^{1/2}$ is extremely high (4.72 liter$^{1/2}$/mole$^{1/2}$·sec$^{1/2}$), so inherently molecular weight is high and polymerization is rapid. Polymerization is slower at higher pH, but the ratio of $k_p/k_t^{1/2}$ is almost constant, so molecular weight is virtually unaffected by pH. The rate constants for transfer to monomer and initiator are very small (0.22 liter/mole·sec and 9.0 liter/mole·sec, respectively), which further supports growth of very long chains and hence high polymer molecular weight. Polymerization

of acrylamide using the sodium chlorate-sodium sulfite redox couple at 50°C gives a similar value of $k_p/k_t^{1/2}$ (5.47 $liter^{1/2}/mole^{1/2}\cdot sec^{1/2}$) (1.22). Activation energy over the temperature range 15-75°C is 7.3 kcal/mole. Initial polymerization rate is first order in monomer concentration while polymerization rate at any time is proportional to the 5/2 power of the remaining monomer concentration. This discrepancy indicates that the polymer formed binds part of the remaining monomer, rendering it unavailable for polymerization. The polymerization rate is found to be first order in free monomer concentration. Termination was indicated to occur by disproportionation. Termination by disproportionation was confirmed in a later study in which an azo initiator was used (1.17). Chain transfer to monomer becomes dominant in controlling molecular weight when the molecular weight exceeds a few million in polymerization initiated by 4,4'-azobis-4-cyanovaleric acid (1.17).

The structure of the polyacrylamide chain has been found to depend strongly on polymerization temperature but not on initiator concentration (1.13). With an ammonium persulfate-sodium metabisulfite redox initiator, polymerization at 50°C forms almost exclusively linear polymer, even with very high levels of initiator, while polymerization at 78°C forms polymer chains having one to seven branches.

The polymerization of acrylamide using persulfate initiator has been studied in aqueous surfactant solution (1.23). The rate of polymerization and polymer molecular weight are unaffected by the

presence of anionic or nonionic surfactants, either above or below the critical micelle concentration (CMC). Cationic surfactants similarly have no effect below the CMC, but they lower both polymerization rate and polymer molecular weight above the CMC. This is attributed to retarded decomposition of persulfate ions which are bound to or adsorbed onto the surface of a cationic micelle, compared to persulfate ions in aqueous solution. Similarly, Trubitsyna et al. studied polymerization of acrylamide initiated by potassium persulfate in both water and dimethyl formamide in the presence of the cationic surfactant cetylpyridinium chloride (1.24). A model is proposed in which polymerization is initiated by radicals formed by the decomposition of an acrylamide-persulfate donor-acceptor complex.

C. Purpose and Scope of the Present Work

The most recent study of inverse emulsion polymerization was DiStefano's study of acrylamide polymerization, using o-xylene continuous phase, benzoyl peroxide initiator, and Tetronic 1102 emulsifier (block copolymer based on ethylene diamine to which is added propylene oxide and then ethylene oxide, sequentially; BASF Wyandotte Co.) (1.25). Several unusual results were found in this study. Rate of polymerization was found to be second order in initiator concentration and first order in emulsifier concentration at 60°. As discussed above, free radical polymerization of acrylamide in solution is classically expected to be half order in initiator concentration and zero-order in surfactant concentration. For in-

verse emulsion polymerization, Vanderhoff et al. (1.1) found polymerization rate to be 0.58 order with respect to surfactant concentration for sodium p-vinylbenzene sulfonate polymerization initiated benzoyl peroxide at 60°C and Kurenkov et al. (1.4) found polymerization rate to be 0.9 order with respect to initiator concentration for acrylamide polymerization initiated by potassium persulfate. Hence DiStefano's kinetic results indicate that this system displays features of both solution and emulsion polymerizations.

Another unusual feature in DiStefano's study was the morphology of the monomer emulsion droplets and latex particles as observed by transmission electron microscopy. Both monomer emulsion droplets and latex particles formed multicelled structures of 50-200 nm overall diameter with internal droplets of 20-50 nm. The droplet morphology was a function of agitation rate, with higher agitation rate forming droplets with more complex inner structure. The size and morphology of the monomer emulsion droplets and the final latex particles were strongly correlated. This correlation was taken as evidence of initiation in monomer droplets.

A final unusual feature of the inverse emulsion polymerization system studied by DiStefano was the appearance of the conversion-time curves, which were not smoothly sigmoidal but rather reached a plateau followed by a period of strong autoacceleration. A plateau was not observed in the inverse emulsion polymerization systems studied by Vanderhoff et al. (1.1) or Kurenkov et al. (1.4), but such plateaus have been observed in conventional emulsion polymerization of vinylidene chloride and seeded emulsion

polymerization of styrene (1.26). These plateaus have been attributed to monomer starvation due to slow diffusion to the locus of polymerization.

DiStefano also noted a positive practical benefit of the surfactant (Tetronic 1102) used in his system: latex viscosity was lower and stability against sedimentation better than with sorbitan monostearate (Span 60, ICI America), esterified fatty alkanolamide (Witcamide 511; Witco Chemical Co.), or phosphate ester (Emphos F27-85; Witco Chemical Co.) surfactants. Given the severe storage stability problems usually encountered with inverse latexes, this superior stability with Tetronic 1102 warrants further characterization and analysis.

In the present work, a variety of surfactants, initiators, and continuous phases have been screened in order to relate DiStefano's findings on latex morphology to the surfactant structure as well as to identify polymerization systems which combine rapid polymerization rate with high molecular weight and little coagulum. Kinetics and mechanism of inverse emulsion polymerization of acrylamide are elucidated using one of the polymerization systems identified in the screening study. Finally, the mechanism of stabilization of inverse latexes is elucidated as a function of surfactant type and initiator type.

CHAPTER II

Experimental

A. Materials

Reagent-grade inhibitor-free acrylamide (Fisher Scientific Co.) was used as supplied. A fresh aqueous (4.5 M) stock solution was prepared weekly. Initiators potassium persulfate (KPS) (Fisher Scientific Co.) and 2,2'-azobis (2,4-dimethylvaleronitrile) (ADVN--Polysciences, Inc.) were used as supplied. Fresh stock solutions (0.0188 mM) of these were prepared every three days. Monomer and initiator solutions were stored in the refrigerator. Continuous phase o-xylene (Koch Refining Co.) and Isopar M (Exxon Corp.) were used as supplied. Surfactants were used as supplied; those which separated into two phases were homogenized before use. Distilled deionized water was used in all experiments.

B. Surfactant Characterization

1. Identification of the Continuous Phase

A surfactant suitable for inverse emulsion polymerization must be soluble in the continuous phase and must form a water-in-oil emulsion. Surfactant solubility was tested by mixing 5.0 ml continuous phase and 0.5 g surfactant in a vial using the Touch-Mixer. Solid surfactants were heated in the continuous phase at 70°C for 2 minutes before mixing. Dye solubilization was used to determine which phase was continuous: 3.5 ml aqueous methylene blue solution (0.0002%) was pipetted into the surfactant solution

and mixed using the Touch-Mixer. If the resulting emulsion was white, the oil phase was continuous. Emulsion stability was measured by observing how long the emulsion remained stable after agitation ceased: emulsions are considered stable if they remain homogeneous for at least two minutes.

2. Optical Microscopy

Surfactant solutions and emulsions were studied under normal and polarized light using the Reichert Zetopan Microscope. A drop of sample was placed on a microscope slide and covered with a cover slip. For studies at elevated temperature, the Reichert HTl heating stage with regulating transformer was used.

3. Light Scattering

Emulsion droplet size was measured by dissymmetry of light scattering using the Brice-Phoenix Light Scattering Photometer. The ratio of the scattering intensities at 45^{o} and 135^{o} was measured at several very low concentrations and using light of three different wavelengths (489 nm with the red filter, 411 nm with the green filter, and 328 nm with the blue filter). The average particle size of the spheres was calculated from the dissymmetry ratio using Beattie and Booth's tables (2.1).

4. Electron Microscopy

Particle size and morphology was studied using the Philips 300 Transmission Electron Microscope equipped with the cold stage holder. Emulsion samples were studied as prepared; latex samples were diluted with o-xylene to ca. 0.5% concentration. Specimen

substrates were prepared by coating a 1/8-inch diameter 200-mesh stainless steel grid with Formvar film and then with evaporated carbon. A drop of sample was placed on this substrate and then the drop was contacted with filter paper to remove all except a thin film of sample. The substrate was then positioned on the cold stage holder; the holder was placed in the electron microscope column and filled with liquid nitrogen so that the thin film of sample was quickly frozen and the volatiles sublimed by the high vacuum of the microscope. The low vapor pressures of water and o-xylene at liquid nitrogen temperature make it unlikely that these components were completely removed by the vacuum sublimation. The sample was examined at 80 kV. These staining agents were used to further elucidate the droplet morphology: phosphotungstic acid (PTA), a negative stain capable of hydrogen bonding; ruthenium tetroxide (RuO_4), a selective stain for polyethers and polyamides; and iron pentacarbonyl ($Fe(CO)_5$), a metal compound insoluble in the aqueous phase.

5. Interfacial Tension

Interfacial tension was measured by the spinning drop method using the EOR SITE Interfacial Tensiometer. A drop of solution containing 10% surfactant in o-xylene was injected into the spinning capillary through which distilled deionized water was flowing. Data were analyzed using the following a theoretical optical equation to correct droplet diameters for the refraction of

the light beam as it passes obliquely through the various media to the optical microscope (2.2):

$$D_{act} = D_{opp} \cdot (RI_o/RI_c)$$

where D_{act} is the corrected droplet diameter, D_{app} is the apparent droplet diameter, and RI_o and RI_c are the refractive indices of the thermal oil and continuous phase, respectively, at the temperature of interest. Visual evidence for the formation of interfacial films was generated by observing and photographing, as a function of time, the viscous "tails" which form at the ends of the drop in the rotating capillary.

6. Nuclear Magnetic Resonance

High resolution ^1H nuclear magnetic resonance spectra were obtained at 89.55 MHz using a JEOL FX90Q Fourier Transform NMR spectrometer. During operation, the spectrometer was locked on an internal deuterobenzene signal at 7.15 ppm. Typically, spectra were recorded with 8200 data points. One hundred transient spectra were sufficient to get good signal-to-noise ratio. The temperature T_p of the probe was calibrated by measuring the chemical shift difference between the methylene and hydroxyl protons of ethylene glycol and applying the Van Geet equation (T_p = 193.25-1.1167ΔHz) (2.3). Samples of surfactant solution were prepared by mixing surfactant with deuterobenzene; emulsion samples were prepared by adding an equal volume of water dropwise to the surfactant solution. Samples were filtered through a fritted

glass filter to remove particulate contaminants and poured into 10 mm precision NMR tubes.

7. Differential Scanning Calorimetry

Thermograms were obtained using a Perkin-Elmer Model IIB Differential Scanning Calorimeter. Typically a scan speed of 5°K/min was used with initial temperature 295°K. Sample size ranged from 5-15 mg.

8. Viscosity

Relative viscosity of surfactant solutions and emulsions was measured as a function of temperature using a Cannon viscometer immersed in a water bath. The Weissenberg Rheogoniometer was used in the cone-plate mode to measure the viscosity at several shear rates.

C. Measurement of Kinetic Parameters

1. Polymerization Recipe

A polymerization recipe comprises these eight factors: volume ratio of aqueous phase to organic phase; monomer concentration; method of emulsion preparation; agitation rate; initiator type; initiator concentration; emulsifier concentration; polymerization temperature.

In this study, the first four of these were kept constant. The volume ratio of aqueous phase to organic phase was maintained at 1/2. The emulsion was prepared by dropwise addition of monomer solution (4.5 M acrylamide) at a rate of 2-3 ml/min to a surfactant solution in xylene. In this recipe, latex solids content is 10%.

The stirring rate (rpm) was adjusted to keep agitator tip speed constant (10^4 cm/min) at a constant ratio of round-bottom flask diameter to stirrer diameter of 1.5/1. Monomer emulsions were prepared in 200 ml round bottom flasks stirred with a 5-cm paddle type mechanical stirrer at 637 rpm; polymerizations were carried out in 25 ml round-bottom flasks stirred with 1.4 cm magnetic stirrer.

The variables in this study were: initiator type and concentration; emulsifier concentration; and polymerization temperature. These are described in the following section.

2. Fractional Factorial Experimental Design

Full factorial experimental designs are perhaps the most widely used experimental strategies for studying the effect of several different independent variables (factors) on a dependent variable (response) (2.4,2.5). They are useful because they allow the experimenter to measure the effect of the factors on a response both singly (main effects) and jointly (interaction effects). However, if more than a few factors are included, the number of experiments becomes unwieldy. For example, to study two levels of each of eight factors, 2^8 (i.e., 256) experiments are necessary. Interpreting the large number of interaction effects can also be unwieldy and difficult. For example, from these 256 experiments, one can calculate 8 main effects, 28 two-factor interactions, 56 three-factor interactions, 70 four-factor interactions, 336 five-

factor interactions, 56 six-factor interactions, 8 seven-factor interactions, and 1 eight-factor interaction. In most physical situations, it is difficult to believe that three or more factors can act in a concerted manner to affect a response; that is, measuring interactions of more than 2 factors is physically meaningless and hence merely provides an estimate of the error (i.e., is redundant). Ignoring higher-order interaction terms in a factorial experimental design is analagous to truncating higher order terms in a Taylor series expansion of a function. Hence only a fraction of a full factorial is necessary in order to estimate main effects and two-factor interactions, if these are confused (confounded) only with higher-order interactions.

A factorial design for a factor at 4 levels can be constructed by dividing the factor into two dummy factors at two levels each. This can be represented by the following matrix in which the 4 levels of factor R are denoted by R_1, R_2, R_3, and R_4, the dummy factors are X and Y, the low and high settings of the dummy factors are - and + (respectively):

		Y: -	Y: +
X	-	R_2	R_3
	+	R_1	R_4

A fractional factorial experimental design for factors at two and four levels can be constructed using this approach.

The factors included in the kinetic study were initiator type

(water-soluble KPS, oil-soluble ADVN); surfactant concentration (2-12% on continuous phase); initiator concentration (0.01-0.10 mole % on moles monomer which is equivalent to 0.144-1.44 mM on monomer phase); and polymerization temperature (50-65°C). Four levels of each of the last three factors were studied by using two dummy factors for each as described above. The design chosen is a 1/4 replicate of a seven-factor design (i.e., 2^{7-2}). Since not all two-factor interactions are clear in this design, the variables are lettered so that only interactions between the two dummy factors which compose a real factor (these interactions are physically meaningless) are confounded with each other. Hence the factors are lettered as follows:

Letter	Description
A	Initiator type (I)
B D	4 levels of initiator concentration ([I])
C F	4 temperatures (T)
E G	4 levels of surfactant concentration ([E])

The design layout used is Plan 4.7.4 from the National Bureau of Standards Applied Mathematics Series (2.6). In order to run two polymerizations in a water bath simultaneously, experiments were grouped by temperature. To ensure that this grouping does not introduce a systematic error, replicates are run after every eight experiments. The layout and experimental settings are given in

Tables 2.1 and 2.2 and Figure 2.1.

Data were analyzed by multivariate regression analysis using the subprogram REGRESSION from the Statistical Package for the Social Sciences (SPSS). To eliminate dependence on the scale used, factor settings for the low and high level were input and 1 and 2, respectively.

3. Conversion-Time Curves

Conversion-time curves were generated using a dilatometer. Dilatometry is based on the difference in density between monomer and polymer: as monomer is converted to polymer, the density change is quantified by measuring the volume contraction of the reactor charge by using a calibrated capillary. The relationship between volume contraction and conversion can be generated in either of two ways: by calculation, from literature values of the monomer and polymer densities and the known capillary diameter; or empirically, by measuring conversion gravimetrically at a given volume contraction. Because of the scatter in literature values for polyacrylamide density, the empirical method was used. Conversion was determined gravimetrically by pipetting an exact volume of polymer into a preweighed dish, coagulating the polymer with acetone and decanting the supernatant, and washing with water and then again with acetone. The polymer was then dried in the vacuum oven at ca. 10^{-3} torr and 60°C for 48 hr. The decrease in height of the 2.0 mm ID capillary was 35 cm at 100% conversion.

The dilatometer used in this study was based on a design by C.

TABLE 2.1

Factor Settings

Run	A	B	C	D	E	F	G	[I]= BxD	T= CxF	[E]= ExG
1	-	-	-	-	-	-	-	2	2	2
2	+	+	+	-	+	-	-	3	3	3
3	+	-	-	+	+	+	+	1	1	4
4	-	+	+	+	-	+	+	4	4	1
5	-	+	-	+	+	+	+	4	1	4
6	+	-	+	+	-	+	+	1	4	1
7	+	+	-	-	-	-	-	3	2	2
8	-	-	-	-	+	-	-	2	3	3
9	+	+	+	+	+	+	-	4	4	3
10	-	-	-	+	-	+	-	1	1	2
11	-	+	+	-	-	-	+	3	3	1
12	+	-	-	-	+	-	+	2	2	4
13	+	-	+	-	-	-	+	2	3	1
14	-	+	-	-	+	-	+	3	2	4
15	-	-	+	+	+	+	-	1	4	3
16	+	+	-	+	-	+	-	4	1	2
17	+	+	+	+	+	-	+	4	3	4
18	-	-	-	+	-	-	+	1	2	1
19	-	+	+	-	-	+	-	3	4	2
20	+	-	-	-	+	-	-	2	1	3
21	+	-	+	-	-	+	-	2	4	2
22	-	+	-	-	+	+	-	3	1	3
23	-	-	+	+	+	-	+	1	3	4
24	+	+	-	+	-	-	+	4	2	1
25	-	-	-	-	-	+	+	2	1	1
26	+	+	+	-	+	+	+	3	4	4
27	+	-	-	+	+	-	-	1	2	3
28	-	+	+	+	-	-	-	4	3	2
29	-	+	-	+	+	-	-	4	2	3
30	+	-	+	+	-	-	-	1	3	2
31	+	+	-	-	-	+	+	3	1	1
32	-	-	+	-	+	+	+	2	4	4

TABLE 2.2

Layout and Order of Experiments

Experiment Order	Run	I	[I]	T	[E]
1	1	ADVN	0.04	55	6
2	7	KPS	0.07	55	6
3	12	KPS	0.04	55	12
4	14	ADVN	0.07	55	12
5	18	ADVN	0.01	55	3
6	24	KPS	0.10	55	3
7	27	KPS	0.01	55	9
8	29	ADVN	0.10	55	9
9	2	KPS	0.07	60	9
10	8	ADVN	0.04	60	9
11	11	ADVN	0.07	60	3
12	13	KPS	0.04	60	3
13	17	KPS	0.10	60	12
14	23	ADVN	0.01	60	12
15	28	ADVN	0.10	60	6
16	30	KPS	0.01	60	6
17	4	ADVN	0.10	65	3
18	6	KPS	0.01	65	3
19	9	KPS	0.10	65	9
20	15	ADVN	0.01	65	9
21	19	ADVN	0.07	65	6
22	21	KPS	0.04	65	6
23	26	KPS	0.07	65	12
24	32	ADVN	0.04	65	12
25	3	KPS	0.01	50	12
26	5	ADVN	0.10	50	12
27	10	ADW	0.01	50	6
28	16	KPS	0.10	50	6
29	20	KPS	0.04	50	9
30	22	ADVN	0.07	50	9
31	25	ADVN	0.04	50	3
32	31	KPS	0.07	50	3

Figure 2.1

Design Layout

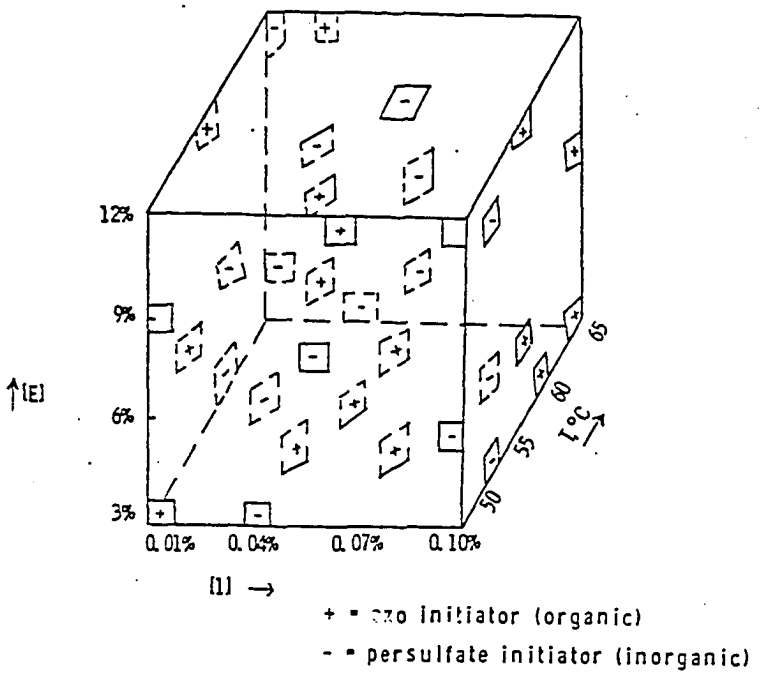

M. Tseng (Ph.D. Thesis, Lehigh University, 1983) and is shown schematically in Figure 2.2. The monomer emulsion, prepared as described above, was charged to the dilatometer flask and purged with nitrogen for 45 min; a reservoir of monomer emulsion was simultaneously purged. If the emulsion was foamy, the dilatometer flask and reservoir were set into the heated water bath for several minutes to break the foam. The 25 ml dilatometer flask was then filled to the brim (total volume 33.5 ml) by pipetting additional emulsion from the reservoir, and then the capillary was inserted. The dilatometer was placed in a heated water bath, stirring was begun, and the flask allowed to equilibrate for 15 min. Then initiator solution (warmed to room temperature) was injected into the flask through the capillary using a polyethylene tube attached to a syringe. A nitrogen blanket was put on the top of the capillary. The liquid level in the calibrated capillary was recorded every 2-3 min.

4. Particle Size

Particle size was measured using the cold stage of the Philips 300 Transmission Electron Microscope, as described earlier. At least 250 particles were measured using the Zeiss MOP-3 Analyzer to determine average particle diameter.

5. Initiator Partition Coefficient

Emulsion samples were prepared by pipetting aqueous and organic phases into a bottle, adding ADVN initiator solution with a

Figure 2.2

Schematic Representation of the Dilatometer

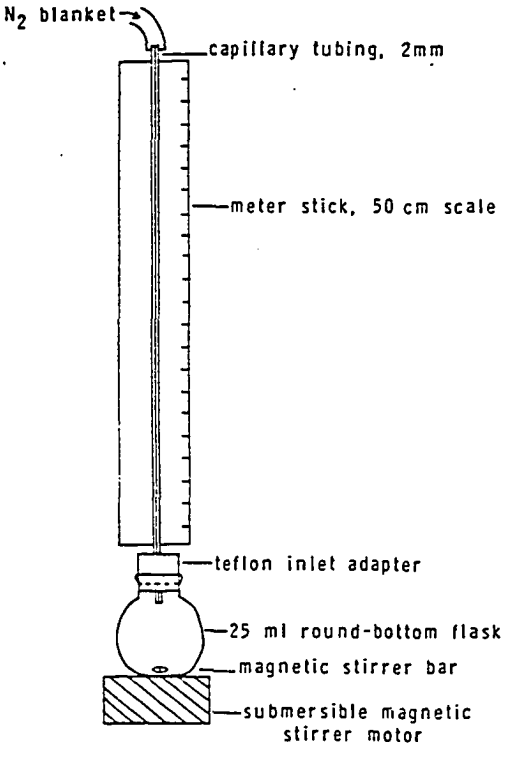

syringe, shaking by hand, and then agitating in a Blue M shaker bath. Emulsions are then broken by centrifugation: if no surfactant had been added, the emulsion was broken by centrifuging in the Sorvall SS-1 centrifuge at 10,000 rpm for 20 min; if surfactant had been added, the emulsion was centrifuged in the IEC Preparative Ultracentrifuge Model B-35 at 40,000 rpm for 60 min. Concentration of ADVN was measured using high performance liquid chromatography (HPLC) with a UV detector set at 365 nm. Samples were injected onto a C_{18} column in the IBM LC9533 using acetonitrile eluant at a flow rate of 1.0 ml/min. The LC procedure used in this work is stored on disk under the name AZO1 with method name AZO.

6. Solution Polymerization Rate

The rate of polymerization of 4.5 M acrylamide is determined gravimetrically as a function of initiator concentration (0.01-0.10 mole % KPS on moles monomer) and temperature (50-60°C). Dilatometry was not suitable for this study due to formation of polyacrylamide gel in the capillary. Portions of acrylamide solution are pipetted into each of 6 test tubes, placed in a Blue M shaking water bath, and initiator solution is injected into each test tube. Every 3 minutes a test tube is removed from the bath and its contents poured into a beaker of acetone setting in an ice bath. Samples are dried in vacuo at 60°C for 48 hr.

7. Solubility of Acrylamide in Organic Phase

Solubility of acrylamide in o-xylene was quantified at

temperatures of 20 to 70°C by stirring monomer in o-xylene in a jacketed cell for 2 hr, allowing monomer to settle and then pipetting the supernatant into a clean flask and diluting 1/1 with acetone to ensure that the monomer remained in solution at room temperature. Acrylamide concentration is measured using infrared absorbance at 1080 cm^{-1} (C-N stretch).

8. Molecular Weight

Characterization of a polymer's molecular weight is important for both fundamental and practical reasons. The weight-average molecular weight $\bar{M}_w$ is related to properties such as strength and melt viscosity. The number-average molecular weight $\bar{M}_n$ is a function of the polymerization rate constants. The breadth of the molecular weight distribution not only affects mechanical properties but also gives additional insight into the polymerization mechanism: in free radical polymerization the polydispersity ratio ($\bar{M}_w/\bar{M}_n$) is greater when termination occurs by disproportionation rather than by combination, and in emulsion polymerization the polydispersity ratio is increased by chain transfer reactions or by a high rate of termination relative to the rate of radical entry or re-entry into particles (2.7).

Number-average molecular weight can be measured by colligative methods or endgroup analysis; of these methods, membrane osmometry is most successful for high polymers. Weight-average molecular weight can be measured by light scattering and equilibrium

sedimentation. Molecular weight can be empirically correlated to the intrinsic viscosity, which is a measure of molecular size. Molecular weight distribution can be measured by techniques such as fractionation (2.8), viscometric methods (2.9), turbidimetric titrations (2.10) and chromatographic methods.

Chromatographic methods are advantageous in that they give the entire distribution and not just the polydispersity ratio. Of these methods, gel permeation chromatography (GPC) is perhaps the most rapid, versatile, and widely used method. In any chromatographic method, fractionation occurs in the column and the broadening of the signal band results from both the molecular weight distribution and instrumental spreading (2.11). The broadening due to instrumental spreading can be accounted for by using standards of varying molecular weight with very low polydispersity. This technique is inapplicable for water soluble polymers because suitable standards are not commercially available; however, techniques based on cumulative molecular weight distribution using standards with broad molecular weight distribution have been developed (2.12-2.15). The need for well-characterized standards can be eliminated by using a detector capable of continuously measuring absolute molecular weight, i.e. a low-angle laser light scattering photometer (LALLS), instead of the usual differential refractometer (2.16-2.18). The possibility of using hydrodynamic chromatography (HDC) to measure molecular weight distribution of high molecular weight water-soluble polymers is

apparent from recent work of Prud'homme et al. in which xanthan polysaccharide molecules (molecular weight 2-50 million) are successfully separated (2.19,2.20). Using this HDC technique, separation is achieved by flow through interstitial regions rather than through pores of the column packing as in GPC.

Molecular weight determination of polyacrylamide has been particularly difficult. Use of intrinsic viscosity is suspect because of shear degradation (2.21,2.22). Polyacrylamide molecular weight has been found to be especially difficult to measure by GPC due to solution instability and adsorption effects (2.23). GPC is unsuitable for measurement of high molecular weight polyacrylamide because many samples approach or exceed the exclusion limit of commercially available columns ($2x10^6$-$5x10^6$, depending on packing). In the present work, four methods have been used to characterize molecular weight: GPC; LALLS; GPC-LALLS; HDC.

a. GPC

Solutions of polyacrylamide in water were prepared at 0.2 weight % by tumbling on a roller mill for 3 days. Samples were injected onto a set of 3 TSK-GEL PW columns (Toyo Soda Co.): G6000 PW + G5000 PW + G3000 PW. Samples were eluted using pure water at flow rate 1.0 cm^3/min. A universal calibration curve was prepared using dextran (Pharmacia Fine Chemicals T10, T40, T70, T500) and polyacrylamide (Polysciences 8247, 8249, 8251) standards. These standards were extremely broad and had, in some cases, a bimodal

distribution (2.24). Exclusion limit was found to be $2x10^6$; this was too low for many specimens of interest and hence prompted a search for another method.

b. LALLS

Scattered light intensity at low forward scattering angles can be used to calculate weight-average molecular weight by simple linear extrapolation to zero concentration rather than by graphical extrapolation (Zimm plots) using the Chromatix KMX-6 LALLS Photometer at 6^o angle. Samples of polyacrylamide in water having concentration 0.1-0.5 mg/ml were prepared and filtered through 0.2 μm Millipore filter. The scatter and noise in the data were unacceptably high, probably due to molecular association in the polyacrylamide solution, so this technique was considered inapplicable.

c. GPC-LALLS

Even though the polymers of interest were above the exclusion limit of the GPC columns, the Chromatix KMX-6 LALLS photometer was coupled to the GPC effluent in the hope that passing the samples through the columns would break up the polyacrylamide associations which has confounded the earlier work using LALLS. The set of GPC columns described above were installed in the Waters 150C using the Chromatix CM-X100 LALLS detector at 6^o angle. Data were digitized using two A/D modules in the DEC 1103 PDP-11 system with Chromatix software MOLWT-2. Samples were filtered through 0.5 m filter cup and eluted at 1.0 cm^3/min. This procedure successfully

eliminated the scatter and noise observed in the off-line LALLS experiment. Since the separation was incomplete because the columns' exclusion limit was exceeded, only $\bar{M}_w$ was accurately measured. Low-angle laser light scattering is an absolute method of determining $\bar{M}_w$, so separation is not required. However, LALLS is only a relative method for determining $\bar{M}_n$, so good separation is necessary for accurate determination of $\bar{M}_n$.

d. HDC

Although the GPC-LALLS method was successful, it requires delicate and expensive equipment. Hence the feasibility of using HDC, a simpler and less expensive technique, to measure molecular weight of polyacrylamides was explored.

A schematic diagram of the HDC unit is shown in Figure 2.3. The eluant consists of 1 mM sodium lauryl sulfate with a trace of formaldehyde added to avoid bacterial growth in the column. The column is 1/2" OD, 10 mm ID stainless steel tubing purchased from Anspec Company. The column is slurry packed under pressure to a pressure of 3500 PSI. Two different resins were used as column packings: BC-X35, a 35% crosslinked cation exchange resin having average particle size 15 μm and particle size distribution 12-16 μm purchased from Benson Co., Reno, Nevada; and CMT 6072-74, a 12 μm styrene-divinyl benzene beads prepared in the Emulsion Polymers Institute at Lehigh by Dr. Chi-Ming Tseng. Scanning electron micrographs of the resins are shown in Figures 2.4 and 2.5. The

Figure 2.3

Experimental Apparatus for
Hydrodynamic Chromatography

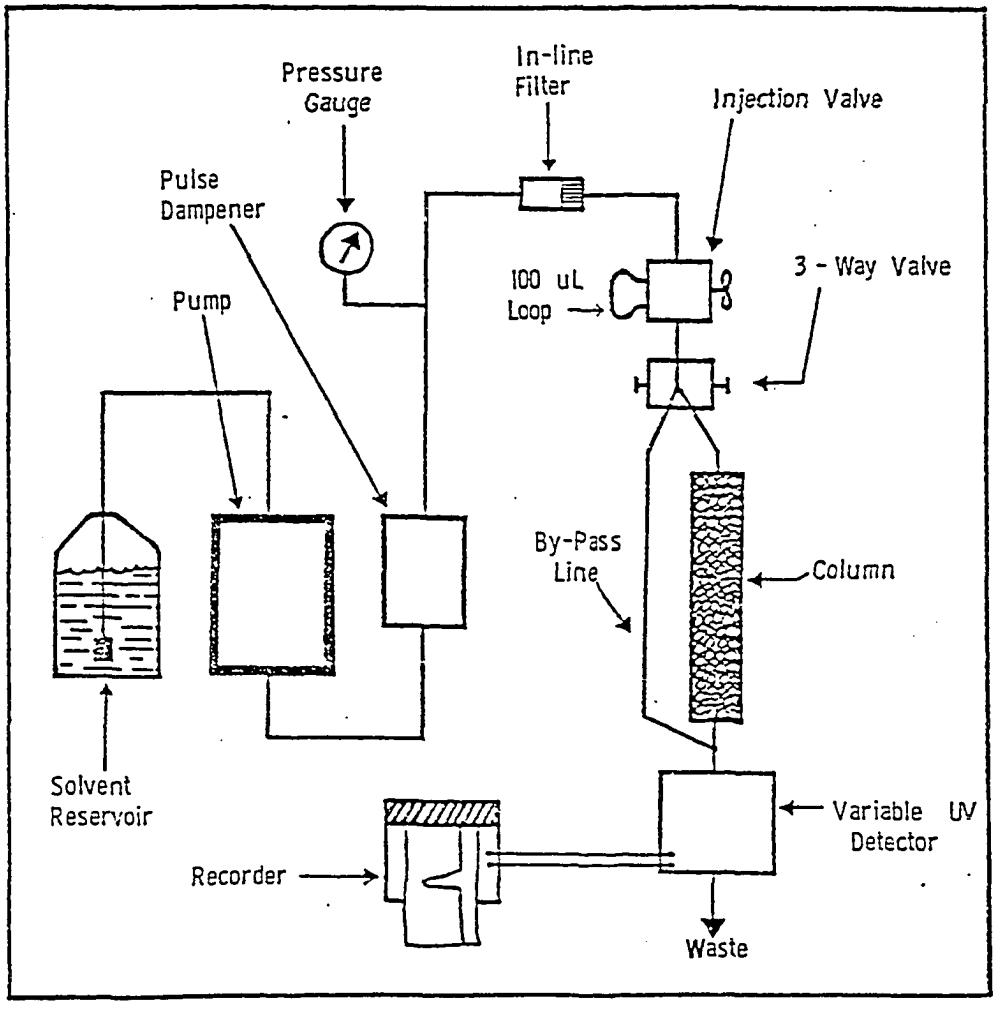

Figure 2.4

Scanning Electron Micrographs of the Benson Resin

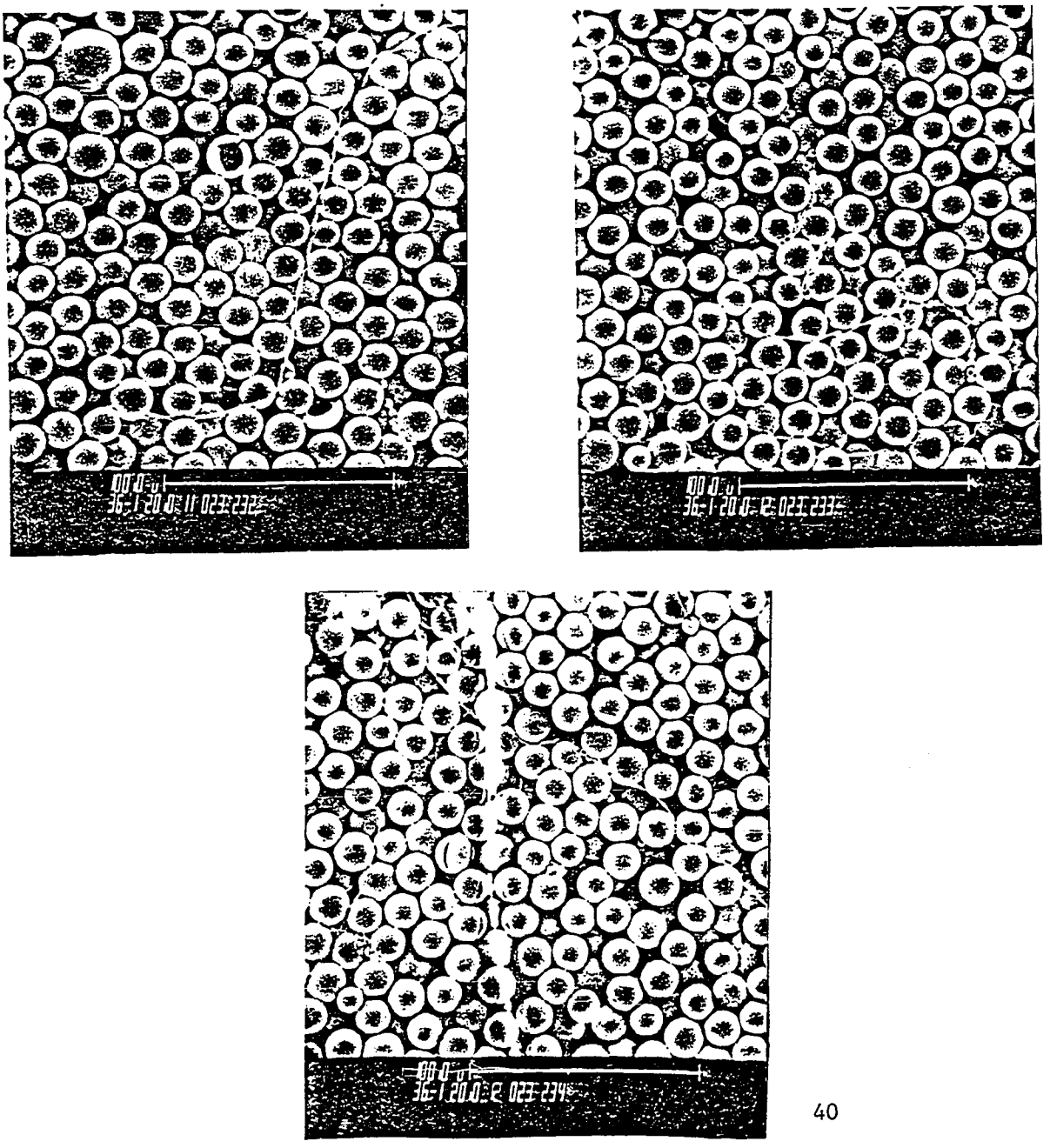

Figure 2.5

Scanning Electron Micrographs of the Lehigh Resin

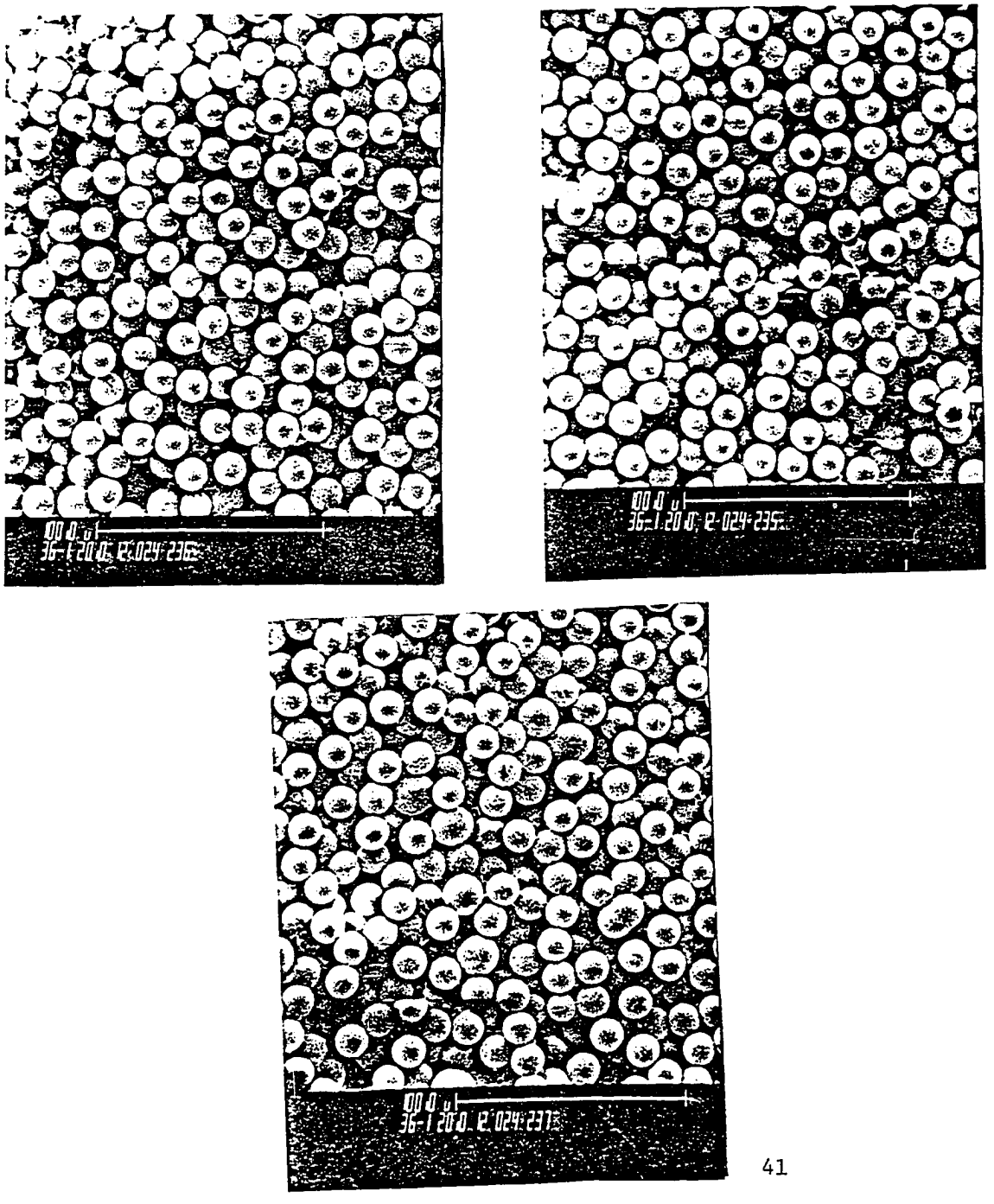

Benson resin contains a significant number of undersized particles; this dispersity is expected to cause band spreading. The Benson resin was used to pack a 0.5 m long column and the Lehigh resin was used to pack a 1.0 m long column. Before packing, resins were washed using the procedure described by Nagy (2.21).

Polyacrylamide, dextran, and poly(vinyl pyrrolidone) were used as standards in order to prepare a universal calibration curve for water-soluble polymers. However, preparation of this curve was not feasible owing to the lack of well-characterized poly(vinyl-pyrrolidone) standards and the apparent absorption of dextran onto the resins. Calibration curves for both the molecular weight ($\bar{M}_w$) and hydrodynamic volume ($[\eta]\bar{M}_w$) as functions of elution volume are shown in Figures 2.6 and 2.7. For both columns, the minimum detectable molecular weight is approximately 10000. Much scatter is seen in the data from the Benson column, probably due to the shorter length and more polydisperse packing of this column. Hence only data from the Lehigh column is used in this study. Since the correlation between elution volume and hydrodynamic volume is approximately the same as the correlation between elutions volume and molecular weight, the latter calibration curve is used for ease of data analysis.

D. Characterization of Latex Stability

1. Brookfield Viscosity

Latex viscosity was measured with a Brookfield model LVT 40874

Figure 2.6

Calibration Curve for Molecular Weight Determination
by Hydrodynamic Chromatography

Lehigh Column

Polyacrylamide Standards

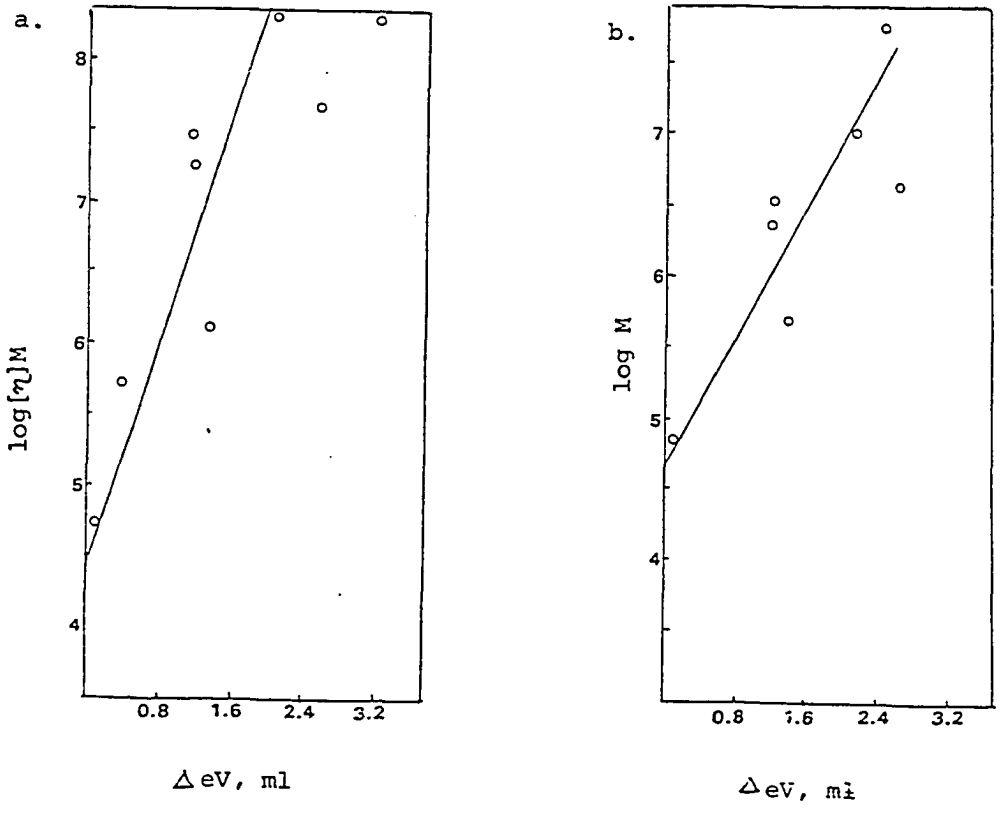

Figure 2.7

Calibration Curve for Molecualr Weight Determination
by Hydrodynamic Chromatography

Benson column

Polyacrylamide Standards

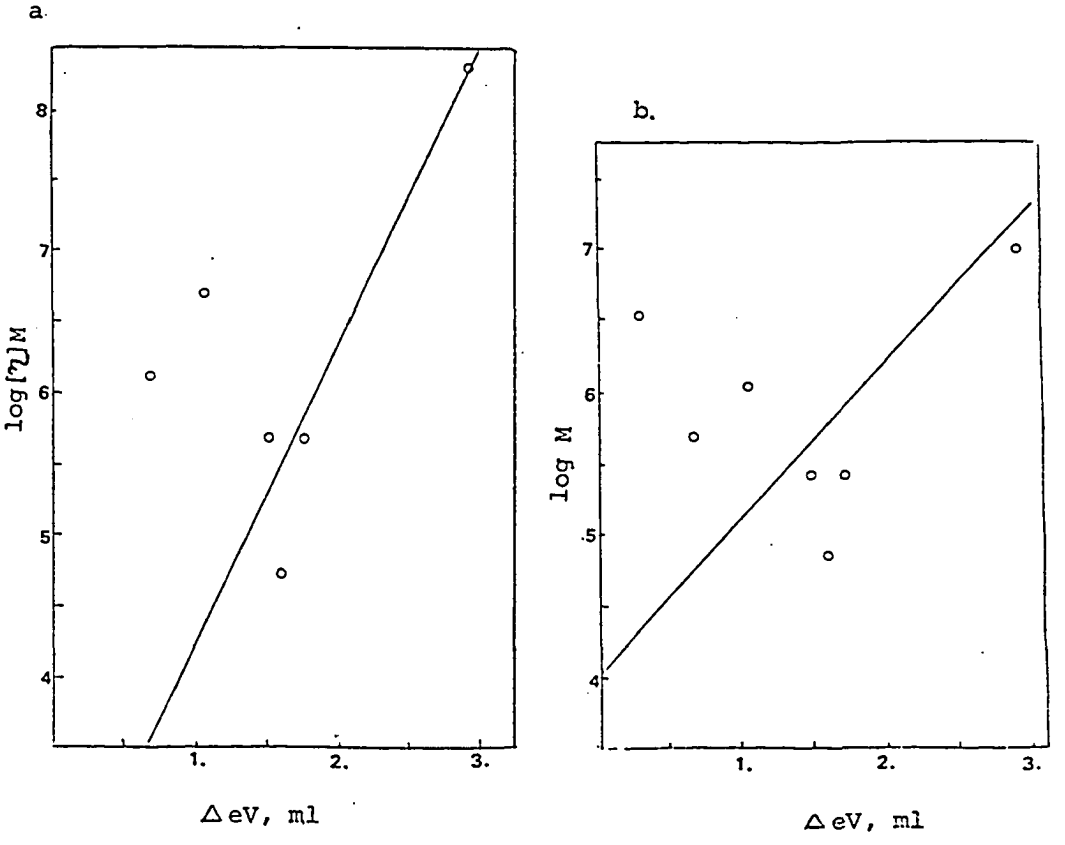

viscometer using a #2 or #3 spindle at 30 or 60 rpm.

2. Viscosity Profile

Latex viscosity as a function of aging time and shear rate (30-1000 sec^{-1}) was measured using the Weissenberg Rheogoniometer (cone and plate viscometer mode with a 1^{o} cone). Viscosity is calculated from the ratio of the measured torsion bar displacement to the applied shear rate.

3. Electrophoretic Mobility

Electrophoretic mobility is measured using the Pen Kem System 3000. The sample is injected into a cylindrical quartz cell having a bore of 0.1013 cm and area of $8.067 \times 10^{-3} cm^2$. Samples are run at $25^{o}C$ using a voltage gradient of 4.97×10^{3} volts/meter over a range of $\pm 2 \times 10^{-8} m^2$/volt sec. Zeta potentials are calculated using the Helmholtz-Smoluchowski equation:

$$Z = \frac{6\pi\eta u}{\varepsilon}$$

where Z is the zeta potential, η is the viscosity of the medium, u is the electrophoretic mobility, and ε is the dielectric constant of the medium.

CHAPTER III

Screening Study: Effect of Recipe Variables on Polymerization Rate, Coagulum Formation, Molecular Weight, and Latex Morphology

A. Introduction

Many references to inverse emulsion polymerization of acrylamide are found in the patent literature and hence it is difficult to select suitable surfactants, initiators, and continuous phases from the abundance of these materials commercially available. Earlier work on inverse emulsion polymerization by F. V. DiStefano using Tetronic 1102 surfactant, benzoyl peroxide initiator, and o-xylene continuous phase produced high molecular weight polymer with little gel; the latex particles were multicellular, although they were an order of magnitude smaller than multiple emulsion droplets previously reported. Hence, in order to define optimal polymerization recipes and put DiStefano's findings (especially regarding latex morphology) in perspective it is necessary to screen a variety of surfactants, initiators, and continuous phases.

B. Materials

Continuous phases used were aromatic o-xylene and aliphatic Isopar M. Initiators used were those having a lower chain transfer constant than the benzoyl peroxide used by DiStefano: water-soluble KPS and oil-soluble ADVN. The more common azo initiator,

azobisisobutyronitrile (AIBN), was unsuitable because of its low solubility in Isopar M. Emulsifiers used (Table 3.1) are representative water-in-oil emulsifers, and include those mentioned in patents on inverse emulsion polymerization. Emulsifier concentration was 10% based on continuous phase and initiator concentration was 0.04 mole % based on moles monomer. The volume ratio of organic phase to aqueous phase was 2/1 and the aqueous phase was 4.5 M acrylamide solution. Total latex solids were 10%. Latexes were prepared dilatometrically.

C. Results

1. Water-in-Oil Emulsion Formation

Surfactants listed in Table 3.1 are tested for water-in-oil (W/O) emulsion formation (Table 3.2). Based on solubility, many more surfactants are suitable for use (i.e., able to form stable emulsions) with o-xylene than with Isopar M compared to o-xylene. If a W/O emulsion was not formed, the emulsifier was not used in a polymerization.

2. Coagulum Formation and Conversion

The amount of coagulum formed is strongly affected by initiator type: generally, more coagulum is formed with water-soluble KPS than with oil-soluble ADVN (Table 3.3). This is not surprising, since formation of radicals in the monomer phase would be more likely to lead to gelation, due either to poor thermal control in this highly exothermic polymerization system or to the presence of

TABLE 3.1

EMULSIFIERS FOR INVERSE EMULSION POLYMERIZATION

Emulsifier

Tetronic 1102: block polymer formed by addition of ethylene oxide to ethylene diamine/propylene oxide (BASF Wyandotte, Inc.).

Tetronic 1502: same composition as Tetronic 1102, different block lengths.

Tetronic 70R2: block polymer formed by addition of propylene oxide to ethylene diamine/ethylene oxide.

Tetronic 130R2: same composition as Tetronic 70R2, different block lengths.

Pluronic L92: propylene oxide/ethylene oxide condensate (BASF Wyandotte, Inc.)

Alkamide HTDE: Stearic diethanolamide (Alkaryl Chemicals, Inc.).

OLOA 340D: amide/imidazoline of isostearic acid and tetraethylene pentamine (TEPA) (Chevron Chemical Company).

OLOA 370: TEPA succinimide of polyisobutylene (PIB)

OLOA 370B: triethylene tetramine succinimide of PIB

OLOA 246A: Calcium sulfonate

OLOA 294: Poly(ethylene oxide), monoalkyl phenyl ether.

Arnnate 462: alkylamine sulfonate (Arjay, Inc.).

Procetyl 10: alkoxylated cetyl alcohol (Croda, Inc.)

Tergitol NP-4: nonylphenol poly(ethylene glycol) ether (Union Carbide Corp.).

Span 60: sorbitan monostearate (ICI Americas, Inc.)

Span 80: sorbitan monooleate.

Hostaphat K0300N: complex ester of phosphoric acid (American Hoechst Corp.).

TABLE 3.2

EMULSIFIERS FOR INVERSE EMULSION POLYMERIZATION:
TEST FOR W/O EMULSION USING METHYLENE BLUE DYE

Emulsifier	HLB	W/O Emulsion in o-xylene[1]	W/O Emulsion in Isopar M[1]
Tetronic 1102	6.0	y-stable**	no-insoluble
Tetronic 1502	5.0	y-stable	no-insoluble
Tetronic 70R2	7.0	no	y-unstable*
Tetronic 130R2	6.0	y-stable	y-unstable
Pluronic L92	5.5	y-stable	no-insoluble
Alkamide HTDE	--	y-stable	no-insoluble
OLOA 340D	--	y-unstable	y-unstable
OLOA 370	--	y-unstable	no
OLOA 370B	--	y-unstable	y-unstable
OLOA 246A	--	y-unstable	y-unstable
OLOA 294	--	y-unstable	y-stable
Arnnate 462	--	y-stable	y-unstable
Procetyl 10	--	no	no
Tergitol NP-4	8.9	y-unstable	y-stable
Span 60	4.7	y-unstable	no-insoluble
Span 80	4.3	y-unstable	y-stable
Hostaphat K0300N	2.5	y-unstable	y-unstable

[1] y = yes

* unstable: emulsion breaks almost immediately when agitation is stopped.

**stable: emulsion stays homogeneous for at least 2 min after agitation is stopped.

TABLE 3.3

INVERSE EMULSION POLYMERIZATION: EFFECT OF RECIPE VARIABLES ON COAGULUM FORMATION AND TOTAL CONVERSION

	o-xylene continuous phase				Isopar M continuous phase			
	I = KPS		I = ADVN		I = KPS		I = ADVN	
Emulsifier	Coagulum	Conversion	Coagulum	Conversion	Coagulum	Conversion	Coagulum	Conversion
Tetronic 1102	some, hard	57	some hard	86	---	---	---	---
Tetronic 1502	none	89	none	80	---	---	---	---
Tetronic 70R2	---	---	---	---	much, soft	86	none	100
Tetronic 130R2	none	100	none	65	much, hard	86	none	9
Pluronic L92	none	75	none	86	---	---	---	---
Alkamide HTDE	some, hard	23	none	100	---	---	---	---
OLOA 340D	much, hard	57	trace	100	much, hard	75	none	80
OLOA 370	none	57	none	57	---	---	---	---
OLOA 370B	some, hard	51	none	43	some, soft	17	none	8
OLOA 246A	none	71	none	17	none	86	none	31
OLOA 294	much, soft	80	much, soft	100	much, soft	100	none	75
Arnnate 462	none	29	none	40	much, hard	86	some, hard	29
Tergitol NP-4	much,	29	trace	63	none	100	none	100
Span 60	none	68	none	100	---	---	---	---
Span 80	some,	51	none	57	none	75	no reaction	
Hostaphat KO300N	none	86	none	100	none	63	none	63

several radicals in a particle simultaneously. Two different types of coagulum were formed in these systems: one type was hard and quite transparent, and the other fluffy and soft. Formation of hard coagulum is generally correlated with use of KPS initiator, which is consistent with crosslinking in these systems. The formation of soft (sticky) coagulum may be related simply to flocculation of latex particles due to poor colloidal stability.

Total conversion is notably low in a number of these systems. Low conversion is not unexpected in systems forming much coagulum, since growing radicals may become entrapped in the coagulum and hence unable to propagate. However, even in polymerization forming no gel, conversion is low (<75%) in some cases (Table 3.4). Low conversion cannot be attributed to overly short reaction times, since reaction mixtures were left undisturbed in the dilatometer for at least 45 minutes after volume contraction ceased. The reason for this is unclear, but, since there is no correlation between initiator type and conversion, it is likely due to chain transfer to surfactant, which wastes radicals.

Generally, conversion was higher in o-xylene systems when polyisobutylene succinimides (OLOA series) and sulfonates (CLOA, Arnnate) surfactants were not used; conversion was higher in Isopar M systems when polyisobutylene succinimides (OLOA series) and polyether (Tetronic, Tergitol) surfactants were used.

TABLE 3.4

Inverse Emulsion Polymerization: Effect of Recipe Variables on Conversion and Polymerization Rate in Systems Forming No Coagulum

	o-xylene Continuous Phase				Isopar M. Continuous Phase			
	I = KPS		I = ADVN		I = KPS		I = ADVN	
Emulsifier	Conversion%	Init. R_p*	Conversion%	Init. R_p	Conversion%	Init. R_p	Conversion%	Init. R_p
Tetronic 1102	---	---	---	---	---	---	---	---
Tetronic 1502	89	81	80	21	---	---	---	---
Tetronic 70R2	---	---	---	---	---	---	100	279
Tetronic 130R2	100	53	65	3	---	---	9	1.5
Pluronic L92	75	120	86	72	---	---	---	---
Alkamide HTDE	---	---	100	24	---	---	---	---
OLOA 340D			100	18			80	31
OLOA 370	57	151	57	19	---	---	---	---
OLOA 370B	---	---	43	13	---	---	80	24
OLOA 264A	71	16	17	3	86	12	31	6.7
OLOA 294							75	24
Arnnate 462	29	36	40	64	---	---	---	---
Tergitol NP-4	---	---	57	13	75	3.6	No reaction	
Span 60	68	162	100	24	---	---	---	---
Span 80	---	---	57	13	75	32.6	No reaction	
Hostaphat KO300N	86	8	100	25	63	64	63	81
Mean		78		24		53		28
Standard Deviation		60		21		40		26

*moles/liter sec $x10^3$

3. Polymerization Rate

The supposition that surfactant could act as a chain transfer agent in these systems and lower total conversion was supported by the correlation between low conversion and low polymerization rate for azo-initiated polymerization shown in Table 3.4; chain transfer to surfactant would tend to lower the polymerization rate. Since such chain transfer must occur at the particle surface rather than in the interior of the particle, it occurs only when radicals are generated in the continuous phase instead of in the monomer phase.

Polymerization was generally more rapid with persulfate initiator than with azo initiator: average polymerization rate, regardless of surfactant type, with KPS was roughly twice the rate with ADVN (Table 3.5).

4. Molecular Weight

Polymer molecular weights are given in Table 3.6. Molecular weights are generally somewhat higher in o-xylene, indicating that Isopar M may cause some chain transfer. Indeed, two molecular weight peaks are found with Hostophat KO300N in Isopar M with both initiators, which also may indicate chain transfer. Highest molecular weights are found using ADVN initiator in o-xylene medium.

5. Latex Morphology

DiStefano's work (3.1) indicated that multicelled monomer emulsion droplets and latex particles were related to the presence

TABLE 3.5

INVERSE EMULSION POLYMERIZATION: EFFECT OF RECIPE VARIABLES ON KINETICS

	o-xylene Continuous Phase		Isopar M Continuous Phase	
Emulsifier	Initial R_p^*	Initial R_p^*	Initial R_p^*	Initial R_p^*
Tetronic 1102	6	16	---	---
Tetronic 1502	81	21	---	---
Tetronic 70R2	---	---	44	279
Tetronic 130R2	53	3	113	1.5
Pluronic L92	120	72		
Alkamide L2	24	---	---	
OLOA 340D	67	18	52	31
OLOA 370	151	19		
OLOA 370B	32	13	16	34
OLOA 246A	16	3	12	6.7
OLOA 294	49	45	25	24
Arnnate 462	36	64	47	27
Tergitol NP-4	55	21	104	33
Span 60	162	24	---	---
Span 80	13	13	32.6	No reaction
Hosta KC300N	8	25	64	81
Mean	57	25	51	28
Standard Deviation	51	20	34	24

*moles/liter sec x 10^3

TABLE 3.6
INVERSE EMULSION POLYMERIZATION: EFFECT OF RECIPE VARIABLES ON HDC AVERAGE MOLECULAR WEIGHT OF POLYACRYLAMIDE INVERSE LATEX

	o-xylene continuous phase		Isopar M continuous phase	
	I = KPS	I = ADVNI	I = KPS	I = ADVN
Tetronic 1102	---	2.4×10^5	---	---
Tetronic 1502	---	---	1.5×10^5	4.6×10^5
Tetronic 70R2	---	---	---	---
Tetronic 130R2	---	---	---	---
Pluronic L92	1.5×10^5	7.5×10^7	---	---
Alkamide HTDE	9.7×10^4	5.6×10^4	---	---
OLOA 340D	---	2.0×10^6	---	2.0×10^6
OLOA 370	---	---	---	---
OLOA 370B	---	9.3×10^7	---	---
OLOA 246A	---	---	---	---
OLOA 294	---	---	---	---
Arnnate 462	---	---	---	---
Tergitol NP-4	---	4.2×10^6	1.9×10^7	1.0×10^4
Span 60	1.2×10^5	1.1×10^6	7.8×10^4	---
Span 80	---	---	1.5×10^5	---
Hosta K0300N	---	---	7.0×10^4 6.5×10^6	3.0×10^3 2.2×10^7
M	1.2×10^5	2.5×10^7	4.3×10^6	4.9×10^6

of two fractions (one hexane-soluble, one hexane-insoluble) in the emulsifier. To verify this, all monomer emulsions used in this study were examined by cold-stage transmission electron microscopy and all emulsifiers were fractionated with hexane (Table 3.7). Multicellular morphology did not correlate with the number of phases but rather with the emulsifier structure: all emulsifiers in which both the hydrophile and hydrophobe were polymeric had multicellular structure. The two-phase composition of the Tetronic and Pluronic surfactants is related to the difficulty in controlling block length during synthesis (3.2). Indeed, emulsions prepared with each fraction separately also have multicellular morphology, further demonstrating that two-phase surfactant composition is not responsible for formation of multicellular emulsions.

D. Conclusions

1. Total conversion can be lowered by formation of coagulum or chain transfer to surfactant.

2. These systems are best for preparation of high molecular weight polyacrylamide at rapid reaction rate with little coagulum:

Pluronic L92/o-xylene
Tetronic 1102/o-xylene
OLOA 340D/o-xylene
Span 60/o-xylene
Tergitol NP-4/o-xylene
OLOA340D/Isopar M

3. Polymerization rate is generally twice as rapid with

TABLE 3.7

EMULSIFIERS FOR INVERSE EMULSION POLYMERIZATION: FRACTIONATION IN HEXANE

Emulsifier	No. of Phases (hexane)	Multicellular Emulsion Morphology
Tetronic 1102: block polymer formed by addition of ethylene oxide to ethylene diamine/propylene oxide	2	yes
Tetronic 1502: same composition as Tetronic 1102, different block lengths	2	yes
Tetronic 7PR2: block polymer formed by addition of propylene oxide to ethylene diamine/ethylene oxide	3	yes
Tetronic 130R2: same composition as Tetronic 70R2, different block lengths	2	yes
Pluronic L92: propylene oxide/ ethylene oxide block copolymer	2	yes
Alkamide HTDE: Stearic diethanolamide	-	no
OLOA 340D: amide/imidazoline of isostearic acid and tetraethylene pentamine (TEPA)	1	no
OLOA 370: TePA succinimide of poly-isobutylene (PIB)	1	no
OLOA 370B: triethylene tetramine succinimide of PIB	1	no
OLOA 246A: Calcium sulfonate	1	no
OLOA 294: Poly(ethylene oxide), monoalkyl phenyl ether	1	no
Arnnate 462: alkylamine sulfonate	1	no
Procetyl 10: alkoxylated cetyl alcohol	1	no
Tergiton NP-4: nonylphenol poly(ethyl-ene glycol) ether	1	no
Span 60: sorbitan monostearate	1	no
Span 80: sorbitan monooleate	1	no
Hostaphat K0300N: complex ester of phosphoric acid	2	no

persulfate initiator compared to azo initiator on an equimolar basis.

4. Multicellular monomer emulsion morphology is correlated to the use of block copolymeric surfactant.

CHAPTER IV

Characterization of the Polymerization Surfactant

The surfactant selected for use in the study of the kinetics and mechanism of inverse emulsion polymerization of acrylamide is Tetronic 1102. This surfactant is a block copolymer containing an ethylene diamine center linkage to which are attached blocks of hydrophobic propylene oxide capped by blocks of hydrophilic ethylene oxide:

$$(EO)_5\text{-}(PO)_{20}\diagdown \qquad \diagup (PO)_{20}\text{-}(EO)_5$$
$$\qquad\qquad N\text{-}CH_2\text{-}CH_2\text{-}N$$
$$(EO)_5\text{-}(PO)_{20}\diagup \qquad \diagdown (PO)_{20}\text{-}(EO)_5$$

It has an average molecular weight 6300 and HLB 6.

Block copolymer molecules in solution have been found to have unusual properties. In this introduction, the behavior of these molecules in solution is reviewed with particular attention to the behavior of molecules having one hydrophobic block and one hydrophilic block.

1. Structure of Block Copolymers with Blocks of Differing Solubilities

The solubility properties of a block copolymer is a combination of the properties of each block. Clearly, if one block is hydrophilic and one is hydrophobic, the blocks are incompatible and the molecule will be non-uniformly soluble in either hydrophilic or

hydrophobic solvents. This solubility behavior, which has been described as "heterogeneous solubility" (4.1), causes one block to have a more extended conformation in solution than the other block and hence leads to phase separation.

2. Block Copolymer Molecules in Solution

Because of the incompatible nature of the blocks, block copolymers form rigid structures such as cylinders and lamellae in concentrated solution (4.2), while they form micelles having a core of the less soluble block and a shell of solvated blocks in dilute solution (4.3). If the molecules do not associate, they phase-separate to form structures which some authors call monomolecular micelles having coiled structure analogous to globular protein; if the molecules associate, they form structures which some authors call polymolecular micelles (Fig. 4.2). Generally, only poly-blocks or highly grafted polymers form "monomolecular" micelles. Qualitatively, the existence of "polymolecular" micelles is shown by the cloudiness of the solution; quantitative determination of the aggregation number can be derived from techniques such as small-angle x-ray scattering and electron microscopy. These techniques have been reviewed by Tuzar and Kratochvil (4.3).

The process of micelle formation can be described as either a closed process, in which the system consists of molecularly dispersed unimers in equilibrium with associates of n-mers, or an open process, in which the system consists of a continuous

distribution of associates of 1 to n unimers. Early work reviewed by Tuzar and Kratochvil (4.3) indicated that association is usually closed, but the experimental studies cited were not unambiguous. Later studies have showed that, although it is a closed process, it is not as simple as closed association of classical non-polymeric soaps. Prasad et al. have shown that Pluronic copolymers in water do not associate at very low concentration ($0.5\text{-}5\times10^{-6}$ M); at higher concentration ($0.005\text{-}1.5\times10^{-2}$ M) molecular association occurs (4.4). Whether the association process in the regime of "polymolecular micelle" formation was closed was not determined by Prasad et al. Mandema et al. have shown that, although association is a closed process, the structure formed is temperature-dependent: the micelles having a compact core which are formed at room temperature, dissociate at low temperature and then re-associate to form cylinders or lamellae (4.5).

Studies of the structure of the "polymolecular micelle" using very sensitive techniques such as small-angle x-ray scattering have shown that the picture of the micelle's structure described above (i.e., a compact core and solvated shell) is too simple: between the core and shell there exists an interfacial region in which the blocks mix and interpenetrate (4.7). The thickness of this region decreases as temperature decreases. Aggregation into nonspherical geometry may occur if the solvated block is too short to cover the insoluble block (4.8). Triblock (ABA) copolymers may form more

complex, network-like micelles due to successive aggregation of two A blocks in the molecules (4.9).

Since low molecular weight amphiphiles such as soaps and surfactants can be used as emulsifiers, the ability of block copolymers to function as emulsifiers and solubilizers in analogy to conventional surfactants has been studied in several systems. In an early study, Molau and Wittbrodt showed that solubilization of homopolymer A by an A-B block copolymer is possible even in concentrated solution: as more homopolymer is added, the micelles increase in size and eventually become elliptical (4.10). An emulsion of a polymer in a nonsolvent which is stable for many months can be formed using a graft copolymer as emulsifier (4.11). Adsorption of an ABA block copolymer onto a polystyrene latex is Langmuirian, and the hydrophilic chains adsorb as loops (4.14). Recent work (4.12) shows that solubilization of homopolymer B by micelles of triblock polymer ABA depends on the relative molecular weight of the homopolymer and the B block. If the homopolymer's molecular weight is relatively low, true solubilization into spherical micelles occurs; otherwise, macroemulsion-like droplets form. If the B block is very long, stable mixed micelles are formed. Marie, Gallot, et al. have used block copolymers to stabilize water/toluene/2-propanol microemulsion. The aggregation of the block copolymer molecules in this system is a closed process, but the aggregation number depends on the ratio of water to propanol (4.6). They find that the phase segregation is less

complete, and more cosurfactant is required for microemulsion formation, with a block copolymeric emulsifier than with conventional ionic or nonionic soaps (4.13). This incomplete segregation leads to a schematic model in which the copolymer molecules' hydrophobic segments are solvated by toluene and cosurfactant, the hydrophilic segments solvated by water and a small amount of cosurfactant, and the continuous phase is a ternary solvent mixture.

3. Formation of Ordered Phases in Block Copolymer Solutions

The ability of heterogeneously soluble block copolymeric molecules to form ordered structures such as cylinders and lamellae at high concentration (as they do in bulk) and certain temperatures has long been recognized (4.1). The types of structures have been described in a review by Gallot (4.15).

Liquid crystalline structures formed by block copolymers in a solvent selective for one block or a solvent blend containing one selective solvent for each block have been extensively studied by Gallot et al. (4.16-4.18). They show that the ordered structures formed (cylinders, lamellae) depend solely on the length of the insoluble block in the copolymer molecule: they are the same regardless of the concentration of polymer in solution. The solution concentration affects only the size of the structures and not their morphology (4.16). These ordered structures are, however, formed only at moderate to high solution concentrations of copolymer (>10-20%); at very low concentration (0.1%), the mole-

cules phase separated (i.e., "monomolecular" micelles are formed) and at higher concentrations (0.1-10%) the molecules associate (i.e., "polymolecular" micelles are formed) (4.17). The number of liquid crystalline structures formed depends on the nature of the blocks: if both are amorphous, only one structure is formed; if one is amorphous and one crystallizable, two mesophases (one corresponding to a folded crystallized chain structure, one to an amorphous chain structure) are formed. Increasing the content of solvent for the crystallizable block causes refolding of the chains with no net change in morphology (4.18).

Liquid crystalline mesophases can be classified in two ways: according to their region of existence on a phase diagram, as proposed by Windsor (4.21); or according to their symmetry, as proposed by Friedel (4.22). Since the latter method provides a more general description of molecular order, it is used in the present work.

Classification of liquid crystals according to symmetry distinguishes three major classes: nematic, cholesteric, and smectic. The nematic order is fluid, non-birefringent, and has orientational order in which the molecules tend to align parallel to each other. The cholesteric phase is also fluid and similar to the nematic phase except that the orientational order is helical and hence the material is usually at least slightly birefringent. Nematic and cholesteric liquid crystals are really subclasses of the same family: nematic liquid crystals are formed by optically

inactive molecules, and cholesteric liquid crystals by optically active molecules (4.23). The third class of liquid crystals, the smectic phase, has a layered structure and hence is birefringent and much more viscous than nematic or cholesteric liquid crystals.

X-ray diffraction (4.24) and nuclear magnetic resonance have been widely used to study liquid crystals. Nuclear magnetic resonance signals from all three types of liquid crystals have distinctive spectra: the signals have a characteristic "super-Lorentzian" shape in which the ratio of the line width at eighth-height to the line width at half-height (a parameter designated R(8/2) is greater than or equal to 4. In the Lorentzian line shape found in isotropic materials, R(8/2) has the value 2.67 (4.25,4.26). The broadening in nematic and cholesteric phases is attributed to orientation of the phase by the magnetic field, whereas broadening in the smectic phase is attributed to orientation of the molecules.

B. Results

1. Morphological Studies

Tetronic 1102, in o-xylene solution, forms multicelled droplets as seen by cold stage transmission electron microscopy (Figure 4.1a). These particles are 0.1-0.2 um in diameter and all of them are multicellular. The smallest particles contain only one or a few cells whereas the larger particles contain many cells. Most of the cells are 0.01-0.02 um in diameter. Similar reticulated particles are also observed for Tetronic 1102 in water

Figure 4.1

SURFACTANT SOLUTIONS WITH 10% TETRONIC 1102

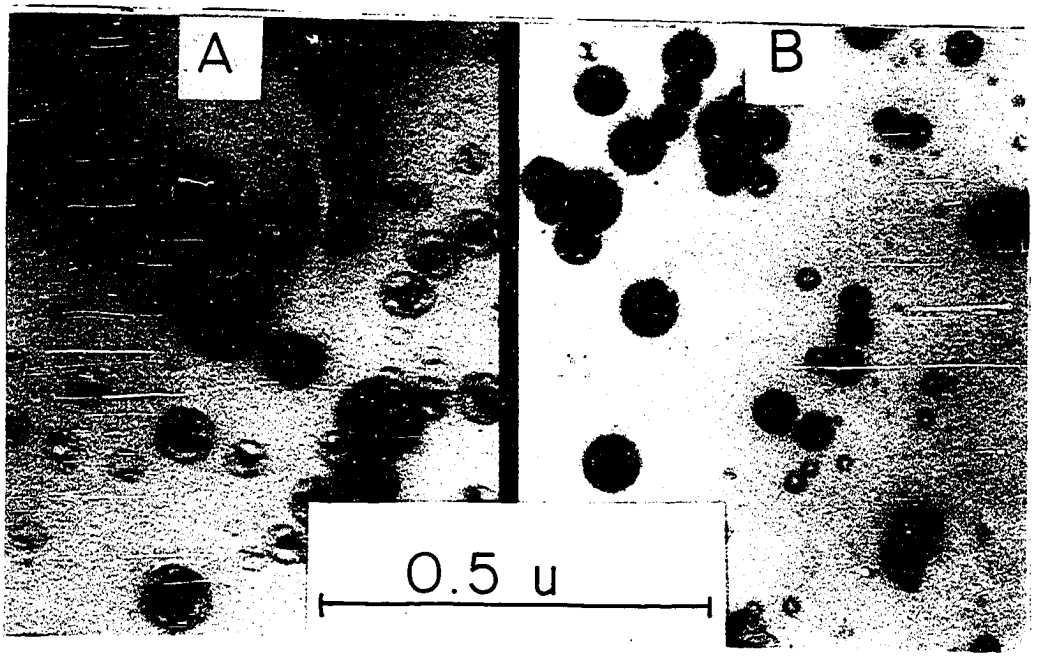

O-XYLENE AQUEOUS

(Figure 4.1b). Thus the emulsifier itself forms 0.1-0.2 um diameter reticulated particles with 0.01-0.02 um diameter cells.

In order to ensure that these reticulated droplets were not formed during the preparation of the electron microscope specimens (a process which included freezing, exposure to high vacuum, and electronic irradiation), the dissymmetry of light scattering was measured for Tetronic 1102 solutions in o-xylene and water. The dissymmetry measured as a function of Tetronic 1102 concentration was extrapolated to zero concentration, and this value was used to calculate the weight-average particle diameter. For Tetronic 1102 in o-xylene, these diameters are 0.177, 0.222, and 0.259 um for ultraviolet, yellow, and red light, respectively. For Tetronic 1102 in water, the diameters are 0.174 and 0.247 um for ultraviolet and yellow light, respectively; the value for red light is indeterminate, presumably because of the small number of particles in the 0.2-0.3 um size range. These results confirm the presence of a colloidal dispersion of Tetronic 1102 particles in both o-xylene and water. Moreover, these weight-average diameters, which give greater weight to the larger particles in the 0.05-0.30 um size range, are in good agreement with the results of the transmission electron microscopy.

Electron microscopic specimens prepared by freeze fracture technique also showed that spherical particles were formed in emulsion (Figure 4.2).

Figures 4.3b, c, and d show electron micrographs of the Tetronic 1102 dispersion of Figure 2a after addition of 4.5M aqueous acrylamide in 20/80, 40/60, and 60/40 aqueous acrylamide/o-xylene phase volume ratios. For the 20/80 volume ratio (Figure 4.3b), the particles are reticulated but smaller in size than those without aqueous acrylamide (Figure 4.3a); many particles are smaller than 0.01 um. For the 40/60 phase ratio (Figure 4.2c), the particles are generally larger than those without aqueous acrylamide, and the 0.01 um-or-smaller particles observed for the 20/80 phase ratio (Figure 4.3b) were not seen; moreover, the surface cells of the larger particles appeared to be swollen with a liquid (presumably aqueous acrylamide) so that some cell walls were ruptured, forming larger cells near the surface than in the center. For the 60/40 phase ratio (Figure 4.3d), the particles were also larger than those without aqueous acrylamide, but there were still many particles smaller than 0.01 um; compared with the 40/60 ratio, the surface cells of the larger particles appeared to be even more swollen with liquid so that even more cell walls were ruptured, forming larger irregularly-shaped cells near the surface.

Figure 4.2

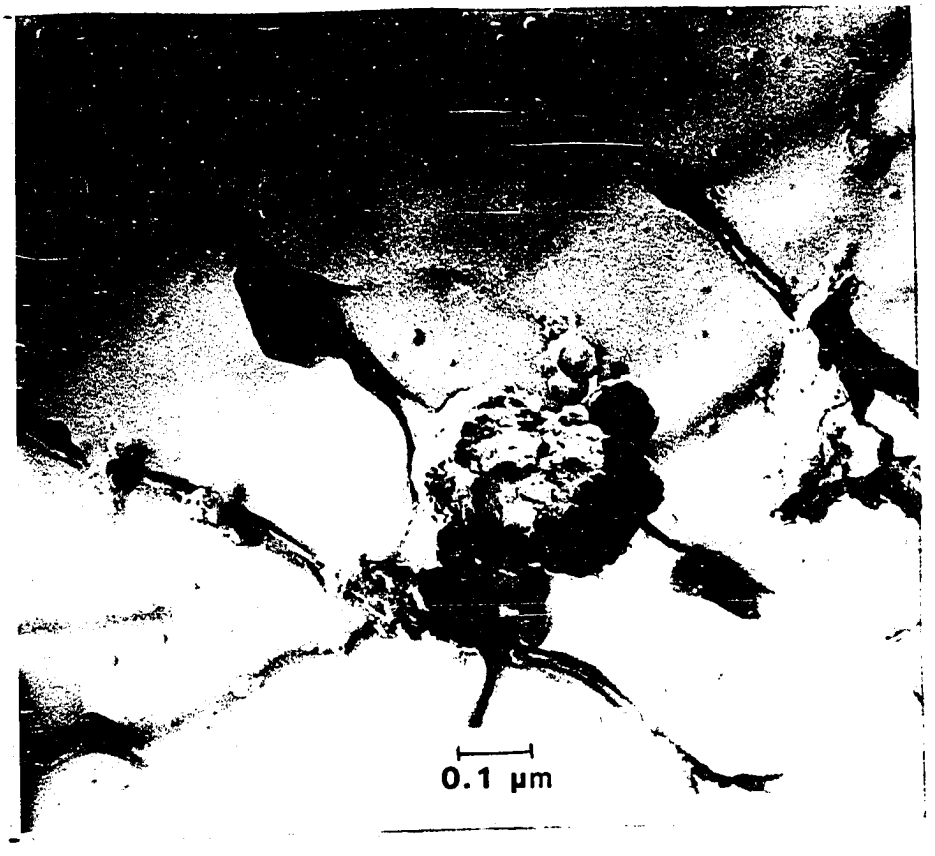

1/1water/o-xylene emulsion containing 10% Tetronic 1102 prepared using freeze-fracture technique

Figure 4.3

Monomer Emulsions Prepared at Varying Phase Ratios

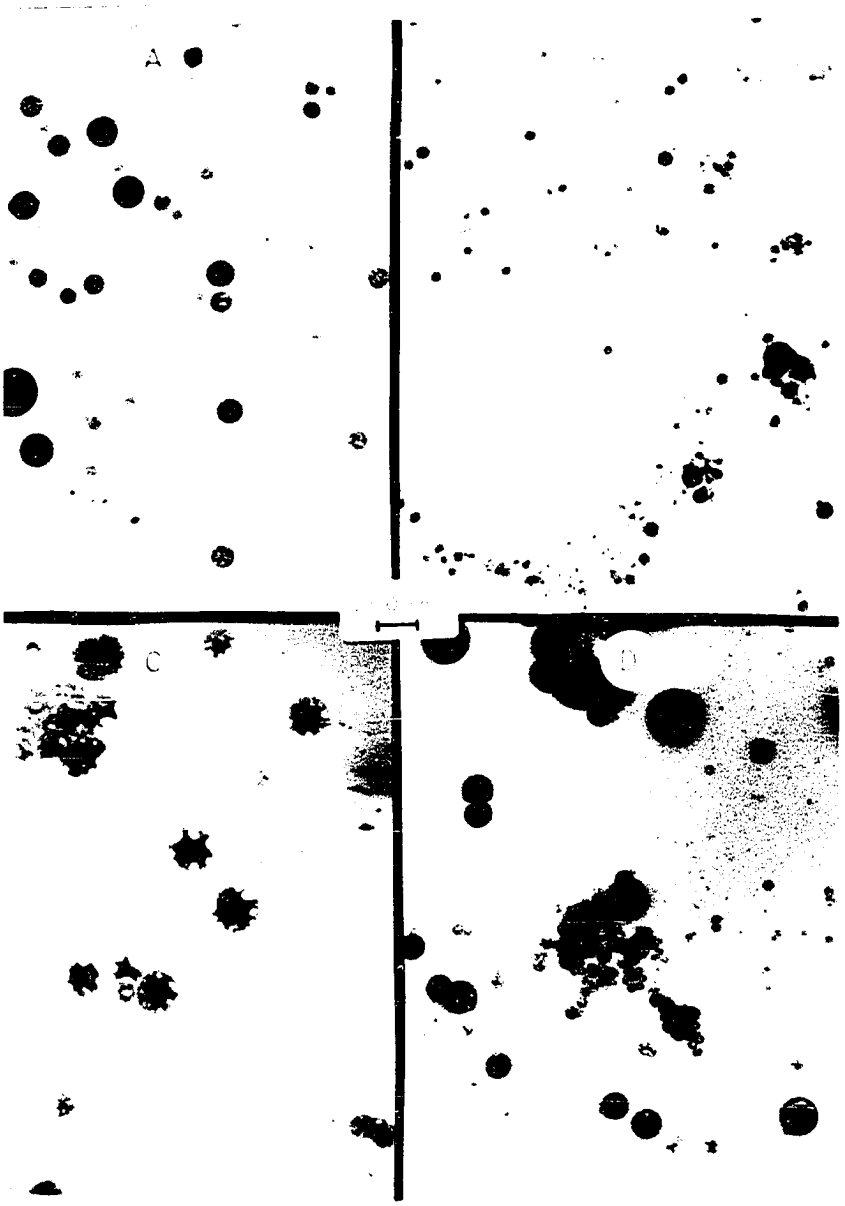

Electron Micrographs of Aqueous Acrylamide Emulsions prepared using 10% Tetronic 1102 and different Acrylamide/o-xylene Phase Ratios: A. 0/100; B. 20/80; C. 40/60; D. 60/40.

These electron microscopic studies do not reveal what is contained inside the cells of the multicelled particles of Tetronic 1102. Centrifugation of both emulsions and solution of Tetronic 1102 in o-xylene and water shows that these cells do not contain voids, since there is no evidence of creaming. Since dye solubilization studies using the water-soluble dye methylene blue show that Tetronic 1102 does indeed form a water-in-oil emulsion, it seems likely that the cells of Tetronic 1102 particles contain entrapped solvent which is displaced by aqueous phase when an emulsion is formed. A variety of electron microscopic staining techniques were used to elucidate the inner structure of the Tetronic 1102 particles. Phosphotungstic acid (PTA), a water-soluble compound capable of hydrogen bonding, was added to emulsions and surfactant solutions. The presence of short, needle-like liquid crystals which were electron-transparent in the continuous phase was revealed (Figure 4.5). Also, these liquid crystals appeared to be oriented normal to the particle surface and thereby form the walls of the multicelled droplets (Figure 4.5). Ruthenium tetraoxide (RuO_4), a selective stain for polyethers and polyamides (4.19,4.20), was used to enhance electron density contrast of the polyacrylamide as well as the surfactant molecule. The stain was added as an 0.5 wt% aqueous solution. Adding this stain to polyacrylamide solution increases solution viscosity almost to the point of gel formation. Because RuO_4 reacts explosively with aromatic hydrocarbons, o-xylene was replaced by

carbon tetrachloride. Tetronic 1102 is equally soluble in carbon tetrachloride and o-xylene. Emulsions were prepared in carbon tetrachloride (CCl_4) in the absence of stain to confirm that the multicellular droplet structure was not affected by changing the continuous phase (Figure 4.6). A coarse emulsion formed by mixing a stained polyacrylamide solution with CCl_4 consists of lightly stained droplets of polyacrylamide (Figure 4.7a). Addition of the RuO_4 solution to an inverse emulsion acrylamide polymer confirmed the presence of the liquid crystals seen in the continuous phase; however, the RuO_4 appeared to preferentially stain the surfactant, so the contents of the inner cells was not elucidated (Figure 4.7b). To eliminate this preferential staining, a polyacrylamide solution was mixed with RuO_4 solution before adding it to the Tetronic 1102 solution in CCl_4. Emulsion preparation was difficult because of the high viscosity of the polyacrylamide solution stained with RuO_4. Electron microscopic examination of this emulsion showed multicelled droplets with swollen and darkened walls as well as a general darkening of the interior of the cells (Figure 4.8). These results indicated that the polyacrylamide both swells the surfactant molecules forming the cell walls and fills the interior of the cells, but since the presence of such a stain typically darkens the background of the entire micrograph, the presence of only aqueous phase in the interior of the cells was not confirmed. Metal compounds which do not react with either the polymer or surfactant but which

are soluble in only one of the phases can be used to preferentially stain that phase in an emulsion. Two such metal compounds were used to elucidate the composition of the interior of the cells in Tetronic 1102 solutions and emulsions: water-soluble silver nitrate and organic-soluble iron pentacarbonyl. Use of the silver nitrate stain shows that the aqueous phase is indeed segregated inside the cells (Figure 4.9a). However, use of the iron pentacarbonyl stain shows that some of the organic phase remains entrapped inside the cells and also swells the surfactant (Figure 4.9b). Hence the segregation of the oil and water phases is not as complete with Tetronic 1102 as with conventional soaps.

Since a polymer chain conformation can be affected by changing temperature, the formation of these multicelled droplets may be expected to be a function of temperature. To investigate these temperature effects, surfactants solutions and emulsions were prepared at 4 and 70°C by equilibrating all ingredients at the desired temperature for 16 hr, preparing the samples at the same temperature and equilibrating them for 16 hr. Samples were kept at constant temperature until preparation of specimens for electron microscopy. Electron microscopy shows that this reticulated structure is found both in surfactant solutions in o-xylene and in water-in-o-xylene emulsions prepared at temperatures ranging from 4 to 70°C (Figures 4.4a,b,c,d). At the low temperature, rodlike structures are seen in the surfactant-in-o-xylene solution, although they are absent in the emulsion. Since rods have greater

Figure 4.4

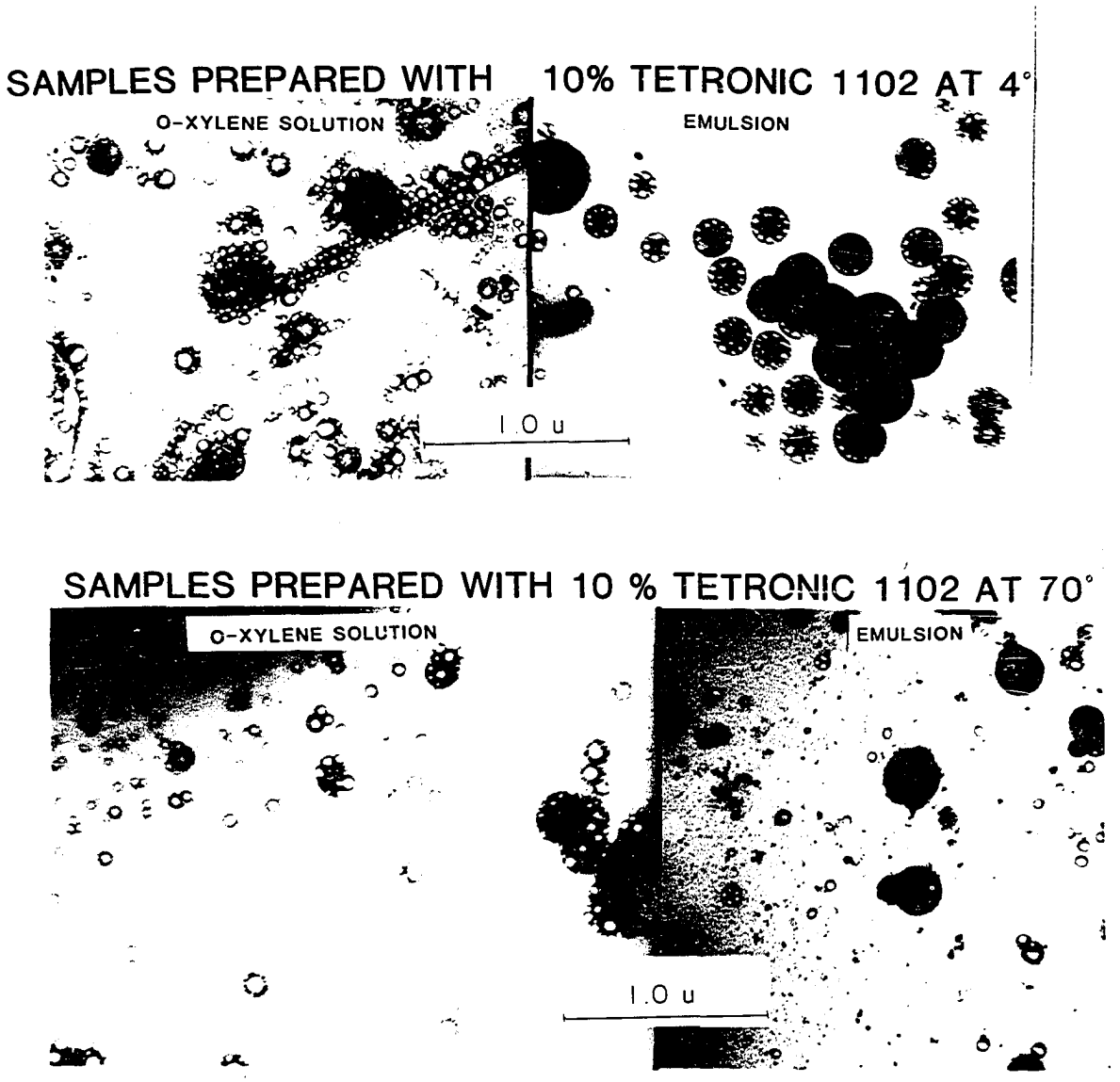

Effect of Temperature on Morphology of Emulsions and Surfactant Solutions Containing Tetronic 1102

Figure 4.5

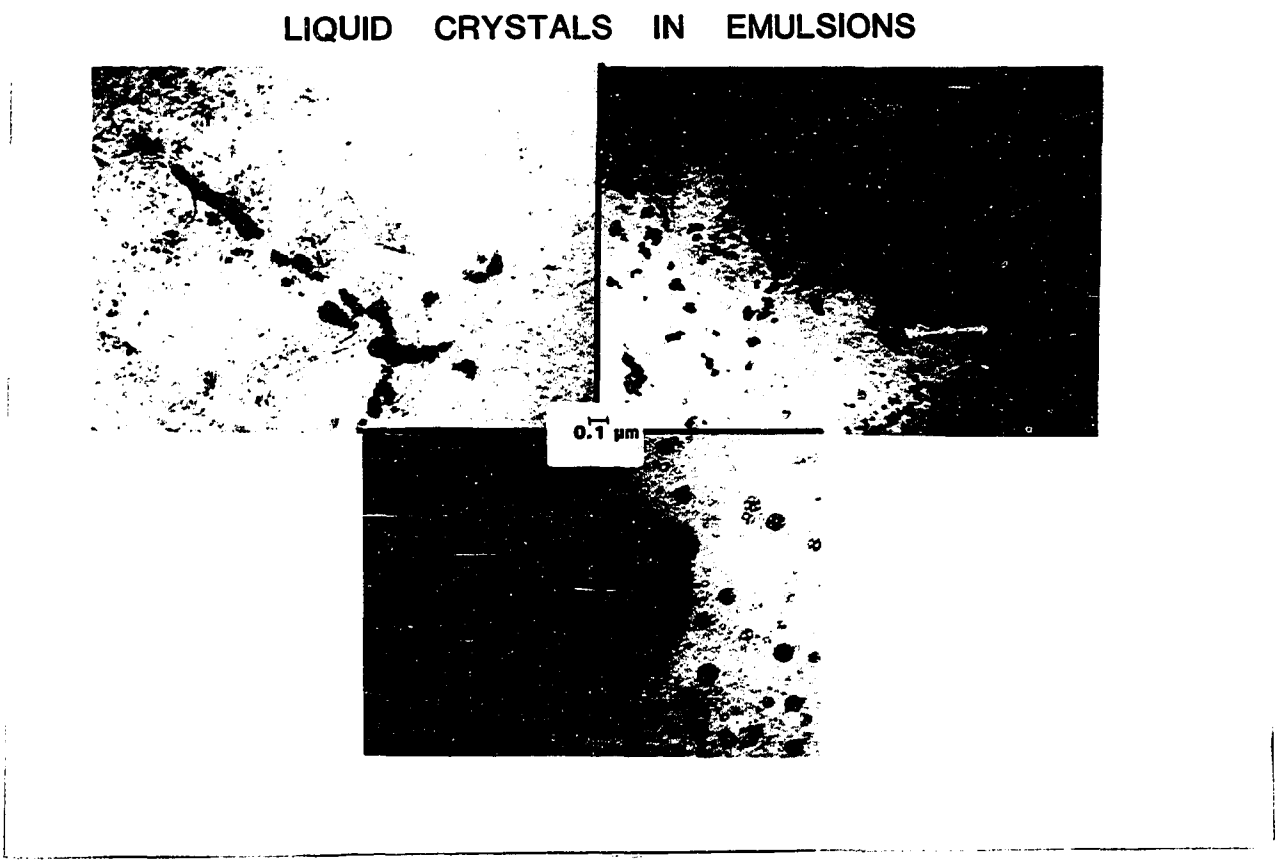

1/1 o-xylene/water emulsions prepared with 10% Tetronic 1102 stained with phosphotungstic acid (PTA)

Figure 4.6
Surfactant Solutions and Emulsions Stained with Ruthenium Tetroxide

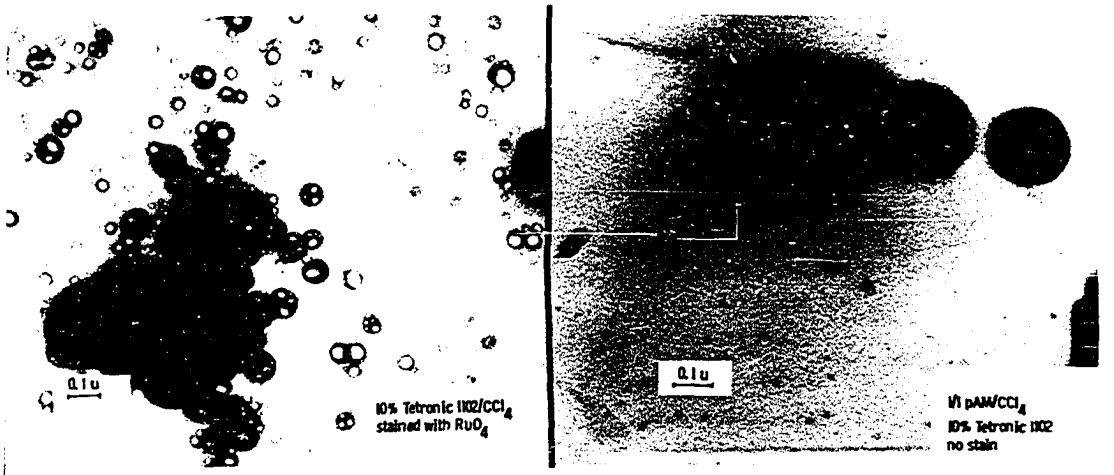

Surfactant solution and emulsion prepared with 10% Tetronic 1102 stained with Ruthenium Tetroxide, a selective stain for polyethers and polyamides

Figure 4.7a
Emulsion Stained With Ruthenium Tetroxide

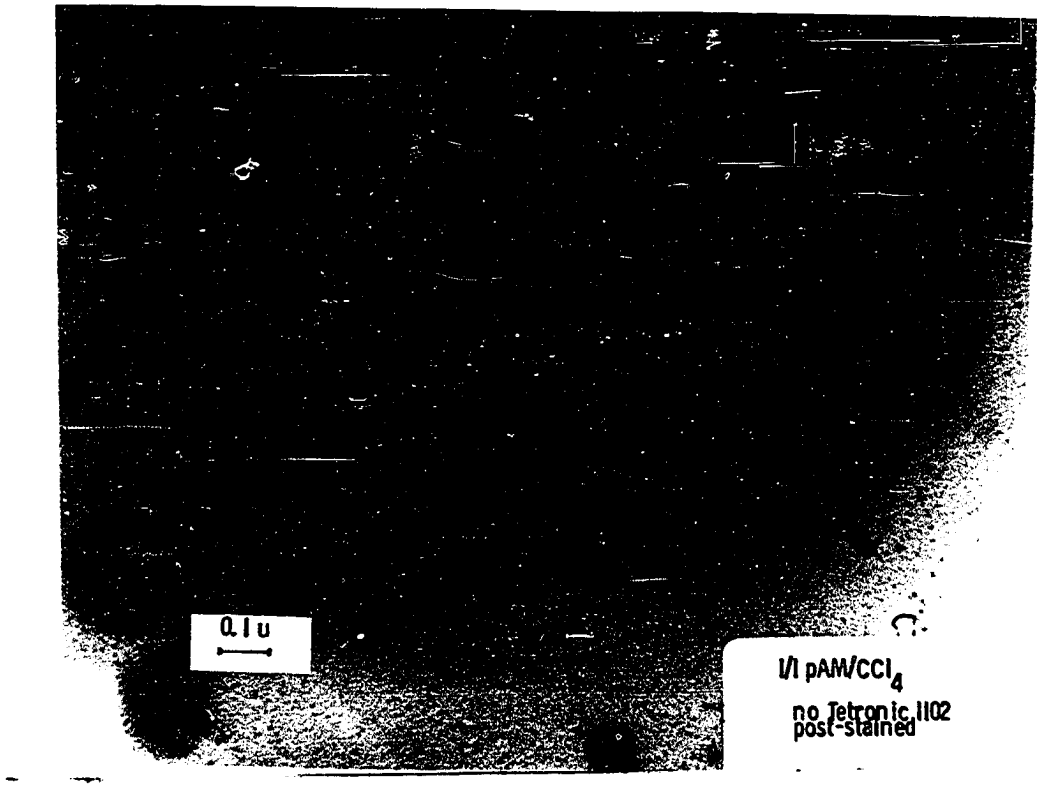

Coarse emulsion (prepared without surfactant) stained with Ruthenium Tetroxide, a selective stain for polyethers and polyamides

Figure 4.7b

Emulsions Stained with Ruthenium Tetroxide

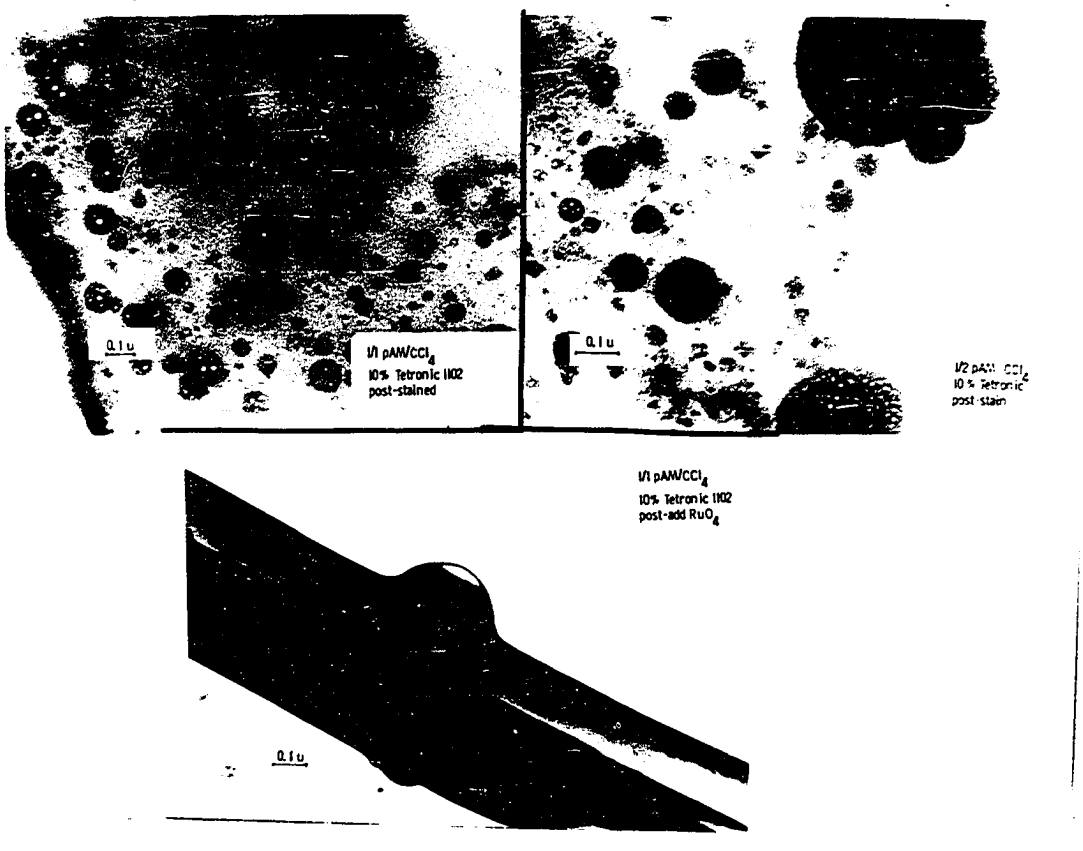

Emulsions prepared with 10% Tetronic 1102 stained after emulsification with Ruthenium Tetroxide, a selective stain for polyethers and polyamides

Figure 4.8

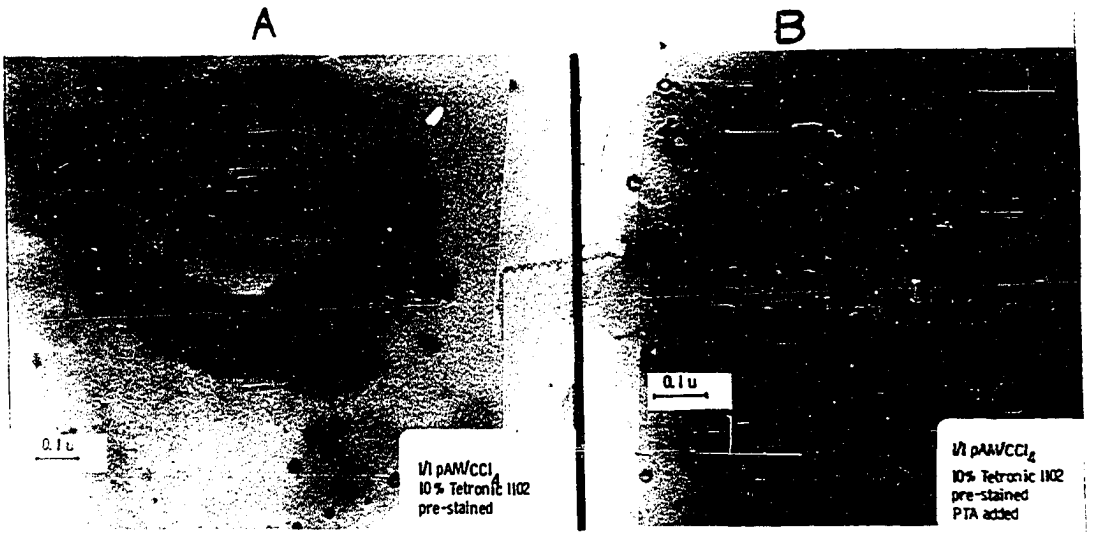

Emulsions prepared with 10% Tetronic 1102 stained before emulsification with Ruthenium Tetroxide, a selective stain for polyethers and polyamides. Figure B has also been stained with a negative stain, Phosphotungstic Acid (PTA)

Figure 4.9a

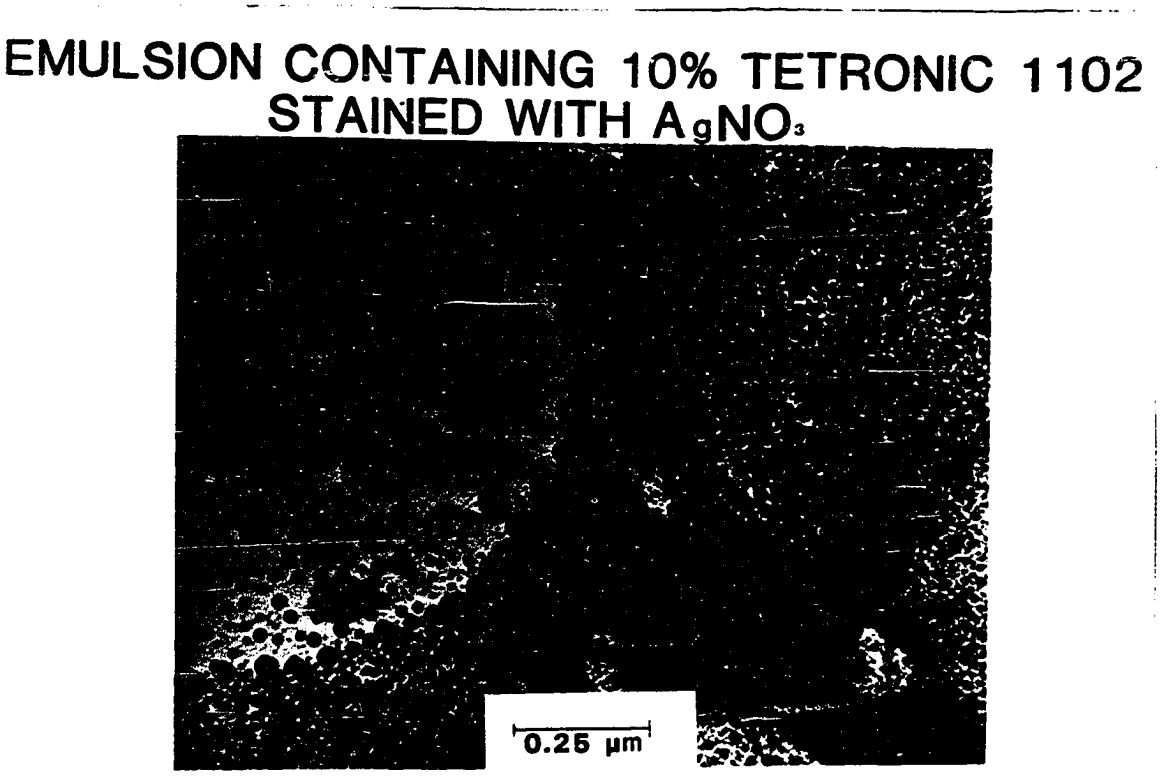

Emulsion prepared with Tetronic 1102 containing a water-soluble staining agent, Silver Nitrate

Figure 4.9b

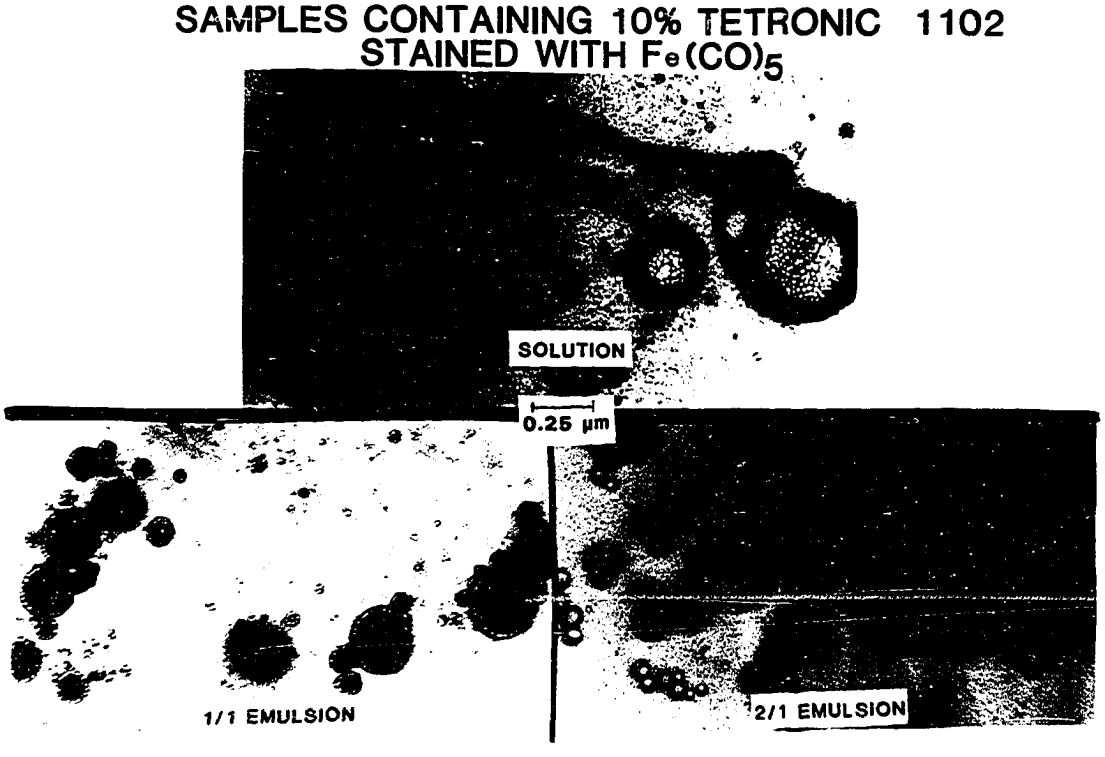

Emulsion prepared with Tetronic 1102 containing an oil-soluble staining agent, Iron Pentacarbonyl

surface area than spheres of equal volume, the surface concentration of the hydrophobic groups must be higher. Formation of rodlike structures is favored by stronger interactive forces (i.e., hydrogen bonding) between the hydrophilic groups.

Although the structure of the multicelled emulsion droplets does not change with changing temperature, studies of viscosity, calorimetry, optical and electron microscopy, interfacial tensiometry, and NMR spectroscopy show that the structure of the surfactant molecule is indeed affected by temperature.

Reduced viscosity (measured in a Ubbelohde viscometer) of aqueous and o-xylene surfactant solutions and emulsions is greatly affected by temperature. Solutions of 4% and 12% Tetronic 1102 in o-xylene show steadily decreasing viscosity as temperature is varied from 20 to 65°C; this is not unexpected, since viscosity typically decreases with temperature (Fig. 4.10a and b). Viscosity of a 12% solution of Tetronic 1102 in water dramatically changes as temperature increases: viscosity increases approximately 70% as temperature increases from 44.5 to 50°C (Figure 4.11) and the solution, translucent at lower temperature, becomes opaque white at 50°C. The emulsion shows a similar increase in viscosity over this temperature range (Fig. 4.12). This indicates that a phase transition occurs at 50° if water is present.

Differential scanning calorimetry shows a crystalline melting transition occurs at 62°C in aqueous surfactant solution and in

Figure 4.10

Reduced Viscosity Of Tetronic 1102 in

O-Xylene

a. 4% Tetronic 1102

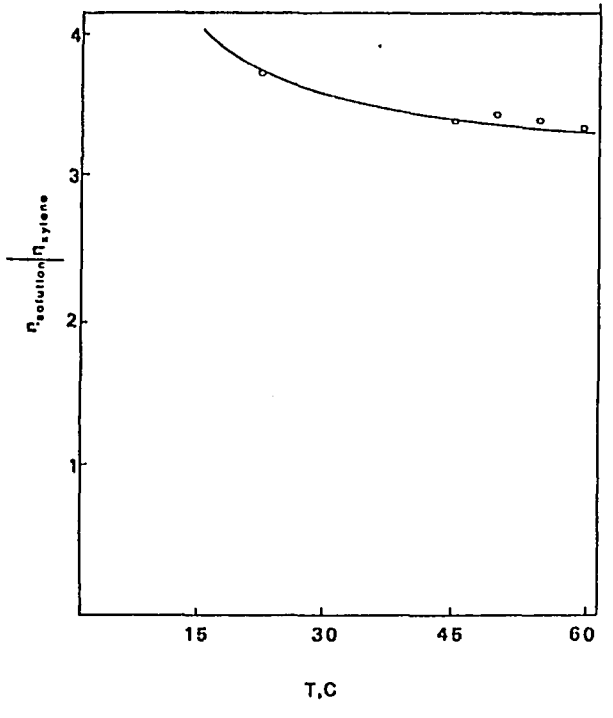

b. 12% Tetronic 1102

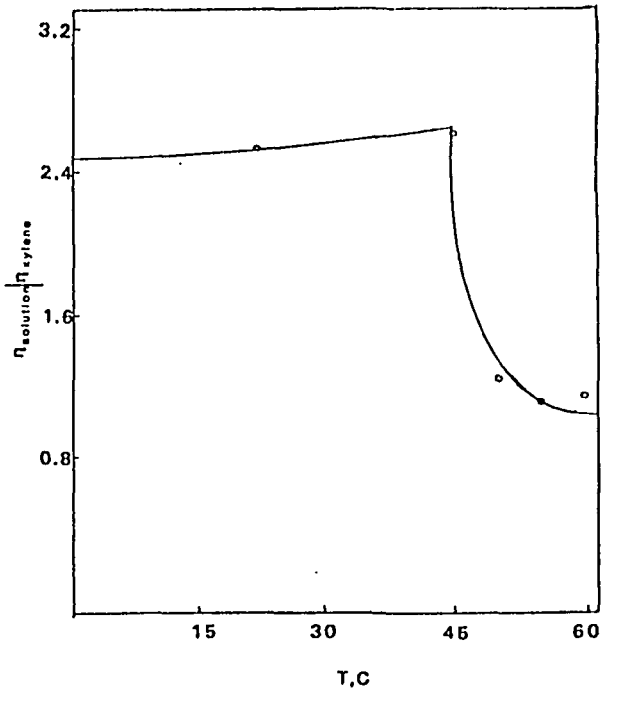

83

Figure 4.11

Reduced Viscosity of 12% Tetronic 1102
in Water

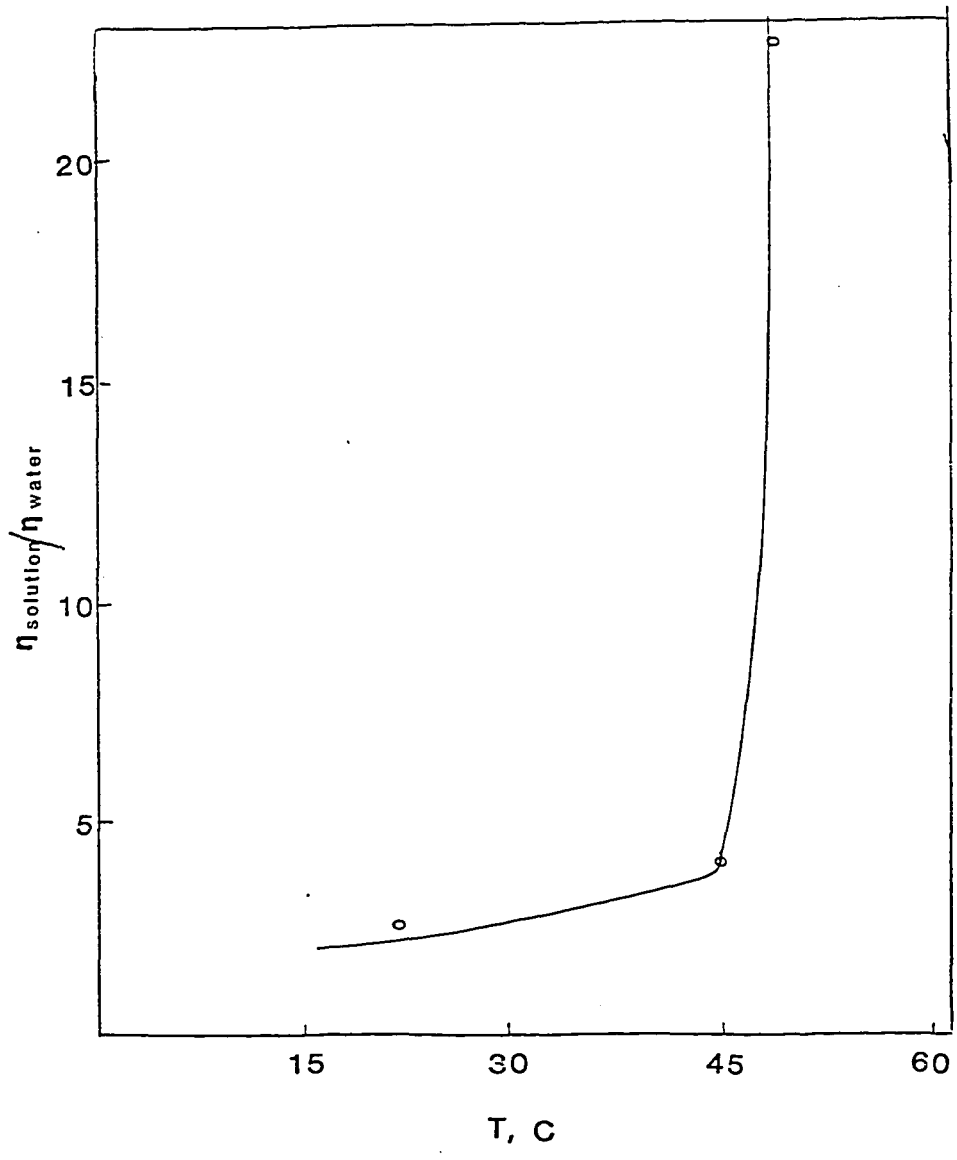

Figure 4.12

Reduced Viscosity of 1/1 o-xylene/water
Emulsion Containing 12% Tetronic 1102
on Volume of Oil Phase

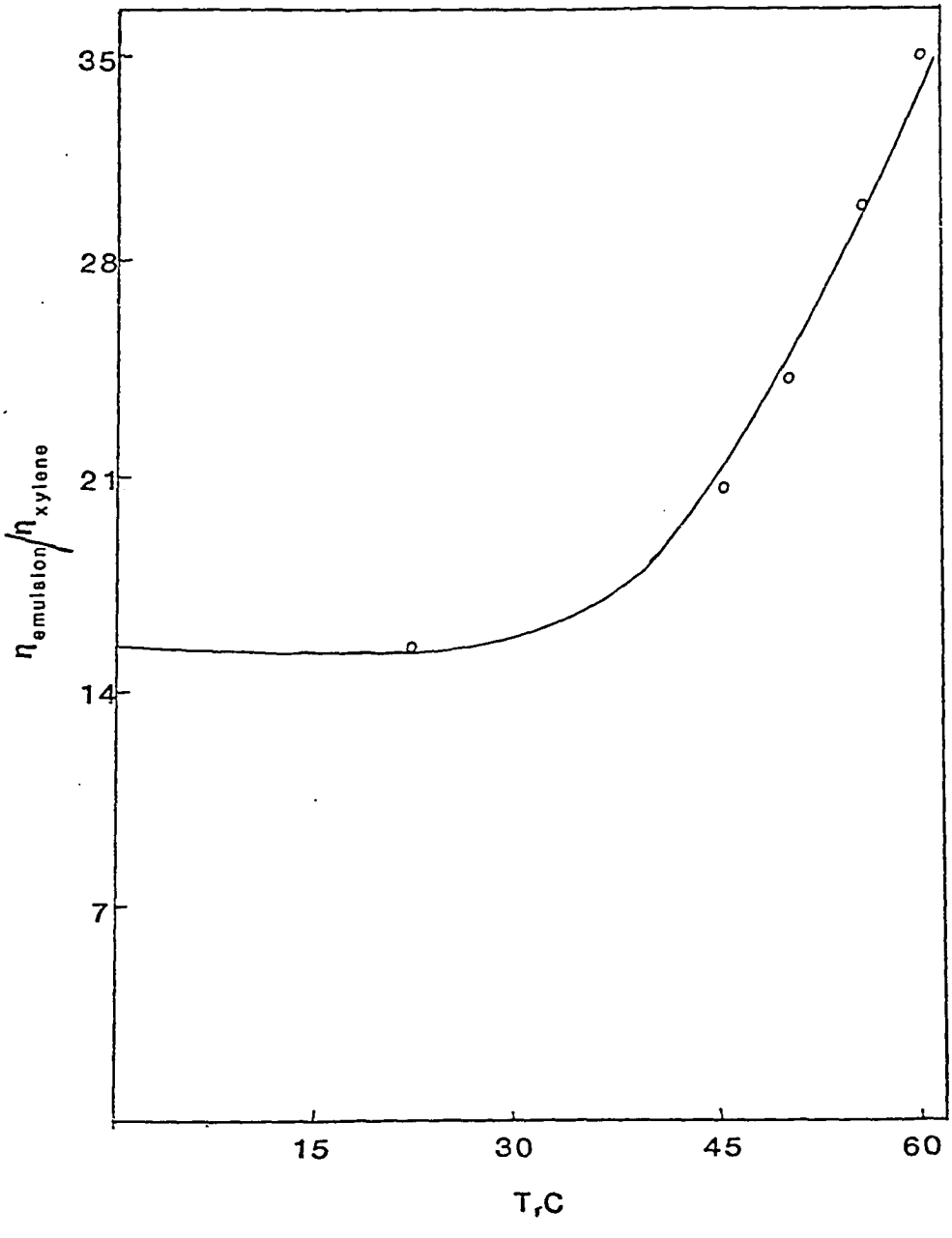

emulsion and is not seen in o-xylene solution or in bulk surfactant. This transition must be due to the poly(ethylene oxide) segments of the surfactant molecule, since poly(propylene oxide) in Tetronic 1102 is atactic, and poly(propylene oxide) is not crystalline unless it is stereoregular (4.27). A melting temperature of 62°C corresponds to a poly(ethylene oxide) molecular weight of 6000 (4.27). Since the average molecular weight of the poly(ethylene oxide) hydrophile in a Tetronic 1102 kmolecule is 1260 g/mole, forming crystallites of molecular weight 6000 would require aggregation of 4 to 5 molecules of Tetronic 1102.

Optical microscopy shows that aqueous Tetronic 1102 solution is isotropic at room temperature but suddenly becomes ordered at 50°C; the structure of the ordered regions changes at 60°C (Figure 4.13). Similar transitions are seen in emulsions. Neither the surfactant solution nor the emulsion are birefringent at any temperature. Electron micrographs of aqueous surfactant solution and emulsion with and without PTA stain taken at temperature ranging from liquid nitrogen temperature to 70°C and back to liquid nitrogen temperature show subtle changes over the temperature range of 45-50°C (Figure 4.14,4.15). These changes are less obvious than those observed with the unaided eye or with the optical microscope (Figure 4.13), probably because of the dearth of solvent present at such high vacuum.

Interfacial tension, which is 2.8 dynes/cm at 25°C, rises

Figure 4.13

OPTICAL MICROSCOPY OF SURFACTANT SOLUTION

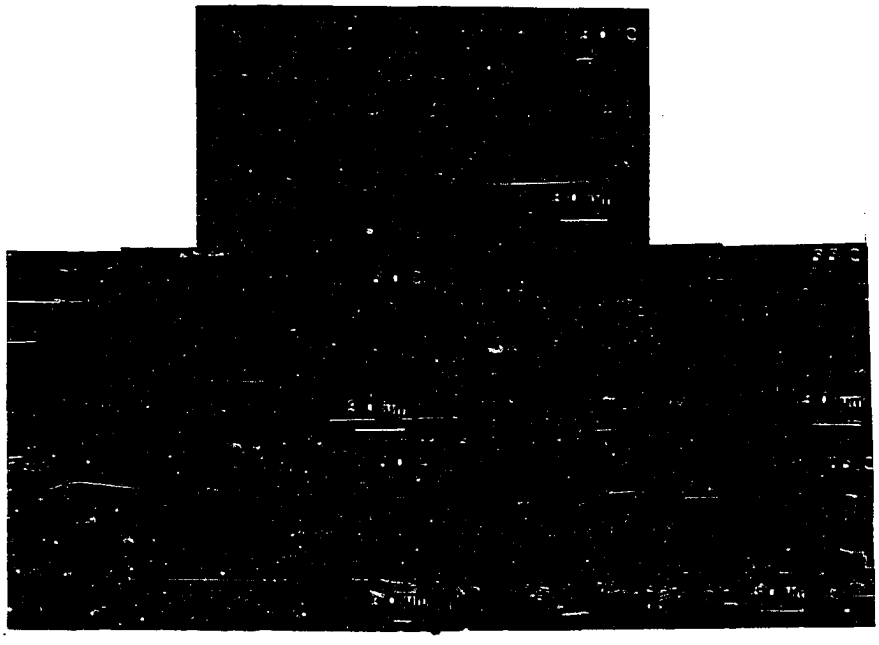

optical micrographs taken using normal (unpolarized) light at various temperatures

Figure 4.14

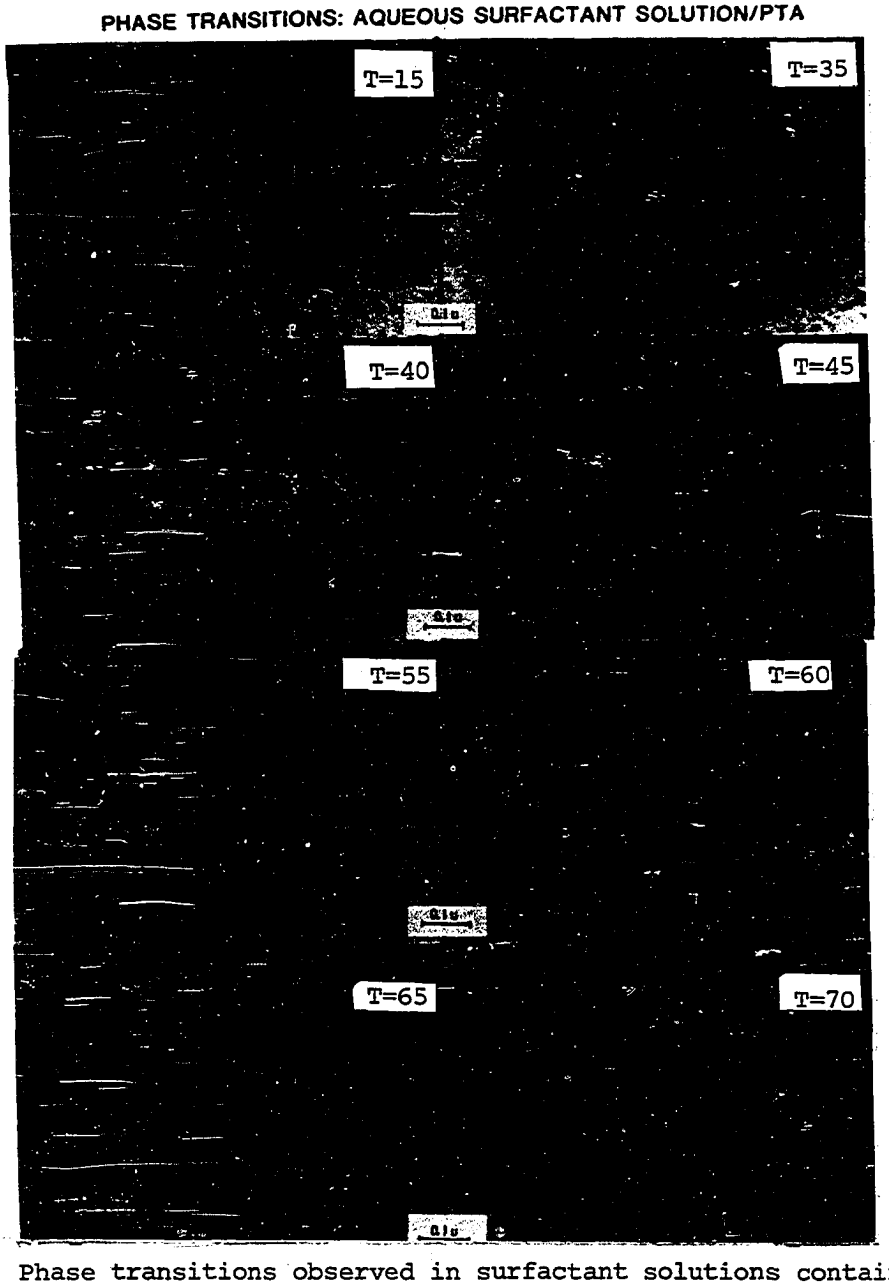

Phase transitions observed in surfactant solutions containing 10% Tetronic 1102 stained with phosphotungstic acid (PTA)

Figure 4.15

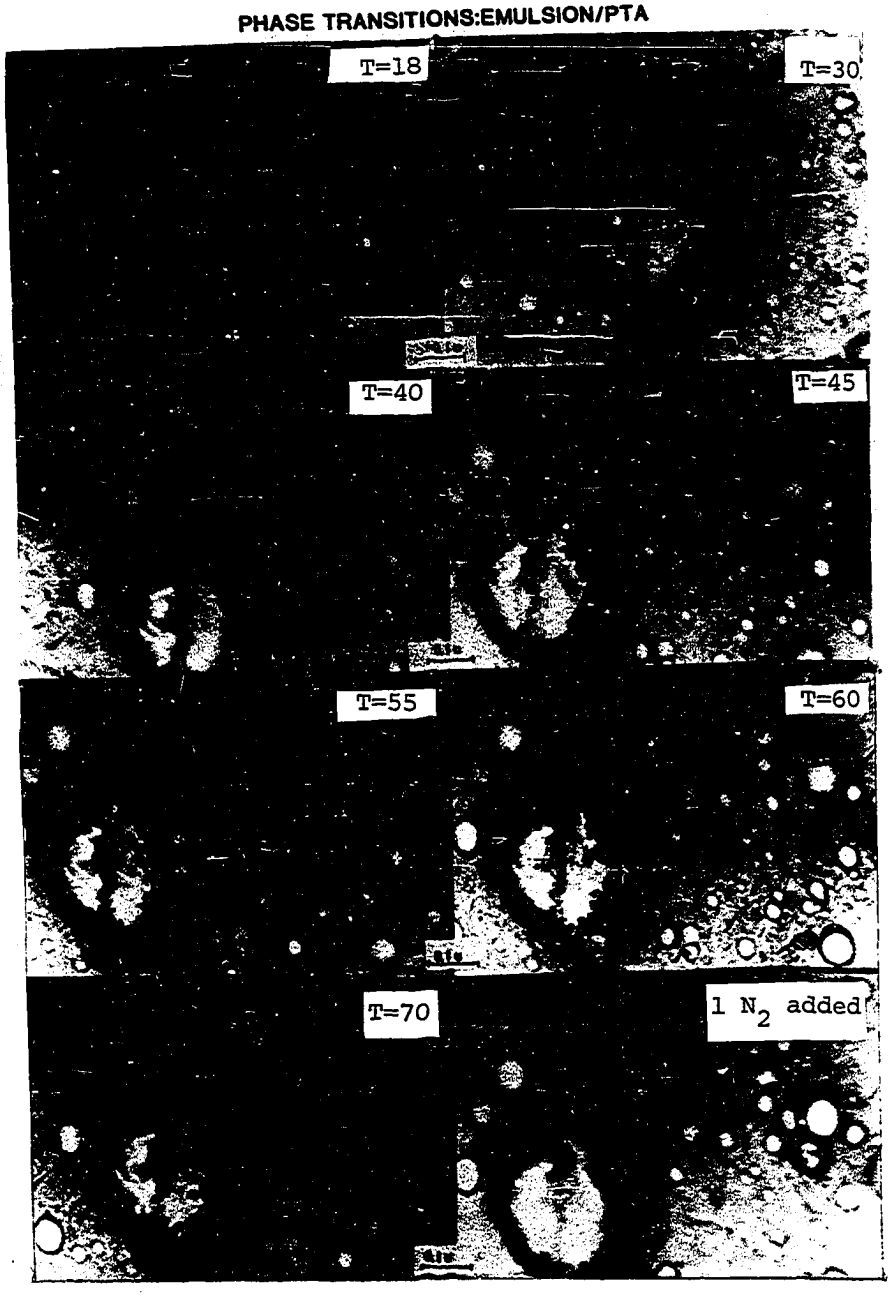

phase transitions observed in 1/1water/o-xylene emulsions containing 10% Tetronic 1102 stained with phosphotungstic acid (PTA)

sharply above the cloud point (30°C) to 16.5 dynes/cm, which is close to the 18 dynes/cm expected* for water in o-xylene with no surfactant. This is not unexpected, since typically surfactants become less hydrophilic (less water soluble) at their cloud points. However, as the temperature is further increased above the cloud point, interfacial tension decreases rapidly to 0.5 dynes/cm and then, above the phase inversion temperature (50°C), rises again to a plateau value of 16 dynes/cm (Figure 4.16). Interfacial tension changes of this magnitude are characteristic of bulk movement of surfactant molecules from one phase to another. Extremely low interfacial tension, such as that found between 50 and 60°C in this system, is typically found when a surfactant phase is formed (4.28). Evidently an ordered phase is formed over a rather narrow temperature range in this system; once the upper temperature limit of its existence is exceeded, the interfacial tension returns to a higher value. Evidently the strong swelling required for a stable emulsion does not occur above the phase inversion temperature, since the emulsion breaks above this temperature. The formation of viscous "tails" on the ends of the droplets in the spinning capillary have been correlated with the presence of an ordered phase (4.35). In the Tetronic 1102 system, increasingly viscous "tails" form at temperatures between 40 and 55°C (Figure 4.17).

---

*Value from Lange's Handbook of Chemistry.

Figure 4.16

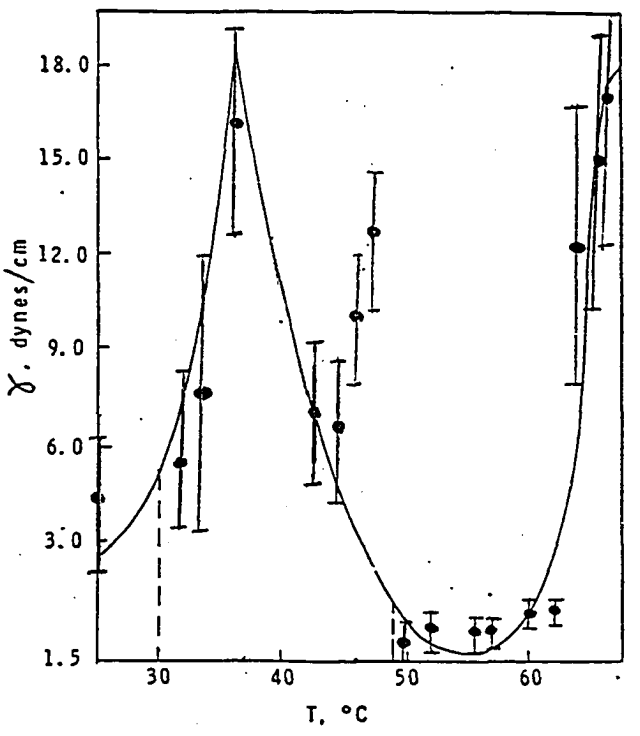

Interfacial Tension (Spinning drop method) of water in o-xylene emulsion containing 10% Tetronic 1102.

Figure 4.17

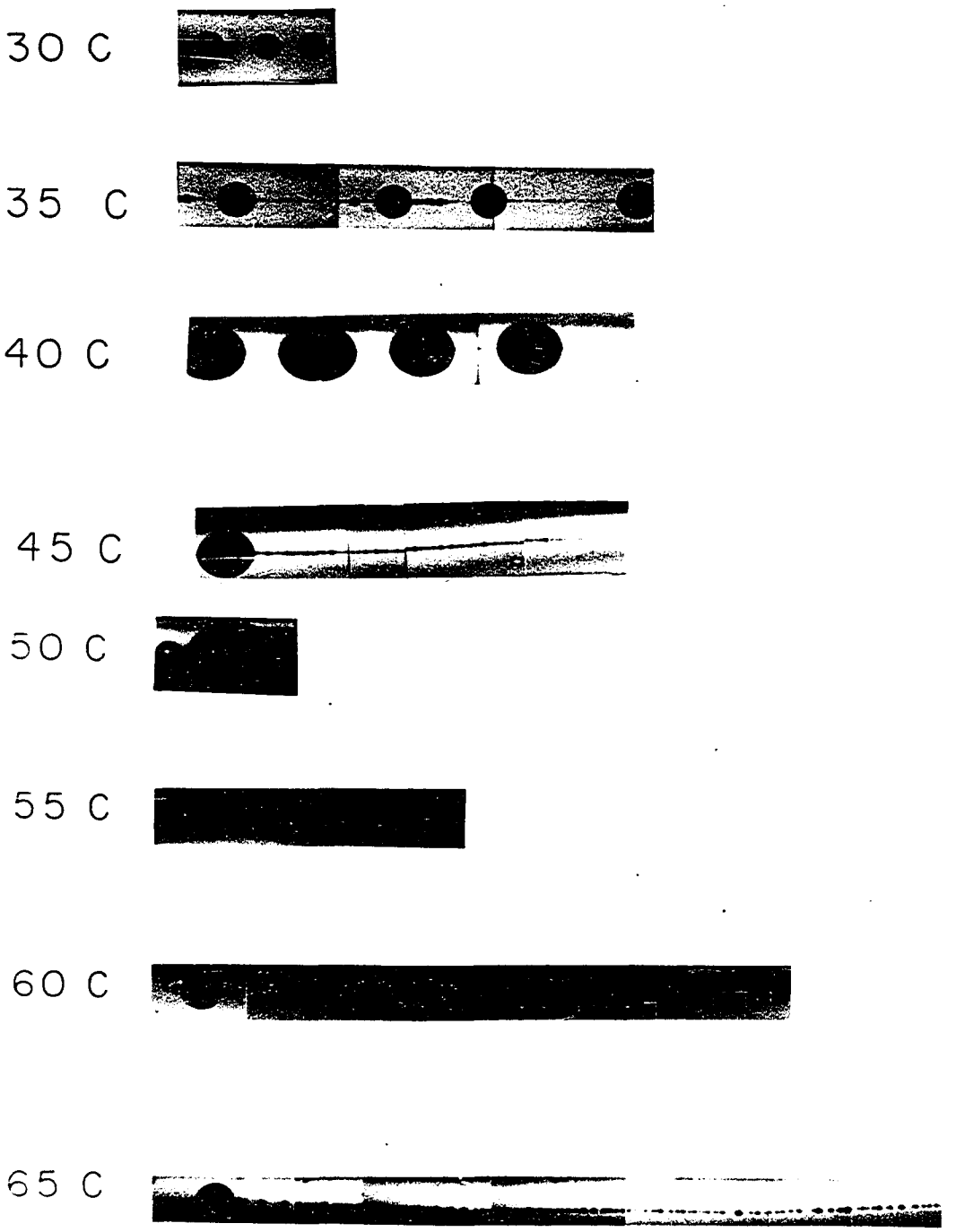

Change in the shape of droplets and droplet "tails" observed as a function of temperature in the Spinning Drop Interfacial Tensiometer

^{1}H NMR spectra show two peaks: a peak at 1.1 ppm due to the methyl protons in the poly(propylene oxide) hydrophobe; and a peak at 3.4 ppm due to the methylene protons found in both the hydrophilic and hydrophobic blocks (Figure 4.18). Both of these peaks broaden when temperature is increased from 25 to 55°C; this is unexpected, since normally NMR signals become sharper at higher temperature because of more rapid exchange (Figure 4.19). The increased broadening indicates that the molecule is assuming a more rigid structure at higher temperature, which is consistent with formation of an ordered phase.

An emulsion of 50/50 volume ratio water/o-xylene with 10% Tetronic 1102 (on continuous phase) shows no settling on storage at ambient temperature after storage for many months. However, when stored at 70°C for 24 hr, the emulsion droplets begin to settle; after 48 hr, the emulsion breaks but the emulsifier remains soluble in the o-xylene; after 72 hr the emulsifier is not soluble in either phase but instead forms a cream layer at the interface.

C. Discussion

The formation of multicelled droplets in solutions of Tetronic 1102 in o-xylene or water results from its block copolymeric structure. Because of the relatively high molecular weight of the poly(propylene oxide) hydrophobic portion, the molecule cannot form a true solution in hydrophilic solvents; similarly, the molecular weight of the poly(ethylene oxide) hydrophilic portion is too high

Figure 4.18

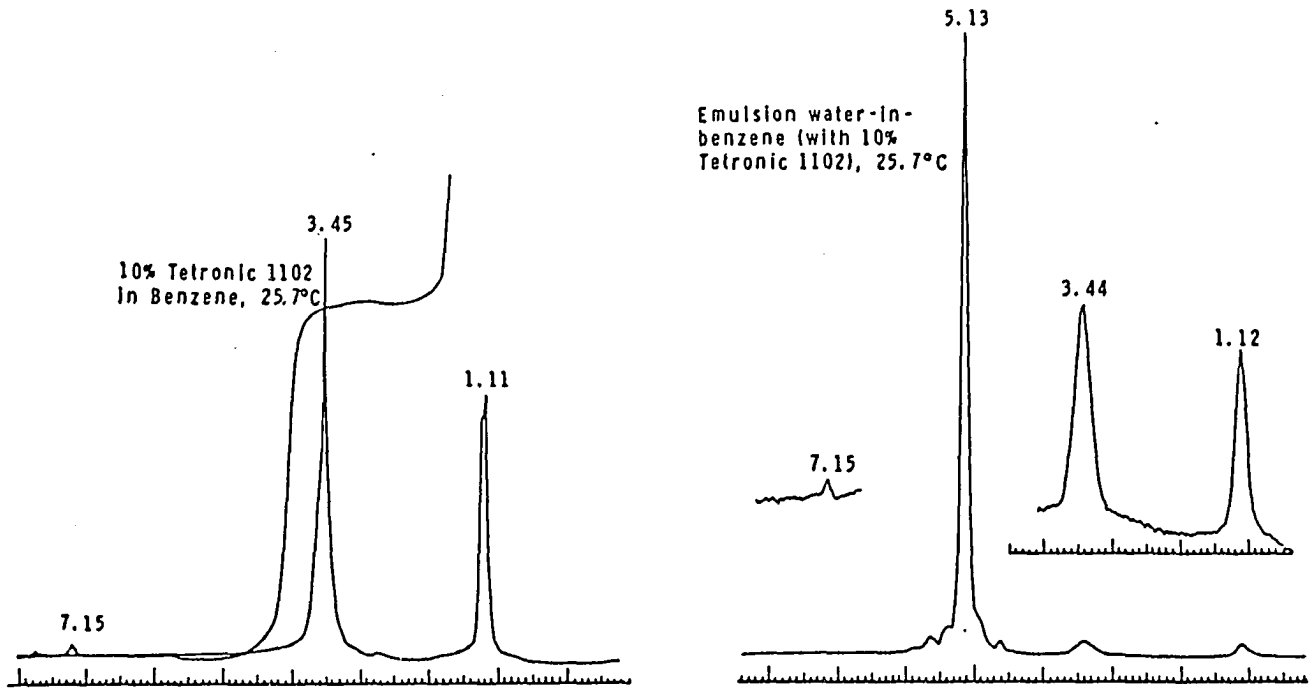

^{1}NMR of surfactant solution and emulsion containing 10% Tetronic 1102 at 25°C prepared using water and d_6 benzene. Internal lock = d_6 benzene at 7.15 ppm.

Figure 4.19

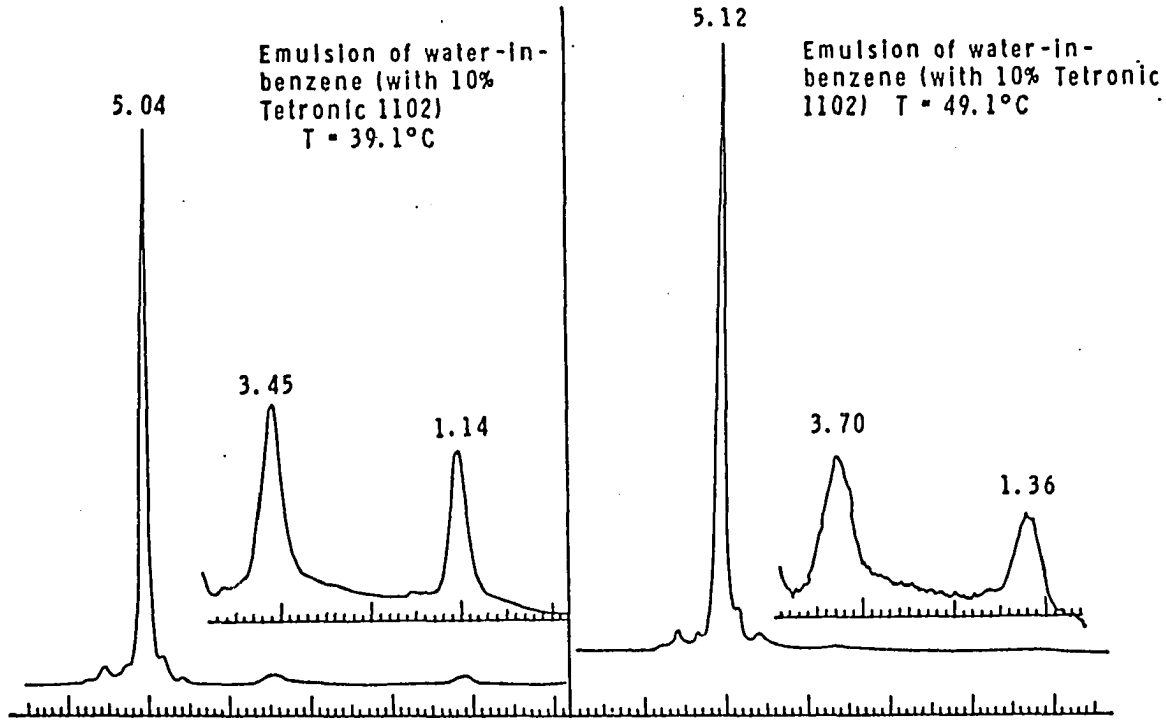

^{1}NMR spectra of emulsions prepared at elevated temperatures.

for true solubility in organic solvent.

Structural considerations as well as molecular weight can affect the solubilization of a block copolymer. Block copolymers in a solvent which is good solvent for one block as well as a nonsolvent for the other block can form phase separated structures (which some authors call "polymolecular" micelles) having a compact core containing the insoluble block, an interfacial region in which the blocks partially mix, and a shell of solvated blocks of the soluble component. The formations of these heterogeneously soluble structures which results in intermolecular phase separation, has been attributed to intermolecular association in the copolymer molecule, as discussed above (4.7-4.9). Surfactant molecules having a swollen block may self-associate in a closed process and in turn may be solubilized by the heterogeneously soluble aggregate. This process would result in entrapment of solvent in the interior of the micelle and result in formation of the seemingly void interior cells seen in electron micrographs of the surfactant solution. Hence the multicelled droplets are caused by the incomplete solution of the block copolymeric surfactant molecules in water or organic solvent, which causes coagulation of the insoluble block and micellization by means of intermolecular association between the surfactant molecules.

Since the formation of these multicelled droplets in solution, then, is due to the preferential solution of one of the blocks, the persistence of this structure on addition of a solvent selective for the other block (i.e., on emulsification) must be

explained. Gervais and Gallot have shown, in a series of papers (4.18), that a solvent selective for the crystallizable block of a block copolymer having one crystallizable block (poly(ethylene oxide)) and one amorphous block (polystyrene or polybutadiene) cannot dissolve more than 10% of the crystallizable block; increasing the solvent content causes the crystallizable block to crystallize with a lower thickness than it had originally.

In the multicelled emulsion droplets seen with the Tetronic 1102, then, there is no great change in the morphology of the droplets as the volume of interior phase increases because the crystallizable hydrophiles cannot be completely solvated. Diffusion of aqueous phase into the interior of the droplets drives out the organic solvent which was entrapped in the droplets when the surfactant solution was prepared and hence the areas inside the droplets which originally contained entrapped solvent now contain water.

These multicelled emulsion droplets, then, bear a superficial resemblance to oil-in-water-in-oil multiple emulsion droplets which have been extensively studied (4.29-4.34) in terms of morphology as well as incomplete phase segregation; but they are profoundly different in that they also form in a single-phase surfactant solution and they are due to the block copolymeric nature of the surfactant.

There is much evidence for formation of ordered (liquid

crystalline) mesophases in this system in the presence of water. Optical microscopy, interfacial tensiometry, and viscometry suggest a mesophase transition occurring at approximately 50°C. Formation of this phase causes the NMR signal to be much greater at 1/8 height than at 1/2 height and hence the signal can no longer be described by a Lorentzian line shape. This super-Lorentzian line shape is characteristic of nematic liquid crystals (4.25). The absence of birefringence is also characteristic of nematic liquid crystals. Evidence for liquid crystals at room temperature is more subtle: the aqueous solution is not birefringent, the NMR signal is Lorentzian, and the interfacial tension is high, but liquid crystals are clearly seen in electron micrographs. These results indicate that the liquid crystals present at room temperature are too few or perhaps too small and imperfect to be detected by NMR. Since the interfacial tension increases drastically and approaches the maximum of 18 dynes/cm as the temperature is increased above 60°C, evidently the liquid crystalline structure is destroyed above the melting temperature of the poly(ethylene oxide).

D. Conclusions

The multicelled particles formed with the block copolymeric emulsifier Tetronic 1102 are reticulated emulsifier particles. The addition of aqueous acrylamide to o-xylene dispersion of these particles fills the particle cells to form water-in-emulsifier-in-oil particles; in addition, the emulsifier phase may

be swollen with o-xylene or aqueous acrylamide, so phase segregation is less complete in these droplets compared to droplets formed using conventional soaps.

The surfactant undergoes liquid crystalline transitions over the temperature range 25-62°C. All liquid crystalline order is destroyed above the melting temperature of the poly(ethylene oxide) segments.

CHAPTER V

Kinetics and Mechanism of Inverse Emulsion Polymerization

A. Introduction

Elucidating the mechanism of an emulsion polymerization includes calculation of rate constants and initial rate of polymerization per particle and determination of locus of initiation and method of particle growth. In this study, two techniques are used to elucidate the mechanism: measurement of kinetic parameters as a function of polymerization recipe variables; and measurement of the amount of oil-soluble initiator which partitions into each phase in the system.

The polymerization recipe variables included in this study are: initiator type (oil-soluble 2,2'-azobis (2,4-dimethylvaleronitrile)-(ADVN) or water-soluble potassium persulfate (KPS); initiator level (0.01-0.10 mole % on moles monomer), emulsifier concentration (3-12% Tetronic 1102 on continuous phase volume); polymerization temperature (50-65°C). Conversion-time curves are measured dilatometrically. Details of sample preparation and dilatometric apparatus are given in Chapter II.

The amount of oil-soluble initiator which partitions into each phase is measured in the presence as well as in the absence of emulsifier. Experimental details are given in Chapter II.

B. Experimental Results

1. Kinetic Study

Data are analyzed by multivariate regression analysis. The regression models are used to generate curves relating the responses to the parameters. Results are discussed below.

a. Rate of polymerization

Regression analysis shows that the factors most strongly affecting rate of polymerization as main effects are the initiator concentration, the emulsifier concentration, and the polymerization temperature. Several pairs of factors also interact to significantly affect polymerization rate: these are initiator concentration-emulsifier concentration; initiator concentration-temperature; and emulsifier concentration-temperature. Multivariate regression analysis using these factors and pairs of factors gives a regression model (equation) having a correlation coefficient of 0.92 at the 98% confidence level. Polymerizations forming much coagulum are excluded from the analysis because the magnetic stirrer bar may have been trapped during polymerization and hence the rate may be nonreproducible.

Graphical analysis of the results of the regression analysis is shown in Figures 5.1-5.4. Rate does not show the expected power-law dependence on emulsifier concentration or initiator concentration: rather, there is a maximum or minimum in these dependences. The significance of this is unclear, since emulsion polymerization kinetics are best studied on the basis of rate per

Figure 5.1

Polymerization Rate as a Function of Initiator Concentration

ADVN Initiator

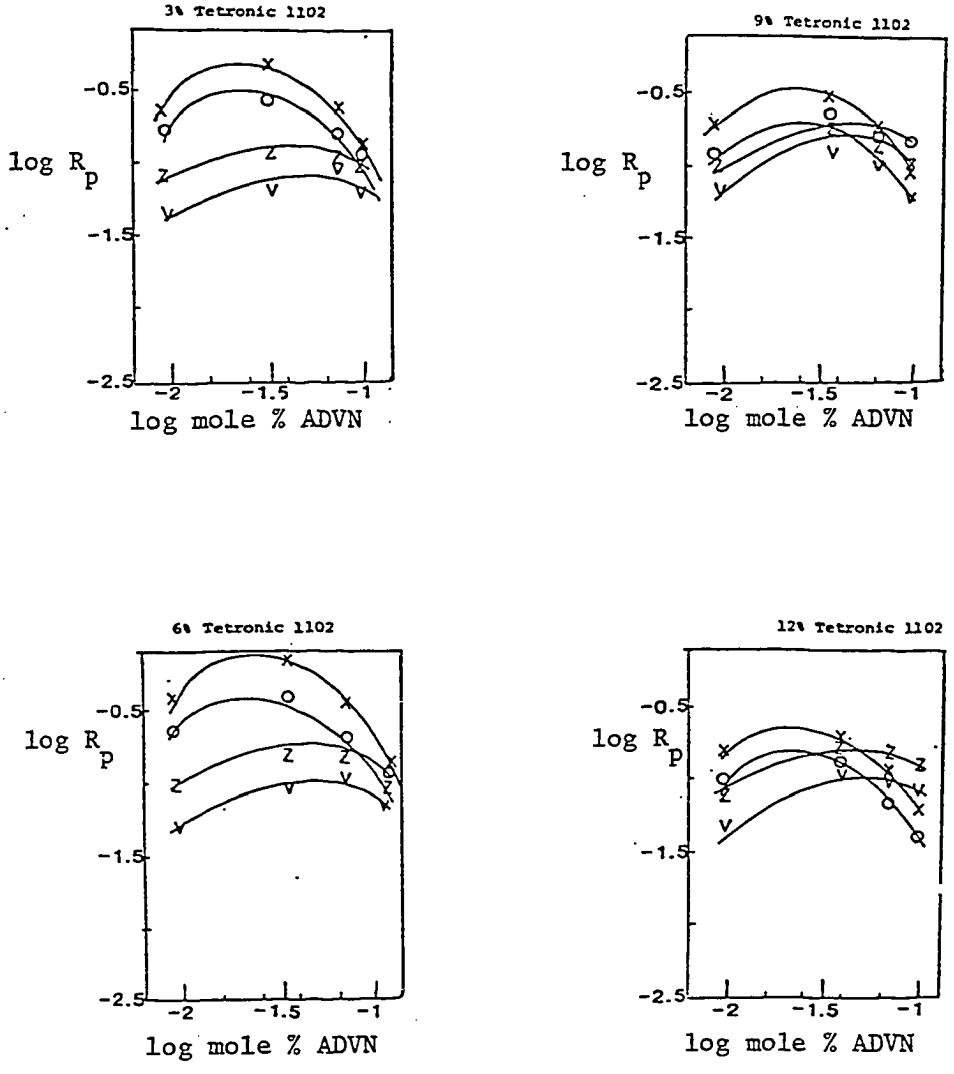

Figure 5.2

Polymerization Rate as a Function of Initiator Concentration

KPS Initiator

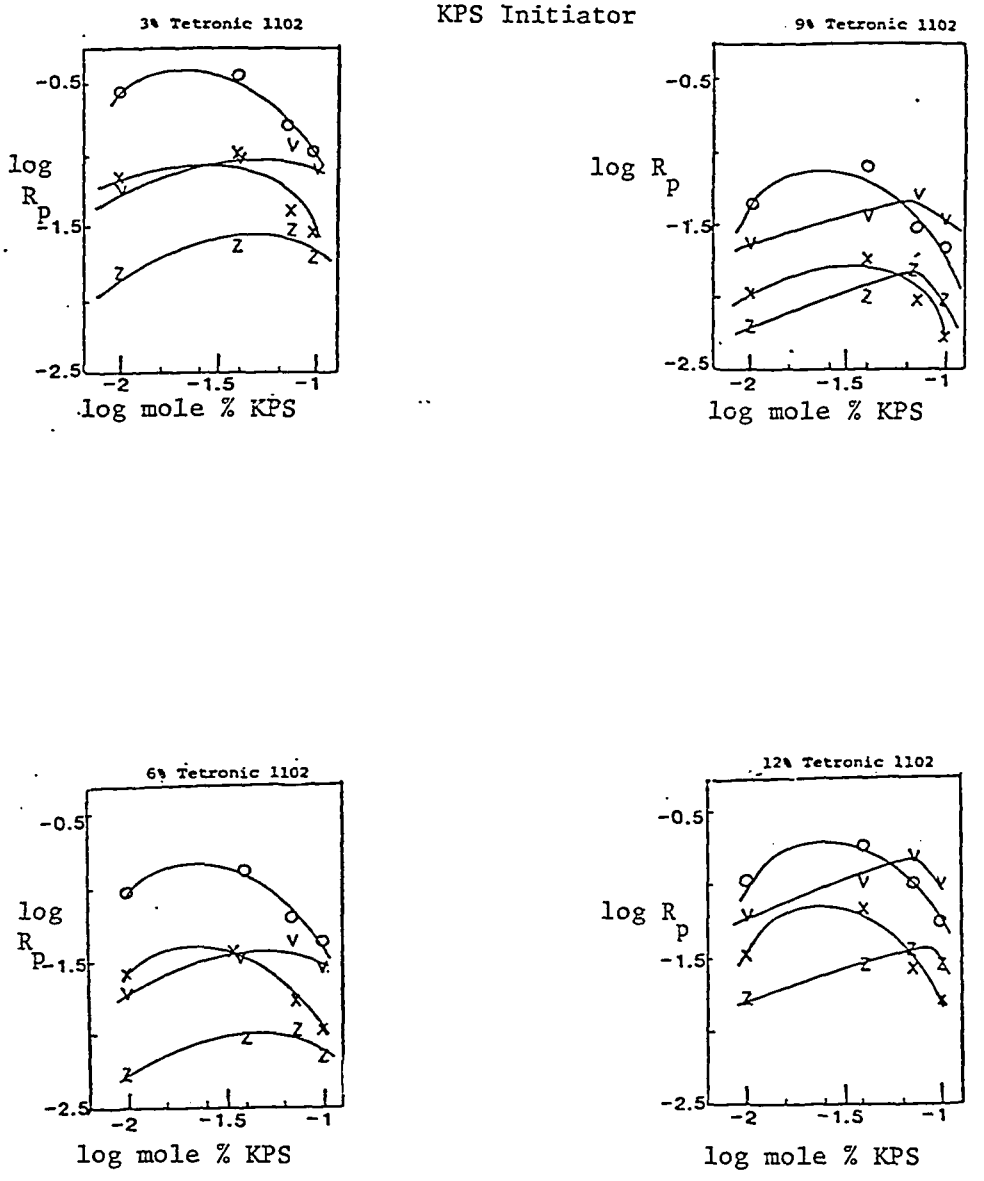

Figure 5.3

Polymerization Rate as a Function of Emulsifier Concentration

ADVN Initiator

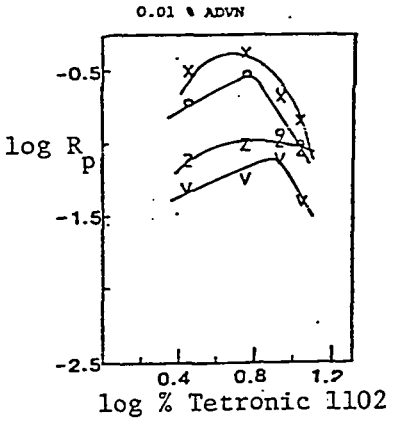

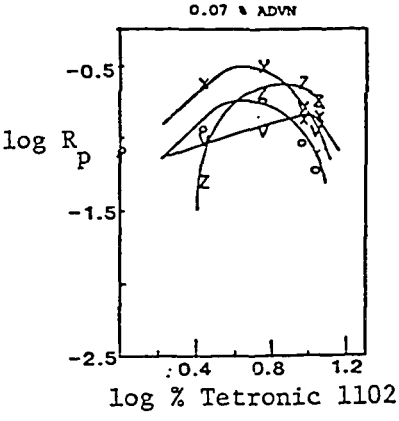

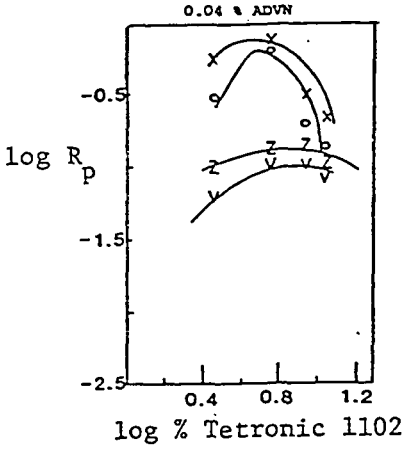

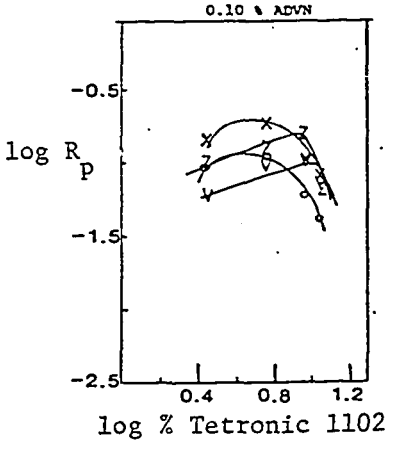

V 50 C

o 55 C

X 60 C

Z 65 C

Figure 5.4

Polymerization Rate as a Function of Emulsifier Concentration

KPS Initiator

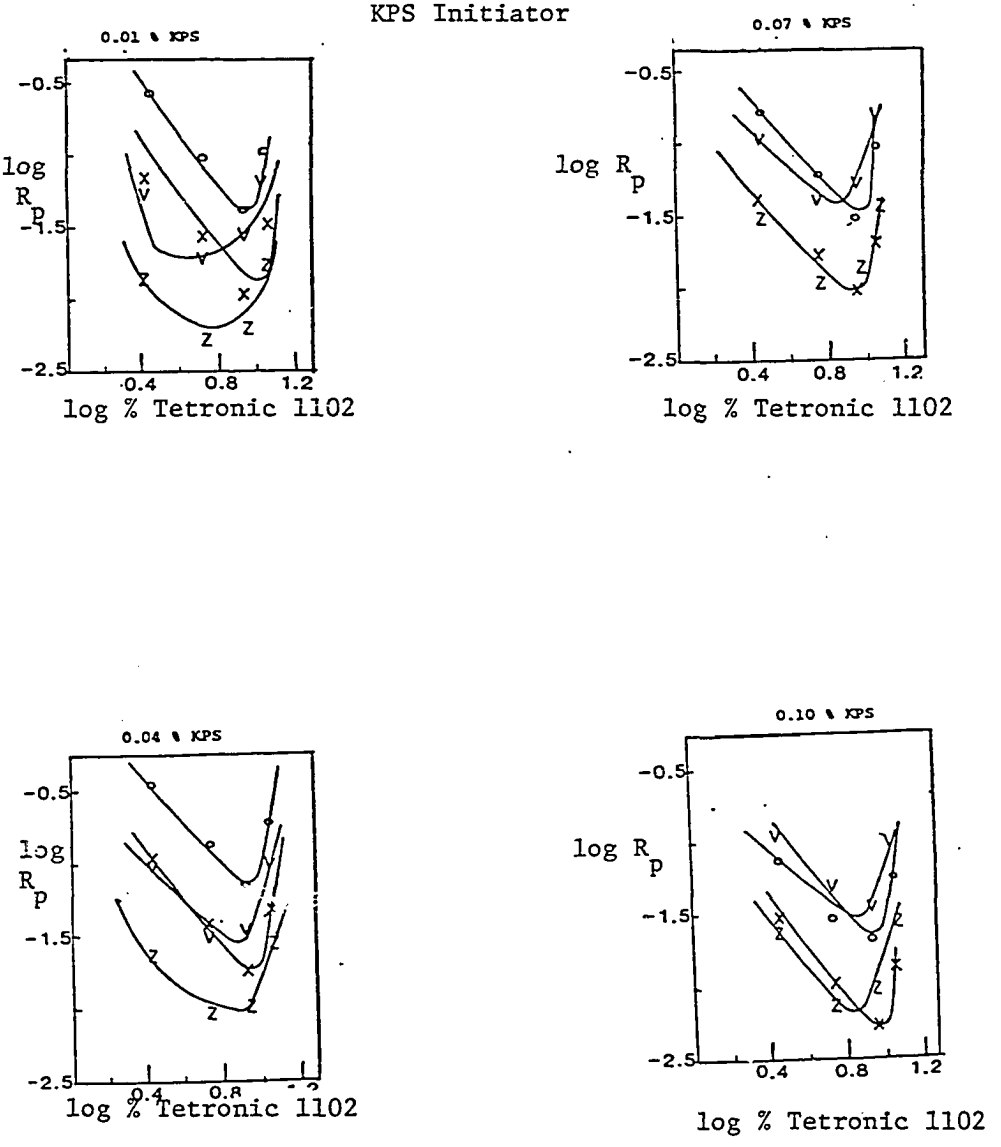

particle and these results may be confounded by particle size effects.

The activation energy of polymerization can be determined from the regression model by considering only the terms containing an expression for temperature in order to generate an Arrhenius plot (Fig. 5.5). This plot shows a dramatic change in slope at polymerization temperature of 65°C, indicating that the reaction mechanism depends on whether the polymerizations temperature is above or below the melting temperature of the poly(ethylene oxide) segments of the surfactant molecule (i.e., 62°C). Since the activation energy is a thermodynamic characteristic of the polymerization system, changes in activation energy are probably really due to changes in energies of association between components of the system. This is analogous to a change in the observed enthalpy of a solution polymerization reaction when the solvent is changed which results from changed energy of association in the monomer (5.17).

b. Multicelled latex particles

Under some conditions, multicelled monomer emulsion droplets do not survive polymerization to form multicelled latex particles. To elucidate the reason for this change in morphology, multivariate regression analysis was done using presence or absence of multicelled latex particles as response. A regression model having a correlation coefficient of 0.99 at the 99% confidence level was generated. The main effects influencing the latex morphology are

Figure 5.5

Arhennius Plot

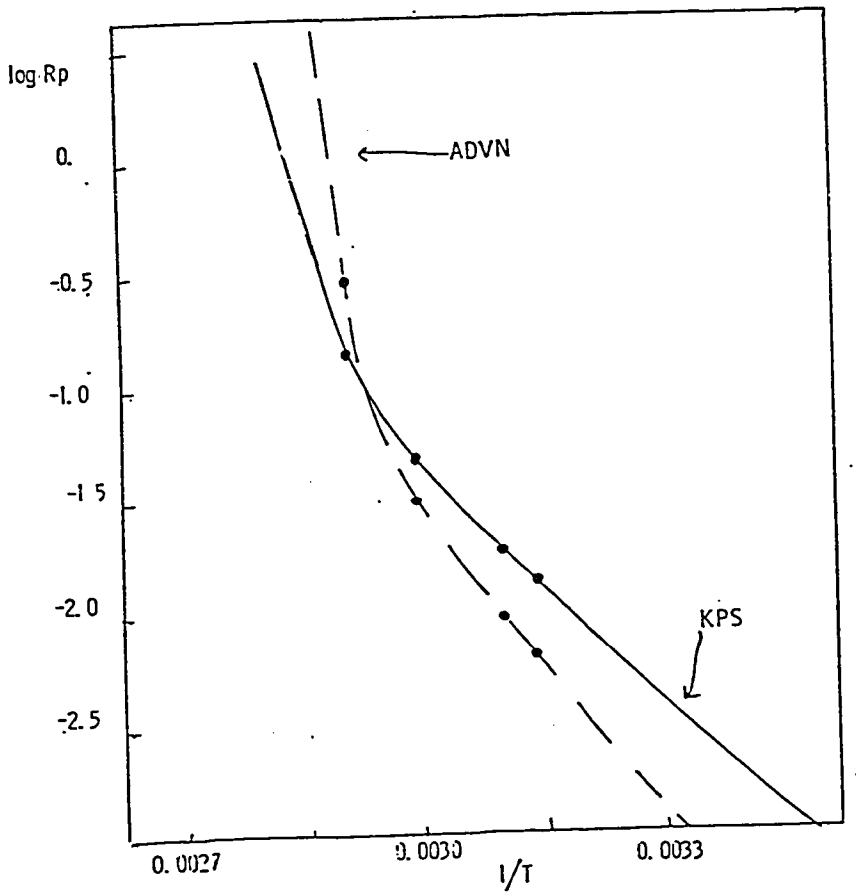

polymerization temperature and initiator concentration. Multicelled latex particles are generally not formed when the polymerization temperature is 65°C, indicating that the surfactant structure affects latex morphology. However, the surfactant being below the melting temperature of the poly(ethylene oxide) segments of the surfactant molecule is necessary but not sufficient for the formation of multicelled latex particles. Regardless of initiator type, multicelled latex particles are generally not found when the initiator concentration is 0.01% and the polymerization temperature is 50°C, and when the initiator concentration is 0.04% or 0.07% and the polymerization temperature is 60°C. The reason for this dependence of morphology on the combination of initiator concentration and polymerization temperature is unclear. It may indicate that latex morphology may be affected by internal viscosity (i.e., molecular weight as affected by initiator concentration), or perhaps a slower initiation rate leads to growth of single interior cells to mature particles. Figures 5.6-5.9 show points for the presence (Y) or absence (N) of multicelled latex particles placed on the curves for rate of polymerization as a function of initiator or emulsifier concentration. Generally polymerization rate is highest when the latex particles are multicellular: this indicates that either the subdivision factor for emulsion polymerization or the rate constants are affected by latex morphology.

c. Polymer Molecular Weight

Regression analysis shows that molecular weight is relatively

Figure 5.6

Correlation Between Polymerization Rate and the Presence (Y) or absence (N) of Multicelled Latex Particles

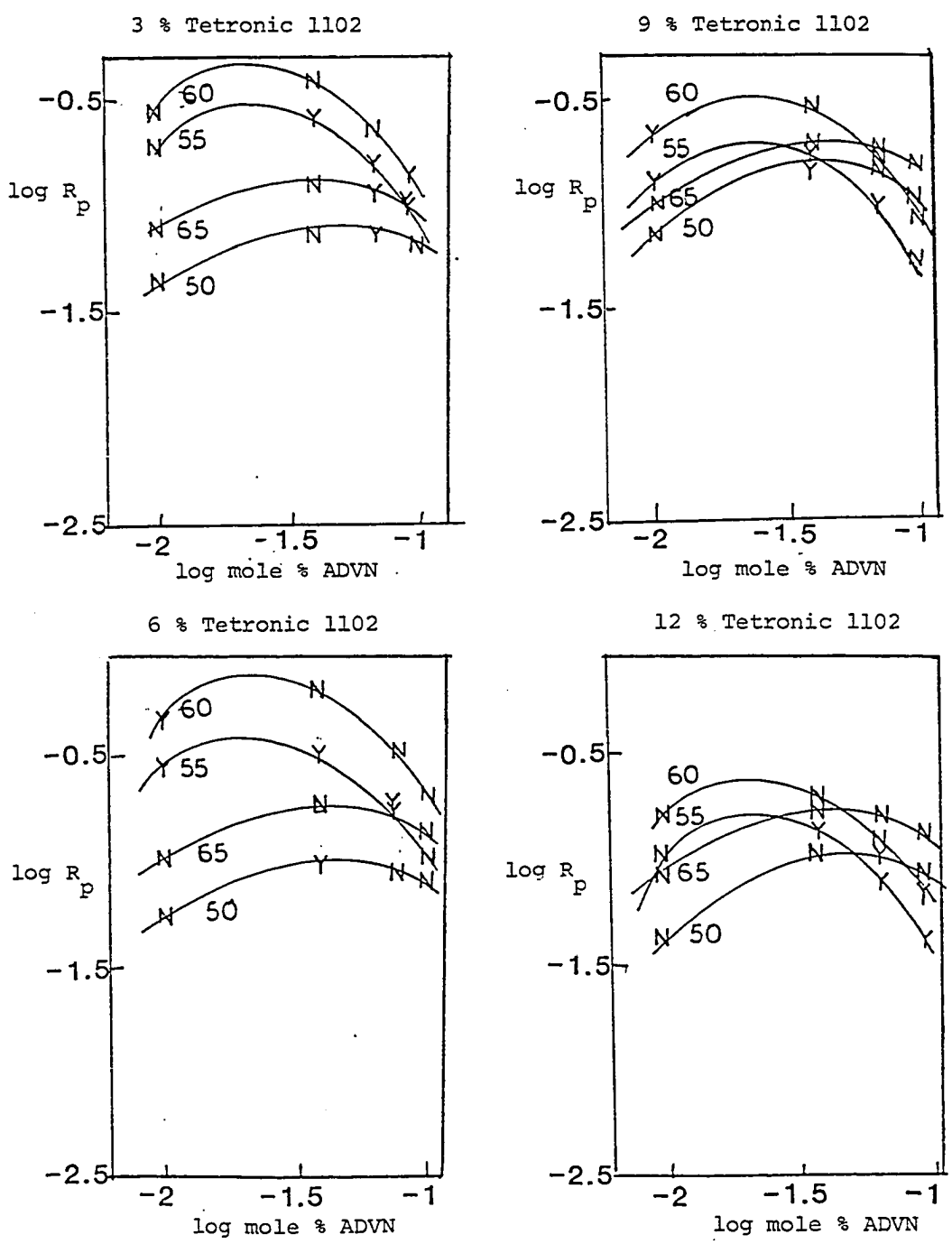

Figure 5.7

Correlation Between Polymerization Rate and the Presence (Y) or Absence (N) of Multicelled Latex Particles

KPS Initiator

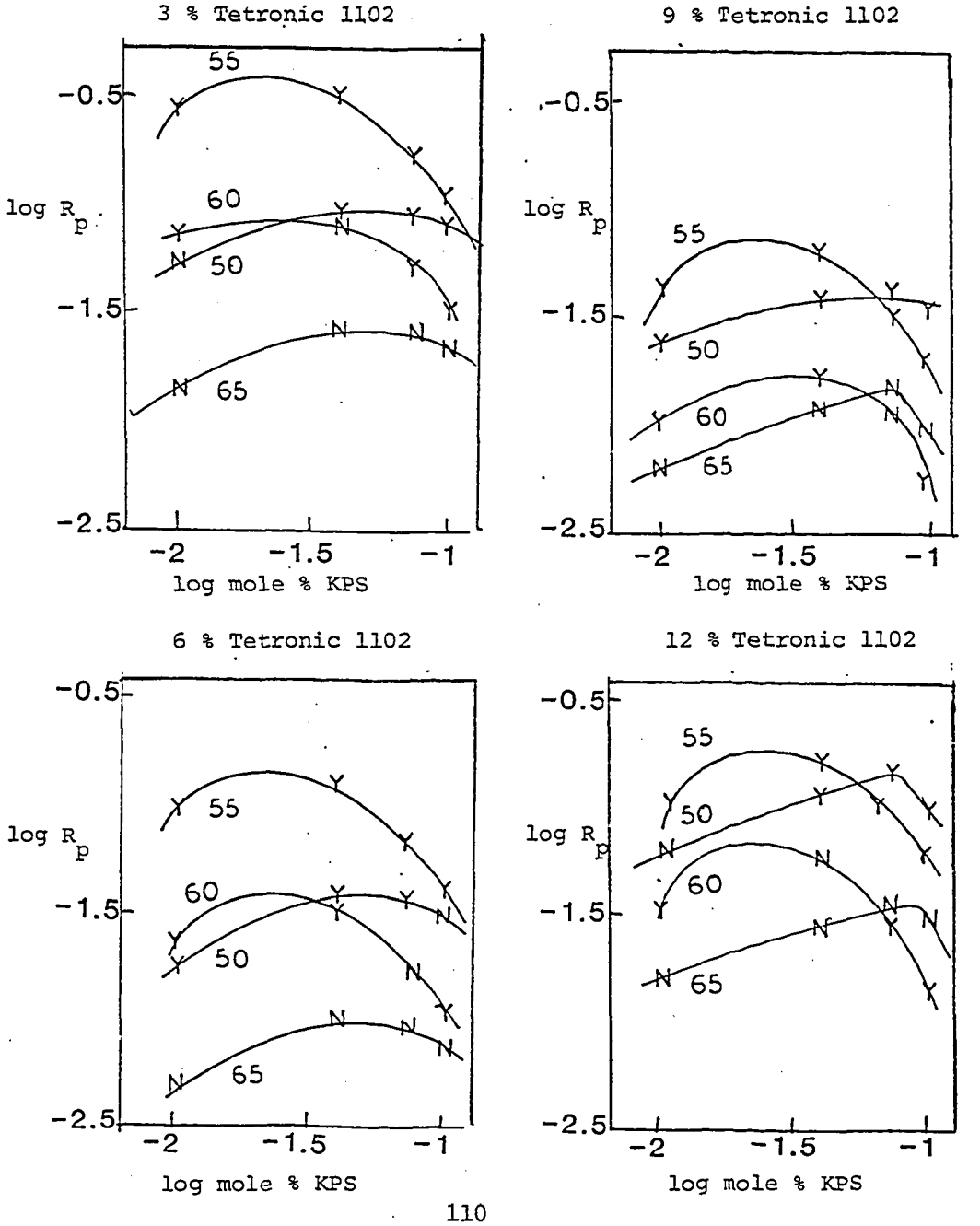

Figure 5.8

Correlation Between Polymerization Rate and the Presence (Y) or Absence (N) of Multicelled Latex Particles

ADVN Initiator

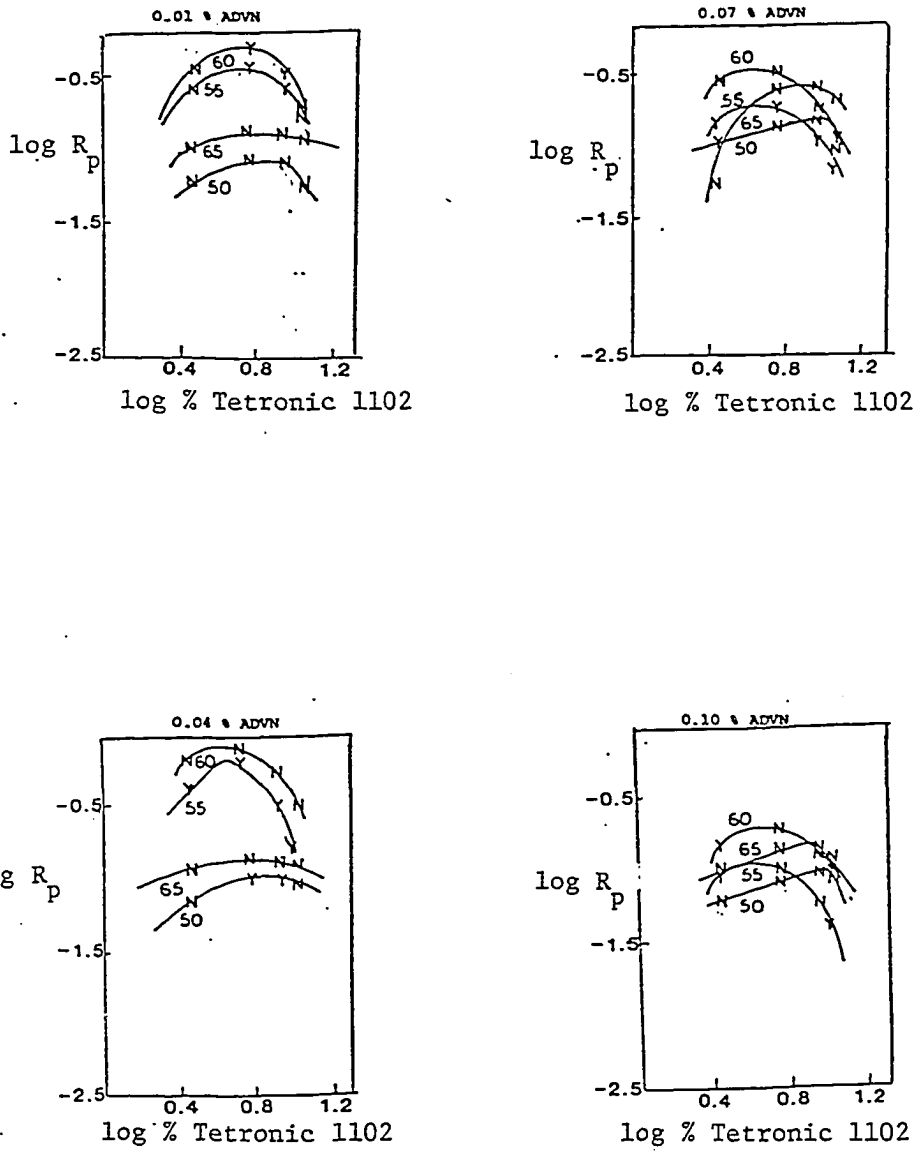

Figure 5.9

Correlation Between Polymerization Rate and the Presence (Y) or Absence (N) of Multicelled Latex Particles

KPS Initiator

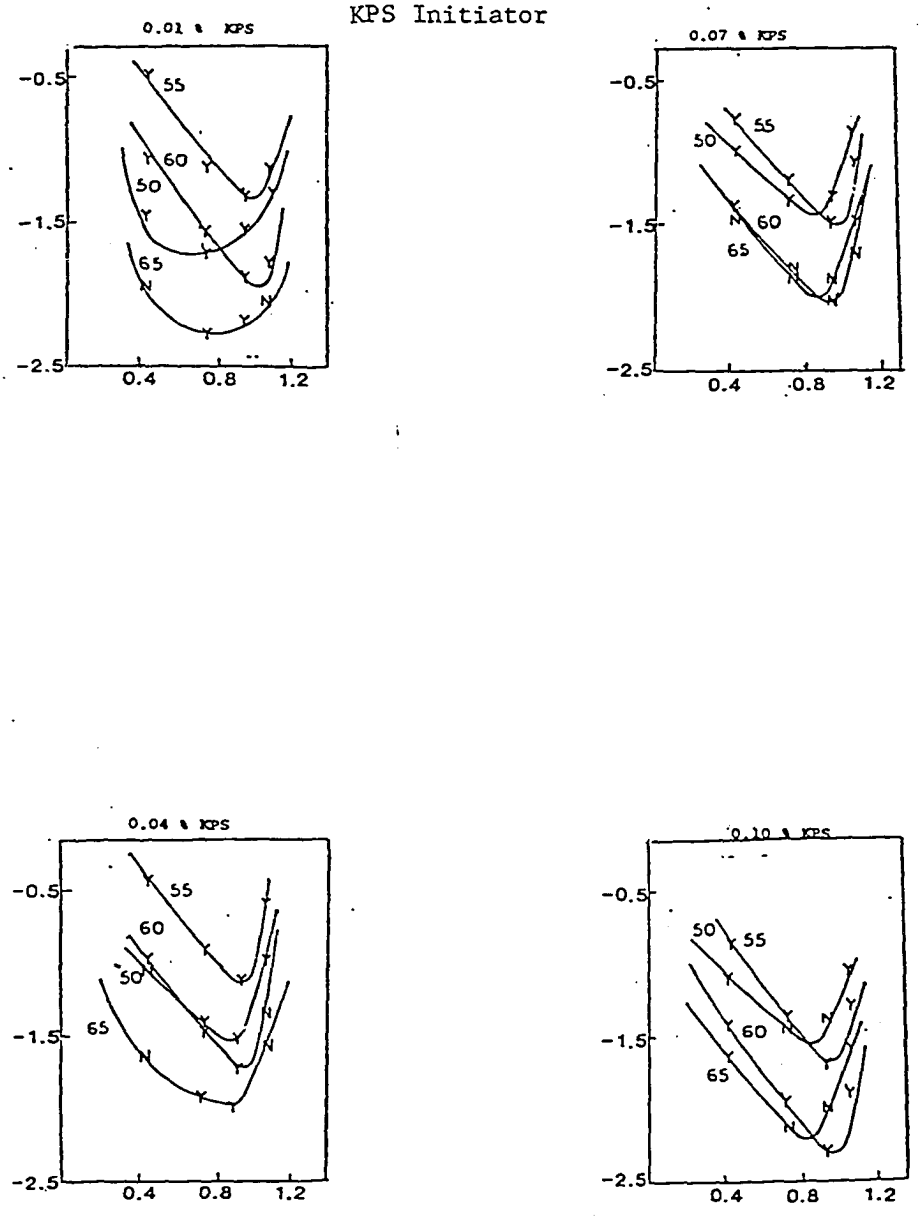

insensitive to initiator concentration. Molecular weight is insensitive to emulsifier concentration if polymerization is initiated by azo initiator but it is very sensitive to emulsifier concentration in persulfate-initiated polymerizations. In addition to this emulsifier concentration-initiator type effect, other factors affecting molecular weight are interactions between initiator concentration and emulsifier concentration and between temperature and initiator concentration. Multivariate regression analysis using the logarithms of the molecular weight yields a correlation coefficient of 0.96 at the 92% confidence level.

The physical meaning of these statistically significant interactions is not immediately obvious; so, in order to interpret the physical meaning of the regression model, molecular weight is plotted as a function of initiator and emulsifier concentration for both ADVN and KPS initiated polymerization (Figs.5.10-5.13). In polymers initiated with ADVN, molecular weight decreases as initiator concentration increases only at the highest initiator concentration used (0.1%) and then only if the polymerization temperature is 50°C. Average molecular weight at any initiator concentration generally decreases as polymerization temperature increases from 50 to 60°C; at 65°C, polymer molecular weight is higher than at 60°C. The failure of polymers prepared at 65°C to follow trends seen in the temperature range 50-60°C is further evidence of the critical importance of the surfactant mesophase structure to the polymerization reaction. Emulsifier concentration

Figure 5.10 - Molecular Weight as a Function of Initiator Concentration.

ADVN Initiator

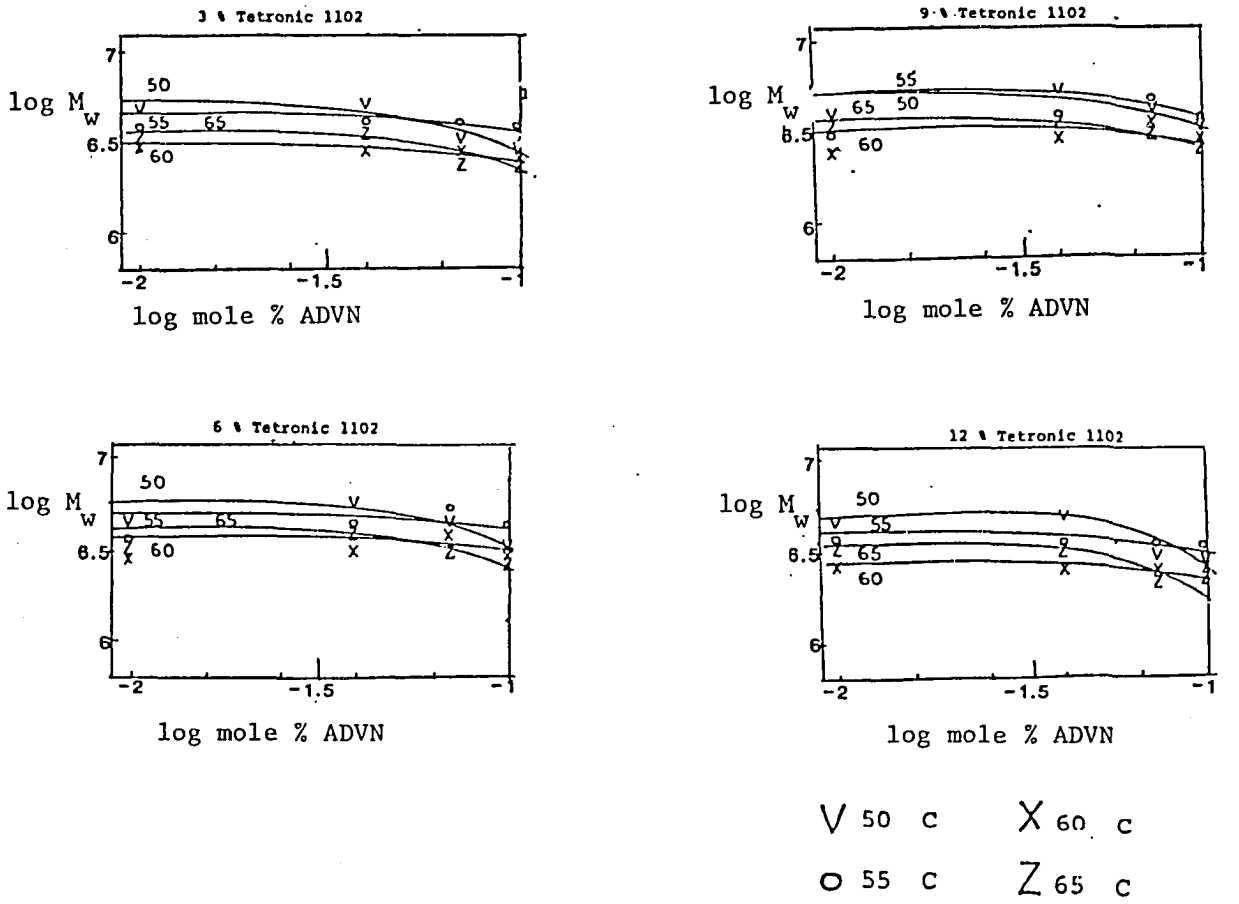

V 50 C X 60 C

O 55 C Z 65 C

Figure 5.11

Molecular Weight as a Function of Initiator Concentration

KPS Initiator

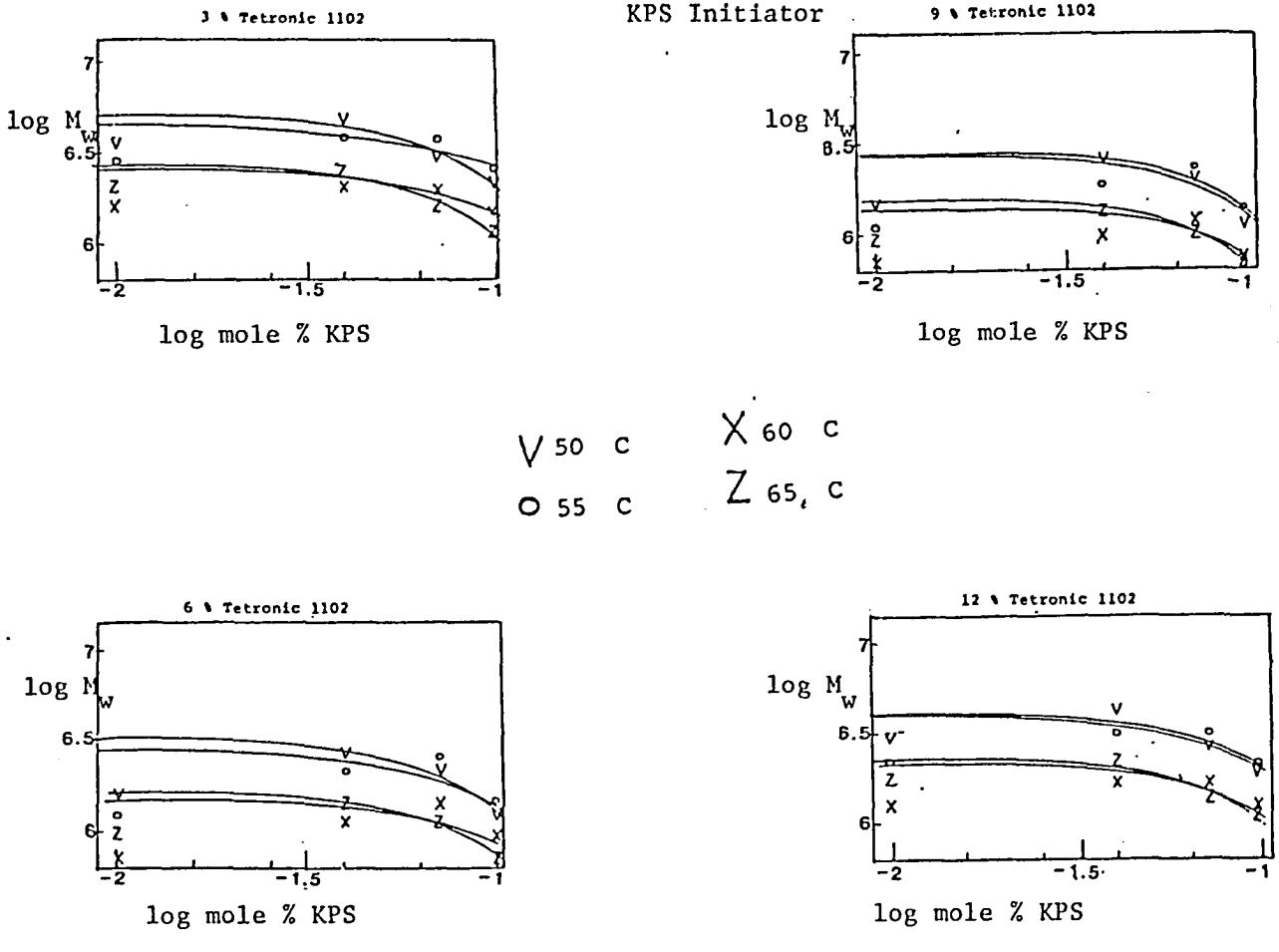

Figure 5.12 - Molecular Weight as a Function of Emulsifier Concentration.

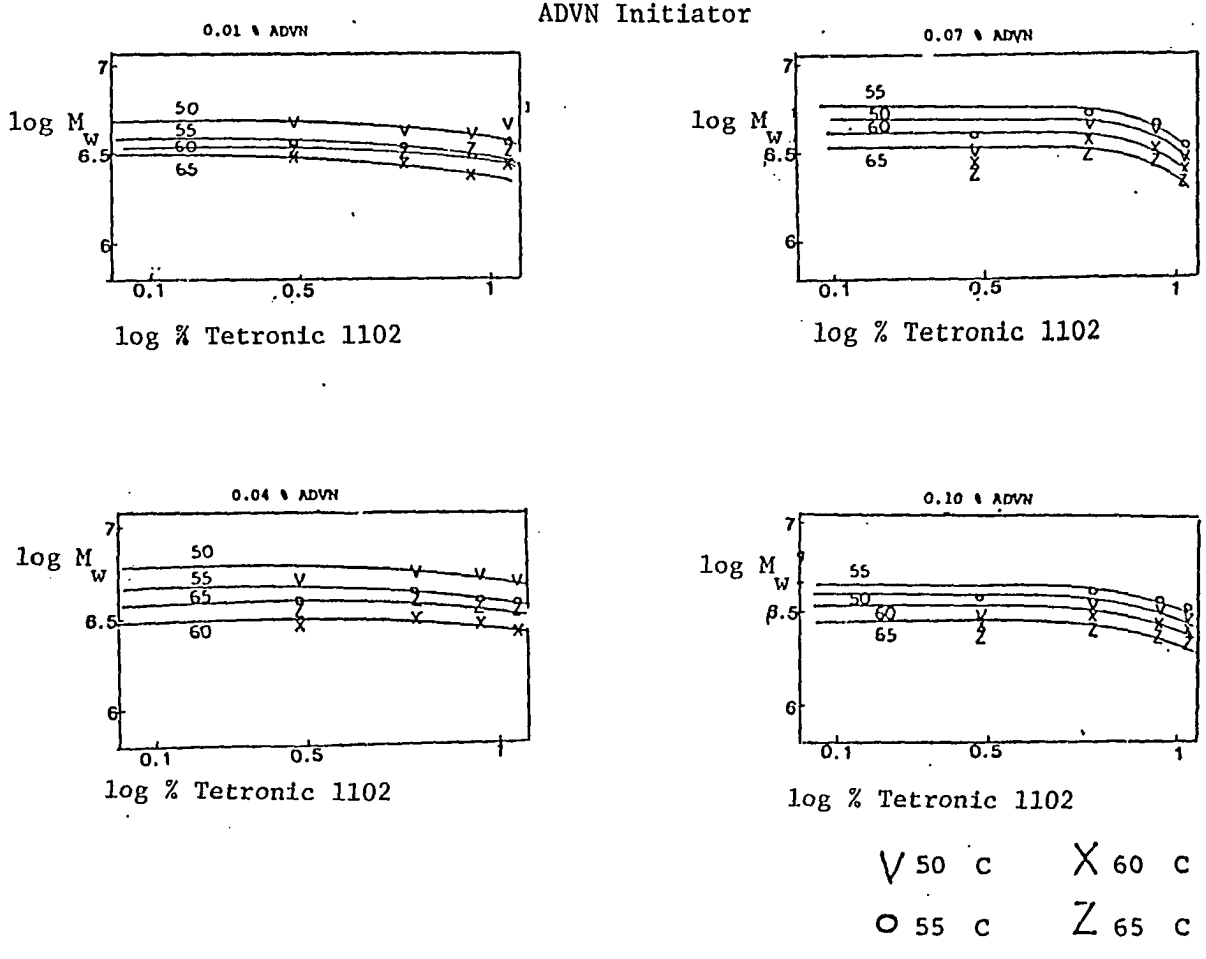

Figure 5.13 - Molecular Weight as a Function of Emulsifier Concentration

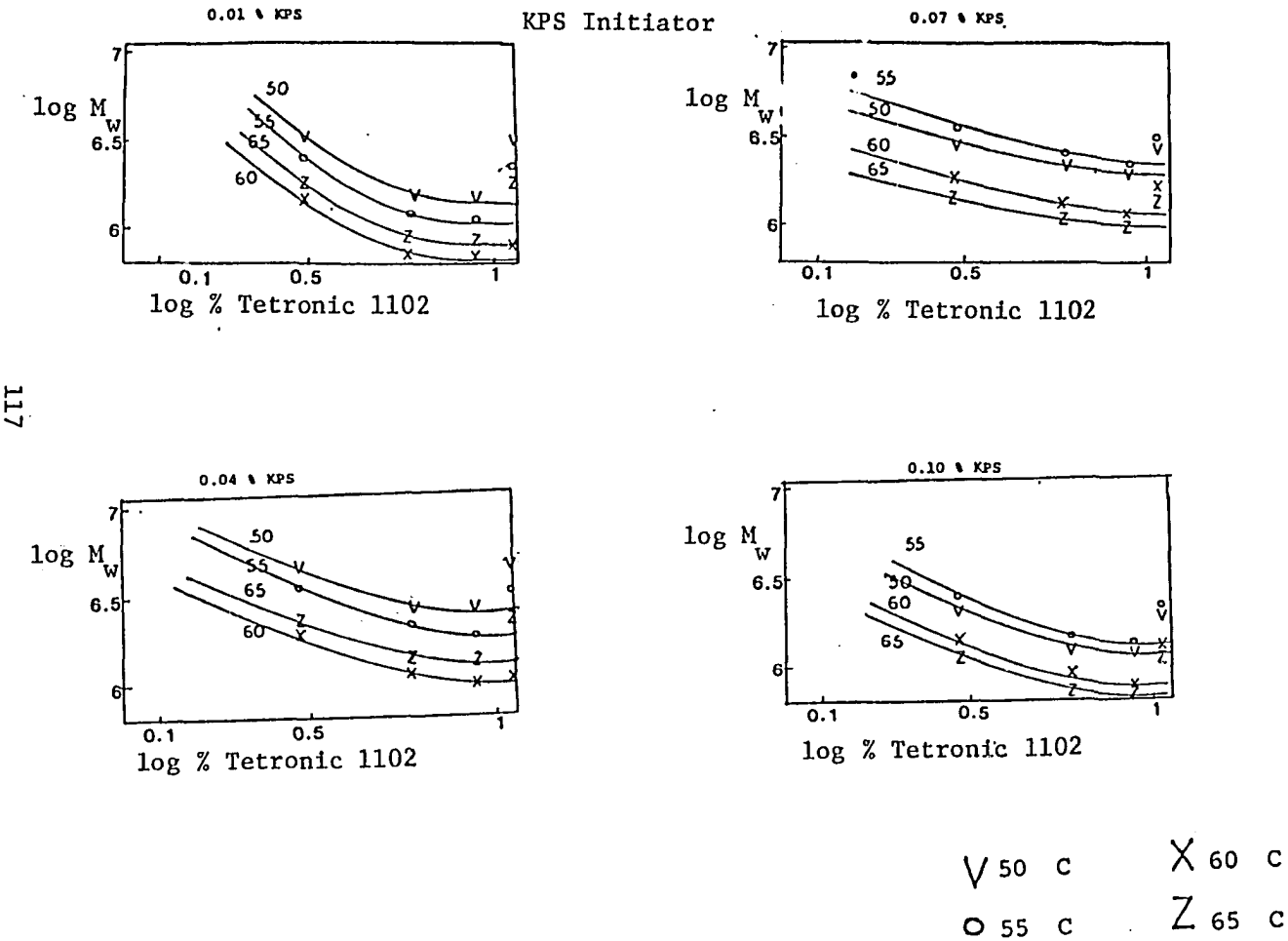

has essentially no effect on molecular weight of azo-initiated polymers, indicating that the emulsifier does not act as a chain transfer agent in these systems. This confirms the earlier work of DiStefano, which showed that Tetronic 1102 did not cause chain transfer (5.1). Polymers prepared with KPS initiator are somewhat more sensitive to initiator concentration than those prepared with azo initiator: polymer molecular weight decreases at the two highest initiator concentrations regardless of polymerization temperatures and emulsifier concentration. The effect of polymerization temperature on molecular weight is the same for persulfate-initiated polymerization and azo-initiated polymerizations: molecular weight decreases as polymerization temperature increases from 50°C to 60°C. Emulsifier concentration strongly affects molecular weight of polymers prepared with KPS initiator: molecular weight decreases sharply to a limiting value as emulsifier concentration increases. This difference in the effect of emulsifier on molecular weight in KPS-initiated polymers compared to ADVN-initiated polymers is probably related to the difference in mode of radical generation and will be discussed later.

d. Average latex particle diameter

Measuring particle volume is critical in calculating kinetic parameters for emulsion polymerization because these parameters should be calculated per particle. In the case of multicelled latex particles, measuring particle volume is not straightforward, since it is not immediately obvious if the appropriate particle

diameter is the overall diameter or the diameter of the interior cells. However, as a first attempt, overall diameter of the particles is measured: this would seem to be a more generally useful parameter since not all particles are multicelled. Regression analysis shows that latexes prepared with KPS initiator have generally larger average diameters than those prepared with ADVN. Other significant correlations exist between the average particle diameter and the initiator concentration, and between the average particle diameter and interactions of the initiator concentrations with temperature, and emulsifier concentration with temperature. Surprisingly, the emulsifier concentration does not affect particle size except as an interaction effect; this demonstrates that the process of colloidal particle formation is much different with the heterogeneously soluble Tetronic 1102 molecule than with conventional emulsifiers.

The regression model generated from these factors and interactions has correlation coefficient 0.99 at the 99% confidence level. Average particle diameters calculated using this regression model will be used in the calculation of rate per particle necessary for determination of kinetic parameters. Knowing average particle diameter, the rate per particle can easily be calculated in latexes where multicelled particles are not formed. In these cases, polymerization rate per particle shows the expected power law dependence on initiator concentration at low initiator concentration and emulsifier concentration, although there is some

scatter in the data (Figs. 5.14-5.17). At higher initiator concentration, polymerization rate decreases, indicating that initiator radicals may recombine rather than react with monomer. This may indicate that radicals are not formed on the continuous phase and diffuse into particles as in the traditional Harkins-Smith-Ewart model of emulsion polymerization, but rather radicals are formed in a more restricted volume and hence are more likely to recombine. The linear relationship between polymerization rate per particle and the concentration of initiator or emulsifier is, therefore, derived using only the lower concentrations of initiator or emulsifier.

e. Latex polydispersity

Latex particle size polydispersity is modeled by regression analysis in order to gain insight into the mechanism of particle growth. The most important factors are interaction effects between emulsifier concentration and initiator concentration and between emulsifier concentration and initiator type. Particle size distribution is broader with persulfate initiator and at higher concentrations of initiator and emulsifier. Multivariate regression gives a correlation coefficient of 0.96 at the 99% confidence level.

f. Skewness of the latex particle size distribution

The skewness of the latex particle size distribution in Interval II has been shown to give insight into the mechanism of particle growth. Positive skewness was related to growth by

Figure 5.14

Rate per Particle as a Function of Initiator Concentration
Latexes without Multicelled Particles

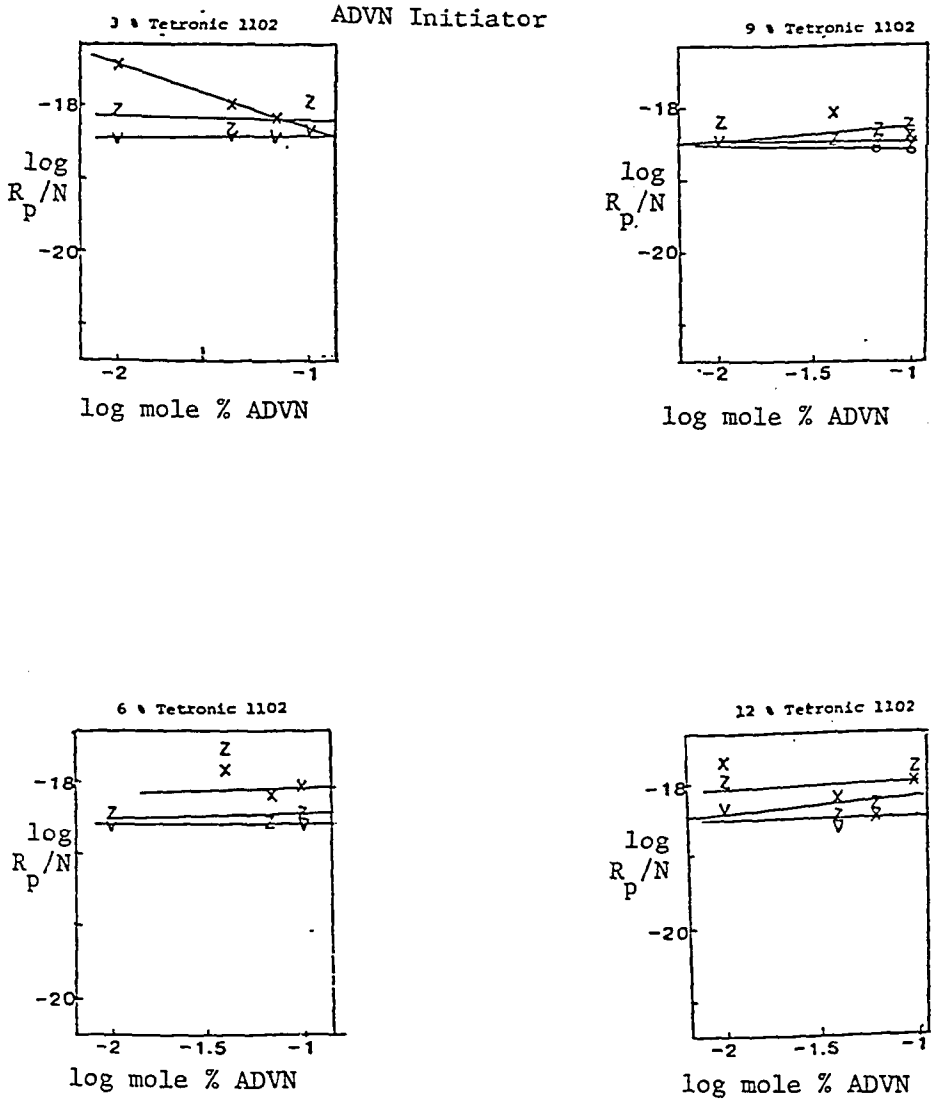

V 50 C
O 55 C
X 60 C
Z 65 C

Figure 5.15

Rate per Particle as a Function of Initiator Concentration

Latexes without Multicelled Particles

KPS Initiator

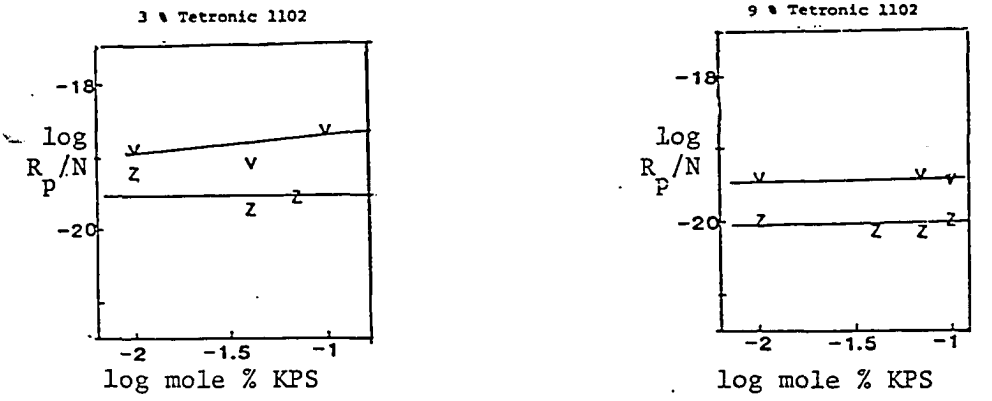

Figure 5.16

Rate per Particle as a Function of Emulsifier Concentration

Latexes without Multicelled Particles

ADVN Initiator

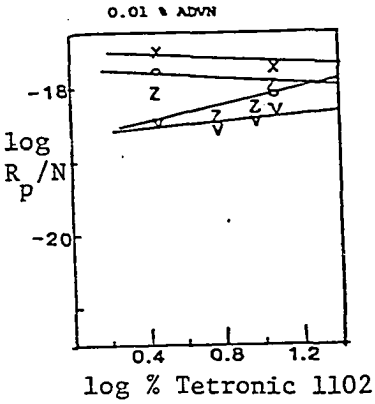

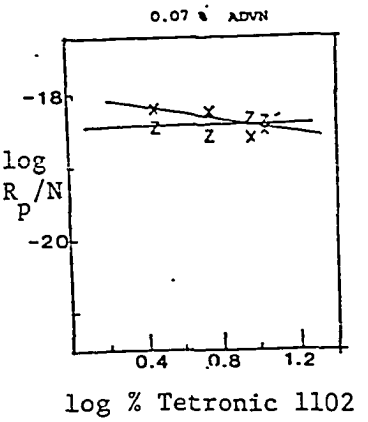

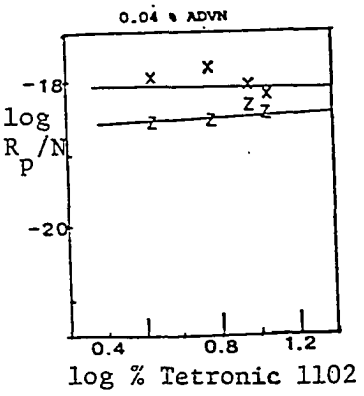

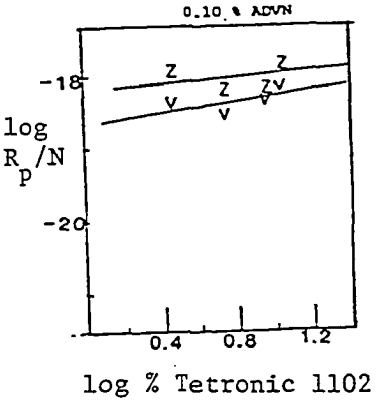

V 50 C

O 55 C

X 60 C

Z 65 C

Figure 5.17

Rate per Particle as a Function of Emulsifier Concentration
Latexes without Multicelled Particles

KPS Initiator

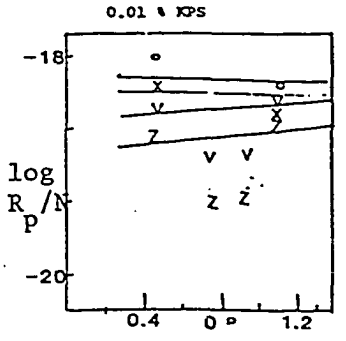

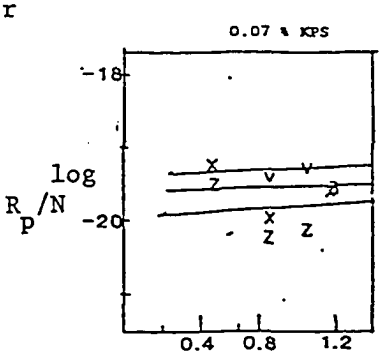

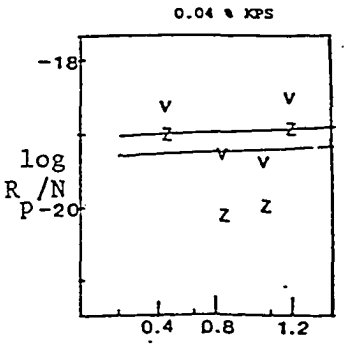

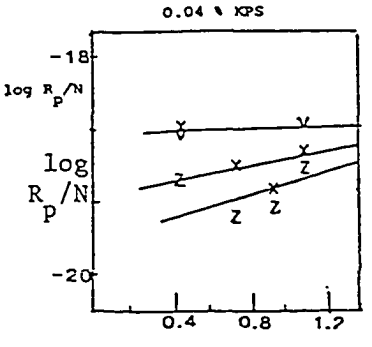

V 50 C

O 55 C

X 60 C

Z 65 C

coagulation and negative skewness to growth by nucleation (5.2). This interpretation cannot be applied directly to the data in this series because particle size distribution was measured at the end of the polymerization instead of during Interval II, and new particle generation is possible after completion of Interval II. Hence negative skewness in the present study may mean either growth by nucleation, or particle nucleation occurring in Interval III.

Skewness is defined as the third moment about the mean of a distribution. In this study the coefficient of skewness, γ_1, is used instead of the third moment about the mean m_3 as a way to quantify skewness in order to eliminate dependence on the scale on which data are recorded

$$\gamma_1 = m_3/(m_2)^{3/2}$$

The skewness coefficient is always positive, indicating particle growth by coagulation.

Multivariate regression analysis shows that the most significant factors affecting the magnitude of the skewness coefficient are interactions between emulsifier concentration and temperature, between initiator concentration and temperature, and between initiator concentration and emulsifier concentration. The skewness coefficient, while always positive, decreases in magnitude as the emulsifier concentration increases, especially if the latex is prepared with azo initiator. Regression analysis

gives correlation coefficient of 0.94 at the 98% confidence level.

Skewness coefficient as a function of emulsifier concentration is shown in Figures 5.18 and 5.19. Skewness coefficient is not a linear concentration of emulsifier level but rather shows a maximum or minimum. The significance of this is not immediately obvious; however, it has been shown earlier that the monomer emulsion is also very polydisperse in this system due to the heterogeneous solubility of the surfactant molecules. Hence analysis of the ratio of the skewness of the particle size distribution of the latex compared to the monomer emulsion may be a more appropriate way to analyze the polydispersity.

The monomer emulsion skewness is always positive and goes through a maximum at 9% Tetronic 1102 (Fig. 5.20): this may correspond to an optimum in droplet stability due to an optimum aggregation number for surfactant molecules at the particular mechanical shear rate used to prepares the monomer emulsion.

Dividing the latex skewness coefficient by the monomer emulsion skewness coefficient gives a function having a power law dependence on emulsifier concentration for persulfate-initiated polymerizations but shows a maximum or minimum for azo-initiated polymerizations (Fig. 5.21, 5.22). This power law dependence in persulfate-initiated polymerizations is good evidence of polymerization in monomer droplets, since it indicates no change in polydispersity and hence no net transport of material between particles during polymerization. The nonlinearity of this rela-

Figure 5.18

Latex Skewness Coefficient as a Function
of Emulsifier Concentration

ADVN Initiator

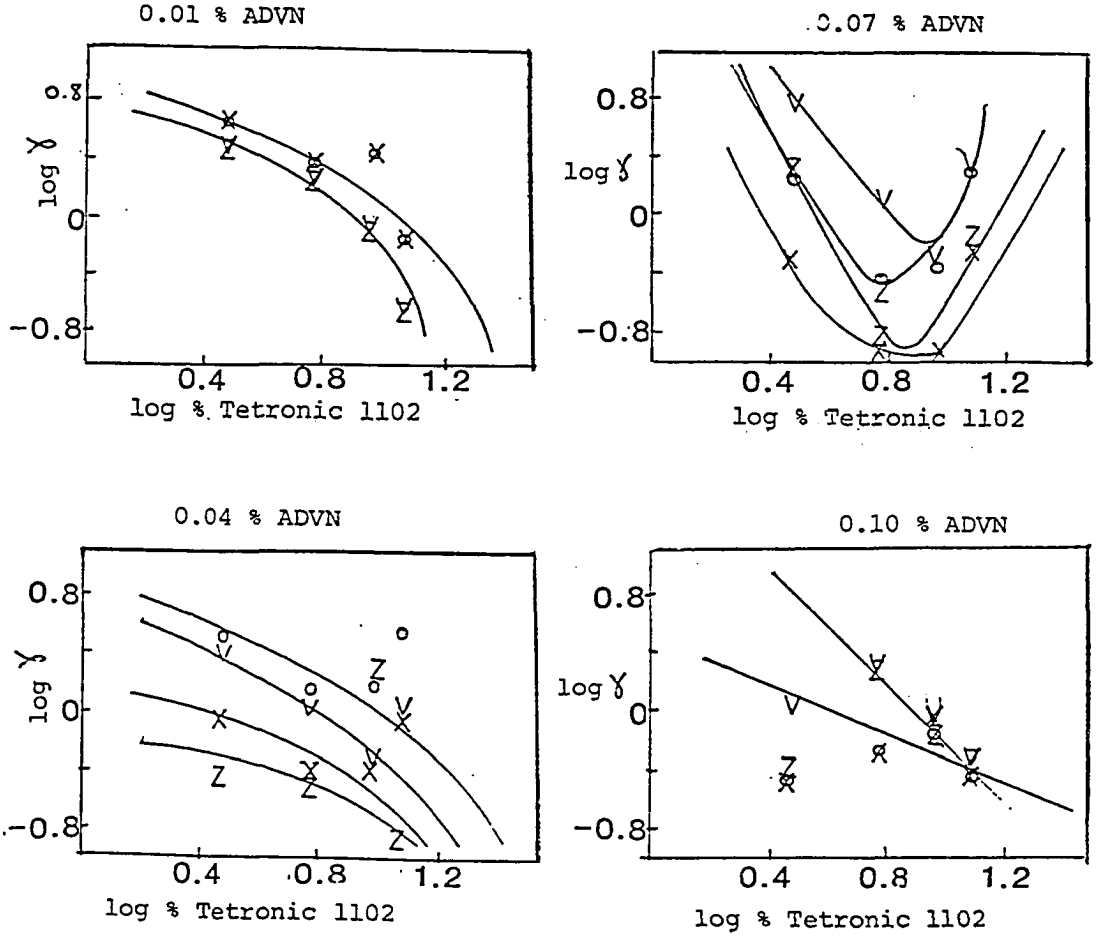

V 50 C

O 55 C

X 60 C

Z 65 C

Figure 5.19

Latex Skewness Coefficient as a Function of Emulsifier Concentration

KPS Initiator

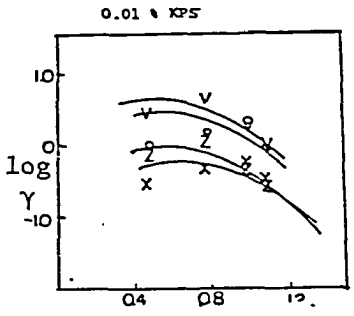

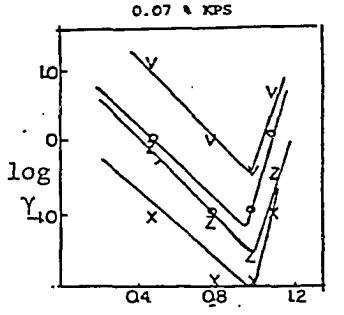

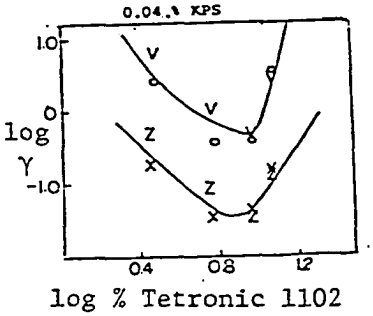

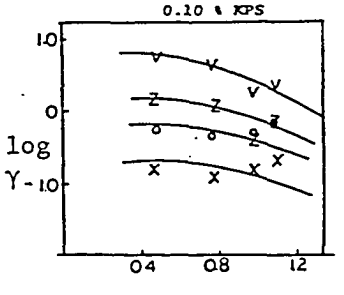

V 50 C

O 55 C

X 60 C

Z 65 C

Figure 5.20

Skewness Coefficient of Monomer Emulsion
as a Function of Emulsifier Concentration

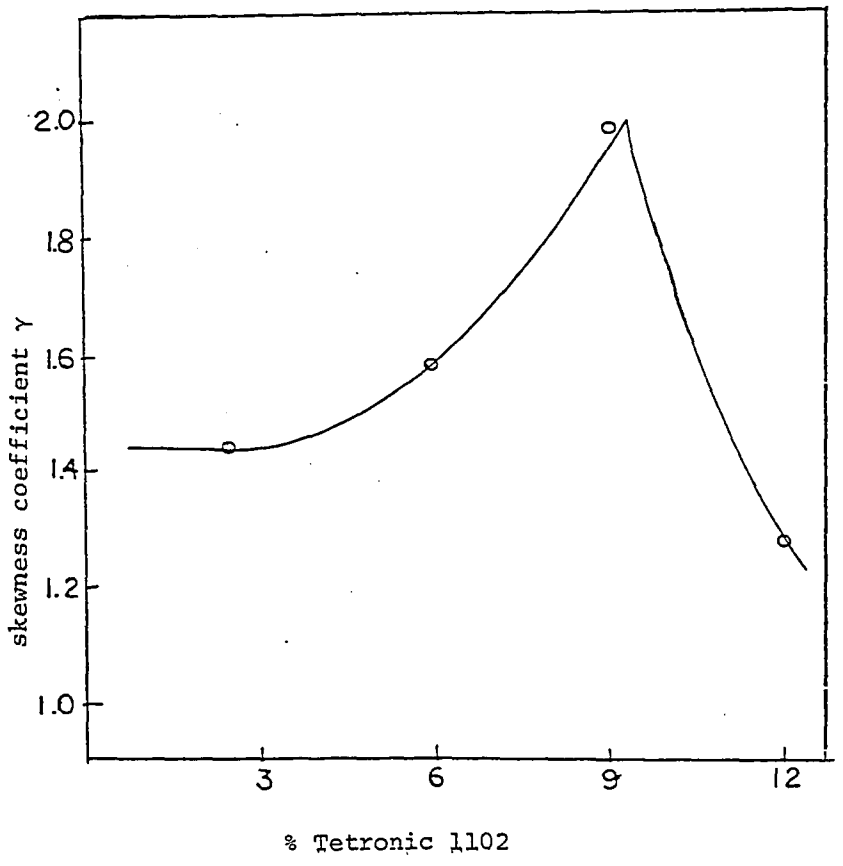

Figure 5.21

Ratio of Latex Skewness (γ_l) to Monomer Emulsion Skewness (γ_m)

KPS Initiator

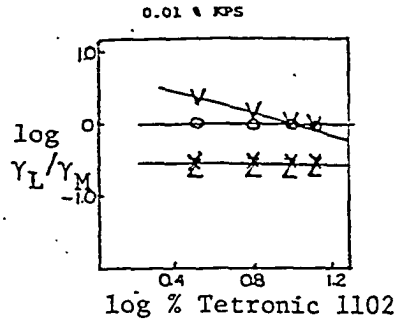

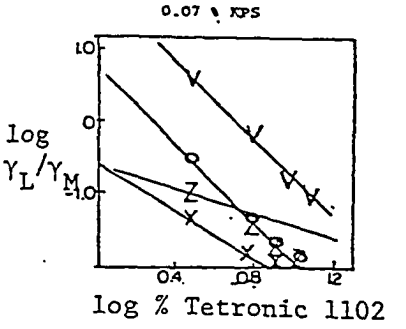

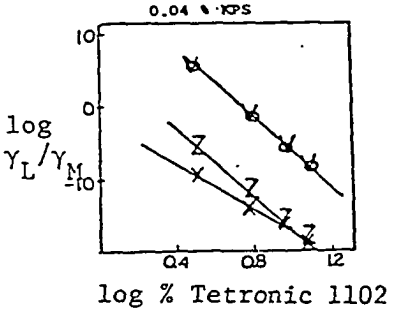

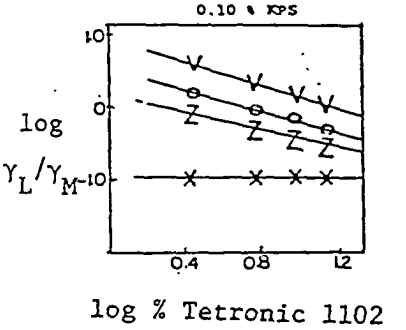

V 50 C

O 55 C

X 60 C

Z 65 C

Figure 5.22

Ratio of Latex Skewness (γ_l) to
Monomer Emulsion Skewness (γ_m)

ADVN Initiator

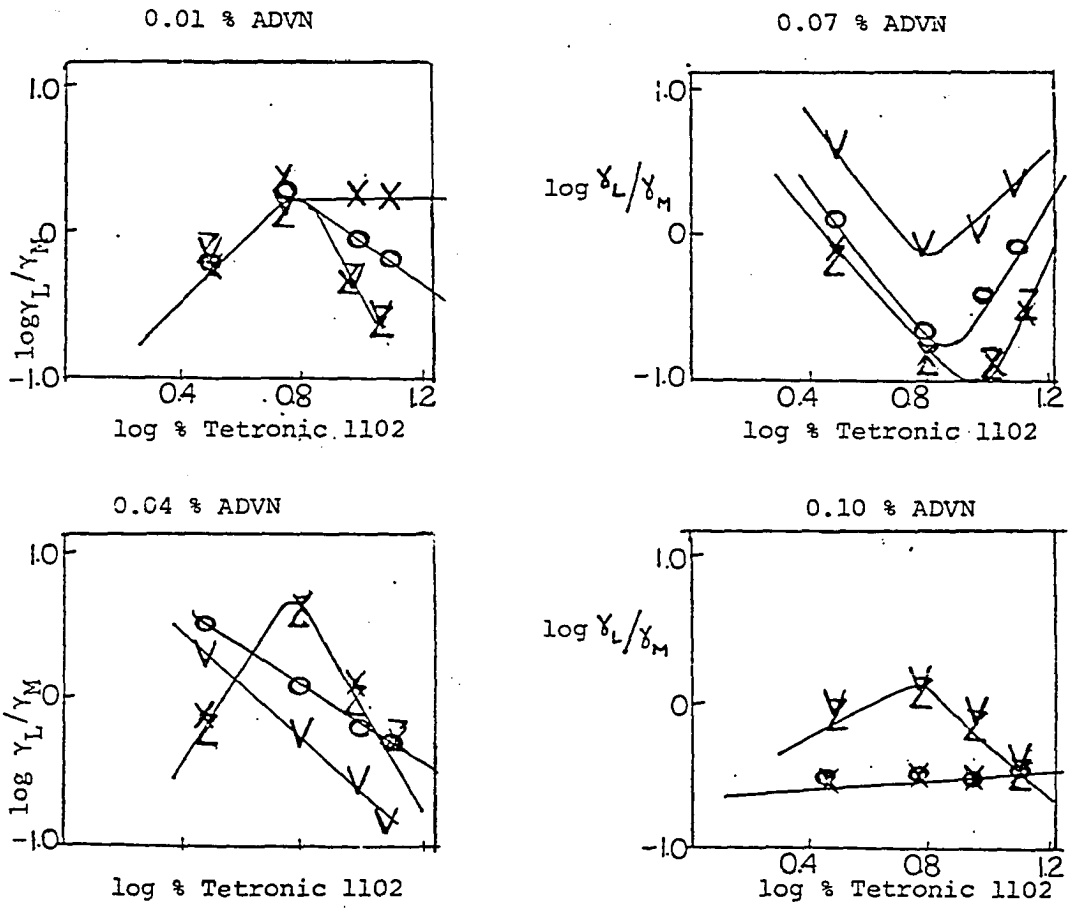

V 50 C

o 55 C

X 60 C

Z 65 C

tionship with azo-initiated polymerizations indicates competing mechanisms of particle growth and hence there may be more than one locus of initiation.

g. Shape of conversion-time curve

The conversion-time curves for acrylamide polymerization with Tetronic 1102 emulsifier are not always smoothly sigmoidal but in some cases polymerization ceases at moderate conversion, followed by a period of autoacceleration. Multivariate regression analysis was done, using the presence or absence of a plateau in the conversion-time curve as the response. The correlation coefficient for this regression model is 0.97 at the 94% confidence level. The presence of the plateau was found to be independent of initiator type or emulsifier concentration but is favored by polymerization temperatures of 50°C or 65°C, but not 55°C and 60°C.

h. Quantity of coagulum

Coagulum is generally formed in an emulsion polymerization due to either rapid autoacceleration ("runaway polymerization") or poor colloidal protection. Analysis of the amount of coagulum does not give insight into the reaction kinetics and mechanism, but is useful in development of polymerization recipes.

Multivariate regression analysis done using the weight of coagulum formed as the response shows that coagulum formation is mainly affected by the initiator type and level. Coagulum formation is a much more severe problem with persulfate initiator than with azo initiator. Much coagulum is formed only in

persulfate initiated polymerizations only at higher levels of initiator (0.07 and 0.10%); however, polymerizing at a temperature of 65°C always forms much coagulum with persulfate initiator at all initiator levels. The correlation coefficient for this regression model is 0.99 at the 99% confidence level.

The coagulum formation at 65°C is likely due to poor colloidal protection, since the polymerization rate is not maximum at this temperature, but the interfacial tension is high, indicating that the emulsifier has partitioned into the continuous phase. Since persulfate is soluble in the monomer phase, it is more likely to cause locally high radical flux and lead to coagulum formation due to "runaway polymerization."

i. Type of coagulum

The type of coagulum formed in these inverse emulsion polymerizations is of two distinctly different types: one type is soft, white and fluffy; the other is hard, clear and granular, and looks and feels like a suspension polymer. Multivariate regression analysis is done using the presence of hard or soft gel as the response in order to gain some insight into the structure of the polymer and the mechanism of the reaction by characterizing conditions under which these types of gel form. The analysis showed that the type of gel formed depended strongly on the polymerization temperature and initiator type and level. The regression model had a correlation coefficient of 0.99 at the 99% confidence level.

The formation of hard gel is strongly correlated to use of persulfate initiator at 65°C. Indeed, these conditions fit the description of a classical suspension polymerization, i.e. a system in which the initiator is soluble in the monomer phase and the continuous phase contains a swollen, moderately high molecular weight species as a "protective colloid."

2. Partitioning of the Oil-Soluble Initiator

The oil-soluble initiator used in this study (ADVN) is a highly hydrophobic molecule:

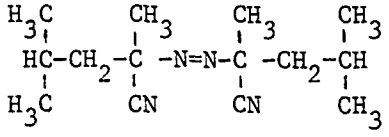

Literature values for its solubility at 25°C are 0.009 g/100 ml in water and 70 g/100 ml in xylene (5.3). The method of transporting these bulky radicals into the monomer phase is not immediately obvious. To gain insight into the means of transport and hence the locus of initiation, the quantity of initiator partitioning into each phase is measured at various initiator concentrations, emulsifier concentrations, and temperatures.

The saturation concentration of ADVN in water at 25°C decreases rapidly to a limiting value as the concentration of Tetronic 1102 increases (Fig. 5.23). The saturation concentration of ADVN in o-xylene is much less significantly decreased by the presence of Tetronic 1102 (Fig. 5.24). Both the experimentally determined

Figure 5.23

Saturation Concentration of ADVN in Water at 25°C:

Effect of Tetronic 1102 Concentration

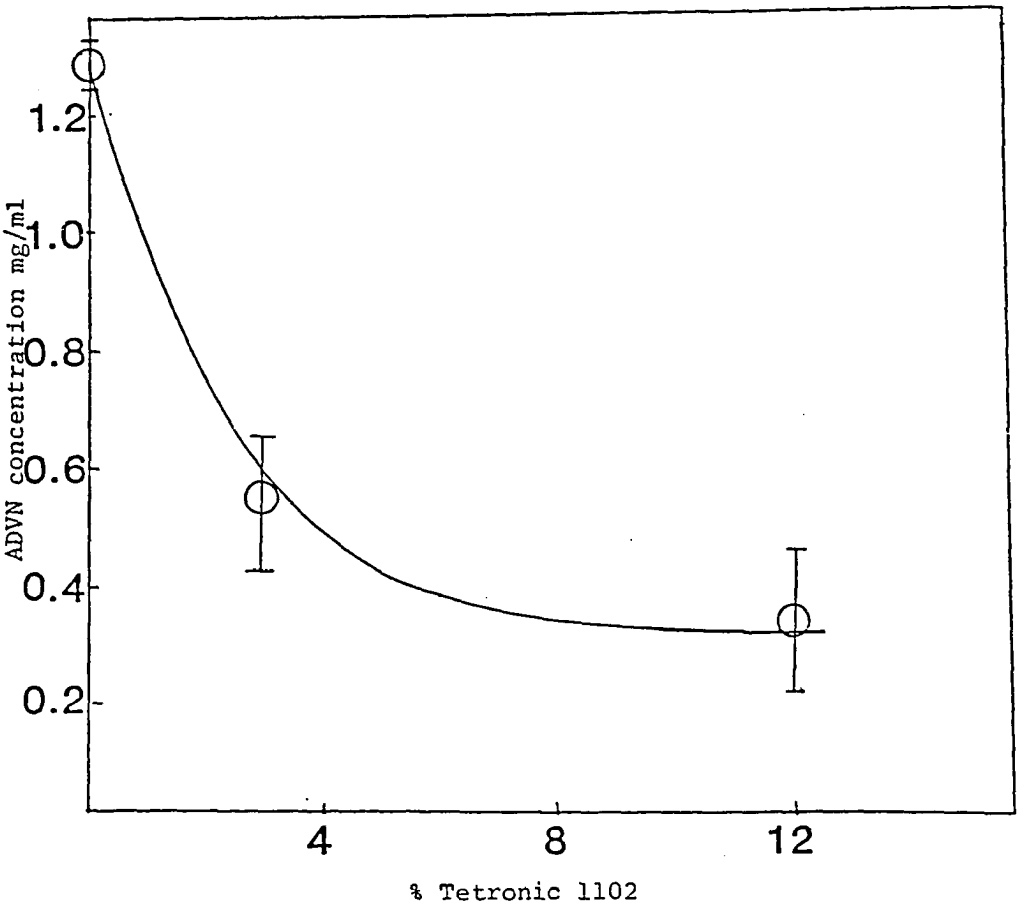

Figure 5.24

Saturation Concentration of ADVN in O-Xylene at 25°C:

Effect of Tetronic 1102 Concentration

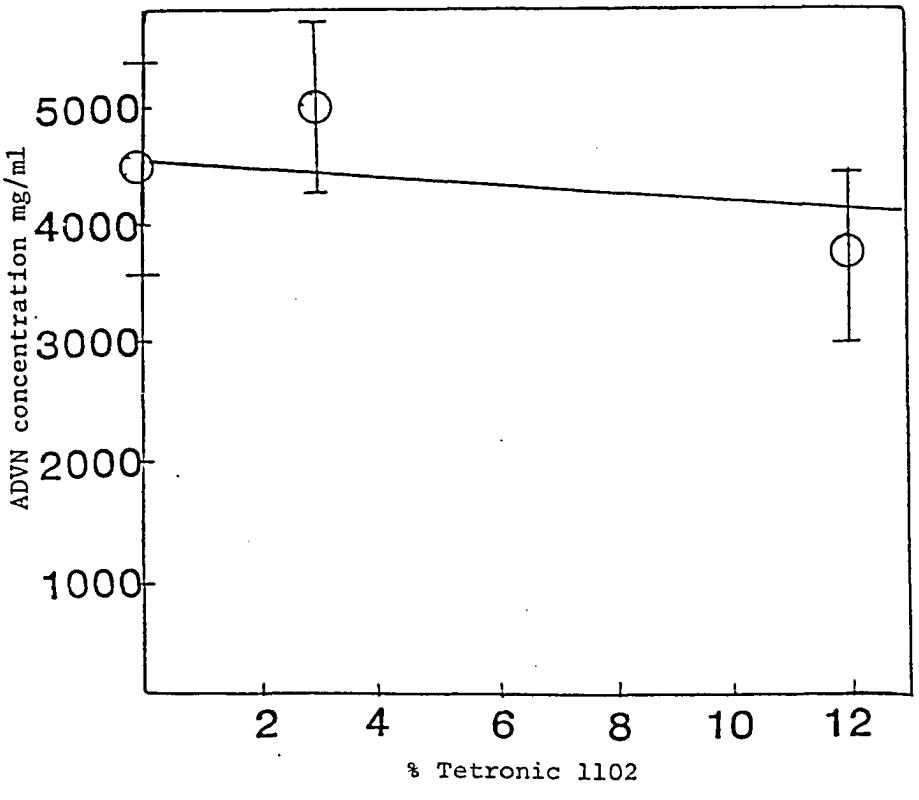

saturation concentration of ADVN in water in the absence of Tetronic 1102 (0.12 g/100 ml) and the experimentally determined saturation concentration in o-xylene (450 g/100 ml) are significantly higher than the literature values at the same temperature (0.009 and 79 g/100 ml, respectively); no reason for this difference is apparent. The method of measurement was the same in both the experimental and literature studies, i.e. ultraviolet spectroscopy.

Adding Tetronic 1102 raises the partition coefficient greatly, indicating that more of the initiator resides in the organic phase (Fig. 5.25). This would seem to indicate that the initiator molecules increasingly disfavor the monomer phase as emulsifier concentration increases. However, quantitative analysis of the amount of ADVN solubilized in each layer shows that this hypothesis is not complete. As the emulsifier concentration increases, the small amount of ADVN solubilized in the aqueous phase becomes somewhat smaller (Fig. 5.26). However, the quantity in the organic phase decreases drastically (Fig. 5.27). Calculation of the quantity solubilized in the cream layer (i.e., the layer formed between the oil and aqueous layers after ultracentrifugation of the emulsion) shows that the ADVN molecules are preferentially solubilized into this layer (Fig. 5.28). If the correlation between the composition of cream layer formed on centrifugation of the emulsion and the composition of the interfacial layer is accepted, these results indicate that the interfacial layer may also serve as a

Figure 5.25

Effect of Tetronic 1102 on the Partition Coefficient of of ADVN

($K_D = W_{org}/W_{aq}$)

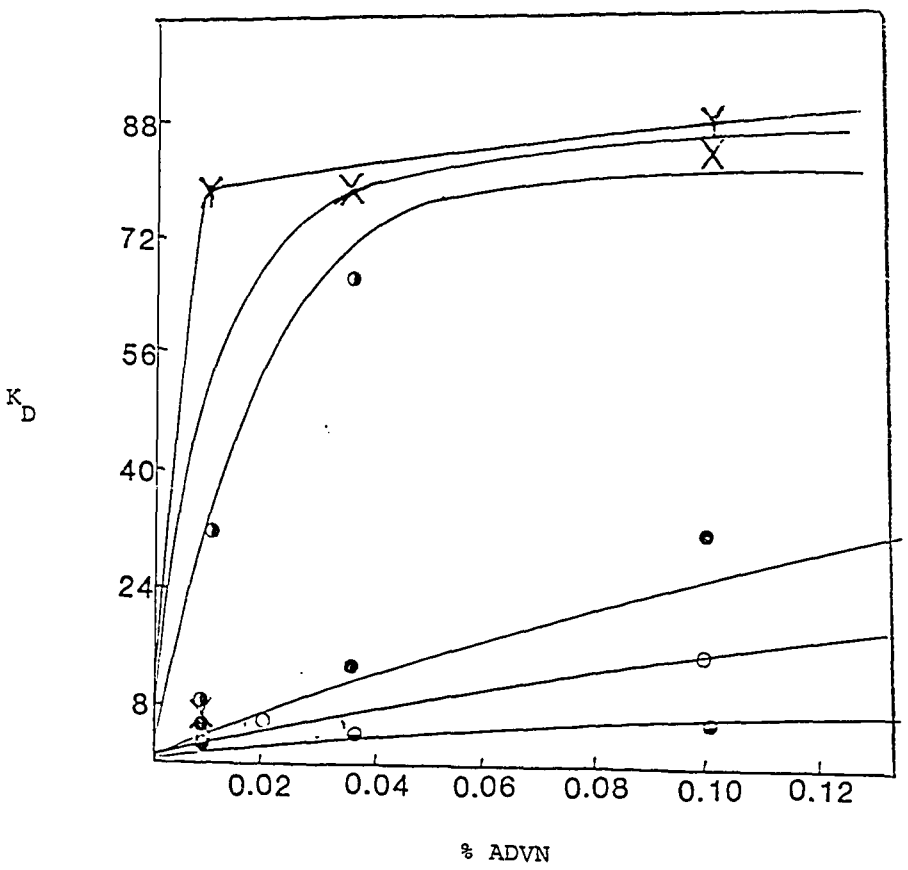

Figure 5.26

Quantity of ADVN Solubilized in the Aqueous Layer as a Function of the Total Quantity of ADVN Added to the System

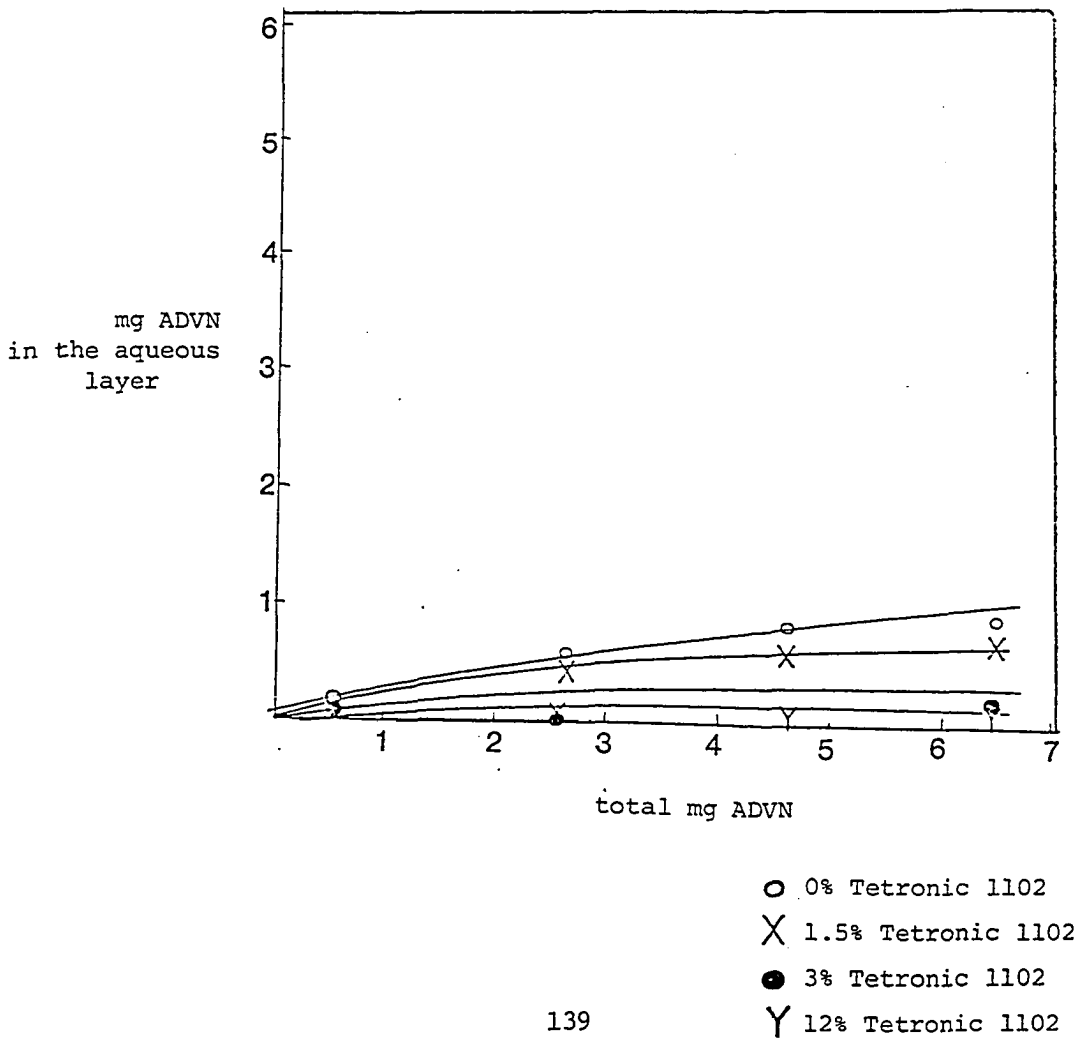

Figure 5.27

Quantity of ADVN Solubilized in the Organic Layer as a Function of the Total Quantity of ADVN Added to the System

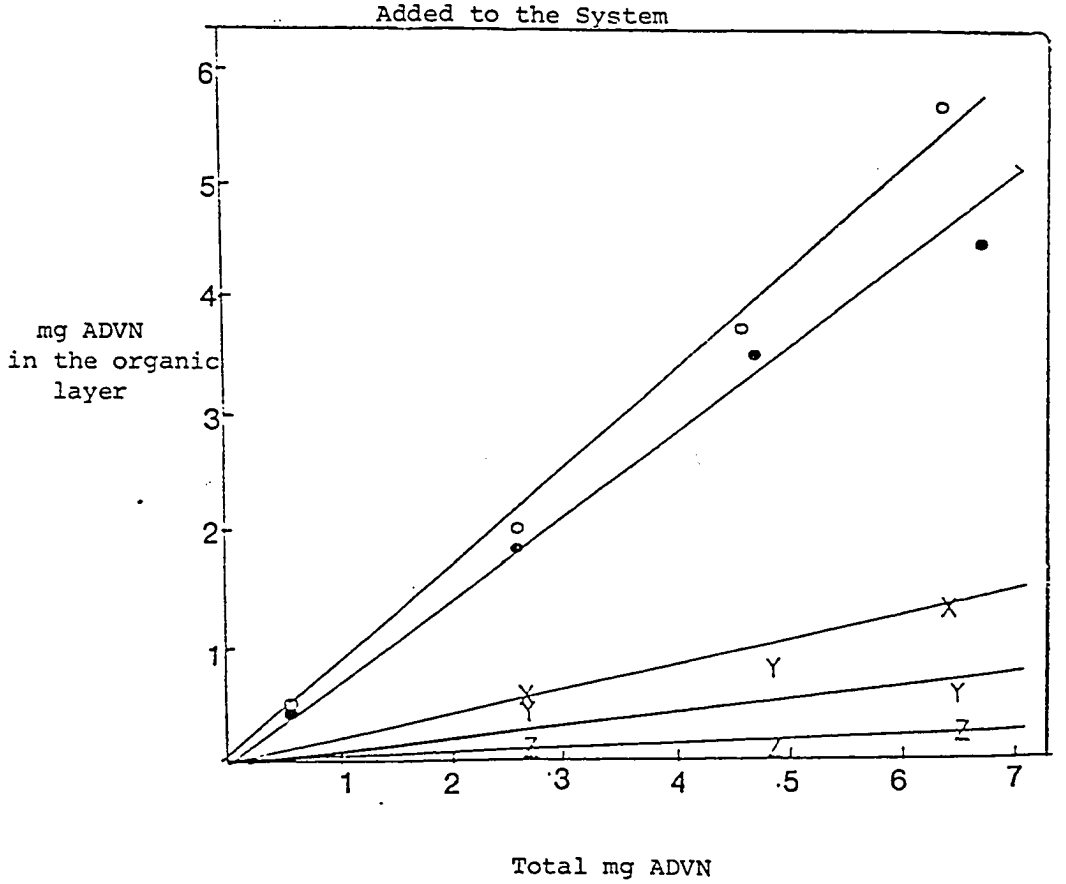

Figure 5.28

Quantity of Solubilized ADVN as a function of the Total Quantity of ADVN added to the System

3% Tetronic 1102

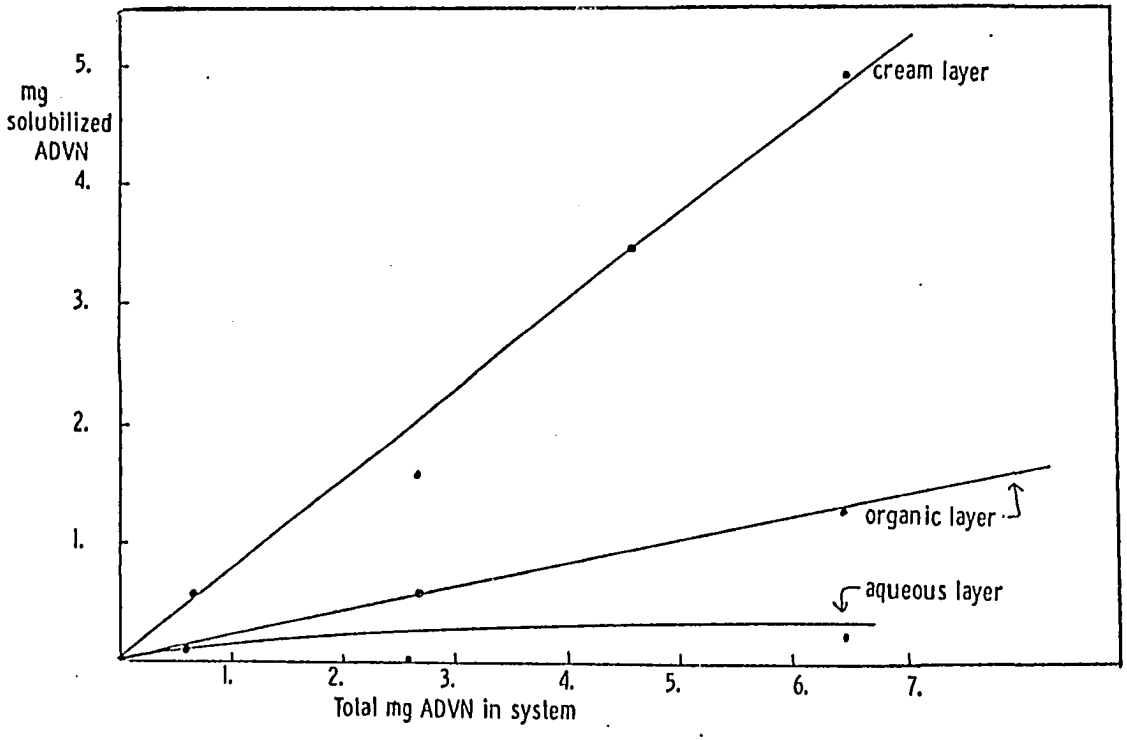

locus of initiation for polymerization.

The partition coefficient studies described above were performed using distilled deionized water as the aqueous phase to facilitate analysis. To ensure that partitioning is not affected by the composition of the aqueous phase, the partition coefficient is measured using propionamide, at the same molar concentration (4.5 M) normally used for acrylamide in these studies, as the aqueous phase. Propionamide has the same structure as acrylamide except for saturation of the vinyl group. Comparing Figure 5.29, which depicts the system containing propionamide, to Figure 5.25 shows that the composition of the aqueous phase indeed does not affect the partition coefficient.

To minimize the possibility of decomposing the initiator, these studies were carried out at room temperature after mixing the samples for 30 min. Raising the temperature or increasing the mixing time raises the partition coefficient to further favor the organic phase (Fig. 5.30); hence the higher temperature used for polymerization does not increase the low solubility of ADVN in the aqueous phase or otherwise affect the partitioning. The cause of higher partition coefficient at longer mixing time is unclear.

3. Solubility of Acrylamide in O-Xylene

The solubility of acrylamide in o-xylene is an important parameter in determining whether polymerization in the continuous phase is important in this system. The solubility of acrylamide in

Figure 5.29

Effect of Tetronic 1102 on the Partition Coefficient of ADVN in the Presence of 4.5 M Propionamide

($K_D = W_{org}/W_{aq}$)

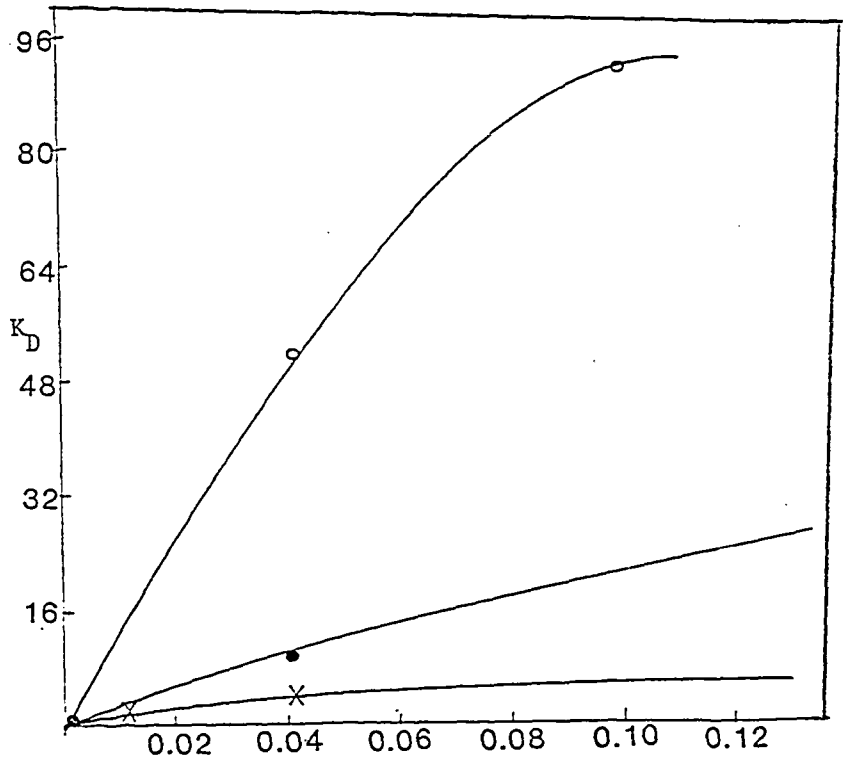

Figure 5.30

Effect of Mixing Temperature and Mixing Time on the Partition Coefficient of ADVN

($K_D = W_{org}/W_{aq}$)

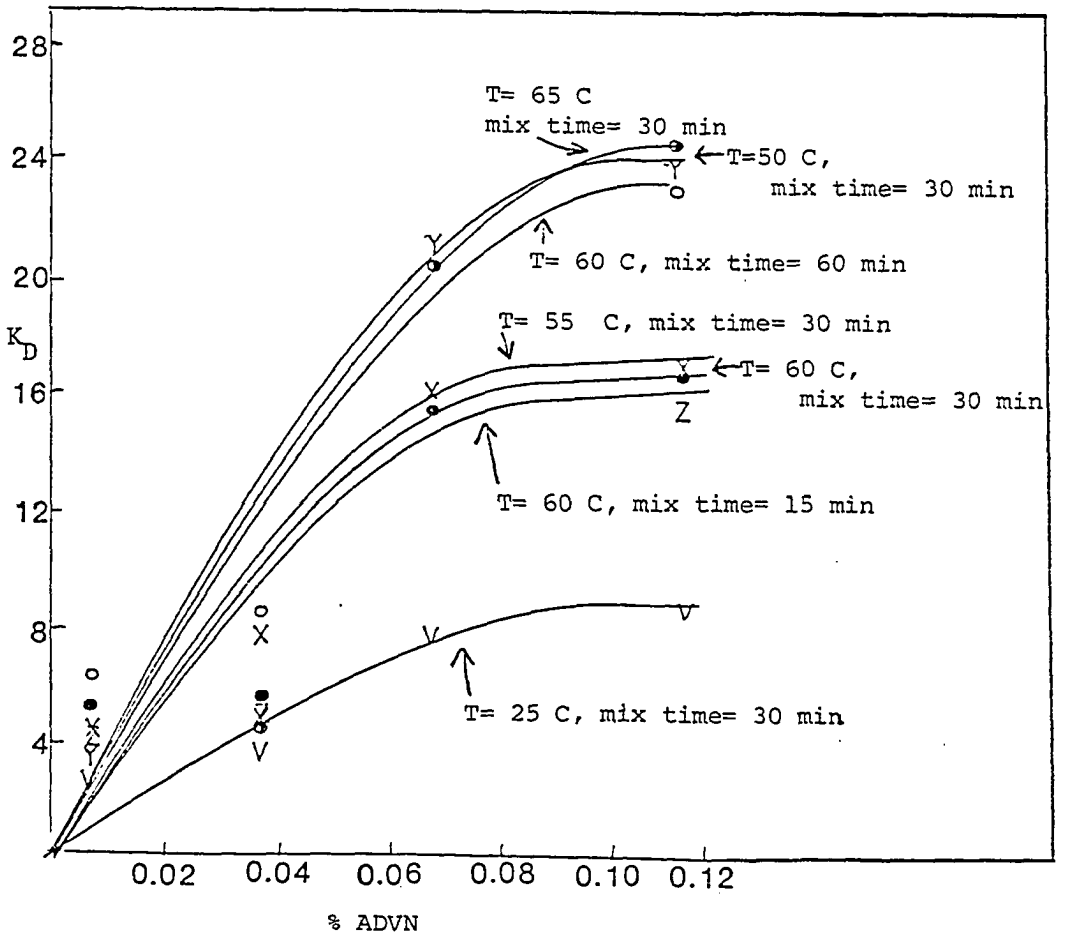

o-xylene increases rapidly as temperature increases, but even at 65°C its solubility is less than 1% (Fig. 5.31). This rapid increase in solubility with temperature and the magnitude of the solubility at each temperature agree well with literature values for the solubility of acrylamide in benzene (5.4). This low solubility argues against significant polymerization in the continuous phase, although in conventional emulsion polymerization, some monomers can polymerize in the water phase at solubilities of 1%.

4. Aqueous Solution Polymerizations of Acrylamide

In order to calculate the subdivision factor for emulsion polymerization, it is necessary to know the rate of polymerization of an aqueous monomer solution having the same concentration as the aqueous solution used in the inverse emulsion polymerization system.

Conversion-time curves for aqueous solution polymerization of 4.5M acrylamide initiated by potassium persulfate have the expected smoothly sigmoidal shape. Rate is plotted as a function of initiator concentration and temperature in Figures A.1 and A.2 in order to determine by extrapolation the rate at temperature and initiator concentrations not measured experimentally. Initial rates of polymerization are summarized in Table 5.1a. In free radical polymerization, rate constants and the initiator efficiency factor f can be calculated from the slope of the rate of polymerization as a function of the square root of the initiator concentration according to the following equation:

Figure 5.31

Solubility of Acrylamide in Aromatic Solvent as a Function of Temperature

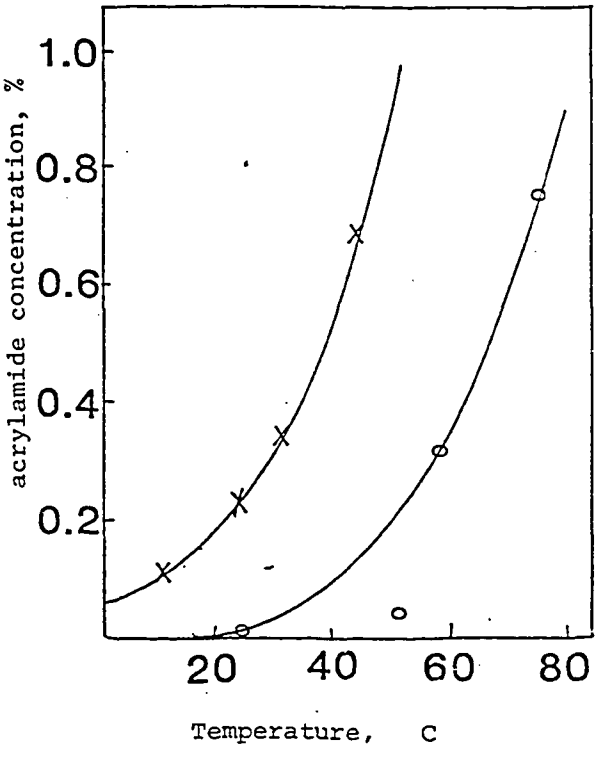

x=benzene (ref. 1.9)

o=o-xylene (this work)

TABLE 5.1a

Initial Polymerization Rate in Aqueous Solution

4.5M Acrylamide

Temperature	Initiator Concentration mole%/moles monomer	Polymerization Rate moles/liter·sec
50	0.01	0.006
	0.04	0.0126
	0.07	0.0138
	0.10	0.212
55	0.01	0.01
	0.04	0.0204
	0.07	0.023
	0.10	0.035
60	0.01	0.0175
	0.04	0.0375
	0.07	0.045
	0.10	0.0635
65	0.01	0.0248
	0.04	0.0565
	0.07	0.0640
	0.10	0.0901

$$R_p = k_p[M](fk_d/k_t)^{1/2}[I]^{1/2}$$

Since the monomer molarity [M] is known and the initiator decomposition rate constant can be found in the literature (5.5), the value of $k_p(f/k_t)^{1/2}$ can be determined from the slope (Figures A.3-A.6). These constants should be equivalent for both solution and emulsion polymerization. These results are given in Table 5.1b.

C. Discussion

Before calculating kinetic parameters, it is instructive to consider the possible descriptive models for polymerization in multicelled particles and the similarity of these models to classical emulsion polymerization.

A multicelled particle can be considered as a single particle containing cells (a) or as an agglomerate of several particles (b):

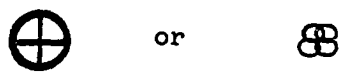

a or b

In both of these cases, the subdivision factor is the same, since there are four small units cosmprising one large unit, but the surface area exposed for possible transfer is larger for the agglomerate (b) than or the cellular structure (a). Hence the radical transfer reactions depend on the configuration of the particle.

The method of transport of initiating radicals into the monomer phase must also be considered schematically. In the classic

Table 5.1b

Polymerization Rate Constants

T	$k_d x 10^{-6}$	Slope of R_p vs $[I]^{1/2}$	$k_p(f/k_t)^{1/2}$
50	1.0	0.304	67.5
55	2.5	0.501	70.4
60	6.9	0.947	80.0
65	11.5	1.33	87.4

Smith-Ewart scheme, radicals are generated in the continuous phase and diffuse into the growing particles; in the Medvedev model, polymerization initiation occurs at the particle surface. In the present system, ADVN radicals may diffuse through the medium into the particles, or, considering the preferential solubilization of ADVN in the cream layer, the ADVN may become solubilized in the interfacial layer and form radicals there. The KPS similarly may form radicals in the continuous phase which diffuse into the particles (although this seems unlikely in nonpolar o-xylene medium) or, since it is added as an aqueous solution, it may form droplets which collide with monomer emulsion droplets and thereby enter the monomer emulsion droplets, or KPS radicals may transfer to emulsion and thereby diffuse to the monomer droplets.

The applicability of the various methematical analyses of emulsion polymerization kinetics must be evaluated in view of these possible descriptive models.

1. Calculation of Kinetic Parameters

a. KPS system

The subdivision factor for emulsion polymerization (z) is defined as the ratio of initial polymerization rate in emulsion to initial polymerization rate in solution, assuming that f, k_p, and k_t are the same in solution and emulsion polymerization at the same temperature. The values of the subdivision factor for the inverse emulsion polymers prepared in this study are listed in Table 5.2. The value of z gives insight into the method of radical generation

Table 5.2

Calculation of Subdivision Factor Z

KPS Initiator

T	[I]	Soln. R_p mole/ℓ·sec	Emulsion R_p mole/ℓ·sec				$Z = R_{pemul}/R_{psoln}$			
			[ε]=3	6	9	12	3	6	9	12
50	0.01	$6x10^{-3}$	0.053	0.019	0.023	0.064	8.8	3.17	3.83	10.7
	0.04	$12.2x10^{-3}$	0.078	0.028	0.035	0.095	6.39	2.30	2.86	7.79
	0.07	$13.8x10^{-3}$	0.111	0.041	0.050	0.136	8,04	2.97	3.62	9.86
	0.10	$2.12x10^{-3}$	0.076	0.028	0.034	0.092	3.59	1.35	1.60	4.34
55	0.01	$10x10^{-3}$	0.25	0.092	0.045	0.123	25.	9.2	4.5	12.3
	0.04	$20.4x10^{-3}$	0.37	0.136	0.066	0.181	18.1	6.7	3.24	8.9
	0.07	$23.0x10^{-3}$	0.167	0.061	0.030	0.082	7.26	2.65	1.30	3.56
	0.10	$35.0x10^{-3}$	0.114	0.042	0.020	0.055	3.26	1.2	0.57	1.57
60	0.01	$17.5x10^{-3}$	0.067	0.025	0.012	0.033	3.83	1.43	0.685	1.89
	0.04	$37.5x10^{-3}$	0.10	0.037	0.018	0.049	2.67	0.98	0.48	1.31
	0.07	$45.0x10^{-3}$	0.045	0.016	0.008	0.022	1.0	0.35	0.18	0.49
	0.10	$63.5x10^{-3}$	0.03	0.011	0.005	0.015	0.47	0.17	0.078	0.24
65	0.01	$24.8x10^{-3}$	0.014	0.0052	0.0064	0.017	0.56	0.21	0.25	0.68
	0.04	$56.5x10^{-3}$	0.021	0.0077	0.0094	0.026	0.37	0.136	0.166	0.46
	0.07	$64.0x10^{-3}$	0.03	0.010	0.013	0.037	0.468	1.72	0.20	0.578
	0.10	$90.x10^{-3}$	0.020	0.0075	0.009	0.025	0.22	0.83	0.1	0.278

in or entry into particles: values of z greater than 1 indicate that the radicals are generated in or enter particles singly, and values of z less than 1 indicate that radicals are generated in or enter particles pairwise. In this study, the value of z is greater than 1 in persulfate initiated polymerizations at temperatures of 50 to 60°C, indicating that there must be a mechanism for generation of single radicals operative in this system. For polymerization at 65°C, the value of z is close to or slightly less than 1, especially at low emulsifier concentration and high initiator concentration, indicating that the structure of the interface can control the generation of radicals or their transport to the locus of initiation.

Mathematical analyses of the kinetics of emulsion polymerization assume a quasi steady state for the distribution of free radicals in the particles. This assumption is clearly valid if radicals are generated in the continuous phase; it is not so obvious if radicals are formed by collision of monomer droplets with initiator droplets. However, O'Toole has shown (5.7) that, in systems like the present one in which radicals are generated pairwise in the monomer phase but kinetically appear singly, this steady-state assumption is valid if no termination occurs in the continuous phase; thqat is, the rate of radical desorption equals the rate of re-entry.

The initial rates of polymerization and the subivision factors are used to calculate kinetic parameters using the following equations taken from the theoretical analyses of Stockmayer (5.6),

O'Toole (5.7), and van der Hoff (5.8):

$$R_p = \bar{n}\, k_p [M]/NaV \qquad (1)$$

$$z = I_m(a)/I_{m-1}(a) \cong \bar{n}/a_4 \qquad (2)$$

$$m = k_{de} V/k_t^* \qquad (3)$$

$$\bar{n} = (0.25 + a^2/16)^{\frac{1}{2}} \qquad (4)$$

where $\bar{n}$ is the average number of radicals per particle, $I_m(a)$ and $I_{m-1}(a)$ are modified Bessel functions of the first kind, f is the average efficiency of both initiator fragments in initiating polymer chains, k_{de} is the rate constant for radical desorption, k_t is the rate constant for termination in the particles, N_A is Avogadro's number, V is the average particle volume, [M] is the monomer concentration in the monomer phase, k_p is the propagation rate constant, and k_t^* is rate constant for termination. Equation (1) cannot be used directly in the present system because it requires measuring the average particle volume which cannot be done unambiguously in a system containing multicelled particles. However, knowing the value of the subdivision factor z, the value of the term a can be calculated using equation (2) if the value of the order (m) of the Bessel functions is known. Assuming no radical desorption from the particles, m equals zero, and the Stockmayer equation can be used to calculate a:

$$z = I_o(a)/I_1(a) \qquad (5)$$

These values are given in Table 5.2 and 5.3. This assumption of no desorption seems to be reasonable in this system. Desorption is thought to result from a transfer reaction with a small molecule rather than with an oligomeric molecule because molecular entanglements lower the ability of oligomers to desorb (5.9). In this polymerization system, the surfactant is oligomeric and hence unlikely to facilitate desorption of radicals. Acrylamide monomer is known from the literature to have a low rate constant for chain transfer to monomer, indicating that radical desorption via chain transfer to monomer is unlikely.

Although the assumption of no desorption makes equation (5) appropriate, using this equation to calculate a leads to practical difficulties due to the properties of Bessel functions: as the value of the argument a decreases, the ratio of $I_o(a)$ to $I_1(a)$ increases drastically. Hence small errors in determination of z (i.e., $I_o(a)/I_1(a)$) lead to large fluctuations in the value of a. To minimize the error in determining a using the ratio of the Bessel function,the values of a were fitted to the following relationship between a and the initiator concentration which applies generally to free-radical polymerization:

$$a = 4(f\, k_d\, [I]/k_t)^{1/2}\, N_a V \qquad (6)$$

where f is the initiator efficiency factor.

The data were analyzed graphically,in two ways: a was plotted as a

Table 5.3

Calculation of a-KPS Initiator

T	[I]	Z				a			
		[E]=3	6	9	12	[E]=3	6	9	12
50	0.01	8.8	3.17	3.83	10.7	0.23	0.665	0.54	0.188
	0.04	6.39	2.30	2.86	7.79	0.32	0.96	0.745	0.258
	0.07	8.04	2.97	3.62	9.86	0.25	0.715	0.57	0.205
	0.10	3.59	1.32	1.60	4.34	0.58	2.4	1.62	0.474
55	0.01	25.	9.2	4.5	12.3	0.08	0.218	0.455	0.163
	0.04	18.1	6.7	3.24	8.9	0.11	0.30	0.645	0.226
	0.07	7.26	2.65	1.30	3.56	0.28	0.815	2.52	0.585
	0.10	3.26	1.2	0.57	1.57	0.645	3.35	2.58	1.67
60	0.01	3.83	1.43	0.685	1.89	0.54	2.00	3.35	1.25
	0.04	2.67	0.98	0.48	1.31	0.80	9.2	2.98	2.5
	0.07	1.0	0.35	0.18	0.49	10.0	1.44	0.72	2.16
	0.10	0.47	0.17	0.078	0.29	2.04	0.68	0.312	0.96
65	0.01	0.56	0.21	0.25	0.68	2.52	0.84	1.04	3.32
	0.04	0.37	0.136	0.166	0.46	1.56	0.54	0.668	2.00
	0.07	0.468	1.72	0.20	0.578	2.04	1.44	0.80	2.64
	0.10	0.22	0.83	0.10	0.278	0.88	4.72	1.6	1.14

$$Z = I_o(a)/I_1(a)$$

function of the square root of [I], which should have an intercept of zero and a slope of $4N_aV(f\ k_d/k_t)^{1/2}$; and log a was plotted as a function of log [I], which should have slope 1/2 and intercept 4 $N_aV(fk_d/k_t)^{1/2}$. Generally the values of a at a given initiator concentration determined by both correlations agreed to within 20%. These a values are listed in Table 5.4. The following relationship between the overall polymerization rate and the value of a can be used to verify the validity of the values of a determined graphically

$$R_p = zk_p[M]a/4N_aV \qquad (7)$$

where k_p is the propagation rate constant and [M] is the monomer concentration in the monomer phase. The relationship between R_p and a was found to have the expected linear relationship (Figures A.7-A.12).

The average number of radicals per particle $\bar{n}$ is a critically important parameter in understanding the mechanisms of an emulsion polymerization. Smith-Ewart Case 2 kinetics apply to $\bar{n}$ equal to 0.5. Case 1 kinetics, in which $\bar{n}$ is much smaller than 0.5, apply to systems where particles are small or radicals rapidly desorb. Case 3 kinetics, in which $\bar{n}$ is much greater than 0.5, apply to systems where the degree of subdivision is not important or the termination rate is depressed (i.e., the Trommsdorff effect is very important) (5.10). The average number of radicals per particle, calculated using equation 4, are listed in Table 5.5. The average

Table 5.4

Values of a from Graphical Analysis

KPS Initiator

T	[I]	[E]							
		3		6		9		12	
		log	linear	log	linear	log	linear	log	linear
50	0.01	0.25	0.2	0.73	0.6	0.57	0.48	0.19	0.15
	0.04	0.32	0.36	0.93	1.15	0.72	0.92	0.26	0.28
	0.07	0.36	0.48	1.05	1.54	0.8	1.23	0.27	0.37
	0.10	0.39	0.58	1.10	1.78	0.85	1.42	0.31	0.45
55	0.01	0.08	0.10	0.22	0.26	0.46	0.38	0.165	0.14
	0.04	0.11	0.19	0.28	0.53	0.60	0.74	0.23	0.38
	0.07	0.18	0.25	0.32	0.70	0.63	0.97	0.24	0.36
	0.10	0.23	0.30	0.34	0.84	0.70	1.16	0.26	0.45
60	0.01	0.52	0.44	0.9	0.53	1.06	1.08	1.04	1.04
	0.04	0.78	0.9	1.23	1.0	2.6	2.15	1.9	2.08
	0.07	0.9	1.2	1.45	1.44	2.65	2.85	2.20	2.75
	0.10	1.00	1.42	1.60	1.70	2.8	3.37	2.4	4.74
65	0.01	1.25	0.78	0.9	0.42	0.58	0.32	1.70	0.98
	0.04	1.70	1.55	1.20	0.85	0.70	0.65	2.25	2.0
	0.07	1.80	2.04	1.35	1.15	0.77	0.86	2.50	2.62
	0.10	2.05	2.34	1.45	1.32	0.80	0.98	2.70	2.98

TABLE 5.5 Values of $\bar{n}$ Calculated from Values of a from Graphical Analysis

KPS Initiator

T	[I]	Value of a [E]				Value of $\bar{n}$ [E]			
		3	6	9	12	3	6	9	12
50	0.01	0.23	0.66	0.52	0.17	0.50	0.53	0.52	0.50
	0.04	0.34	1.04	0.82	0.27	0.51	0.56	0.54	0.50
	0.07	0.42	1.30	1.01	0.32	0.51	0.59	0.56	0.51
	0.10	0.49	1.44	1.13	0.38	0.51	0.62	0.57	0.50
55	0.01	0.09	0.24	0.42	0.153	0.50	0.50	0.51	0.50
	0.64	0.15	0.28	0.67	0.30	0.50	0.50	0.53	0.51
	0.07	0.26	0.32	0.80	0.32	0.50	0.51	0.54	0.51
	0.10	0.27	0.34	0.93	0.36	0.50	0.51	0.55	0.51
60	0.01	0.48	0.90	1.07	1.04	0.51	0.55	0.57	0.56
	0.04	0.84	1.14	2.38	1.99	0.54	0.58	0.78	0.70
	0.07	1.05	1.45	2.75	2.45	0.56	0.62	0.85	0.29
	0.10	1.22	1.65	2.90	3.50	0.58	0.65	0.88	1.01
65	0.01	1.01	0.66	0.45	1.34	0.56	0.53	0.51	0.60
	0.04	1.62	1.03	0.68	2.13	0.64	0.56	0.53	0.73
	0.07	1.92	1.25	0.82	2.56	0.69	0.59	0.54	0.81
	0.10	2.20	1.39	0.89	2.84	0.74	0.60	0.55	0.87

$$n = (0.25 + \frac{a^2}{16})^{\frac{1}{2}}$$

number of radicals per particle is generally close to 0.5 for all polymerization conditions except for polymerizations at high temperature (60-65°C) in which the initiator concentration and the emulsifier concentration are both high. The effect of high initiator concentration is not entirely unexpected, since high radical flux may be expected to increase the number of radicals per particle if autoacceleration occurs early in the reaction; this may occur in the case of acrylamide because of the characteristically high ratio of k_p/k_t. The effect of emulsifier on $\bar{n}$ is, however, unexpected: increasing the emulsifier concentration should decrease the average particle volume, whereas inspection of equations 4 and 6 shows that $\bar{n}$ is directly related to the average particle volume. This may indicate that the emulsifier may play an important role in the polymerization mechanism, and under some conditions this system resembles bulk or suspension polymerization rather than emulsion polymerization.

As discussed earlier, measuring the average particle volume cannot be done directly in this system containing multicelled particles. However, the average particle size can be calculated knowing the values of the propagation rate constant and $\bar{n}$:

$$R_p = k_p[M]\bar{n}/N_a V \qquad (8a)$$

$$V = k_p[M]\bar{n}/N_a R_p \qquad (8b)$$

The value of the propagation rate constant k_p is characteristic of the free radical polymerization of acrylamide and hence the literature values (6000-18000 liter/mole·sec, depending on pH) should be

applicable. The average of these values (12000 liter/mole·sec) is used in the following calculations. The total number of particles N can be calculated knowing the average particle volume V and the total disperse phase volume V_m:

$$N = V_m/V \cdot \qquad (9)$$

This value of N can be compared with the value of N determined from electron microscopic measurements of overall particle diameter in order to understand the effect of multicellular latex morphology on the polymerization mechanism. Results are shown in Table 5.6 and Figures 5.32a-d. The number of particles determined from electron microscopic measurement of particle size is generally much smaller than the number of particles calculated from the polymerization rated over the temperature range of 50 to 60°C. This indicates that the overall multicellular particle cannot be considered to be a single, segregated polymerization reactor. However, the ratio of the number of particles calculated from the polymerization rate to the number of particles measured by electron microscopy is fairly constant (10.4 ± 2.64) over the temperature range from 50 to 60°C (Table 5.7). Earlier calculations had shown that the average number of radicals per particle had a value typical of emulsion polymerization; apparently the multicellular structure simply affects the degree of subdivision in the system.

Further evidence that the emulsifier's structure affects the degree of subdivision and hence the number of particles is found by

TABLE 5.6 Calculation of No. Particles/ml from Polymerization Rate and From TEM
KPS Initiator

T	[I]	$N_{calc} \times 10^{17}$				$N \times 10^{17}$ measured by TEM			
		[ε]=3	6	9	12	3	6	9	12
50	0.01	11.8	3.97	4.92	14.2	1.04	1.56	2.37	1.58
	0.04	16.9	5.56	7.23	21.1	1.56	2.33	3.55	2.37
	0.07	24.1	7.74	9.95	29.7	0.95	1.42	2.15	1.44
	0.10	16.6	5.04	6.65	20.6	0.63	0.95	1.44	0.96
55	0.01	55.6	20.6	9.83	27.3	0.206	0.308	0.713	0.476
	0.04	82.3	30.3	13.9	39.5	0.308	0.46	1.06	0.713
	0.07	37.2	13.3	6.18	17.8	0.427	0.638	1.48	0.987
	0.10	25.3	9.18	4.04	12.0	0.286	0.427	0.99	0.66
60	0.01	14.6	5.07	2.34	6.57	0.206	0.308	0.713	0.476
	0.04	20.6	7.09	2.56	7.78	0.308	0.461	1.06	0.713
	0.07	8.96	2.86	1.04	3.09	0.427	0.639	1.48	0.987
	0.10	5.76	1.88	0.631	1.65	0.285	0.427	0.987	0.66
65	0.01	2.77	1.09	1.39	3.15	1.04	1.56	2.37	1.58
	0.04	3.66	1.52	1.98	3.98	1.56	2.33	3.55	2.38
	0.07	4.83	20.7	2.67	5.08	0.95	1.41	2.15	1.43
	0.10	3.01	1.38	1.83	3.19	0.63	0.947	1.44	0.962

$N_{calc}/N_{TEM} = 10.4$ $\quad N_{calc} = 10.4\ N_{TEM}$

Figure 5.32

Correlation Between Calculated (N_c) and Measured (N_m) Numbers of Particles

KPS Initiator

a. T=50 C

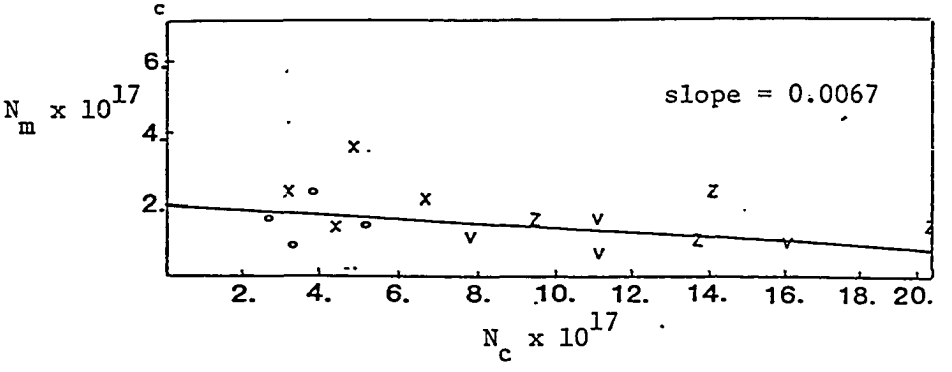

b. T = 55 C

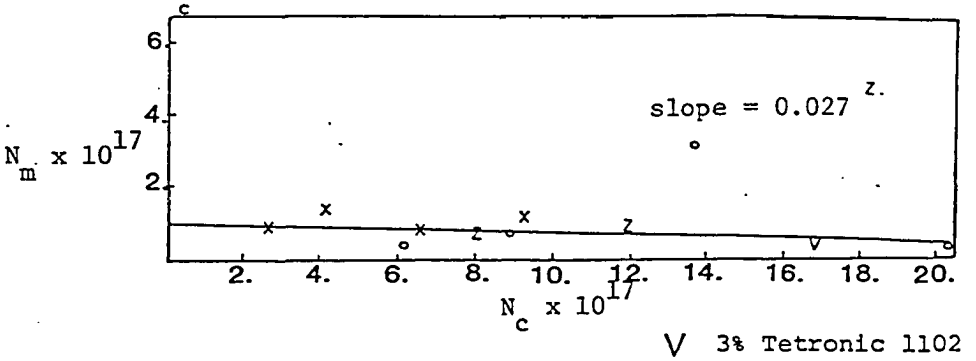

V 3% Tetronic 1102

O 6% Tetronic 1102

X 9% Tetronic 1102

Z 12% Tetronic 1102

Figure 5.32 (Continued)

c. T = 60 C

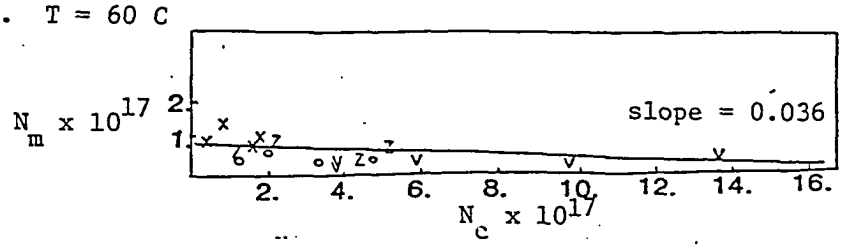

d. T = 65 C

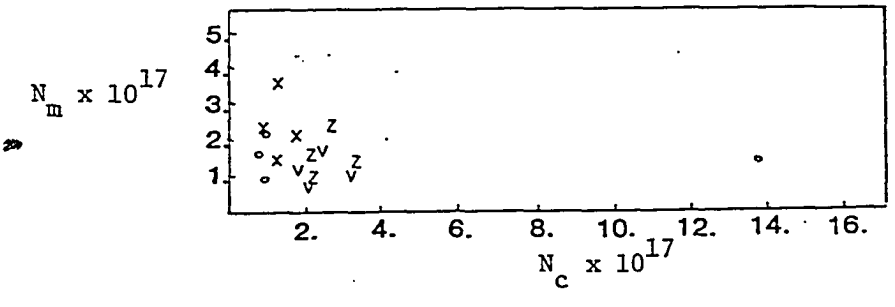

V 3% Tetronic 1102

O 6% Tetronic 1102

X 9% Tetronic 1102

Z 12% Tetronic 1102

TABLE 5.7

Correlation Between N_{calc} and N_{TEM}

KPS (N/ml)

T	[I]	N_{calc}/N_{TEM} [E]=3	6	9	12
50	0.01	11.3	2.54	2.08	8.98
	0.04	10.8	2.38	2.04	8.90
	0.07	25.3	5.45	4.63	20.6
	0.10	26.3	5.30	4.62	21.4
55	0.01	269.	66.9	13.7	57.3
	0.04	267.	65.8	13.1	55.4
	0.07	87.1	20.8	4.17	18.0
	0.10	88.4	21.5	4.08	18.1
60	0.01	7.76	16.5	3.28	13.8
	0.04	66.8	15.4	2.41	10.9
	0.07	20.9	4.47	0.703	3.13
	0.10	20.2	4.40	0.640	2.50
65	0.01	2.66	0.699	0.586	1.99
	0.04	2.35	0.652	0.558	1.67
	0.07	5.08	14.7	1.24	3.55
	0.10	4.78	1.45	1.27	3.32

considering the data at 65°C, which is above the melting temperature of the surfactant. At 65°C, the ratio of the calculated number of particles to the microscopically measured number of particles is 2.22 ± 0.75. This lower ratio may be due either to the formation of solid latex particles or to the structure of the surfactant molecule during the polymerization.

Since the average value of this ratio for the few latexes polymerized at lower temperature which did not form multicelled latexes (8.6 ± 1.05) is within the range for latexes prepared at 50 to 60°C, the structure of the surfactant molecule during polymerization, and not the final latex morphology, affects the number of particles in the system.

Since the measured and calculated values of the number of particles differ by a constant factor over the temperature range from 50 to 60°C, the propagation rate constant can be generated over this range by plotting the polymerization rate as a function of the reciprocal of the measured particle volume using equation (8a) in Figures A.13-A.16. The value of k_p calculated from the slope of this plot is (1.06 ± 0.45) x 10^4 liter/mole·sec, which is within the range of literature values for k_p, and is independent of temperature of polymerization over the range of 50-65°C used in this study.

Smith-Ewart case 2 kinetics predict that the number of particles should vary, in the initial linear region, with the 3/5 power of emulsifier concentration and the 2/5 power of the initiator concentration; the Medvedev model predicts that N should vary with

the 1/2 power of the initiator concentration. Both the measured and calculated values of the number of particles are plotted as functions of the emulsifier and initiator concentrations (Table 5.8, Figures 5.33-5.40). The plot of number of particles as a function of initiator concentration has the same slope for both the calculated and measured numbers of particles. The curves show generally the same shape, i.e. an initial rise followed by a leveling off or decrease at higher initiator concentrations, although there is more scatter in the data for the calculated number of particles. the slope of this curve is approximately 0.40 at polymerization temperatures of 50 to 60°C and 0.29 at polymerization temperature of 65°C. This lower dependence of the number of particles on the initiator concentration further indicates that the degree of subdivision of the polymer phase has become less important. The data for the calculated number of particles as a function of emulsifier concentration shows much scatter, so the relationship between the number of particles and the emulsifier concentration is studied using only the number of particles measured microscopically. The relationship between the measured number of particles and the emulsifier concentration is initially linear followed by a plateau or decreasing region. The slope of this relationship is 0.6 in the polymerization temperature range from 50 to 60°C, in good agreement with the value predicted by Smith-Ewart Case 2. At 65°C, this relationship is much stronger (slope 1.07). In earlier work (5.11), this was attributed to initiation in monomer droplets. However, in the present system

TABLE 5.8. Calculation of Rate/Particle

KPS

T	[I]	gr/sec x 10^{17} $(R_p/N_{tem}/m.)\cdot 32.1\times10^{-3}$ [E]=3	6	9	12	$\bar{V}$ x 10^5 $\bar{V}_{particle,nm}$ 3 = $10^{24}/N_{tem}$ [E]=3	6	9	12
50	0.01	1.63	3.91×10^{-1}	3.12×10^{-1}	1.3	2.98	2.00	1.31	1.96
	0.04	1.60	3.86×10^{-1}	3.16×10^{-1}	1.29	2.00	1.34	0.878	1.31
	0.07	3.75	0.972	0.746	3.03	3.29	2.20	1.45	2.16
	0.10	3.87	0.946	0.758	3.08	4.92	3.29	2.16	3.23
55	0.01	38.9	9.59	2.03	8.29	15.1	10.1	4.37	6.53
	0.04	38.5	9.49	2.12	8.15	10.1	6.76	2.92	4.37
	0.07	12.6	3.07	0.65	2.67	7.29	4.88	2.10	3.15
	0.10	12.8	3.16	0.65	2.67	10.9	7.29	3.14	4.72
60	0.01	10.4	2.60	0.54	2.22	15.1	10.1	4.37	6.54
	0.04	10.4	2.58	0.55	2.21	10.1	6.76	2.92	4.37
	0.07	3.38	0.804	0.17	0.715	7.29	4.88	2.10	3.15
	0.10	3.38	0.827	0.163	0.729	10.9	7.29	3.15	4.72
65	0.01	0.732	0.107	0.0867	0.345	2.98	2.00	1.31	1.96
	0.04	0.432	0.106	0.085	0.351	2.00	1.34	0.879	1.31
	0.07	1.01	0.250	0.194	0.831	3.28	2.20	1.45	2.16
	0.10	1.02	0.254	0.20	0.834	4.93	3.29	2.16	3.24

Figure 5.33

Correlation Between Number of Particles (N) and Emulsifier Concentration

KPS Initiator

Polymerization Temperature = 50°C

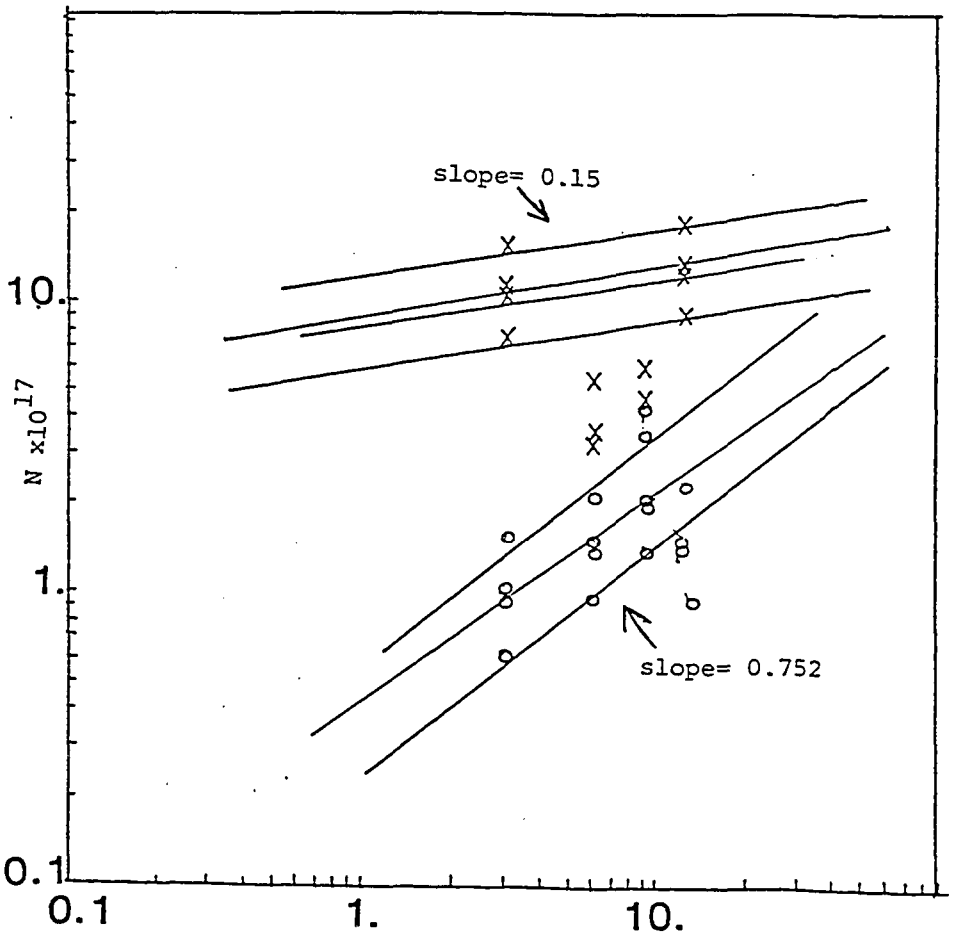

Figure 5.34

Correlation Between Number of Particles (N) and Emulsifier Concentration

KPS Initiator

Polymerization Temperature = 55°C

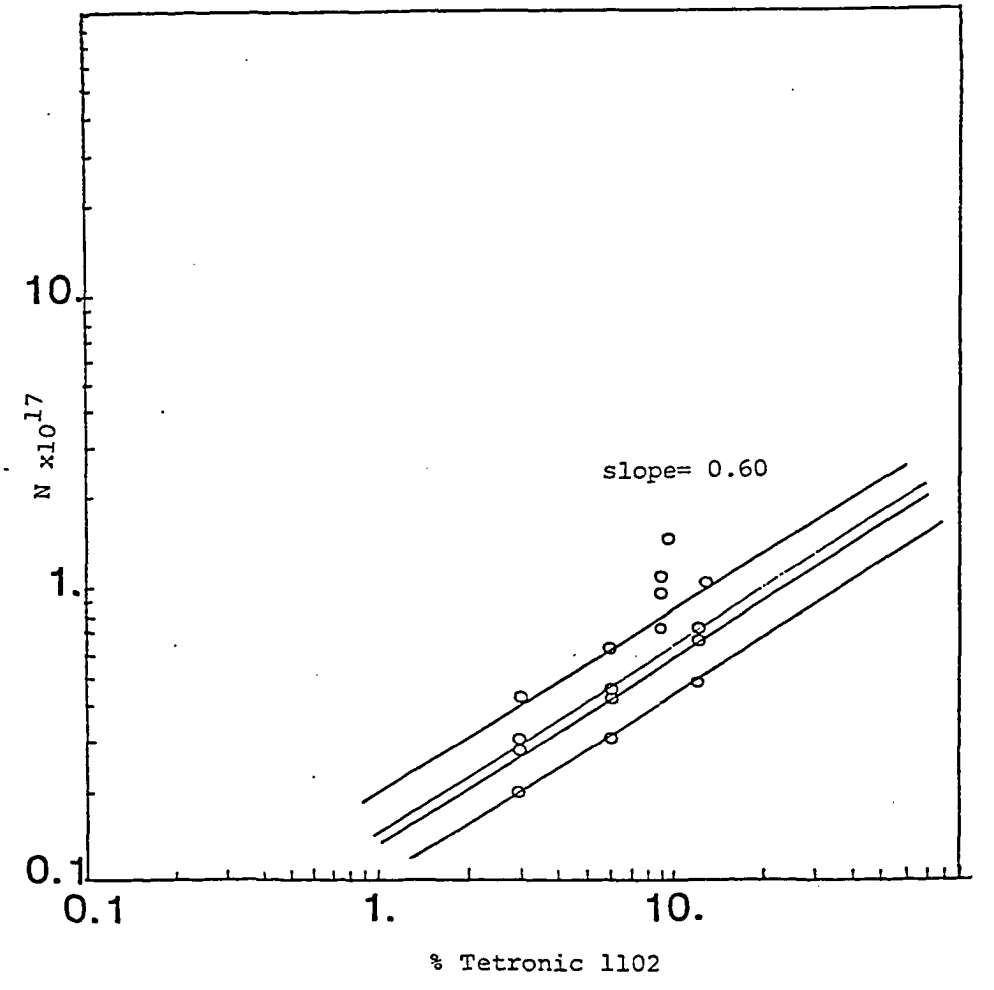

169

X calculated

O measured

Figure 5.35

Correlation between Number of Particles (N) and Emulsifier Concentration

KPS Initiator

Polymerization Temperature = 60°C

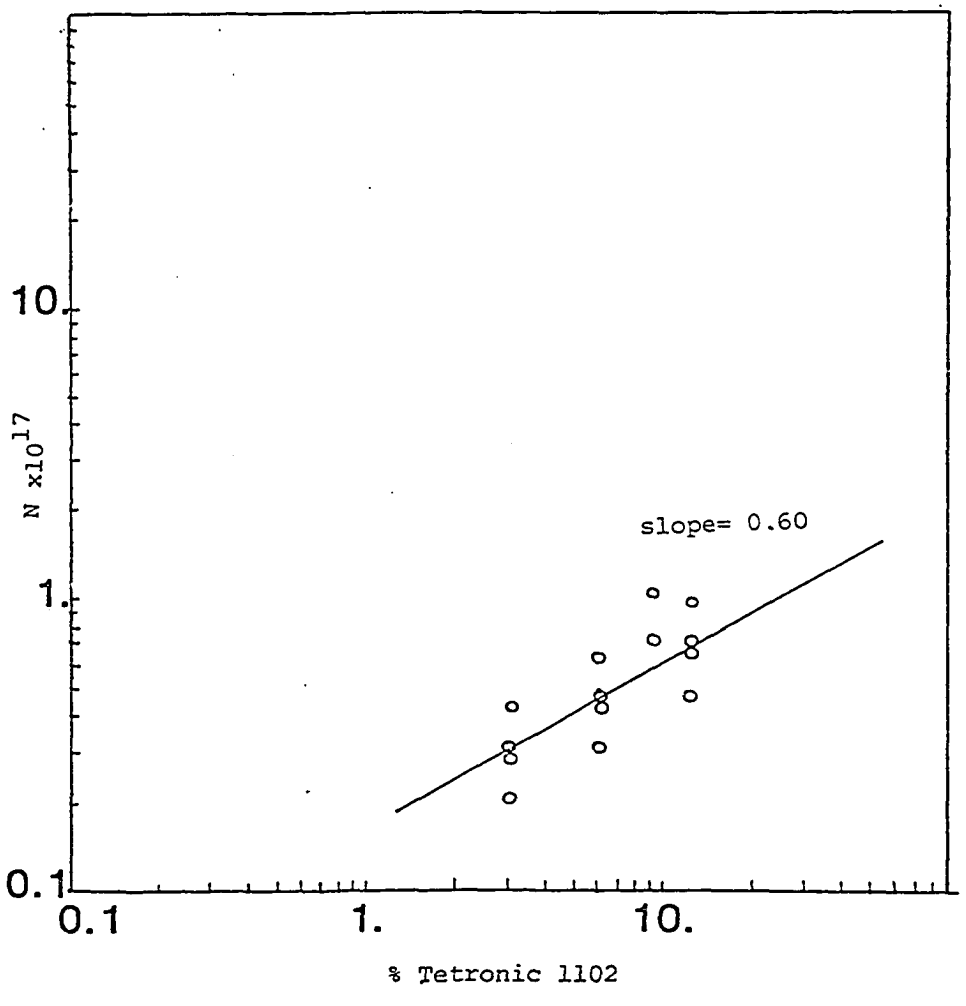

170

O measured

Figure 5.36

Correlation Between Number of Particles (N) and Emulsifier Concentration

KPS Initiator

Polymerization Temperature = 65°C

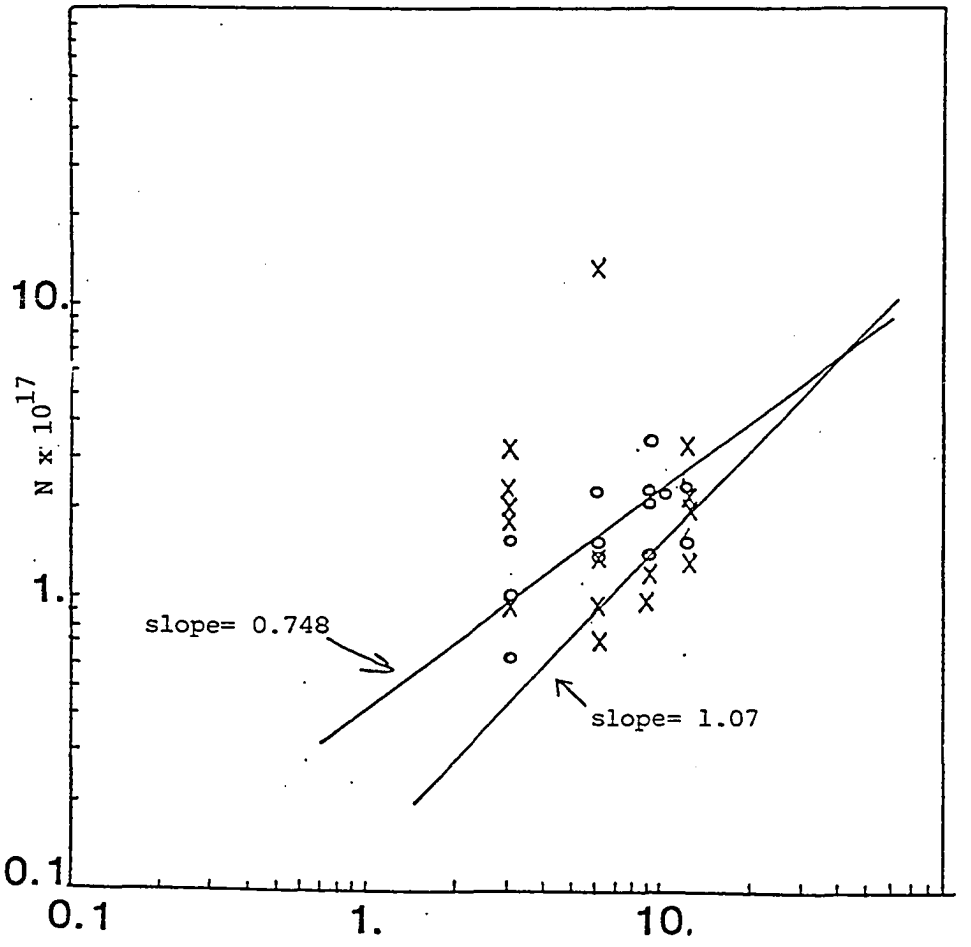

171

X calculated

o measured

Figure 5.37

Correlation Between Number of Particles (N) and Initiator Concentration

KPS Initiator

Polymerization Temperature= 50° C

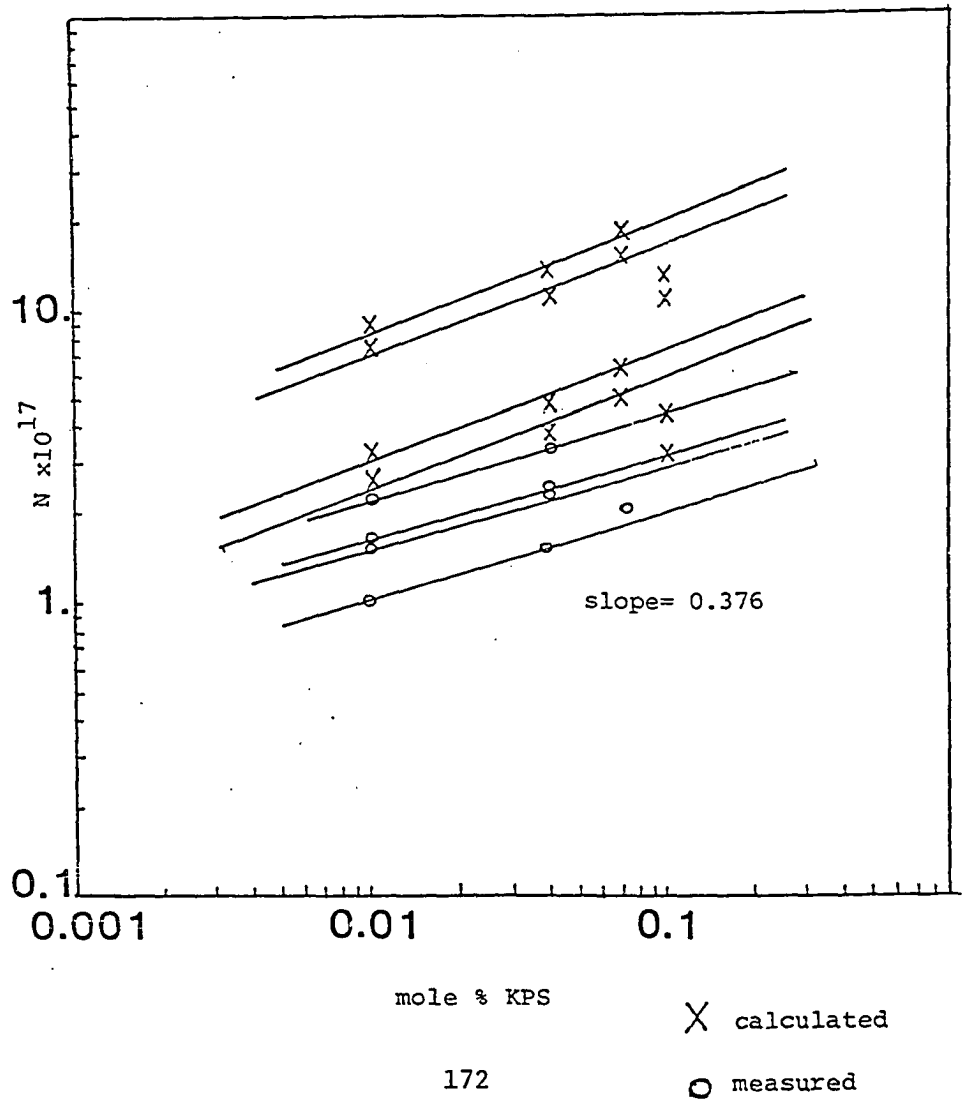

Figure 5.38

Correlation Between Number of Particles (N) and Initiator Concentration

KPS Initiator

Polymerization Temperature= 55°C

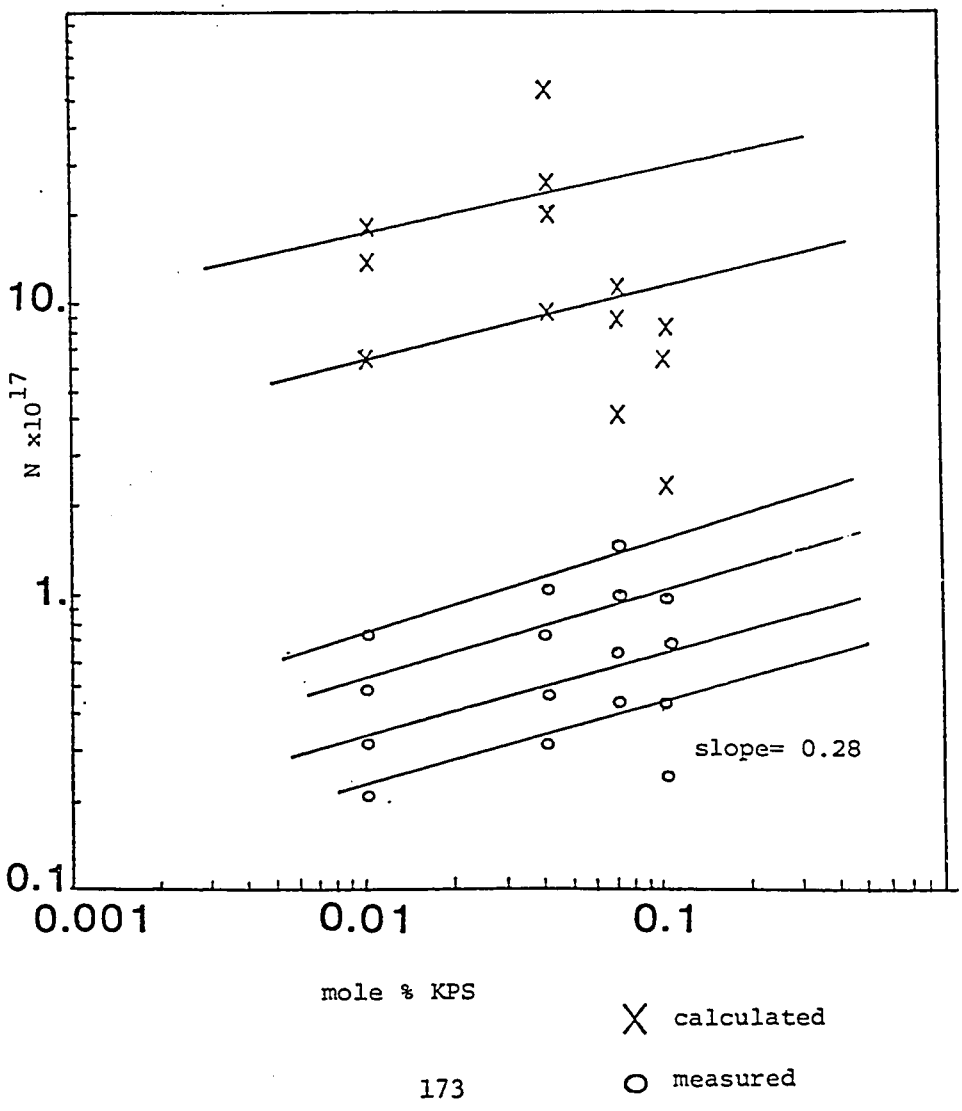

Figure 5.39

Correlation Between Number of Particles (N) and Initiator Concentration

KPS Initiator

Polymerization Temperature= 60 C

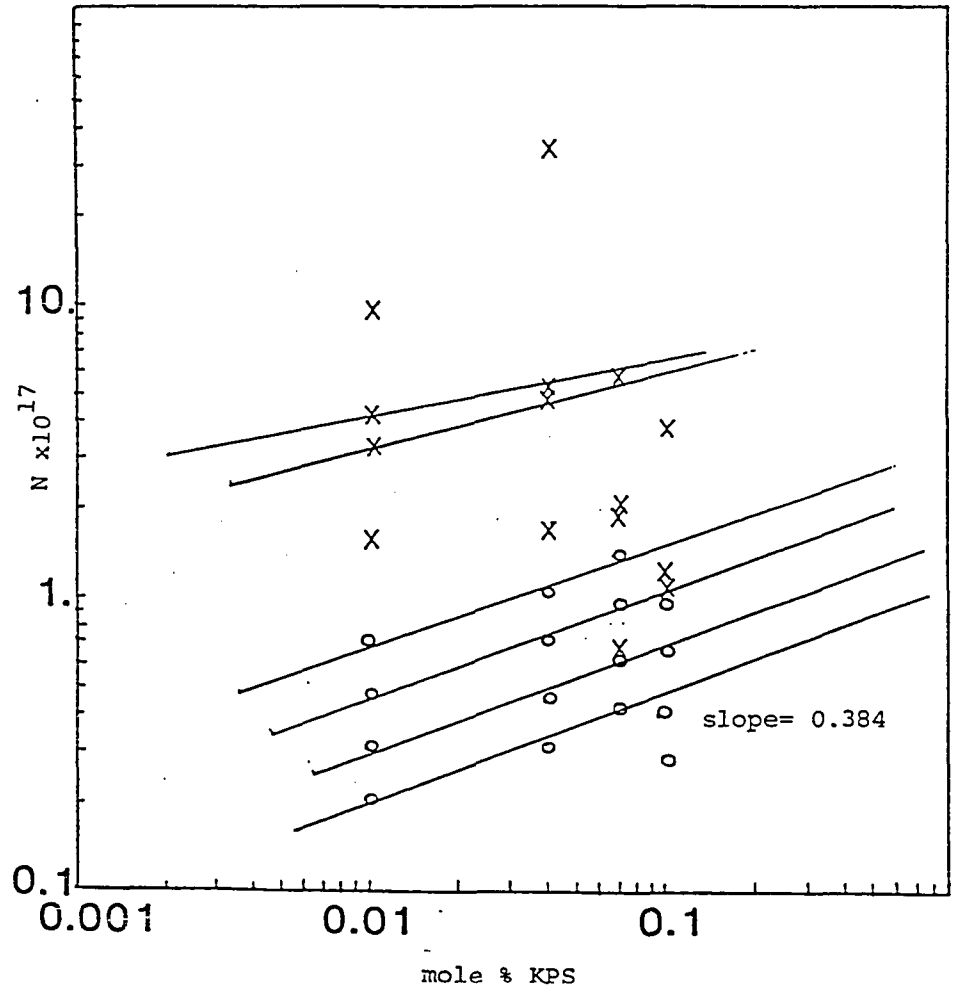

Figure 5.40

Correlation Between Number of Particles (N) and Initiator Concentration

KPS Initiator

Polymerization Temperature = 65°C

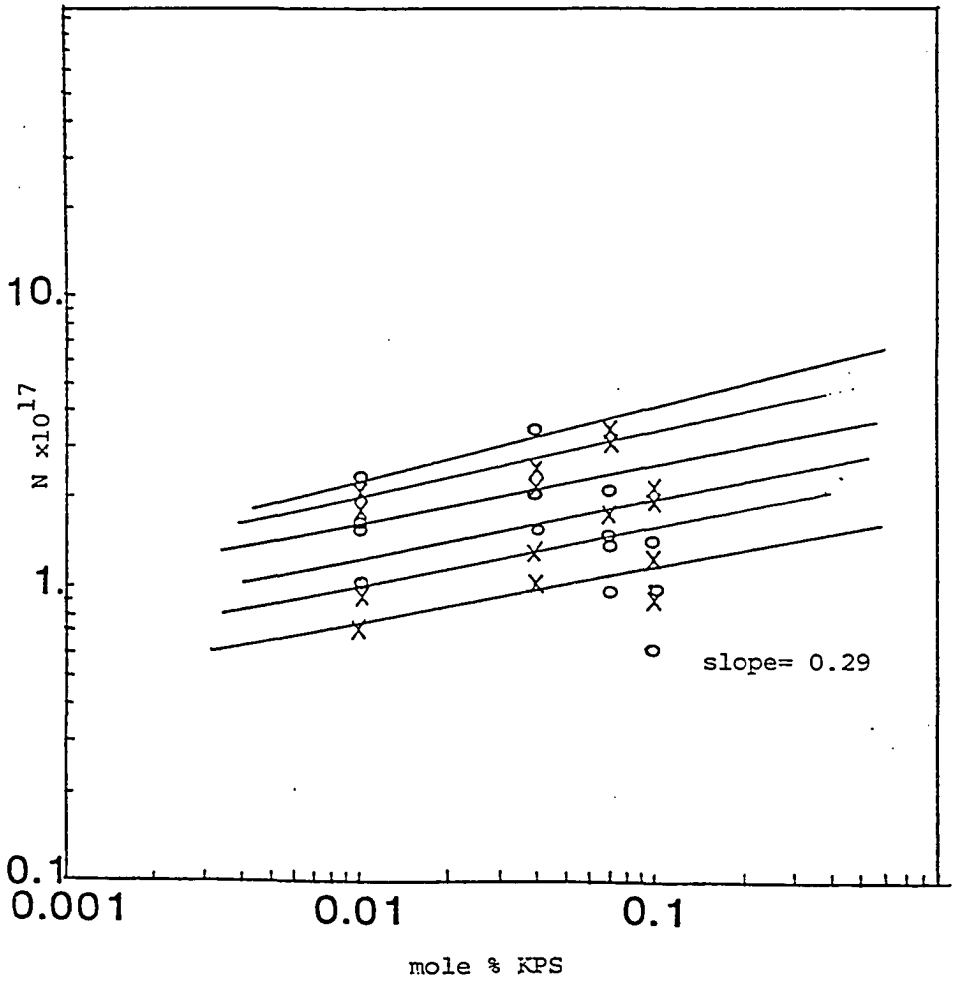

it is probably due to the high interfacial tension of the surfactant at 65°C. High interfacial tension indicates that the surfactant will preferentially partition into the continuous phase; hence surface area maximization is favored, and as a result adding emulsifier forms new particles rather than increasing aggregation.

The variation of rate per particle with average particle volume is shown in Figures A.17-A.22. Rate per particle is independent of temperature at all particle volumes. The slopes of these plots increase only slightly as temperature increases. In all cases, the slope is between 2.01 and 2.6, which is higher than expected for emulsion polymerization and indicates that the subivision effect is less important in this system than in a conventional emulsion polymerization.

At a given initiator concentration and emulsifier concentration, the number of particles decreases as temperature increases (Figure 5.41). The number of particles increases with increasing emulsifier concentration up to a limiting value, then decreases as emulsifier concentration increases further.

The degree of polymerization is related to the initiator concentration in the following way:

$$1/\bar{x}_n = 1/z\ (k_t/k_p{}^2 f\ k_d[I])^{1/2}(1/[M]) + k_{tr}/k_p \qquad (9)$$

where $\bar{x}$ is the number-average degree of polymerization and k_{tr} is the rate constant for chain transfer to monomer. A plot of $1/\bar{x}_n$ as

Figure 5.41

Correlation Between Measured Number of Particles and Polymerization Temperature

KPS Initiator

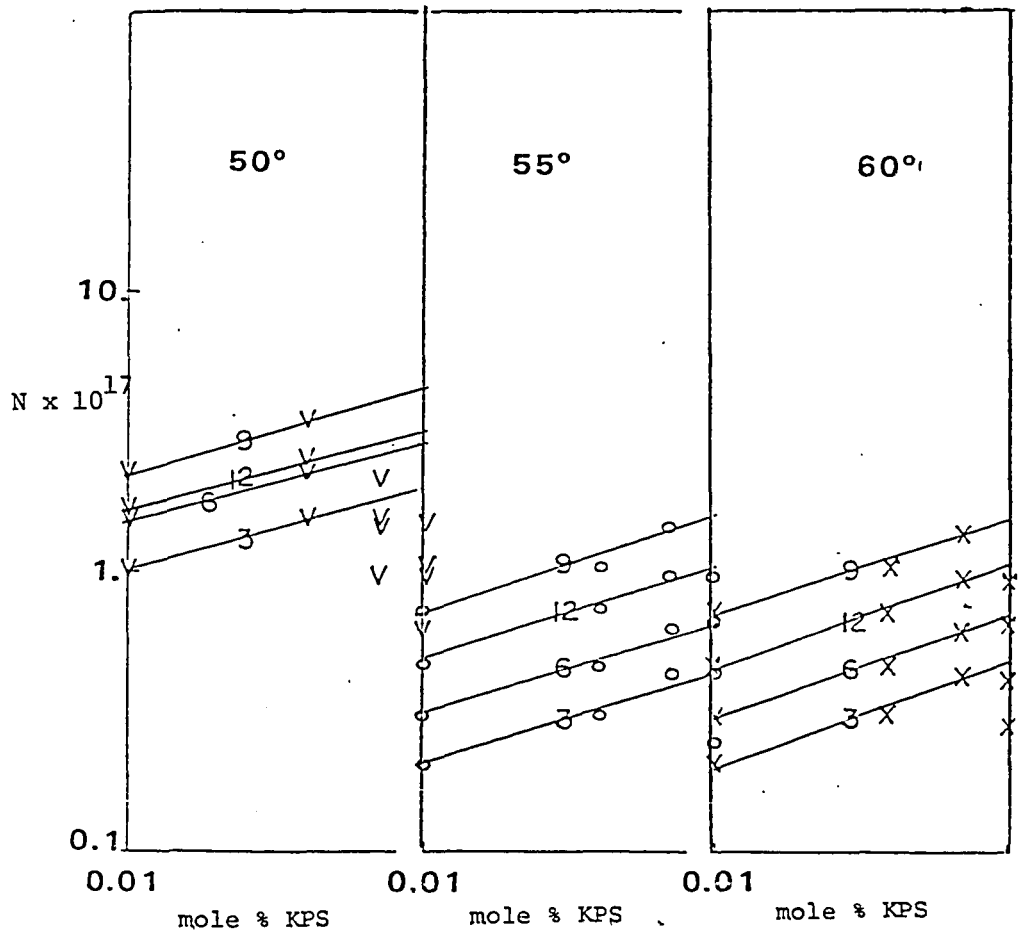

a function of the square root of the initiator concentration will have a slope of $1/z(k_t/k_p^2 f\ k_d)^{1/2}1/[M]$ and intercept of k_{tr}/k_p. In these experiments, $\bar{M}_w$ has been determined rather than $\bar{M}_n$, so the weight-average degree of polymerization $\bar{x}_w$ ($\bar{x}_w = \bar{M}_w/M_o$) will be used to prepare this plot (Figures 5.42-5.45). Polymer molelcular weights are given in Table 5.9. Since these polymers appeared from chromatograms to have fairly narrow molecular weight distributions, use of $\bar{x}_w$ rather than $\bar{x}_n$ will merely introduce a small error in the value of k_{tr}/k_p. The initiator efficiency factor f and the termination rate constant k_t can be determined by combining the value of fk_t calculated from equation 9 with the value of f/k_t determined from the following relationship between the polymerization rate and the square root of the initiator concentration:

$$R_p = z(k_p^2[I]/k_t\ fk_d)^{1/2}[M] \qquad (10)$$

The values of f, k_{tr}, and k_t determined in this way are given in Table 5.10. The transfer rate constant varies from 0.03 to 0.26 liter/mole·sec, which is in the range of the literature value of the rate constant for transfer to acrylamide monomer (0.22 liter-/mole·sec) in solution polymerization. The average value of the initiator efficiency factor f is 0.62, which is rather low but still within the range expected for free radical polymerization. This somewhat depressed value for f may indicate that initiator radicals are trapped within a solvent cage, but more likely it is simply the result of high internal viscosity; high viscosity has been observed

Figure 5.42

Correlation Between Polymer Molecular Weight and Initiator Concentration

KPS Initiator

Polymerization Temperature= 50° C

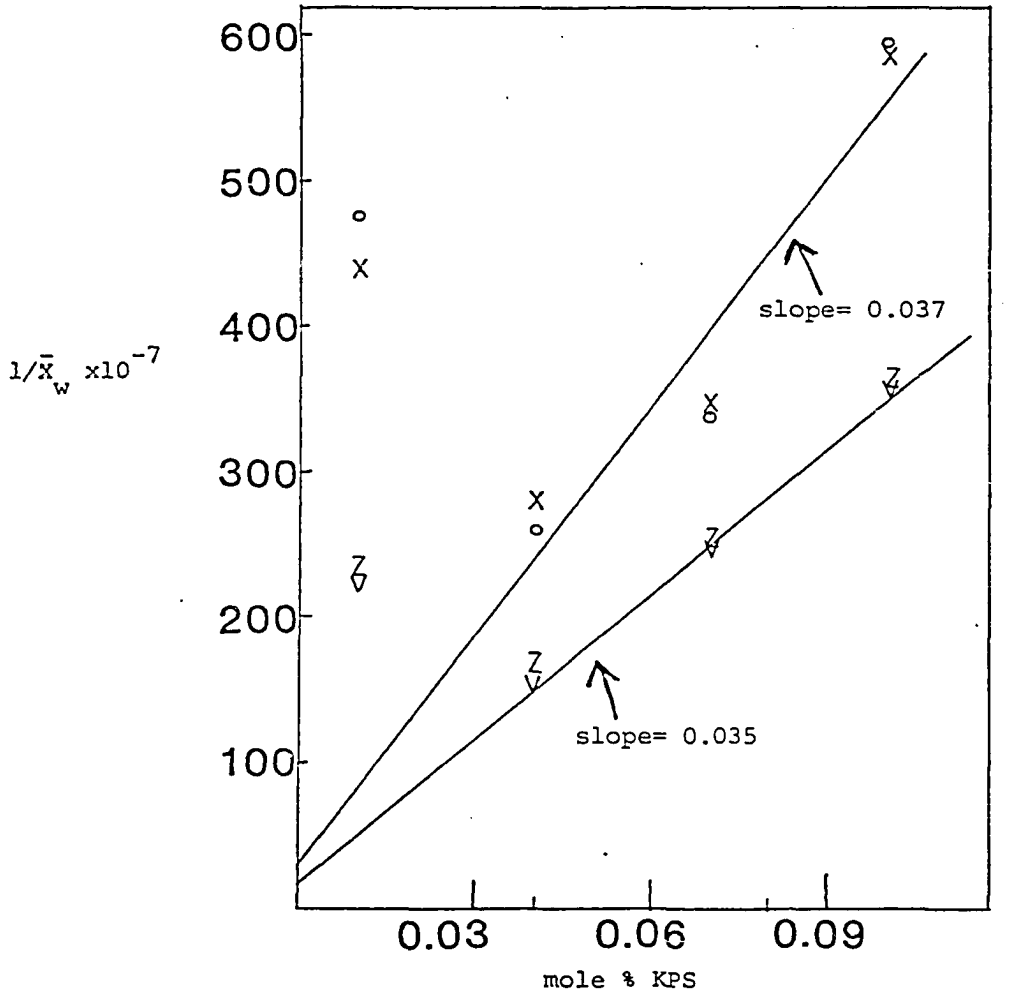

V 3% Tetronic 1102

o 6% Tetronic 1102

X 9% Tetronic 1102

Z 12% Tetronic 1102

Figure 5.43

Correlation Between Polymer Molecular Weight and Initiator Concnetration

KPS Initiator

Polymerization Temperature= 55° C

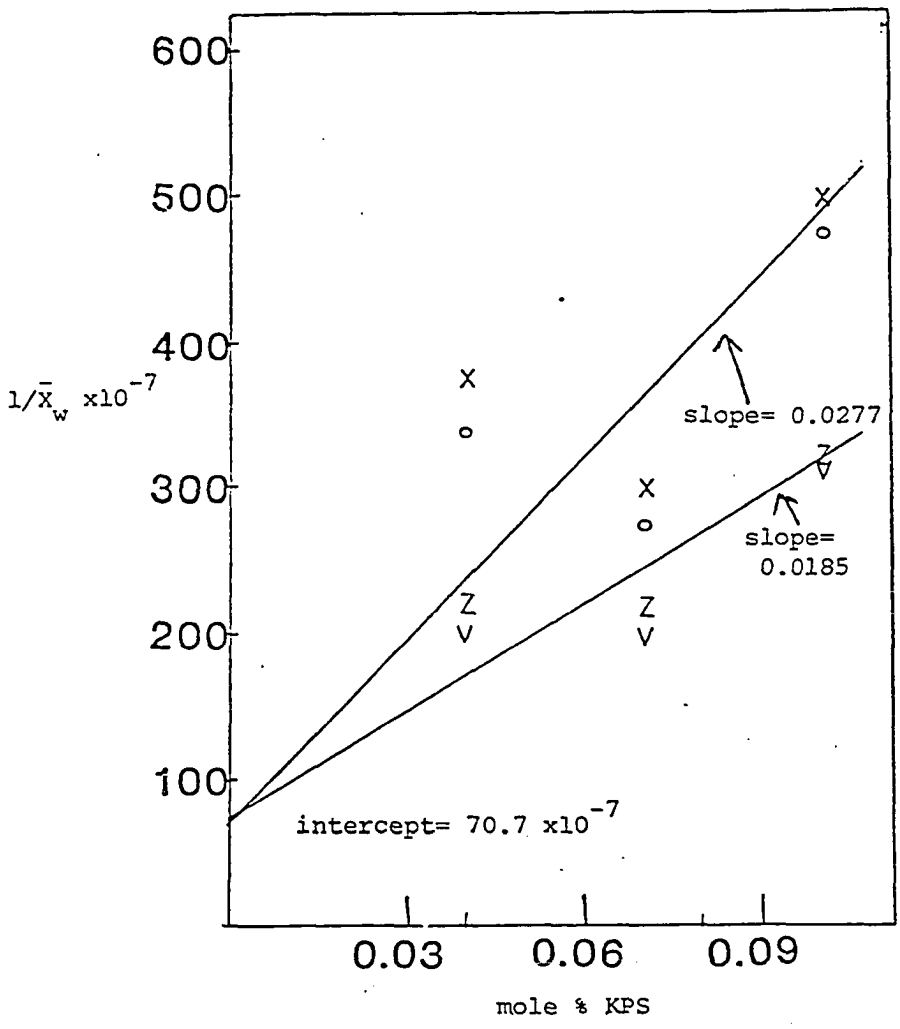

V 3% Tetronic 1102

X 9% Tetronic 1102

o 6% Tetronic 1102

Z 12% Tetronic 1102

Figure 5.44

Correlation Between Polymer Molecular Weight and Initiator Concentration

KPS Initiator

Polymerization Temperature= 60°C

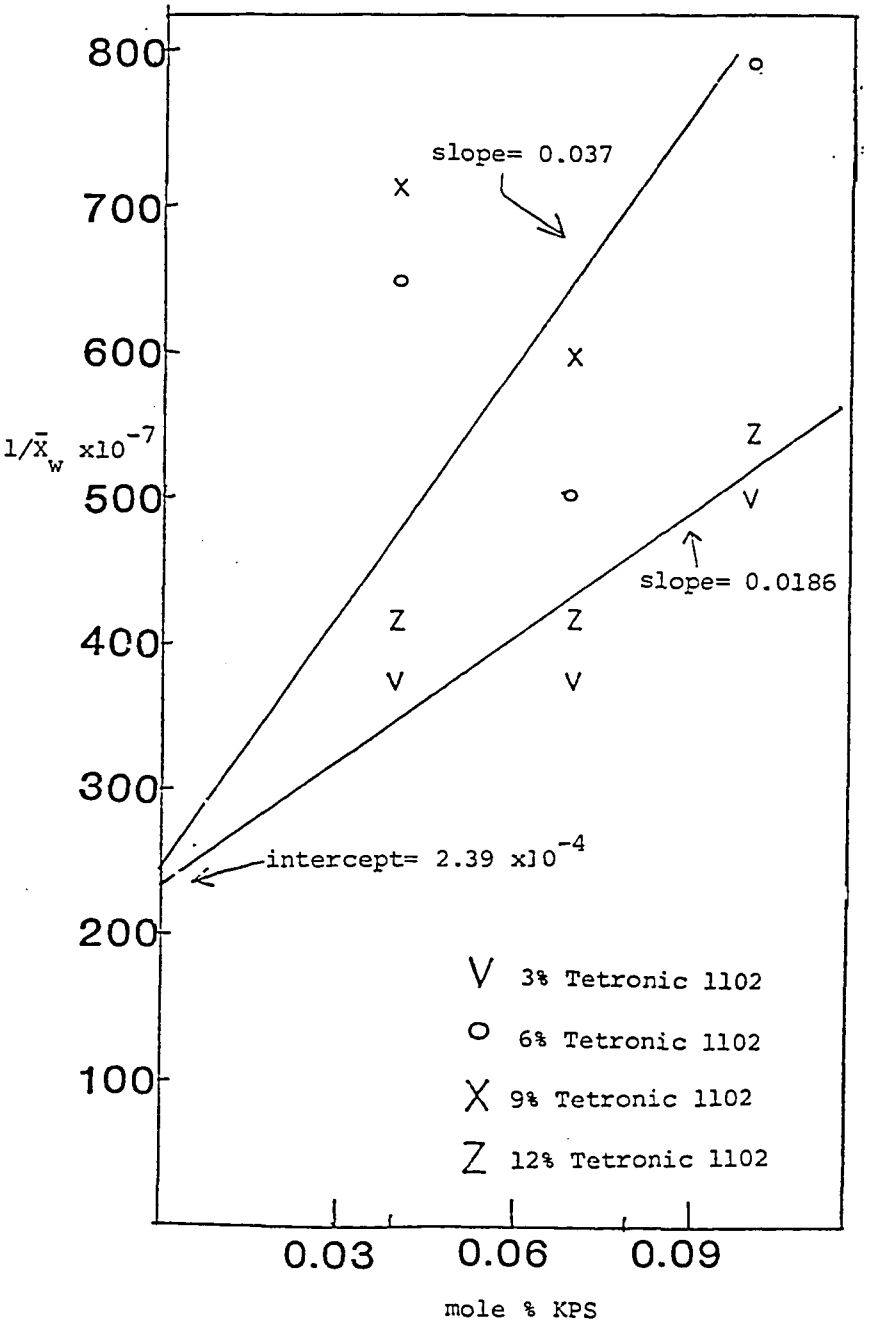

Figure 5.45

Correlation Between Polymer Molecular Weight and Initiator Concentration

KPS Initiator

Polymerization Temperature= 65°C

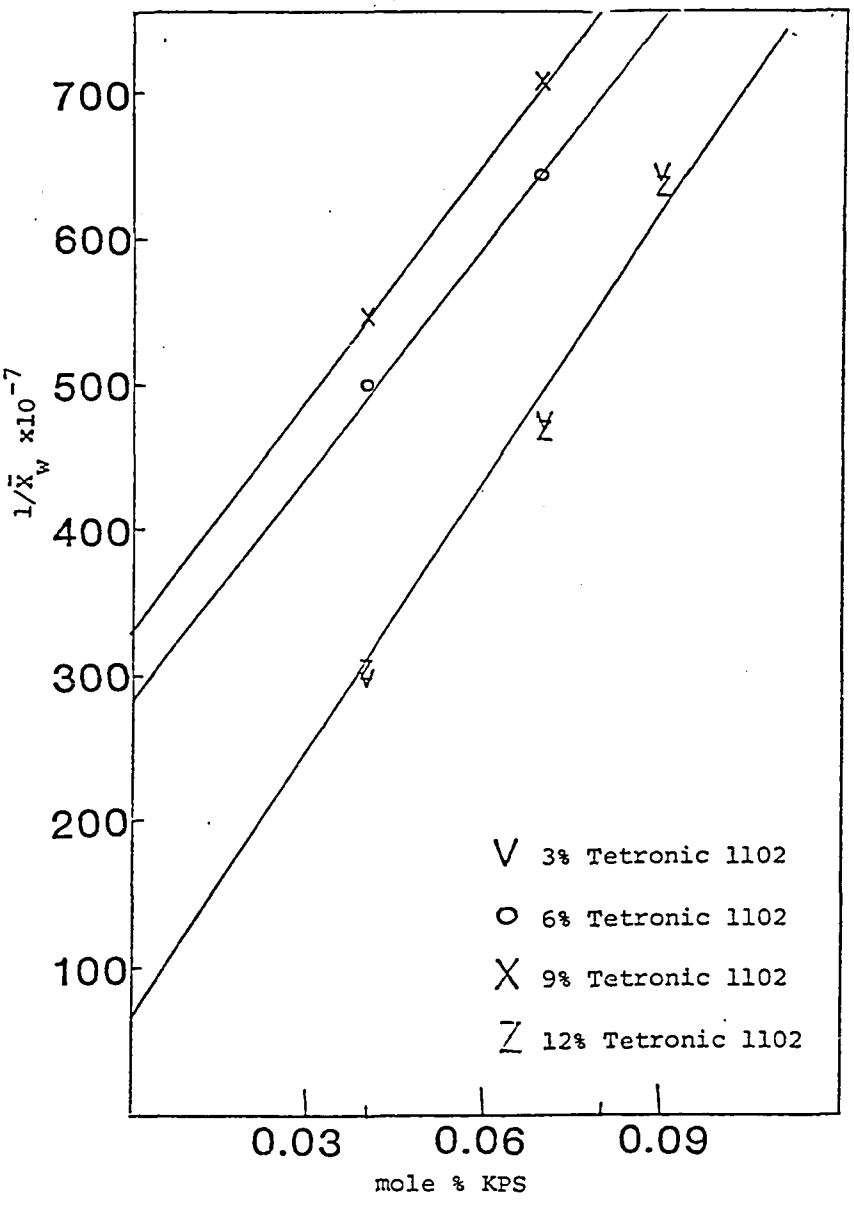

TABLE 5.9

MW of Latex

KPS Latexes

T	[I]	[E]			
		3	6	9	12
50	0.01	3.2×10^{6}	1.6×10^{6}	1.5×10^{6}	3.1×10^{6}
	0.04	4.5×10^{6}	2.7×10^{6}	2.5×10^{6}	4.3×10^{6}
	0.07	2.9×10^{6}	2.1×10^{6}	2.0×10^{6}	2.8×10^{6}
	0.10	2.0×10^{6}	1.2×10^{6}	1.2×10^{6}	2.0×10^{6}
55	0.1	2.5×10^{6}	1.2×10^{6}	1.1×10^{6}	2.3×10^{6}
	0.4	3.6×10^{6}	2.1×10^{6}	1.9×10^{6}	3.2×10^{6}
	0.07	3.6×10^{6}	2.6×10^{6}	2.3×10^{6}	3.2×10^{6}
	0.10	2.6×10^{6}	1.5×10^{6}	1.4×10^{6}	2.2×10^{6}
60	0.01	1.5×10^{6}	7.1×10^{6}	6.3×10^{6}	1.3×10^{6}
	0.04	1.9×10^{6}	1.1×10^{6}	9.9×10^{5}	1.7×10^{6}
	0.07	1.9×10^{6}	1.4×10^{6}	1.2×10^{6}	1.7×10^{6}
	0.10	1.4×10^{6}	8.7×10^{5}	7.7×10^{5}	1.3×10^{6}
65	0.01	1.8×10^{6}	8.9×10^{5}	8.6×10^{6}	1.7×10^{6}
	0.04	2.4×10^{6}	1.4×10^{6}	1.3×10^{6}	2.3×10^{6}
	0.07	1.5×10^{6}	1.1×10^{6}	1.0×10^{6}	1.5×10^{6}
	0.10	1.1×10^{6}	7.0×10^{5}	6.7×10^{6}	1.1×10^{6}

TABLE 5.10

Values of k_{tr} , k_t and f

KPS

T, °C	$k_{tr}/k_p x10^{-7}$	k_{tr}	f	$k_t x10^3$
50	29.	0.032	0.74	2.06
55	70.7	0.055	0.74	1.75
60	240.	0.264	0.68	1.85
65	223.	0.245	0.34	0.67

to increase the lifetime of caged radicals (5.15). The termination rate constant ranges from 670 to 2060 liter/mole·sec. This value is approximately three orders of magnitude lower than the literature value for solution polymerization.

The polymer molecular weight shows the expected direct dependence on polymerization rate (Figures A.23-A.26).

b. ADVN System

The approach used above to generate the kinetic parameters for KPS-initiated polymerizations cannot be used for azo initiated polymerizations because solution polymerization of acrylamide could not be effected using the highly water-insoluble ADVN, and hence the subdivision factor cannot be calculated from the polymerization rates measured under the same conditions in emulsion and in solution unless one makes the tenuous assumption that f, kp, and kt are all the same in KPS and ADVN systems. However, the subdivision of an emulsion polymerization system can also be affected by agitation, since average particle volume decreases as agitation rate increases. Polymerization rate is inversely proportional to average particle volume (equation 8a). Hence changing particle volume by changing agitation rate will change polymerization rate proportionally. The difference in effective (calculated) and measured particle volumes was found in the KPS system to be a constant factor. Polymerization rate and particle volume are measured at varying agitation rates in the ADVN system in order to calculate this constant factor.

Measuring polymerization rate as agitation rate increases

shows that the polymerization rate increases gradually as agitation rate increases up to 500 rpm, then polymerization rate sharply increases (Figure 5.46). Measuring particle volumes and polymerization rates at the varying agitation rate shows that the ratio of pairwise comparisons of the particle volumes to the polymerization rates yields a constant factor (Table 5.11):

$$\frac{V_1^{TEM}/V_2^{TEM}}{R_{p1}/R_{p2}} = 1.74 \pm 0.55$$

This value of this factor is much smaller than the value of 10.4 ± 2.64 found in the KPS system. This difference between the KPS and ADVN systems may be related to the mode of initiation and will be discussed later.

This factor will not be applied to polymerizations carried out at 65°C because this is above the melting point of the surfactant; after rate constants are calculated, the effective particle volume will be calculated from the rate of polymerization using the following equation:

$$R_p = z(f\, k_d\, k_p[I]/k_t)^{1/2}[M]$$

Measuring polymerization rate as a function of the square root of the initiator concentration permits estimation of the factor z. Knowing z, a can be calculated using the graphical method suggested by van der Hoff (5.8) and then the average particle volume can be

Figure 5.46

Effect of Agitation Rate on Polymerization Rate

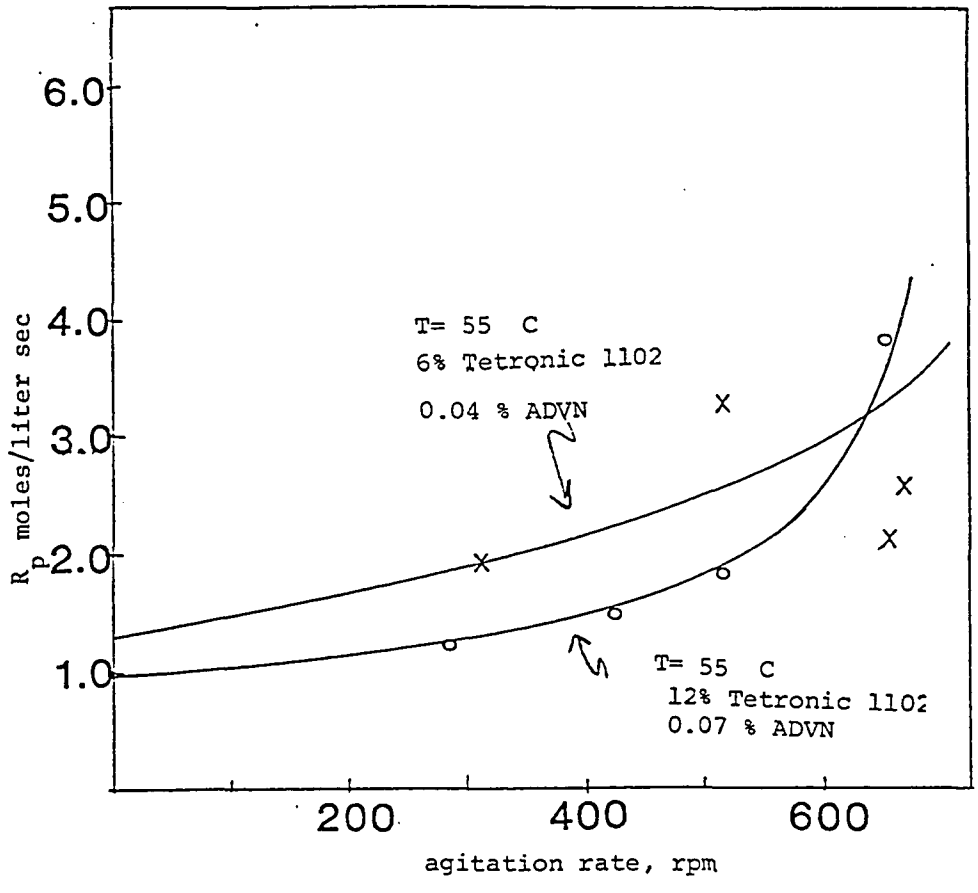

TABLE 5.11. Polymerization Rate and Measured Particle Volume at Varying Agitation Rates

Recipe

T = 55°C

0.04% ADVN

6% Tetronic 1102

Agitation Rate, rpm	$\bar{D}_v$, nm	V, $nm^3 \times 10^5$	R_p moles/liter·sec
280	83.3	3.03	0.0124
425	51.0	0.69	0.015
520	60.0	1.13	0.0182
655	51.5	0.715	0.038
665	58.7	1.05	0.064

$\frac{rpm_1}{rpm_2}$	$\frac{280}{310}$	$\frac{280}{425}$	$\frac{280}{520}$	$\frac{280}{655}$	$\frac{310}{425}$	$\frac{310}{520}$	$\frac{310}{655}$	$\frac{425}{520}$	$\frac{425}{655}$
V_2/V_1	0.462	0.492	0.373	0.236	0.49	0.807	0.51	0.61	0.96
R_{p2}/R_p	1.01	1.69	1.82	1.38	3.57	1.78	1.36	1.35	0.40

F = 1.745 $\quad 1.745 \pm 0.55$

S = 0.785

calculated using equation (6). Results of these calculations will be discussed later.

The values of the parameters a and z can be calculated using the following equation suggested by Vanderhoff (5.11) in which the subscripts A and P denote the azo-initiated and persulfate-initiated polymerizations, respectively.

$$a_A z_A = a_p Z_p (V_A/V_p)(R_{pA}/R_{pp}).$$

Results of these calculations are shown in Table 5.12. The values of az are all very small, ranging from 0.03 to 0.7; according to the theoretical analysis of van der Hoff (5.8), such low values of az indicate that radicals are generated in or enter particles in pairs. This result is unexpected for an initiator soluble in the continuous phase, but is consistent with the findings of Vanderhoff et al. (5.11) for the inverse emulsion polymerization of sodium styrene sulfonate in o-xylene with Span 60 emulsifier.

The average number of radicals per particle ($\bar{n}$) can be calculated from the value of az:

$$\bar{n} = az/4$$

The values of $\bar{n}$, which are all much less than 0.5 (Table 5.12), are in the regime of Smith-Ewart Case 1; this indicates that radical desorption occurs rapidly. In this case, determining the values of the parameters a and z individually is difficult because the relationship between them depends on the parameter m, which indicates the rate of radical transfer out of the particle relative to the

TABLE 5.12 Values of az and $\bar{n}$

ADVN

T	[I]	az				$\bar{n}$ = az/4			
		[E]=3	6	9	12	[E]=3	6	9	12
50	0.01	0.218	0.24	0.188	0.199	0.054	0.060	0.047	0.049
	0.04	0.238	0.232	0.184	0.227	0.059	0.058	0.046	0.056
	0.07	0.604	0.552	0.436	0.480	0.151	0.138	0.109	0.120
	0.10	0.612	0.559	0.628	0.486	0.153	0.134	0.157	0.121
55	0.01	0.0877	0.203	0.273	0.0727	0.022	0.051	0.068	0.018
	0.04	0.106	0.226	0.313	0.103	0.0265	0.056	0.078	0.026
	0.07	0.059	0.123	0.151	0.044	0.015	0.031	0.038	0.011
	0.10	0.034	0.058	0.079	0.022	0.009	0.015	0.019	0.006
60	0.01	0.434	0.330	0.646	0.460	0.108	0.082	0.161	0.115
	0.04	0.431	0.310	0.634	0.609	0.108	0.078	0.158	0.152
	0.07	0.246	0.459	0.436	0.283	0.062	0.115	0.109	0.071
	0.10	0.136	0.251	0.216	0.195	0.034	0.063	0.054	0.048

rate of radical termination within the particle:

$$m = vk_{de}/k_t^*$$

where v is the average particle volume, k_{de} is the rate "constant" for desorption, and k_t^* is the termination constant. In systems where desorption occurs, m is greater than zero. The value of m cannot be determined from these experimental data. k_{de} cannot be measured, and k_t^* cannot be equated with the termination rate constant in bulk because the termination constant is usually several orders of magnitude lower in emulsion than in homogeneous polymerization. Hence the most direct way to proceed with the calculation of a and z is to arbitrarily set m equal to a constant value. In the following analysis, m has been set equal to one. This value of m was also used by Vanderhoff et al. (5.11), so individual values of a and z can be determined from the value of az using the graphical method they suggest. To enhance the accuracy of this method, the values of a determined graphically are plotted against the square root of the initiator concentration. Generally the values of a obtained both ways agreed to within 30%. The values of a and z are given in Table 5.15.

Inspection of equation 7 shows that polymerization rate and the value of the parameter a should be linearly related. This relationship is found at polymerization temperature of 50°C, but at higher temperature a goes through a maximum (Figures A.27-A.32). Presence of a maximum indicates competition between two opposing parameters; in this function, either the subdivision factor z

decreases or particle volume increases as polymerization rate increases (Figures A.33-A.35). The data show that particle volume does indeed not decrease monotonically as polymerization rate increases at higher temperature. Apparently the state of subdivision of this system does not affect polymerization rate in the usual linear way, perhaps because desorption is facilitated by increased particle surface area and hence overall polymerization rate is lower when particles are larger. The variation of rate per particle with average particle volume also is affected by the system's state of subdivision in an unusual manner (Figures A.36-A.41). The slope of the rate per particle as a function of average particle volume is much steeper than expected for conventional emulsion polymerization, especially at higher temperatures, also indicating that the subdivision effect is less important in this system than in a conventional emulsion polymerization.

At a given initiator concentration and emulsifier concentration, the number of particles decreases as temperature increases (Figure 5.47). The number of particles increases with increasing emulsifier concentration up to a limiting value, the decreases as emulsifier concentration further increases. These unusual variations of the number of particles with emulsifier concentration and temperature were also found in the KPS system and indicate that initiation occurs in monomer droplets in this system.

Smith-Ewart Case 2 kinetics indicate that the number of particles should vary with the 3/5 power of the emulsifier concentration and the 2/5 power of the initiator concentration.

Figure 5.47

Correlation Between Calculated Number of Latex Particles and Polymerization Temperature

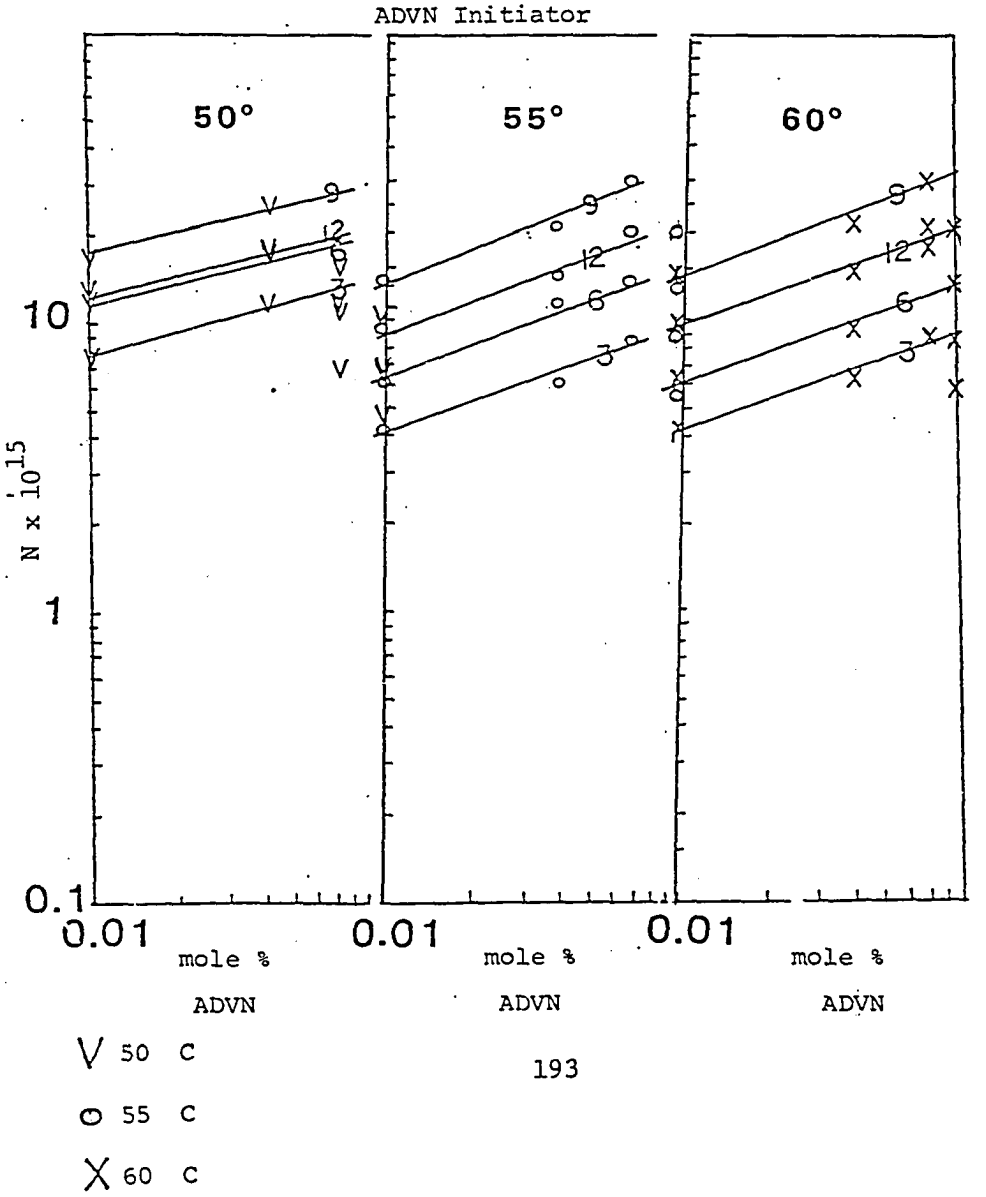

The average number of radicals per particle $\bar{n}$ calculated above indicates that this system does not follow Case 2 kinetics. This behavior is confirmed by the relationship between the number of particles and the emulsifier and initiator concentrations: the number of particles varies with the 4/5 power of the emulsifier concentration and with the 1/5 power of the initiator concentration (Figure 5.48-5.53). The low dependence of number of particles on initiator concentration is another indication that the degee of subdivision is less important. The stronger dependence of the number of particles on the emulsifier concentration at all temperatures indicates initiation in the adsorbed layer, as in the Medvedev model.

Polymer molecular weights are given in Table 5.13. As described above, equations 9 and 10 can be combined to calculate f, k_t, and k_{tr} (Figures 5.54-5.60). The values of f, k_t, and k_{tr} determined in this way are given in Table 5.14. The transfer rate constant varies from 0.016 to 0.028 liter/mole·sec, which is lower than in the persulfate initiated system (i.e., 0.03 to 0.26 liter/mole·sec) but is still close to the literature value (0.22 liter/mole·sec) for solution polymerization. The higher value of k_{tr} in the KPS system indicates that chain transfer to surfactant is more likely with KPS than with ADVN, and hence the method of radical generation is indeed different in the KPS and ADVN systems. The average value of the initiator efficiency factor is notably low (0.31) compared to the value for persulfate (0.62), indicating that

Figure 5.48

Correlation Between Calculated Number of Particles and Initiator Concentration

ADVN Initiator

Polymerization Temperature= 50° C

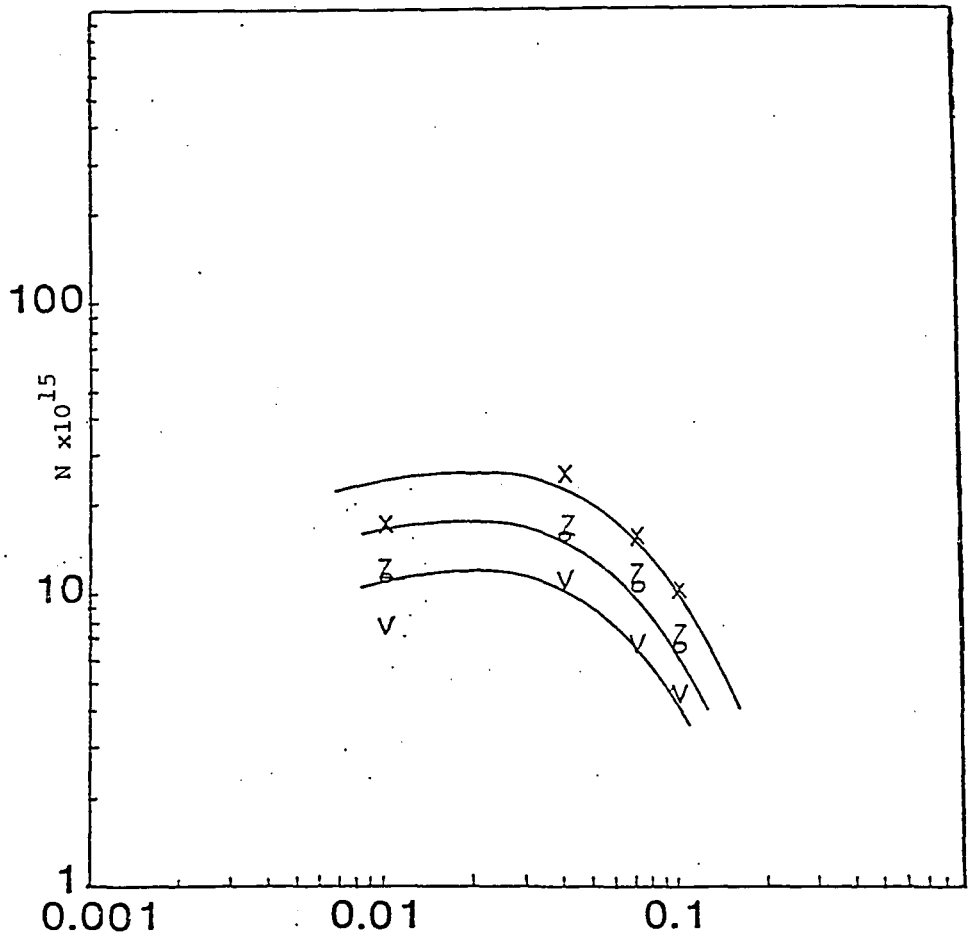

V 3% Tetronic 1102 mole % ADVN

O 6% Tetronic 1102

X 9% Tetronic 1102

Z 12% Tetronic 1102

Figure 5.49

Correlation Between Calculated Number of Particles and Initiator Concentration

ADVN Initiator

Polymerization Temperature= 55° C

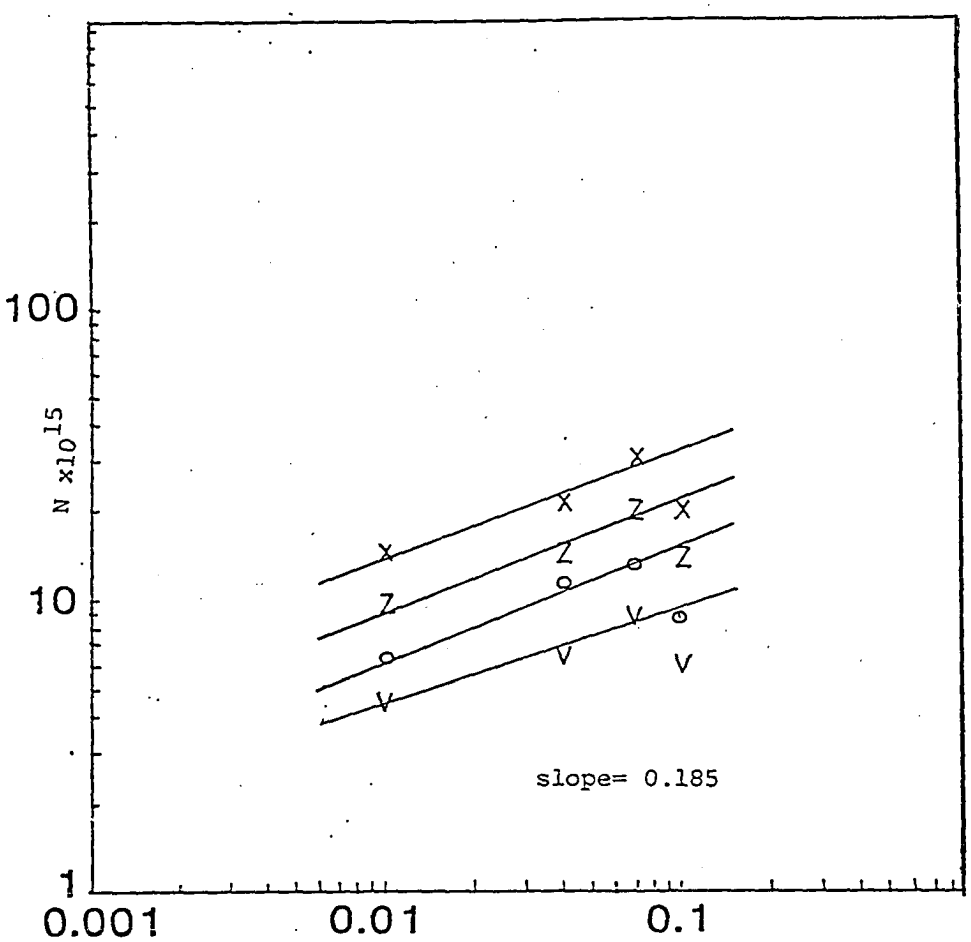

V 3% Tetronic 1102

O 6% Tetronic 1102

X 9% Tetronic 1102

Z 12% Tetronic 1102

Figure 5.50

Correlation Between Calculated Number of Particles and Initiator Concentration

ADVN Initiator

Polymerization Temperature= 60° C

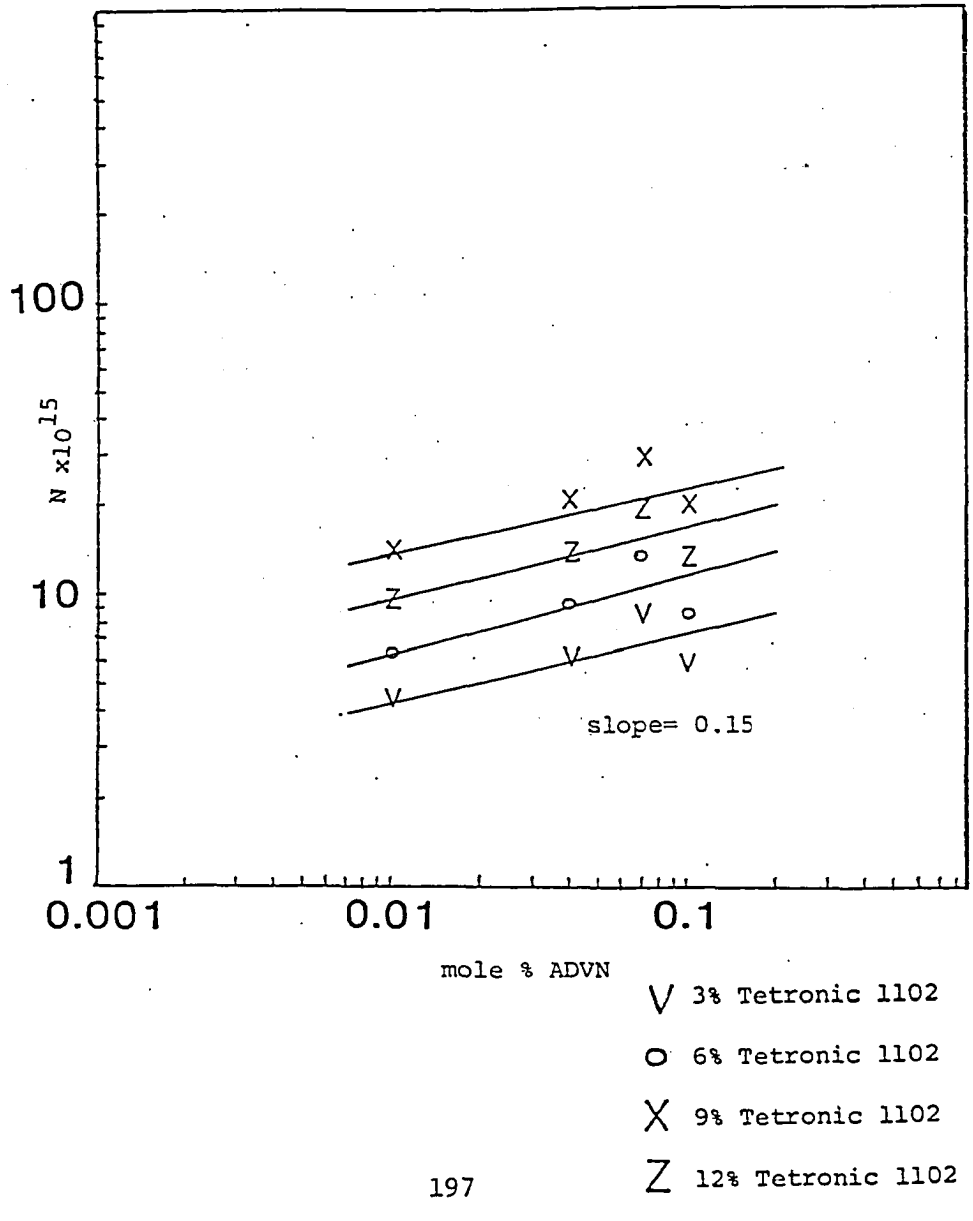

Figure 5.51

Correlation Between Calculated Number of Particles and Emulsifier Concentration.

ADVN Initiator

Polymerization Temperature= 50 C

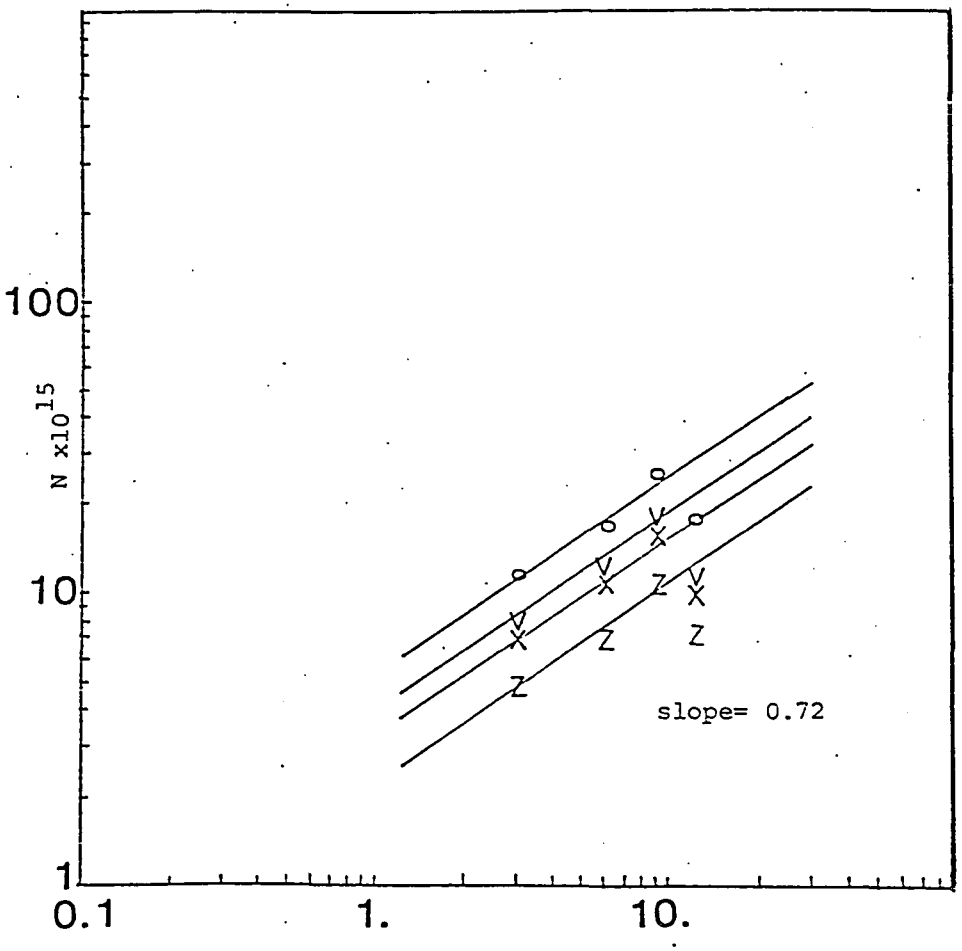

Figure 5.52

Correlation Between Calculated Number of Particles and Emulsifier Concentration

ADVN Initiator

Polymerization Temperature= 55 C

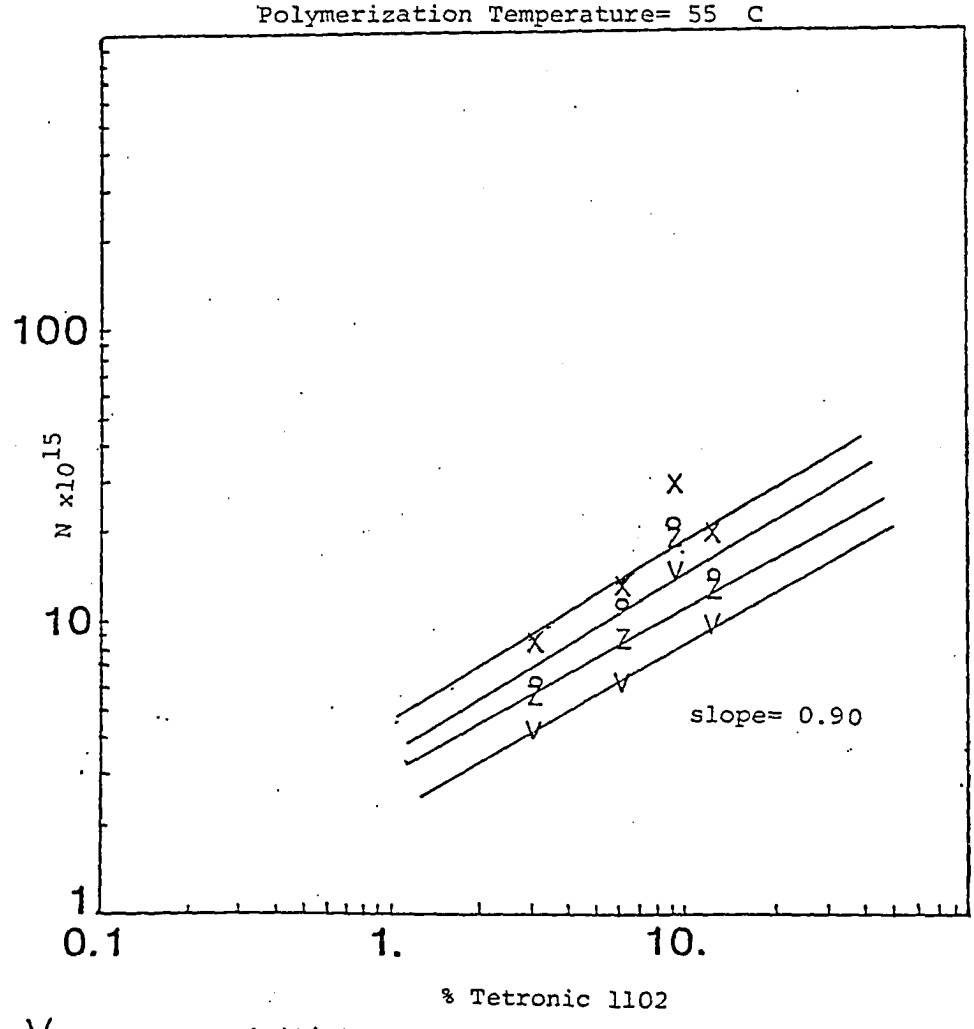

V 0.01 mole % initiator

O 0.04 mole % initiator

X 0.07 mole % initiator

Z 0.1. mole % initiator

Figure 5.53

Correlation Between Calculated Number of Particles and Emulsifier Concentration

ADVN Initiator

Polymerization Temperature= 60 C

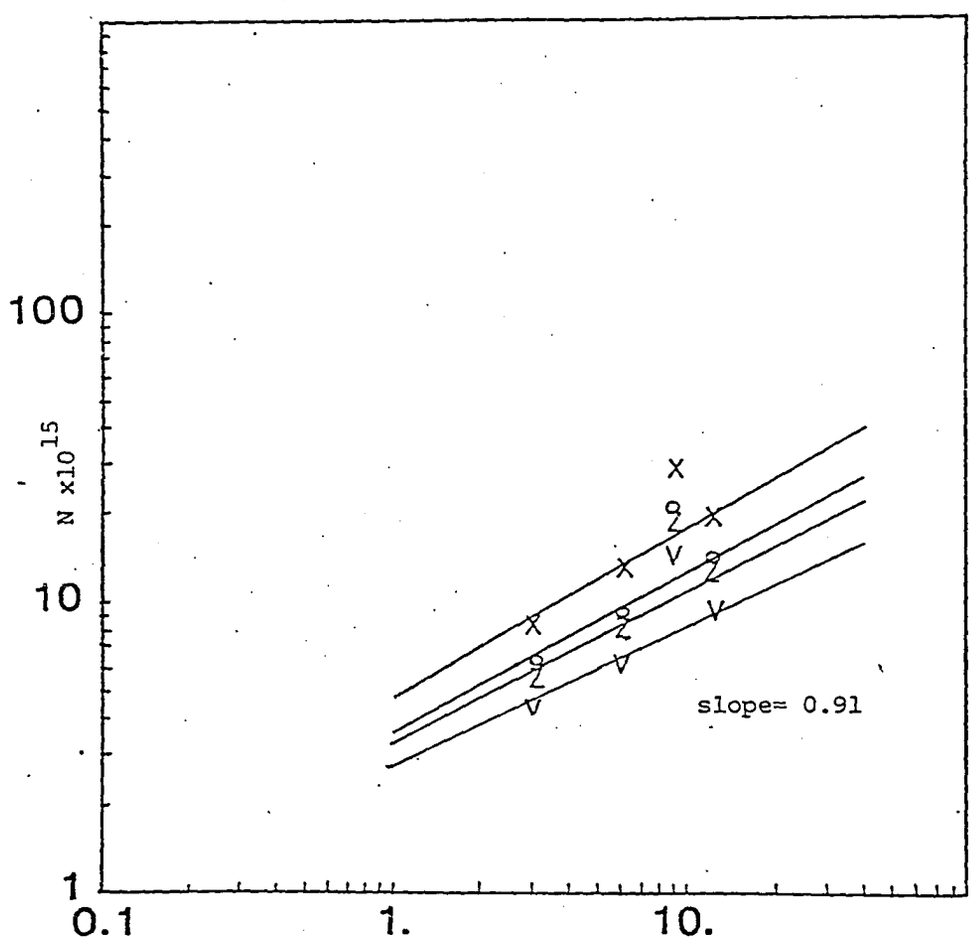

V 0.01 mole % initiator

O 0.04 mole % initiator

X 0.07 mole % initiator

Z 0.1. mole % initiator

Figure 5.54

Polymerization Rate as a Function of Initiator Concentration

ADVN Initiator

Polymerization Temperature= 50° C

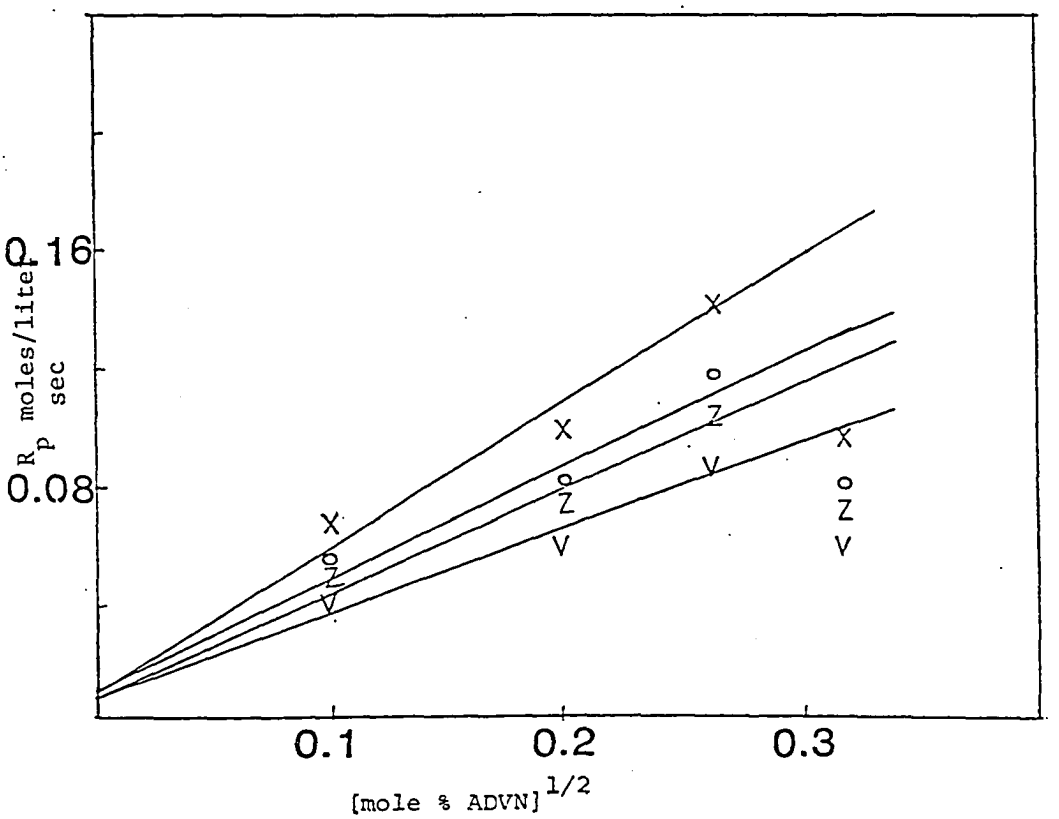

V 3% Tetronic 1102

O 6% Tetronic 1102

X 9% Tetronic 1102

Z 12% Tetronic 1102

Figure 5.55

Polymerization Rate as a Function of Initiator Concentration

ADVN Initiator

Polymerization Temperature= 55° C

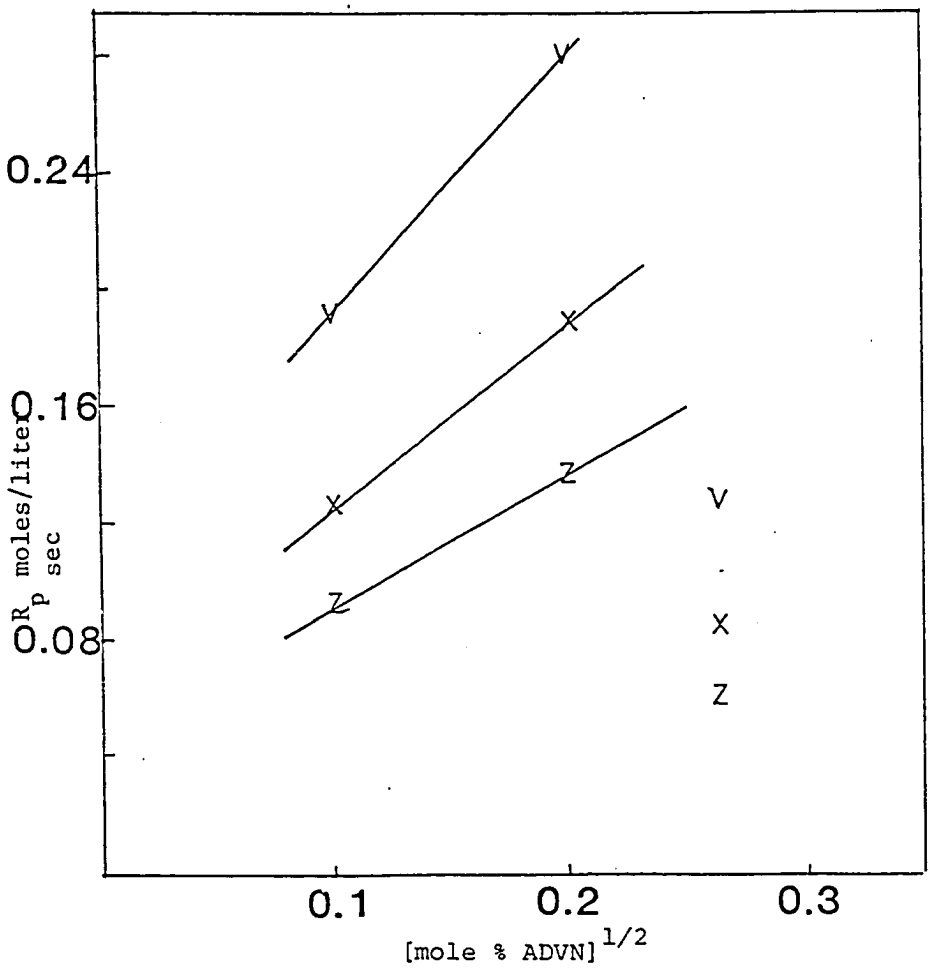

V 3% Tetronic 1102

X 9% Tetronic 1102

Z 12% Tetronic 1102

Figure 5.56

Polymerization Rate as a Function of Initiator Concentration

ADVN Initiator

Polymerization Temperature= 60° C

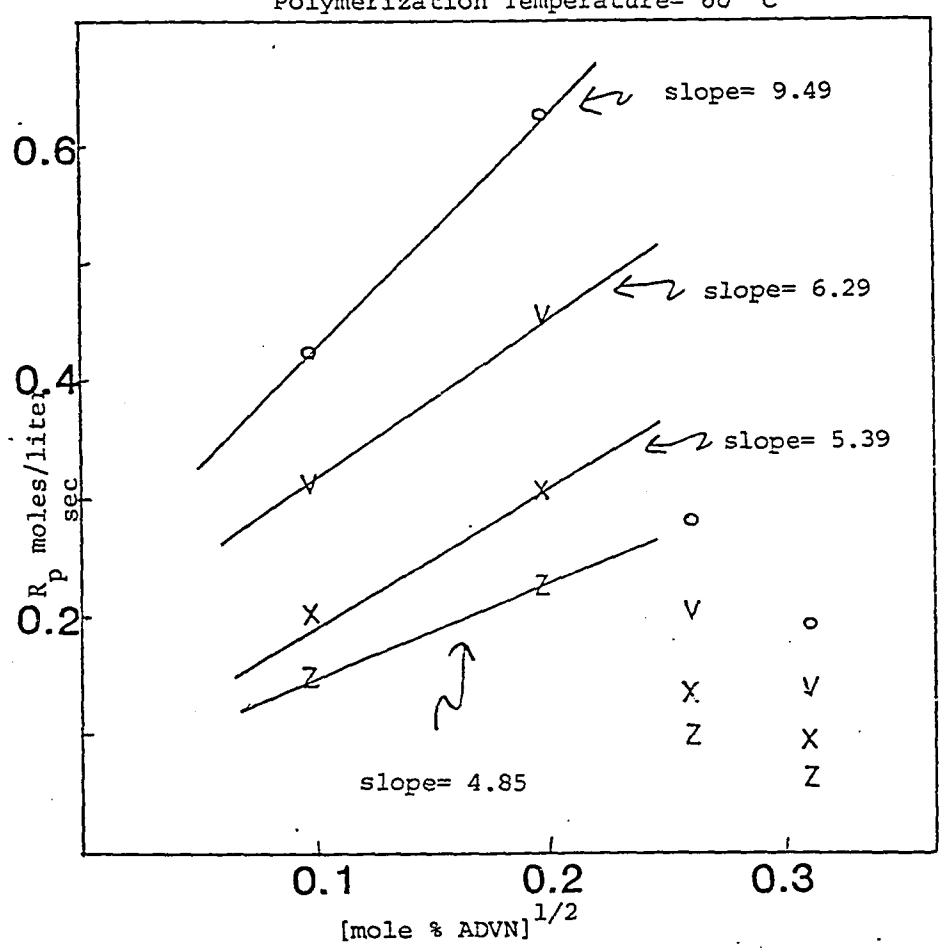

V 3% Tetronic 1102

O 6% Tetronic 1102

X 9% Tetronic 1102

Z 12% Tetronic 1102

Figure 5.57

Correlation Between Polymer Molecular Weight and Initiator Concentration

ADVN Intiiator

Polymerization Temperature= 50° C

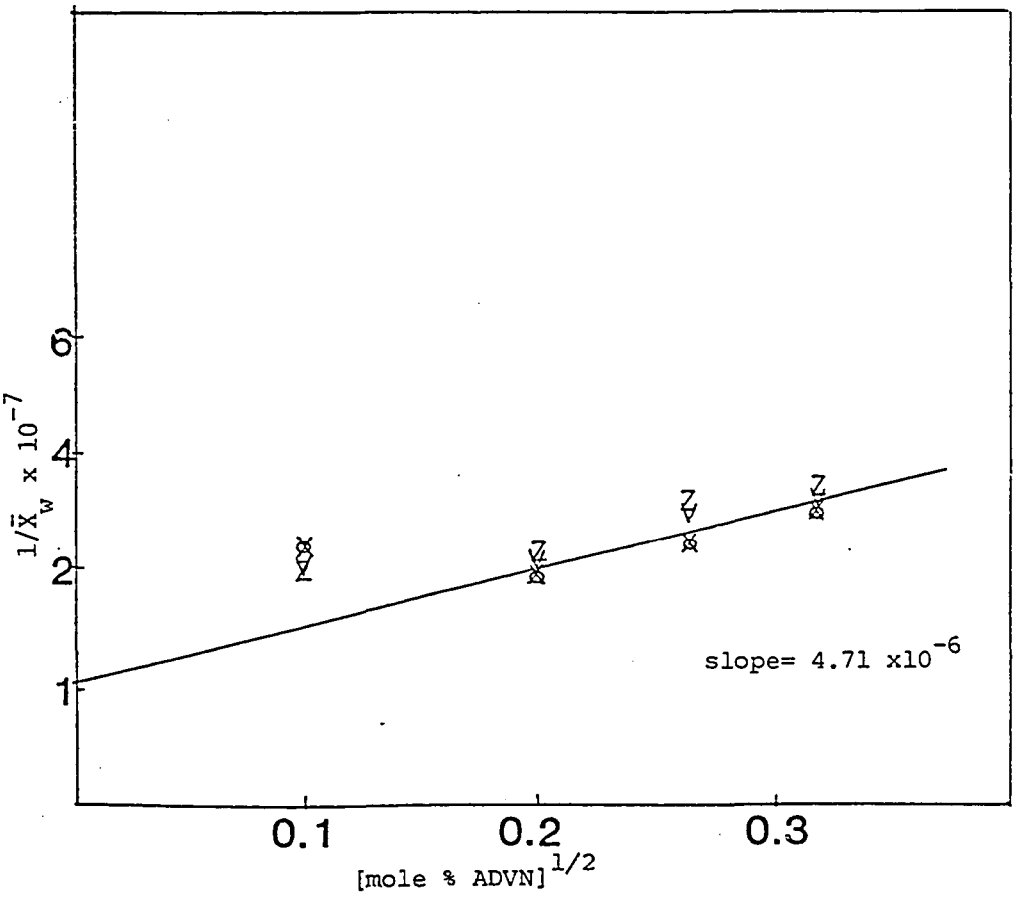

V 3% Tetronic 1102

O 6% Tetronic 1102

X 9% Tetronic 1102

Z 12% Tetronic 1102

Figure 5.58

Correlation Between Polymer Molecular Weight and Initiator Concentration

ADVN Initiator

Polymerization Temperature= 55° C

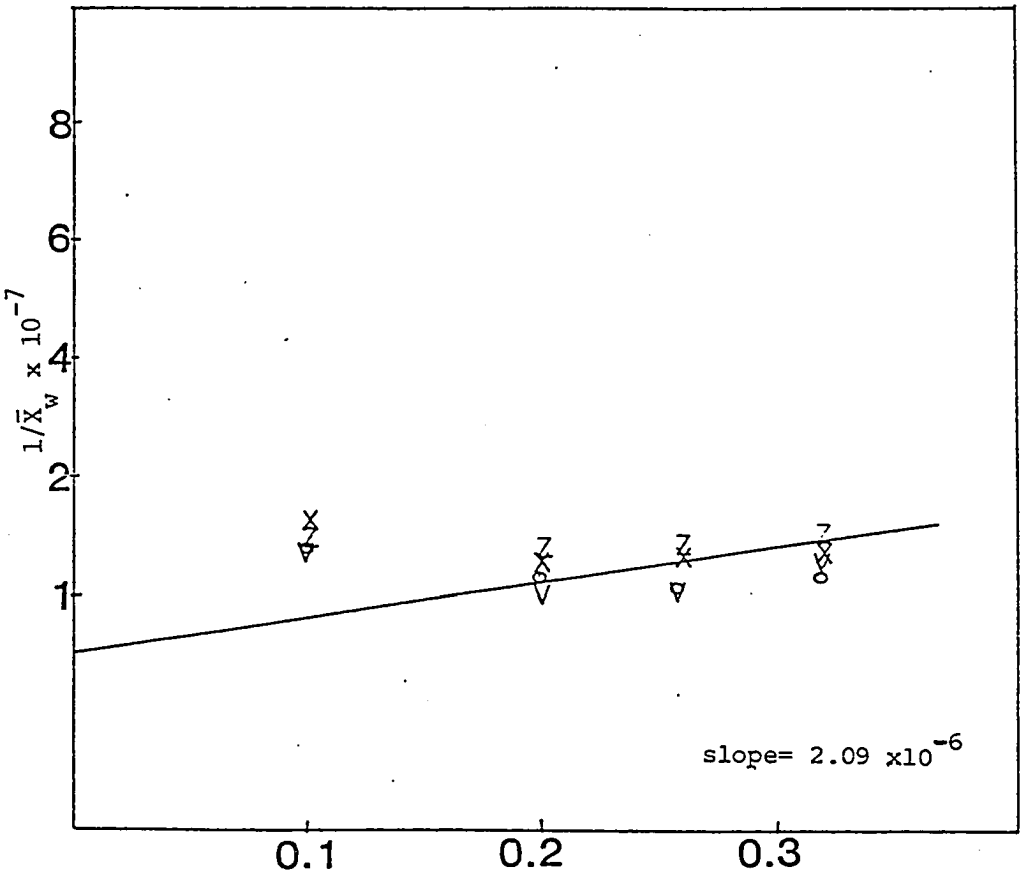

V 3% Tetronic 1102

O 6% Tetronic 1102

X 9% Tetronic 1102

Z 12% Tetronic 1102

Figure 5.59

Correlation Between Polymer Molecular Weight and Initiator Concentration

ADVN Initiator

Polymerization Temperature= 60 C

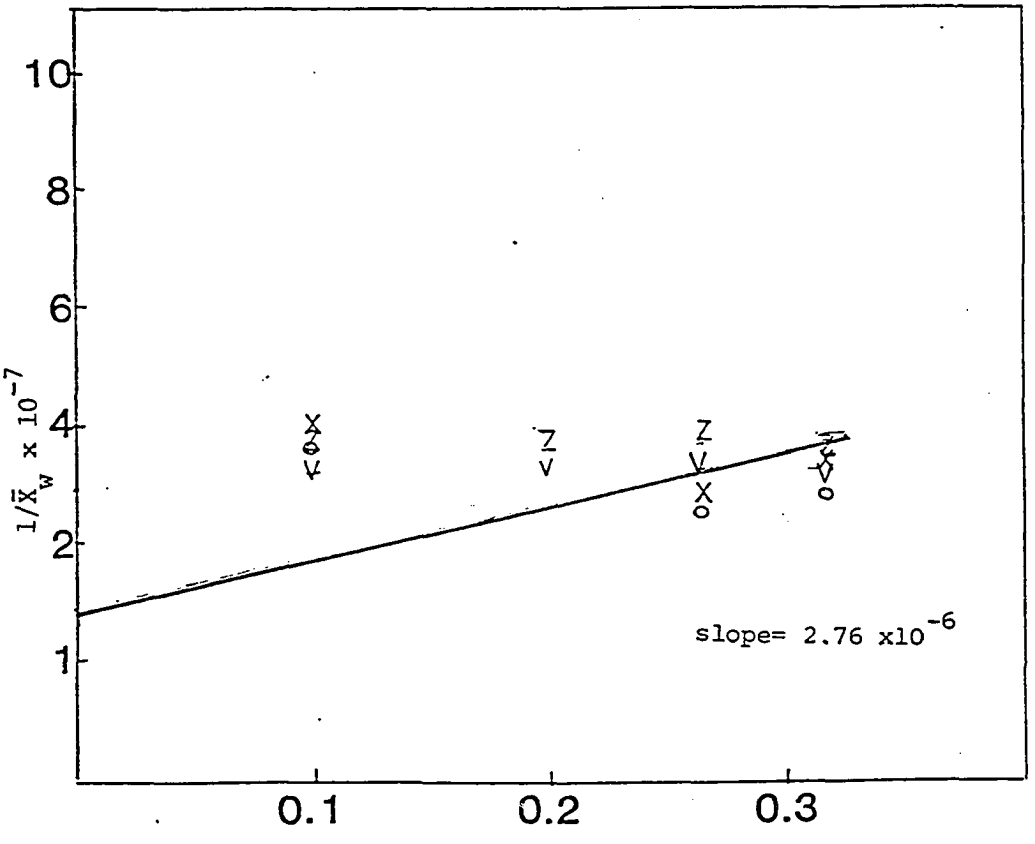

V 3% Tetronic 1102

O 6% Tetronic 1102

X 9% Tetronic 1102

Z 12% Tetronic 1102

Figure 5.60

Correlation Between Polymer Molecular Weight and Initiator Concentration

ADVN Initiator

Polymerization Temperature= 65 C

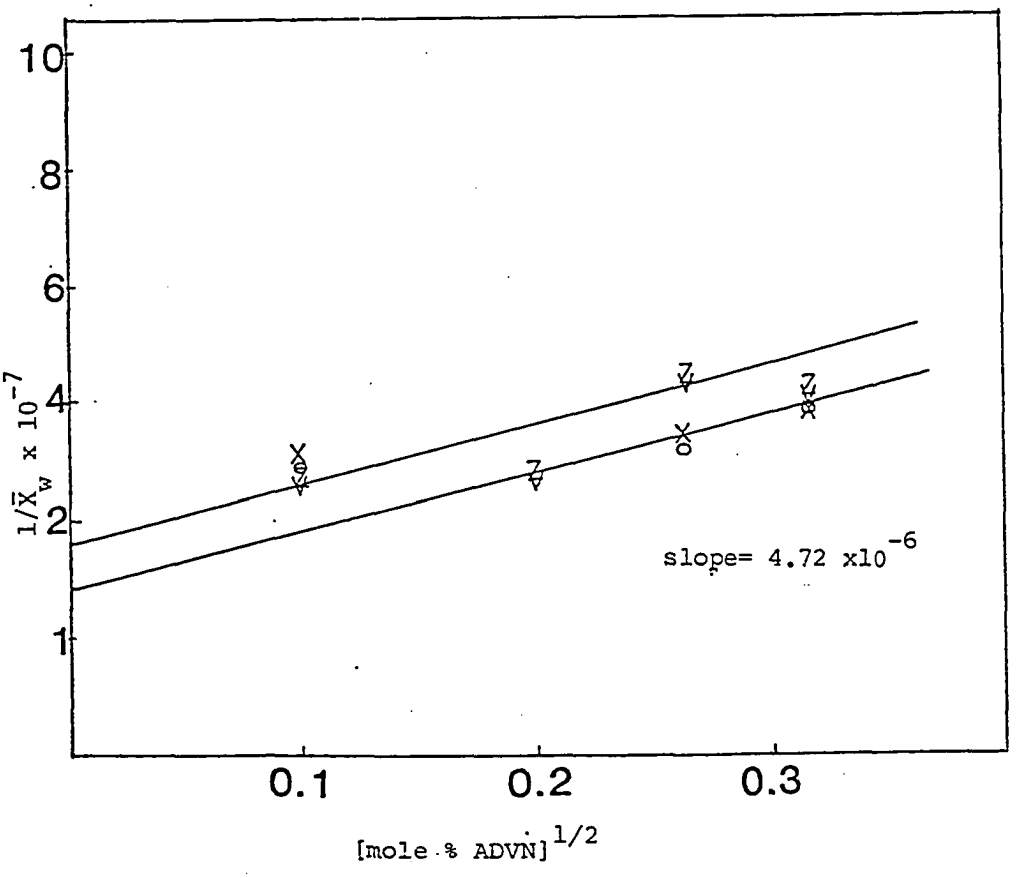

V 3% Tetronic 1102

O 6% Tetronic 1102

X 9% Tetronic 1102

Z 12% Tetronic 1102

TABLE 5.13

ADVN Latexes

$\bar{M}_w$

T	[I]	[E] 3	6	9	12
50	0.01	4.8×10^6	4.3×10^6	4.1×10^6	4.6×10^6
	0.04	5.0×10^6	5.4×10^6	5.2×10^6	4.8×10^6
	0.07	3.2×10^6	4.3×10^6	4.1×10^6	3.1×10^6
	0.10	3.1×10^6	3.4×10^6	3.3×10^6	2.9×10^6
55	0.01	3.8×10^6	3.5×10^6	3.0×10^6	3.4×10^6
	0.04	4.0×10^6	4.4×10^6	3.8×10^6	3.5×10^6
	0.07	4.0×10^6	5.3×10^6	4.7×10^6	3.5×10^6
60	0.01	3.0×10^6	2.7×10^6	2.4×10^6	2.7×10^6
	0.04	2.9×10^6	3.1×10^6	2.8×10^6	2.6×10^6
	0.07	2.9×10^6	3.8×10^6	3.4×10^6	2.5×10^6
	0.10	3.0×10^6	3.4×10^6	2.9×10^6	2.6×10^6
65	0.01	3.8×10^6	3.4×10^6	3.2×10^6	3.6×10^6
	0.04	3.6×10^6	3.9×10^6	3.8×10^6	3.5×10^6
	0.07	2.3×10^6	3.1×10^6	2.9×10^6	2.2×10^6
	0.10	2.4×10^6	2.6×10^6	2.6×10^6	2.3×10^6

$$R_p = \frac{R_i}{2}\bar{X}_n$$

$$= fk_d[I]\bar{X}_n$$

$$\log R_p = \log \bar{X}_n + \log(fk_d[I])$$

TABLE 5.14

Values of k_{tr}, k_t, and f

ADVN

T, °C	k_{tr}	f	k_t
50	0.0164	0.36	55.9
55	0.0232	0.22	53.9
60	0.0268	0.29	61.5
65	0.0280	0.39	62.1

TABLE 5.15

Values of a and z from Graphical Analysis

ADVN

T	[I]	[E] =	a 3	a 6	a 9	a 12	z 3	z 6	z 9	z 12
50	0.01		0.544	0.580	0.468	0.515	0.40	0.414	0.40	0.386
	0.04		0.980	0.973	0.868	0.900	0.243	0.238	0.212	0.252
	0.07		1.36	1.42	1.35	1.38	0.735	0.389	0.323	0.252
	0.07		1.36	1.42	1.35	1.38	0.735	0.389	0.323	0.348
	0.10		1.61	1.58	1.61	1.60	0.380	0.354	0.390	0.304
55	0.01		0.576	0.515	0.595	0.540	0.152	0.394	0.459	0.135
	0.04		0.658	0.960	1.12	0.655	0.091	0.235	0.279	0.157
	0.07		1.15	1.317	1.38	1.12	0.051	0.093	0.109	0.039
	0.10		1.25	1.46	1.57	1.35	0.027	0.039	0.050	0.0162
	0.01		0.62	0.50	0.92	0.65	0.70	0.66	0.702	0.708
	0.04		0.93	1.10	1.03	0.99	0.463	0.282	0.616	0.615
	0.07		1.33	1.38	1.35	1.37	0.185	0.332	0.323	0.206
	0.10		1.46	1.73	1.68	1.63	0.093	0.145	0.129	0.119

the radicals are probably held within a solvent cage. The average termination rate constant is notably low in this system (58.3 liter/mole·sec), and is an order of magnitude lower than with persulfate initiator.

The average particle volume at 65°C can be calculated using these rate constants, and values of a determined graphically, in equations 6 and 7, as described earlier. The ratio of calculated (effective) number of particles to the experimentally measured number of particles is 0.91 ± 0.21 (Figure 5.42). This is lower than the ratio at 50 to 60°C (i.e., 1.74), which is the same trend seen with persulfate initiator.

In emulsion polymerization, the molecular weight is expected to be directly proportional to the polymerization rate. This relationship is indeed found in polymerizations. especially at higher initiator concentrations (Figures A.43-A.46).

2. Locus of Initiation

In the classical Smith-Ewart scheme of emulsion polymerization, radicals formed in the continuous phase diffuse into the micelles and initiate polymerization; the monomer droplets, which are roughly an order of magnitude larger than the micelles, act as reservoirs of monomer as the reaction proceeds. In the present systems, because the monomer droplets are small and because their morphology is controlled by the surfactant, the difference between monomer droplets and micelles is really semantic and hence initiation can be described as occurring in monomer droplets. The description of this process on a molecular level will be discussed

in the following section.

a. KPS initiator

Since potassium persulfate is insoluble in the continuous phase, initiation can occur by diffusion of initiator radicals or molecules into the monomer phase and solubilization in the adsorbed surfactant layer (i.e., the Medvedev model), by transfer of initiator radicals to monomer or emulsifier followed by diffusion into the monomer phase, or by capture and coalescence of initiator solution droplets. Since the potassium persulfate is added as an aqueous solution to a preformed monomer emulsions, the latter seems plausible physically. In this experiment, the initiator solution concentration was kept constant and the volume of solution added varied. Hence, studying the effect of initiator concentration on the number of monomer emulsion and latex particles should give information on the relative importance of radical capture compared to radical transfer or diffusion and solubilization.

The ratio of the number of latex particles to the number of monomer emulsion droplets has been measured as a function of initiator concentration (Figures 5.61-5.64). The magnitude of this ratio is surprisingly high; since the measured volume contraction due to conversion of monomer to polymer is 31.5%, the ratio of the number of polymer particles to the number of monomer emulsion droplets should be 1.46 (i.e., 100/(100-31.5)) if the droplets coalesce rather than simply contract in size. The measured ratio of the number of latex particles to the number of monomer emulsion

Figure 5.61

Number of Monomer Emulsion Droplets as a Function of Emulsifier Concentration

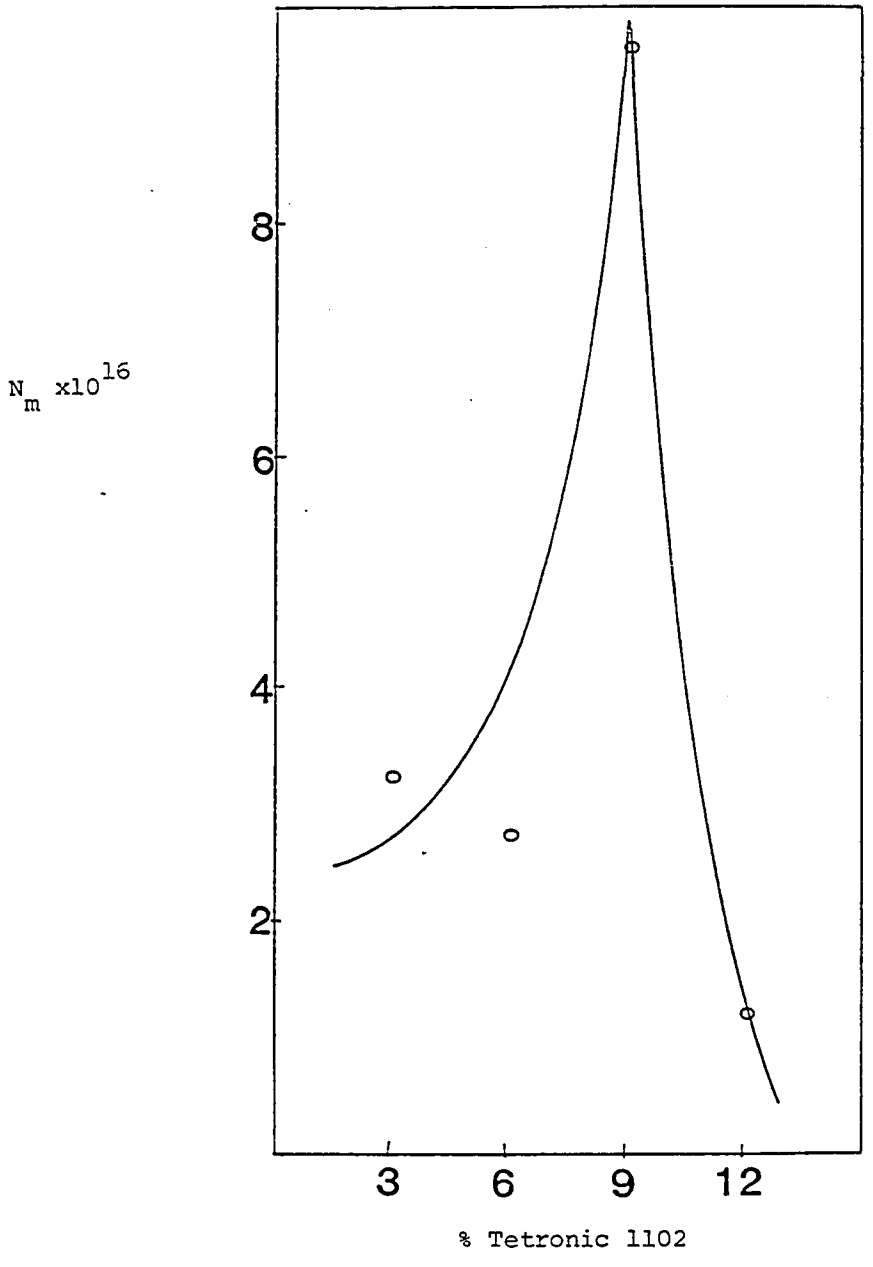

Figure 5.62

Ratio of the Number of Latex Particles (N_l) to the Number of Monomer Emulsion Droplets (N_m)

KPS Initiator

Polymerization Temperature= 50° C

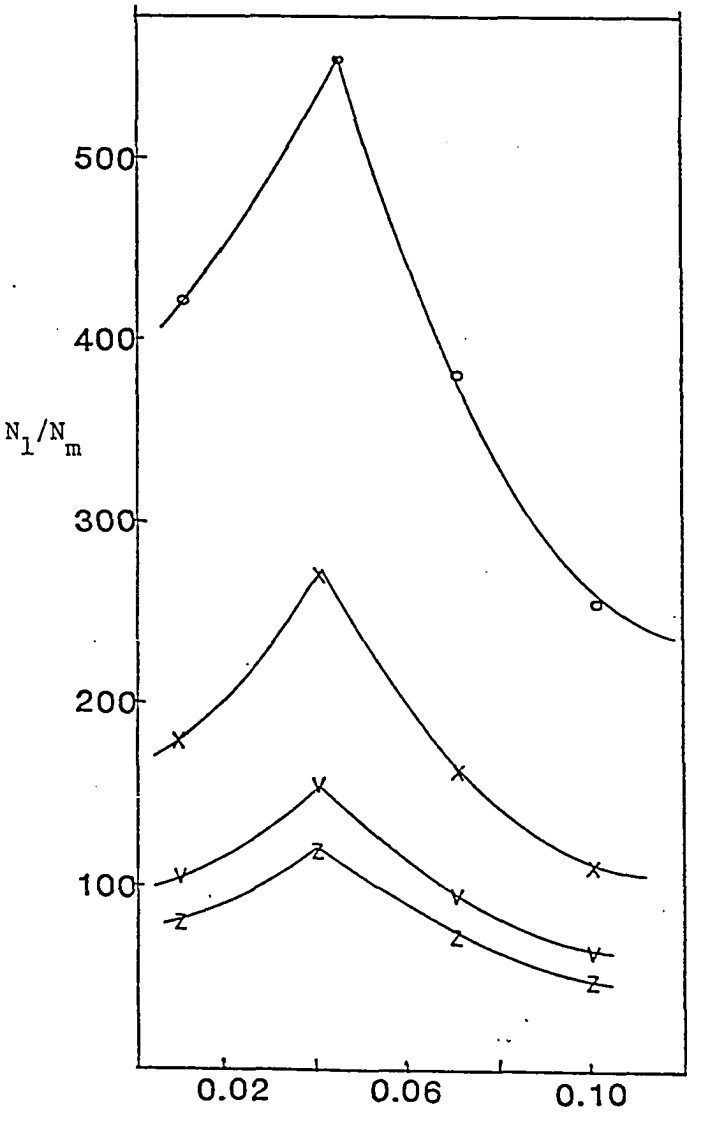

V 3% Tetronic 1102

O 6% Tetronic 1102

X 9% Tetronic 1102

Z 12% Tetronic 1102

Figure 5.63

Ratio of the Number of Latex Particles (N_1) to the Number of Monomer Emulsion Droplets (N_m)

KPS Initiator

Polymerization Temperature= 55° C

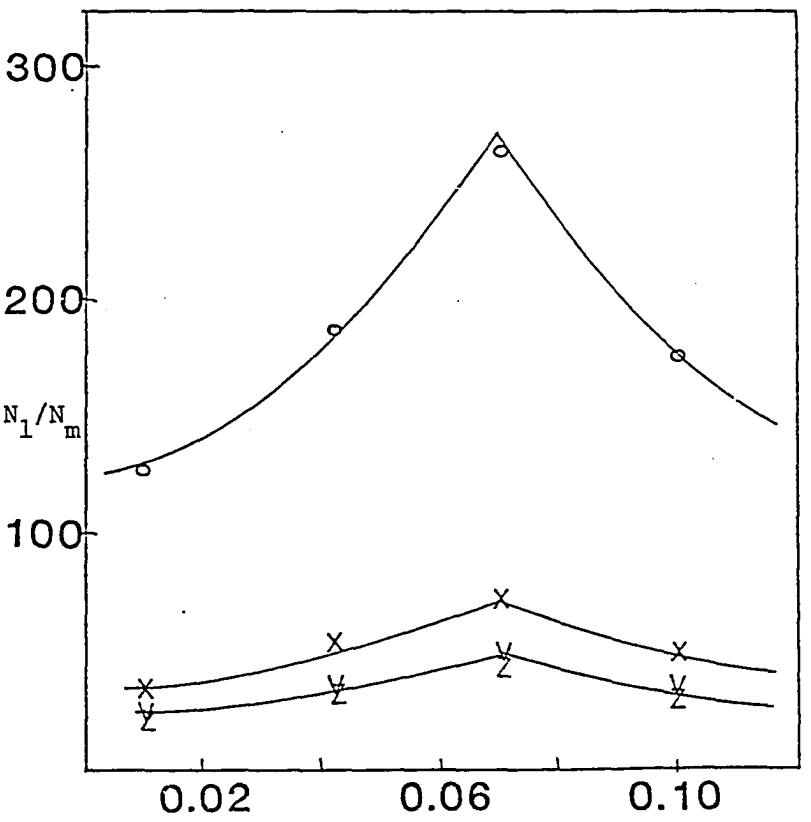

V 3% Tetronic 1102

o 6% Tetronic 1102

X 9% Tetronic 1102

Z 12% Tetronic 1102

Figure 5.64

Ratio of the Number of Latex Particles (N_1) to the Number of Monomer Emulsion Droplets (N_m)

KPS Initiator

Polymerization Temperature= 60° C

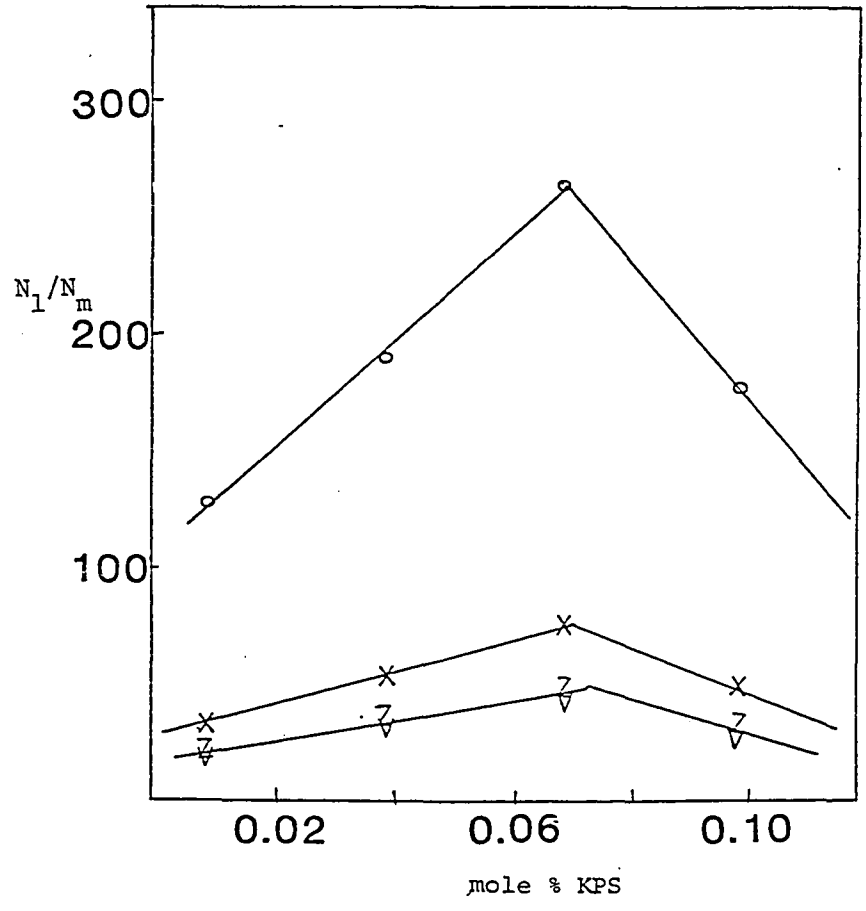

V 3% Tetronic 1102

O 6% Tetronic 1102

X 9% Tetronic 1102

Z 12% Tetronic 1102

droplets is generally much higher than 1.46 (i.e., 50 to 500). This indicates that more latex particles are being nucleated, or that the measured latex particle size is too low, or the measured monomer emulsion droplet size is too high. Earlier analysis of the skewness of the latex particle size distribution showed that particles grew by coagulation rather than by nucleation, so nucleation of new particles is not a plausible explanation for the magnitude of this ratio. However, since Tetronic 1102 forms multicellular particles in solution in the absence of dispersed phase, it is likely that some of the droplets counted as monomer emulsion droplets are actually simply reticulated Tetronic 1102 particles rather than monomer emulsion droplets. Hence the measurement of the number of monomer emulsion droplets may be systematically incorrect; this means that the magnitude of the ratio of latex particles to monomer emulsion droplets is not physically meaningful, but, since the number of monomer emulsion droplets is systematically erroneous, changes in this ratio are meaningful. This ratio increases with increasing emulsifier concentration up to a limiting value, then decreases as the initiator concentration is further increased (Figures 5.61-5.64). This indicates a competition between two processes may be occurring: capture of initiator solution droplets initially increases the ratio of the number of latex particles to the number of monomer droplets, but adding more aqueous initiator solution destabilizes the monomer droplet and causes coalescence. There are two possible reasons for reduced monomer droplet stability when more initiator solution is added: the added aqueous solution

may swell the surfactant layer and make the surface too hydrophilic for stability; or the ionic persulfate molecules may contract the adsorbed layer and thereby reduce stability. Studies on the stability of inverse latexes (discussed in Chapter 6) show that adding electrolyte or using persulfate initiator reduces both the zeta potential and the latex stability against settling and causes the latex viscosity profile to become shear-thinning, indicating that an ionic species can indeed contract the adsorbed layer. Hence the decrease in the ratio of latex particles to monomer emulsion droplets at high initiator concentration can be attributed to destabilization of the particles.

The effect of polymerization temperature on the number of particles also gives some insight into the mechanism of initiation in this system. The number of particles decreases over the polymerization temperature range from 50 to 60°C (Figures 5.41-5.47); this is the opposite of the relationship between the number of particles and the polymerization temperature found in conventional emulsion polymerization using chemical sources of free radicals. However, this decreasing relationship is also found in γ-ray initiated emulsion polymerization of styrene (5.14) as well as in the inverse emulsion polymerization system studied by Vanderhoff et al. (5.11). In a γ-ray initiated polymerization, the free radical concentration is independent of temperature, so the decreasing relationship between the number of particles and the polymerization temperature was attributed to production of larger initial polymer molecules due to

the increased propagation rate at higher temperature and growth of the micelles which have captured radicals at the expense of those which have not. This explanation does not seem to apply in the present system because the activation energies for persulfate and azo decomposition are large enough to override the effect of increased propagation rate. However, if initiation occurs by capture of initiator droplets rather than by diffusion, the distribution of number of initiator radicals per molecule will be very broad; some monomer emulsion droplets will have captured many radicals and some will have captured none. This is analogous to the case of γ-ray initiated polymerization in which the particles which have captured radicals grow at the expense of those which have not. However, since the relationship between polymerization temperature and the number of particles is the same for both azo and persulfate initiators, and since the capture mechanism is inapplicable to the azo initiator, this relationship does not necessarily indicate that initiation occurs by capture with the persulfate initiator.

An unexpected finding in this system is that the value of the subdivision factor z is greater than 1, which indicates generation of single radicals. Since the initiator is soluble in the dispersed (monomer) phase, generation of pairs of radicals was expected. Since the initiator efficiency factor is fairly high, it is unlikely that the release of initiator radicals to the monomer is controlled by cage effects. Desorption of one of the two initiator fragments would also result in single radical generation in the particles, but desorption is unlikely in this system for

reasons discussed earlier. Formation of single radicals by oil soluble initiators in conventional emulsion polymerization, which is analogous to formation of single radical by water-soluble persulfate initiator in inverse emulsion polymerization, has been attributed to mechanisms such as radical diffusion out of the particle or entry of single radicals from the continuous phase (5.9). The former mechanism may be operative in this system: diffusion of an oligomeric or monomeric radical out of the particle and into another particle would not affect the kinetics as long as termination in the continuous phase does not occur. This does not contradict the earlier assumption of no desorption because no continuous phase termination occurs; for each particle losing one radical in a random process, another particle gains a radical in an equally random manner. The high molecular weight of polymer formed in this system is consistent with the diffusion of radicals out of the particle: since the molecular weight depends on the growth time of the radical within the particle, diffusion of radicals out of the particle is consistent with longer growth time and hence higher molecular weight. It is unclear why initiator capture and desorption after forming monomer radicals is preferred over simple diffusion; possibly the nonionic monomer radicals can diffuse more readily than ionic initiator radicals. Another explanation for the formation of single radicals in the particles may be in the mechanism of decomposition of KPS as studied by Kolthoff (5.15):

$$S_2O_8^{2-} \rightarrow 2SO_4^{-}\cdot$$

$$SO_4^{-}\cdot + H_2O \rightarrow HSO_4^{-} + OH\cdot$$

$$2OH\cdot \rightarrow H_2O + 1/2\ O_2$$

The first reaction in this sequence is presumed to be the rate-determining step and the other reactions are presumed to be very rapid; however, if the second step is an equilibrium, and only the sulfate radicals are sufficiently active to initiate polymerization, this scheme could explain the generation of only single radicals by KPS. This process is analogous to the formation of single radicals by hydroperoxides (5.16). Measuring the pH of aqueous acrylamide solution as a function of conversion may indicate if the second step in the above scheme is an equilibrium or if it goes to completion. The dramatic lowering of molecular weight as emulsifier concentration is raised (Figure 5.13) indicates that initiator radicals may transfer to emulsifier and this may be a mechanism of transport of single radicals to the monomer droplets.

b. ADVN Initiator

Partition coefficient studies show that the initiator is preferentially solubilized in the adsorbed layer. This result, combined with low radical efficiencies and generation of pairs of radicals in the particles, indicates initiation in the adsorbed emulsifier layer. The highly hydrophobic ADVN molecules diffuse through the continuous phase into the adsorbed layer, where they form radicals which may be wasted by reacting with each other (the adsorbed layer is somewhat analogous to a solvent cage) or which may react with the monomer molecules which swell the adsorbed layer. These monomeric or oligomeric radicals diffuse into the

interior of the droplets and continue polymerizing.

3. Propagation and Particle Growth

Analysis of the skewness of the particle size distribution in this system indicated growth by coagulation rather than by nucleation. This mechanism is consistent with the mechanism of initiation described above. However, there are several features of this system which require further analysis: the variation between the effective (calculated) and measured numbers of particles; the plateau in the conversion-time curve under some circumstances; the survival of multicellular morphology through polymerization to the final latex.

It is not surprising that the ratio of the effective number of particles to the measured number of particles is greater than one. The number of particles is a measure of the state of subdivision of the system; the multicellular morphology in this system reflects the presence of additional interfaces and hence a greater degree of subdivision than the individual particles. The difference between the effective and measured numbers of particles is greatest for KPS-initiated polymerizations at polymerization temperature below the melting temperature of the surfactant. This is reasonable in light of the proposed polymerization mechanism. The degree of subdivision of the system can be expected to most strongly affect the mechanism when the surfactant molecules form a rigid layer (i.e., below the melting temperature) and when the initiator radicals are not soluble in the interfacial layer but instead must be captured

by monomer droplets in order to propagate polymerization. These conditions describe a system containing KPS initiator at lower temperature. Under other conditions, the presence of additional interfaces due to the multicellular structure have a much less significant effect: the surfactant partitions away from the interface at 65°C and the ADVN initiator is readily soluble in the interfacial layer. Hence the ratio of the number of effective to measured latex particles approaches unity at 65°C or with ADVN.

Under some conditions, a plateau region was observed in the conversion-time curve during which the polymerization reaction essentially halted, then spontaneously began again with roughly the same rate as found initially. Similar plateaus in conversion-time curves have been observed in conventional emulsion polymerization of vinylidene chloride (5.13). These plateaus have been attributed to monomer starvation caused by slow diffusion from coalesced monomer droplets to the growing particles, since the monomer is spanningly soluble in the polymer. Plateaus have also been observed in seeded emulsion polymerization of styrene due to monomer starvation. Other possible factors causing a plateau in the conversion-time curve include high internal viscosity, unstable diffusional flux of radicals, and a phase change in the surfactant due to a sharp increase in the temperature of the system. Multivariate regression analysis shows that, in this system, the presence of the plateau is strongly correlated to polymerization temperature of 50 or 65°C. No other variable in this system is correlated with the presence of this plateau; hence it cannot be attribute to a surfac-

tant phase change or to increased internal viscosity. However, the initial polymerization rate and the presence of the plateau are indeed correlated: polymerization rate is generally lowest under conditions when the plateau is observed (i.e., 50 and 65°C), indicating that slow diffusion causes the reaction to stop temporarily. Preparation of the same polymerization recipe at several different agitation rates shows that polymerization rate increases as agitation rate increases, indicating that diffusion increases with increasing agitation rate; the plateau seen in the conversion-time curve at slower agitation rate disappears at higher agitation rate. Considering the mechanism of this reaction, diffusional problems are not surprising. In the classical Smith-Ewart model, monomer molecules diffuse into the growing particles; this process is facile due to the small size and low viscosity of the monomer molecules. In the proposed mechanism of inverse emulsion polymerization of acrylamide, monomer is transported to the locus of polymerizations by collision and coalescence of monomer droplets. This mechanism is expected to be much more sensitive to agitation rate and less facile due to the high internal viscosity of the growing polymer particles. Hence the presence of this plateau in the conversion-time curve is attributed to temporary monomer starvation due to low diffusional flux.

The correlation between the absence of multicellular latex particles and polymerization temperature of 65°C is easily explained by considering that the surfactant's melting temperature

is 62°C and the surfactant molecules form a less rigid structure above the melting temperature. However, multicellular latex particles are also not found under certain other conditions, such as at low initiator concentration at 50°C and at moderate initiator concentration at 60°C. Microscopic studies of emulsion morphology discussed earlier have shown that the emulsifier molecule is much more electron-dense than either acrylamide or polyacrylamide. Hence if the polymer particle appears solid and dark, the emulsifier must be present as a uniform layer on the surface. Evidently some reaction conditions can affect the conformation of the surfactant molecule. This may be due to transitory effects such as the local reaction rate or initiator concentration. Since the ratio of the effective number of particles to the measured number of particles is the same at temperatures below 65°C regardless of whether the latex is multicellular, these conformational effects apparently do not play an important role in the polymerizations mechanism.

4. Termination

Termination of polyacrylamide chains in solution has been shown to occur by disproportionation in reactions initiated by redox or azo initiators.

This mechanism may not apply directly to inverse emulsion polymerization of acrylamide because the high internal viscosity causes termination to be diffusion controlled. In these experiments, chain transfer reactions do not appear to be very important when ADVN is used because the molecular weight is high and

is not strongly dependent on emulsifier concentration, and the chain transfer constant is low (0.016-0.03 liter/mole·sec); hence termination by combination is likely. In the case of KPS initiated polymerization, termination by chain transfer to surfactant is also important.

D. Conclusions

The average number of radicals per particle ($\bar{n}$), the relationship between the number of particles and the emulsifier concentration, and the single entry of radicals into particles which were found in kinetic analysis of KPS-initiated polymerizations fit the predictions of Smith-Ewart Case 2 theory very well. Hence it is unlikely that the mechanism of this reaction is profoundly different from the model used in deriving Smith-Ewart Case 2. This indicates that initiation is more likely to occur by diffusion of radicals to the locus of polymerization rather than by capture and coalescence of monomer droplets and initiator droplets. Since the KPS is added to the monomer emulsion as an aqueous solution, the initiator solution probably forms droplets which are surrounded by Tetronic 1102. Radicals are transferred to the emulsifier molecule and migrate into the monomer droplets. The important effect of emulsifier on molecular weight in the KPS system and DiStefano's finding that acrylamide can transfer to Tetronic 1102 (5.1) are consistent with this mechanism of initiation. The preferential solubility of ADVN in the adsorbed emulsifier layer, low radical efficiencies, and pairwise entry of radicals into particles indicate initiation in the adsorbed

emulsifier layer. However, analysis of the ratio of the latex skewness to the monomer emulsion skewness indicated that there may be more than one locus of initiation. Measurement of the polymerization rate as a function of the number of particles (Figures 5.65-5.68) extrapolates to a value greater than zero when the polymerization rate is zero. This indicates that some polymerization occurs in the continuous phase, so probably initiation occurs in both the adsorbed emulsifier layer and the continuous phase. With both initiators, polymerization occurs in the monomer droplets and particles grow by coagulation.

The multicellular structure of the emulsifier used in this system introduces an additional level of complexity into the mechanism. The number of latex particles cannot be determined directly and the apparent activation energy of the polymerization reaction changes above the melting temperature of the surfactant.

However, the polymerization mechanism, derived from measurement of kinetic parameters in this system, is remarkably similar to the mechanism of inverse emulsion polymerization of sodium p-vinylbenzene sulfonate as studied by Vanderhoff et al. (5.11). In both systems, the effects of initiator concentration, emulsifier concentration, and temperature on the number of particles are similar but different from conventional emulsion polymerization in that the degree of subdivision is less important in inverse emulsion polymerization. In both the acrylamide and sodium p-vinylbenzene sulfonate systems, radicals are generated singly with

Polymerization Rate as a Function of the Number of Latex Particles

Figure 5.65

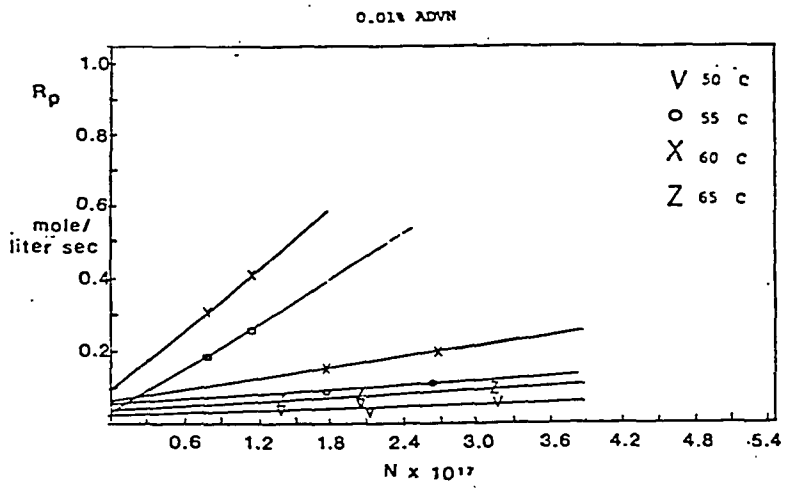

Figure 5.66

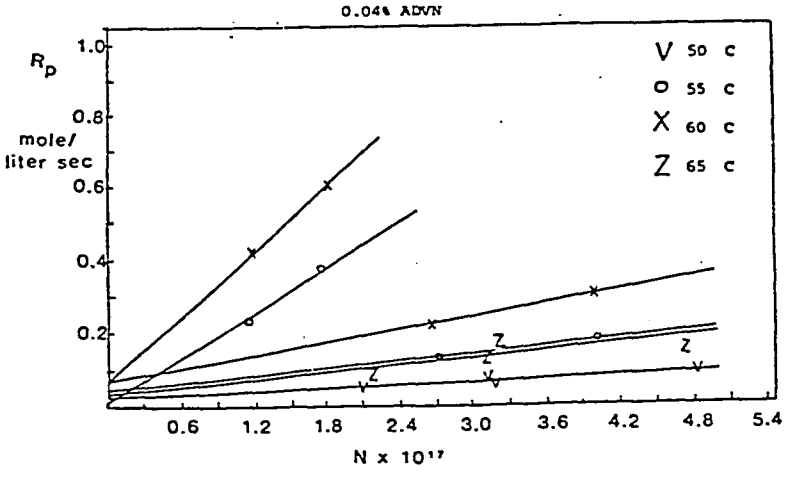

Figure 5.67

Polymerization Rate as a Function of the Number of Latex Particles

Figure 5.67

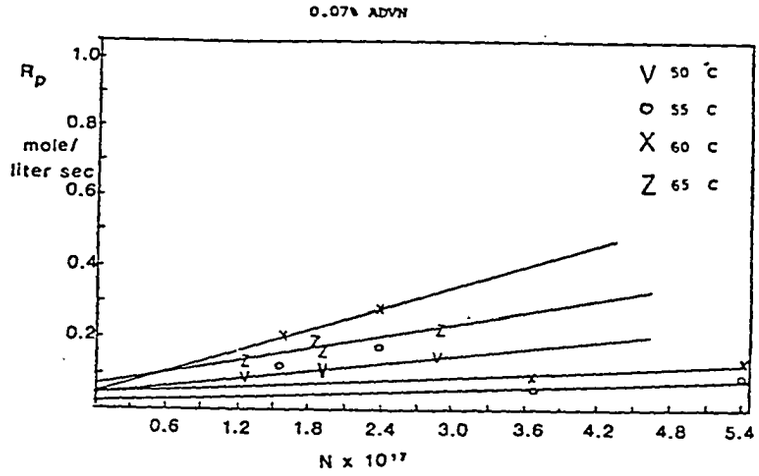

Figure 5.68

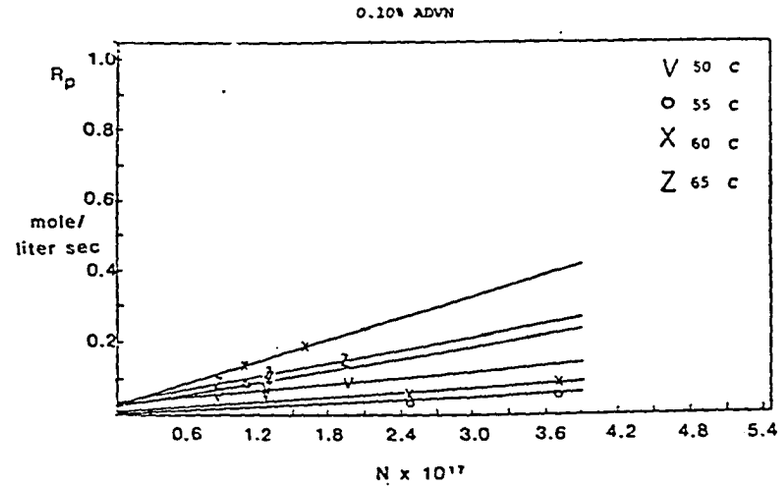

water-soluble initiator and in pairs with oil-soluble initiator. Hence none of the unusual feature of the mechanism proposed in the present work can be attributed to the unusual structure of Tetronic 1102 emulsifier but rather they must be considered characteristic of the inverse emulsion polymerization process. A very fundamental difference between conventional and inverse emulsions is the mechanism of stabilization: inverse emulsions are often not effectively stabilized against flocculation by electrostatic forces, so their intefacial layer is much more structured. Studies discussed later is this dissertation show that electrostatic forces are indeed unable to stabilize inverse polyacrylamide latexes. Transport and diffusion of monomer and initiator species through a structured interface is expected to be a much different process than through an interface covered with a monolayer of surfactant and having a uniform charge. The differences between conventional and inverse emulsion polymerization (i.e., effects of reaction parameters on the number of particles and the method of generation of oil-soluble and water-soluble radicals) are probably related to the characteristics of the interfacial region.

The decrease in polymerization rate at high initiator concentration and the occurrence of chain transfer to surfactant in persulfate-initiated systems both indicate that the surfactant is not simply on the surface of the particles but rather is incorporated inside the particles and affects diffusion. This means that the multicelled particles are best pictured as one particle subdivided into several areas than as an aggregate of several particles.

CHAPTER VI

Stabilization of Inverse Emulsion Polymers

A. Introduction: Stabilization of Water-in-Oil Colloidal Dispersions

In colloid chemistry, "stability" is defined as stability against flocculation: chemical stability is implicit. Generally colloids are stable when the repulsive electrostatic forces are larger than the attractive dispersion forces, as described quantitatively by the DLVO theory of electrostatic stabilization (6.1).

The mechanism of stabilization of water in oil emulsions is a subject of much controversy. Traditionally electrostatic stabilization has often been considered ineffective for colloidal dispersions in organic media because of the difficulty of forming ionized species in a medium of low dielectric constant. Indeed, Osmond and Waite have stated that "the repulsive electrostatic forces of the type generated in aqueous media are not generally available for stabilizing particles in liquids of low polarity such as aliphatic hydrocarbons . . . only relatively few liquids, such as water, with dielectric constants greater than about 50, are able to provide adequate dispersion stability as a result of electric charges on the particles" (6.2). On the other hand, many experimental results refute this opinion: as early as 1952, van der Minne and Hermanie measured the zeta potentials of carbon

black dispersed in hydrocarbons and concluded that the particles did indeed have an electrophoretic mobility and that their zeta potentials were sufficiently high to stabilize a dispersion (6.3). Many later experimental studies (reviewed below) support the conclusion of van der Minne and Hermanie.

The following reviews the possible mechanisms of stabilization of water-in-oil emulsions and evaluates the applicability of these mechanisms of stabilization to inverse polyacrylamide latexes prepared with a variety of surfactants, initiators, and electrolytes.

1. Electrostatic Stabilization

a. Origin of the Surface Charge

There are four mechanisms by which a colloidal particle can acquire a surface charge: dissociation of surface groups; adsorption of ionic surfactants; acid-base interactions at the interface of the surfactant; adsorption of ions; and isomorphic substitution inside a lattice. Only the first three of these appear to be important in organic media (6.4). The ion most commonly responsible for charge transfer between the particle and the medium, in the absence of adsorbed surfactant, is the proton. The particle's surface charge may depend on the relative acidity or basicity of the particle and medium (6.5, 6.6); hence the presence of even trace amounts of water can sometimes greatly influence the sign and magnitude of the surface charge (6.7). Indeed, the sign of the zeta potential may reverse when there is

enough water to form a monolayer (6.8). In a nonaqueous or aqueous colloidal dispersion containing a surfactant, the zeta potential may pass through a maximum as the surfactant concentration increases: this indicates that zeta potential is a complex function of the nature of the surfactant and medium rather than simply being a function of surface composition (6.9). In this case, the double layer is formed when proton transfer from the water to the hydrophile causes dissociation (6.10). In the case of ionic surfactant, this complex function is also affected by competitive adsorption: adsorbing a few surfactant ions initially increases zeta potential, but adding more surfactant increases adsorption of the counter-ion due to electrostatic forces and lowers zeta potential (6.11,6.12).

Zeta potentials measured in hydrocarbon media in the absence of adsorbed dispersant generally range from -52 to +90 mV, although some higher values have been reported; depending on the magnitude of the Hamaker constant, $\pm$30 to 32 mV is adequate for stabilization (6.8).

In the presence of adsorbed surfactant or dispersant, the magnitude and sign of the surface charge depends on the nature of the interaction between the particle's surface and the dispersant. Both proton transfer and electron transfer may occur between the particle surface and the surfactant, resulting in zeta potentials of over 100 mV (6.13). The sign of the particle's charge depends on the attractive forces between the particle and the surfactant:

these forces have been attributed to acid-base interactions (6.9), to the relative adsorbability of the cation and anion due to the polarity of the particle and medium, and to competitive adsorption of the ionic species in conjunction with a solution effect (that is, adsorption of one type of surfactant ions increases the potential, then electrostatic forces are strong enough to increase adsorption of the counter-ions) (6.9).

b. Electrostatic Repulsion

The electrostatic repulsion is controlled by the "thickness" of the double layer calculated from Debye-Huckel theory (6.14):

$$k = \left(\frac{4\, e^2 \Sigma_i z_i^2 n_{io}}{\varepsilon k T}\right)^{1/2}$$

where e is the electronic charge, z_i is the valence, n_{io} is the bulk concentration of ions of type i per unit volume, is the medium's dielectric constant, k is Boltzmann's constant, T is the absolute temperature, and k is the reciprocal double layer "thickness" (i.e., the Debye length). The energy of electrostatic repulsion between charged spheres (V_R) can be calculated using the following equation (6.26):

$$V_R = \frac{\psi_o^2 \varepsilon a^2 \beta}{H+2a} \exp(-kH)$$

where β accounts for electric field distortion as double layers overlap, a is the particle radius, H is the interparticle separation distance, and ψ_o is the surface potential.

The impossibility of electrostatic repulsion in organic media has been argued on two observations: that the Debye length is sometimes so great that the double layers overlap even in dilute solution; and that the low dielectric constant of hydrocarbon media makes the energy of electrostatic repulsion very small, since the repulsion energy is proportional to the dielectric constant.

Data generated using carbon black dispersions in oil medium containing surfactant show that the argument of excessively long Debye length is not universally valid. By assuming that one proton per micelle has been added or removed to provide the charge carrying species, the number of ions per unit volume can be calculated from the conductivity, and a very short Debye length is found because the medium has a low dieletric constant (6.13).

It has been argued that there are too few counter-ions between particles to treat mathematically as a uniformly smeared-out charge, making it difficult to ascribe interparticle repulsion to the interactions of ions far away from the parent particles, so the expression for Coulombic repulsion ($V_R = q^2/((H + 2a)\varepsilon)$ should be used rather than an expression related to double-layer overlap (6.15). However, the expression given above for electrostatic repulsion is not inappropriate because it contains only a correction term for overlapping ionic atmospheres and, in the limit of low K, expresses simply the Coulombic repulsion (6.16) The ϵ ·or introduced in calculating the electrostatic repulsion considering

only Coulombic repulsion is serious for small particle separations (6.17). In this limiting case, this equation shows that large particles can be better stabilized. The observed "limited coalescence" of oil droplets in coarse o/w emulsions (i.e., the coalescence of droplets at a rate decreasing to zero as droplets approach a limiting average size and polydispersity) is another indication of the favored stabilization of larger droplets (6.18).

The argument that low dielectric constant makes electrostatic repulsion impossible is not supported by experimental data: since the dielectric constant for a typical oil is 2 and that of water is 80, if ψ_o of 20 mV is adequate for stabilization in water, then ψ_o of 127 mV is required for the same electrostatic repulsion in oil (6.12). Zeta potentials of this magnitude have been observed in hydrocarbon media (6.8,6.13). Albers and Overbeek find zeta potentials of up to 130 mV for water-in-benzene emulsions stabilized with metal oleates (6.19).

A unique feature of double layers in media of low dielectric constant is low capacitance: small surface charges are sufficient to produce appreciable potentials (6.4). This supports the possibility of significant electrostatic repulsion, although it does make it difficult to consider the double layer as uniformly smeared out.

Configurational effects may also influence electrostatic repulsion. Romo has shown, using dispersions of alumina and

aluminum hydroxide in alcohol, that repulsion decreases as the alcohol's carbon chain length increases: This is attributed to lower structural density of the molecules adsorbed at the surface (6.8).

c. Van der Waals Attraction

Typically, in aqueous dispersions, van der Waals attractive forces are important over a longer range than electrostatic repulsive forces. However, in non-aqueous dispersions, the long Debye length causes the attractive forces to decay more rapidly than the repulsive forces. The Hamaker constant for interparticle interactions (A_{22}) is estimated to be 3-20% smaller in hydrocarbon medium than in aqueous medium (6.20):

$$V_A = -\frac{Ar}{12\pi H^2}$$

where A is the effective Hamaker constant ($A = A_{11}^{1/2} - A_{22}^{1/2}$). Effective Hamaker constants in oil medium have been calculated to be of the same order of magnitude as in aqueous medium (6.21). Indeed, Hamaker constants are truly constant only in hydrocarbon media: in aqueous media they are actually functions of the interparticle distance (6.22). An adsorbed layer having a Hamaker constant different from those of the dispersed phase and medium decreases the attractive energy, owing either to increased interparticle distance or to a change in the effective Hamaker constant (6.23).

d. Total Interaction

The total interaction energy V_T is the sum of V_A and V_R.

Calculating the variation in interaction energy (V_T/kT) as a function of separation distance H, at given values of the zeta potential, shows that the height of the energy barrier is almost independent of the effective Hamaker constant (6.58). This means that the repulsive force has a much greater effect on stability than the attractive forces (6.7). Indeed, the precise value of the attractive energy in an organic dispersion is not important unless a secondary minimum develops (6.9). Particle size, then, affects stability more than the attractive force (6.24,6.25). Increasing the zeta potential, therefore, strongly increases the height of the energy barrier. Because the electrostatic energy barrier extends over a longer distance, particles in concentrated dispersions assemble in a geometric array (6.13).

Albers and Overbeek have shown, however, that stability against coalescence is inversely related to zeta potential for water-in-benzene emulsions stabilized by metal oleates (6.19). They attribute this to the mobility of the molecules at the interface: highly charged molecules form a monolayer rather than a solid-like multilayer which is better able to stabilize. Similar results are reported by Chapman using water-in-paraffin oil emulsions stabilized by a low HLB emulsifier, magnesium stearate (6.10). Other workers have also attributed stabilization in hydrocarbon medium containing surfactant to effects due to the structure of the interface, such as resistance to wetting of

segments of the adsorbed film by the dispersed phase (6.57), formation of liquid crystals (6.27,6.28), formation of a strong interfacial film (6.29) and formation of solid particles at the interface due to surfactant hydrolysis (6.30).

Electrostatic stabilization is, in summary, possibly an effective way to stabilize nonaqueous dispersions, especially dilute dispersions of large droplets. However, factors other than electrostatic effects, such as specific effects due to the structure and rigidity of the interfacial layer, can also have an important effect on colloid stability.

Electrostatic stabilization theory considers only coagulation and coalescence as possible routes to emulsion destabilization. Higuchi and Misra have shown that molecular diffusion may also lead to emulsion destabilization if the aqueous and organic phases are not perfectly immiscible (6.31). In their studies of water-Aerosol OT (dioctyl sodium sulfosuccinate)-hydrocarbon systems, they found that, although the thermodynamic activity of the water was the same in all systems, the solubility of water in solutions of Aerosol OT in hydrocarbon decreased as the hydrocarbon chain length increased. That is, diffusion becomes more difficult as the solubility of the internal phase in the external phase decreases. Hence the driving force for degradation by diffusion is the miscibility of the internal phase as determined by its molal interfacial area. Since diffusion rate is related to surface area, the interparticle difusion rate should also be faster if the

droplets are smaller. Smaller particles are less thermodynamically stable than larger particles because internal pressure increases as particle radius decreases; hence, the larger particles grow at the expense of the smaller ones. This is in agreement with the prediction from electrostatic stabilization theory that stabilization of larger droplets is favored (6.17,6.18). Higuchi and Misra also showed that addition of small amounts of a third component which distributes preferentially into the dispersed phase dramatically increases emulsion stability, which shows that hindering molecular diffusion improves emulsion stability. In the system being studied, the addition of acrylamide, which is unable to diffuse through a hydrocarbon medium, to water inhibits interparticle diffusion of water. Other studies have shown that the increase in stability of water-in-oil emulsions resulting from addition of paraffins or alkanes was greater when the additive's chain length was longer, in agreement with Higuchi and Misra's molecular diffusion theory (6.32,6.33).

2. Steric Stabilization

Steric stabilization is defined as prevention of flocculation by adsorption or chemical bonding of nonionic polymer chains onto the colloidal particle's surface. Colloidal particles are surrounded by clouds of polymer chains which prevent the particles from contacting each other. No electrostatic component is operative (6.56). Steric stabilizers prevent flocculation because

interaction of the polymer chains will increase the free energy of the two particles by increasing enthalpy and decreasing entropy, and lead to repulsion between particles. Steric stabilization is poorly understood fundamentally. A review of the theoretical models is beyond the scope of this report, and the reader is referred to a recently published review (6.2).

The molecular weight and chemical composition of the steric stabilizer, along with polymer-solvent and solvent-surface interactions, determine its effectiveness (6.34). Stabilizer is adsorbed until the surface is saturated. An effective steric stabilizer must be adsorbed sufficiently strongly and irreversibly to maintain complete surface coverage, must be sufficiently concentrated at the interface to generate enough osmotic pressure to resist van der Waals attractive forces, and must form an interfacial layer thick enough to prevent flocculation. Homopolymers and random copolymers are often too weakly and reversibly adsorbed, or form too thin a barrier, to effectively stabilize dispersions in organic media.

The most effective stabilizers have a moiety strongly anchored to the particle's surface so that it is neither desorbed nor displaced when another particle approaches. These stabilizers are graft or block copolymers containing two polymeric components: one insoluble in the continuous phase and the other soluble. The insoluble block anchors the molecule to the particle's surface by associating with the particle; the soluble block provides stability

against flocculation by forming a hydrophobic layer covering the particle's surface. Clearly, such molecules will form aggregates analagous to micelles in the continuous phase. The molecular weight of the insoluble block must be at least 1000 to ensure sufficient insolubility, and the soluble block should have similar molecular weight to ensure formation of a stable micellar solution rather than precipitation. Molecules of this type are conventionally called dispersants.

The most important criterion for selecting the insoluble (anchoring) block is strong attachment to the particle's surface. This can be accomplished by physical adsorption, although stronger forces such as covalent bonding or acid-base interactions may be necessary. The anchor group also must be freely soluble in the dispersed phase in order to form stable dispersions of small particle size (6.34). The criterion for selection of the soluble component is free solubility in the organic medium: solubility parameters are useful in selecting a suitable component. This procedure for selecting the soluble and insoluble blocks is analagous to the HLB concept for surfactants.

Block and graft copolymer molecules form ordered structures in solvent because of microphase separation. In dilute solution of selective solvents (i.e., a solvent or solvent system which solvates one block and precipitates the other) micelles form which possess a compact core consisting of insoluble blocks and a shell

consisting of soluble blocks (6.35). The concentrations normally used for steric stabilization are usually quite dilute (i.e., concentrations of only a few weight percent). In concentrated solution (>20%), rigid, organized structures such as cylinders and lamellae form. Molecules capable of forming such ordered structures may also be capable of liquid crystal formation. Liquid crystalline phases in emulsions have been shown to greatly enhance stability (6.36). The increased stability is attributed to both reduction of the Van der Waals attraction potential during collision as well as increased interfacial viscosity by the multilayer structure formed by the liquid crystals (6.37).

3. Calculation of Dispersion Stability

a. Flocculation Rate

Dispersion stability can be quantified by the half-time for dispersion flocculation, i.e. the product of the stability ratio W and the Smolukowski half-time τ:

$$W = \frac{1}{2a} \int_{o}^{\infty} \exp(V_T/kT)dH$$

$$\tau = 3\eta/4kTv_o$$

$$W\tau = (3\eta/8kTv_o a)\int_{o}^{\infty} \exp(V_T/kT)dH$$

where η is the viscosity and v_o is the number of particles per unit volume before flocculation:

$$v_o = 3/4\ a^3$$

where ϕ is the volume fraction of internal phase.

The relationship between surface potential and dispersion stability calculated in this way for dilute dispersion (i.e. no double layer overlap) is explained well by DLVO theory (6.28). Half-times of several years have been calculated for concentrated organic dispersions containing surfactants (6.13). In contrast to this finding of long half-times, Albers and Overbeek, considering only Coulombic repulsion and neglecting double layer effects, have shown by theoretical calculations that flocculation is rapid and occurs until the droplet concentration is so low that the distance between droplets is much larger than the double layer thickness (6.28). Silica dispersions in alcohol, which are stabilized by electrostatic repulsion due to charge originating from the silanol groups, are stable for many months; if these silanol groups are esterified with higher alcohols such as stearyl alcohol, the dilute dispersion in cyclohexane or octane is stable for several years (6.39). However, in agreement with Albers and Overbeek (6.38), concentrated dispersions (dispersed phase volume fraction greater than 30%) are found to be unstable. Similarly, Feat and Levine have predicted by theoretical studies that double layer effects can not stabilize concentrated nonaqueous dispersions (6.24).

b. Rheological Studies

Rheological studies of colloidal systems can give insight into stability by providing information on the thickness of the adsorbed steric "barrier" as well as on the state of flocculation and

changes in it with changing shear rate.

The rheological behavior of dispersions was first studied by Einstein (6.40), who showed that the viscosity of a dilute (<5 vol %) suspension depends only on volume fraction of the particles and is independent of particle size or polydispersity:

$$\eta_r = \eta/\eta_o = 1 + 2.5\phi$$

where η_r is the relative viscosity, η is the viscosity of the dispersion, η_o is the viscosity of the continuous phase, and ϕ is the volume fraction of the particles. Thomas (6.41) extended this relationship to phase volumes of up to 60%:

$$\eta_r = 1 + 2.5 \quad + 10.5^{2} + 2.73 \times 10^{-3} \exp(16.6\phi)$$

In concentrated dispersions (>40%), particle size significantly affects viscosity: at constant latex solids, viscosity is higher if the particles are smaller (6.42).

b.1. Adsorbed Layer Thickness

The thickness of the adsorbed layer of steric stabilizer can be calculated by comparing the effective hydrodynamic diameter of the particles with the particle diameter measured by an independent method such as electron microscopy. The relationship between reduced viscosity and phase volume is fitted to a quadratic equation similar to the Thomas equation: the difference between the experimentally determined coefficient of the linear term and the value of 2.5 found in Thomas' equation is related to the steric barrier

thickness (6.43). To confirm that the calculated coefficient ratio is indeed due to an adsorbed layer and not to agglomeration or nonspherical particles, a similar relationship has been derived between the effective hydrodynamic phase volume and the average particle diameter D to calculate the thickness of the barrier (6.44):

$$\phi = 2.5 + (15\Delta/D)$$

The thickness calculated in this way is the hydrodynamic thickness, which affects the dispersion's rheological behavior; the steric thickness, which is half the distance between two particles when significant repulsion occurs, is approximately the same as the hydrodynamic thickness if the stabilizer has a narrow molecular weight distribution but may be twice the hydrodynamic thickness if the stabilizer is polydisperse (6.45).

b.2. State of Flocculation

An early attempt to understand the effect of aggregation on flow properties described rheological behavior of a colloidal dispersion in terms of the rate constants for interparticle linkage formation and rupture which are related to the rate constants for flocculation and deflocculation (6.46). Although the rate constants could not be derived from shear stress-shear rate measurements, these parameters were determined: the ratio of the rate constants for shear-induced flocculation compared to Brownian motion-induced flocculation; and the ratio of the probabilities for thermally-induced rupture compared to shear-induced rupture. The

viscosity profile of a colloidal dispersion gives information on its state of flocculation: in dilute systems (<20% by volume), non-Newtonian behavior, thixotropy, and the presence of a yield value indicate flocculation or particle association (6.43,6.44); but in concentrated systems, non-Newtonian behavior is observed due to crowding (6.47). These generalizations are based on a model of the dispersion as a suspension of uniform rigid spheres in which hydrodynamic and Brownian forces are more important than Coulombic and van der Waals forces. However, even dilute dispersions can be non-Newtonian if the dispersed droplets can be deformed by shearing, or if the particle size distribution is very polydisperse, if the particles are nonspherical, or if Coulombic and van der Waals forces are important (6.48).

In cases where flocculation is due to strong van der Waals attractive forces, several attempts have been made to estimate the van der Waals attraction constant from rheological measurements; none of these has been entirely satisfactory (6.30,6.49). A more recent approach has considered the flow unit to be a doublet and has included the energy dissipation due to movement of liquid between the disaggregated spheres in calculation of the total energy dissipation (6.51). The structure of a rapidly settling dispersion is organized on several levels and hence leads to anomalously large sediment volumes: primary particles; flocs of primary particles strongly bonded together; and loose aggregates held

together by mechanical entanglements (6.50).

Changes in w/o emulsion rheology on aging have been studied by Sherman in a classic series of papers (6.52). The decrease in viscosity of water-in-paraffin oil emulsions stabilized by nonionic surfactant is attributed to the increase in the mean droplet size. The van der Waals attractive constant is calculated from the minimum velocity gradient required to deflocculate agglomerated droplets. Shearing a flocculated emulsion at progressively higher shear rates first tightens the initially loose packing but eventually disrupts the floc structure; hence at high shear rates (215.5 sec^{-1}) all emulsions have the same viscosity.

B. Results

Surfactants and initiators used in this study are listed in Table 6.1. Latexes were prepared by bottle polymerization; under this mild agitation, the multicellular monomer emulsion formed with the block copolymeric surfactants Tetronic 1102 and Pluronic L92 does not survive polymerization and hence transmission electron microscopy shows that none of the latexes in this study are multicellular. Both persulfate and azo initiator were used, at a level of 0.04 mole % based on moles monomer, to evaluate the effect of ionic residues. Several surfactant blends mentioned in the patent literature were included. Electrolyte was added in some cases tc evaluate the effect of double layer compression. Latex particle size and polydispersity were measured (Table 6.2).

TABLE 6.1

Latexes Prepared* for Stability Studies

Designation	Surfactant	Surfactant Level[1]	Initiator	Other Additive[4]
A	Tetronic 1102	4%	ADVN	
B	Tetronic 1102	12%	ADVN	
C	Span 60	4%	ADVN	
D	Span 60	12%	ADVN	
E	Pluronic L92	4%	ADVN	
F	Pluronic L92	12%	ADVN	
G	3/1 Span 60/ Tween 61[2]	12%	ADVN	
H	1/1 OLOA 340D/ Emid 6545[3]	12%	ADVN	
I	Span 60	12%	ADVN	5% Na_2SO_4 (on monomer solids)
J	Tetronic 1102	12%	ADVN	" " " "
K	Tetronic 1102	4%	KPS	
L	Span 60	4%	KPS	

*Prepared by bottle polymerization at 55°C.

[1]% on continuous phase volume.

[2]Tween 61 = polyoxyethylene (4) sorbitan monostearate

[3]Emid 6545 = oleic diethanolamide

[4]Added to monomer solution before emulsification.

TABLE 6.2

Latex Particle Size (nm)

Designation	Variables	D_N	D_W	PDI
A	4% Tetronic 1102	33.6	45.8	1.361
B	12% Tetronic 1102	26.6	35.0	1.317
C	4% Span 60	23.1	29.5	1.276
D	12% Span 60	32.8	43.3	1.319
E	4% Pluronic L92	33.1	51.6	1.556
F	12% Pluronic L92	28.8	36.4	1.264
G	3/1 Span 60/Tween 61	34.5	45.3	1.313
H	1/1 OLOA 340D/Emid 6545	36.3	52.1	1.434
I	12% Span 60/Na_2SO_4	34.4	46.8	L.367
J	12% Tetronic 1102/Na_2SO_4	20.8	24.0	1.152
K	4% Tetronic 1102/KPS	30.4	38.8	1.276
L	4% Span 60/KPS	18.6	23.2	1.253

Electrophoretic mobility and specific conductance were measured; from these data, the zeta potential, the Smolukowski half-life for rapid flocculation ($T_{1/2}$), the diffusion coefficient, the concentration of ions per unit volume, and the Debye length (1/k) were calculated (Table 6.3). The difficulty of stabilizing these latexes is apparent on consideration of the Smolukowski time (i.e., the average time between collisions), which is generally less than one millisecond. Since collisions are very frequent, it is difficult to reduce the sticking probability sufficiently to prevent flocculation.

Zeta potentials are all positive, indicating that the polyacrylamide particles are cationic. Hydrolysis of polyacrylamide may also cause positive zeta potentials; however, hydrolysis normally requires more extreme pH and higher temperatures than were used in this study. Evidently the particles are cationic due to acid-base interactions between polymer and surfactant. The zeta potentials are quite large in some cases: they approach or exceed 100 mV in some cases, which is sufficiently high for significant electrostatic repulsion and also for electrostatic stabilization. Zeta potentials are highest in the case of latexes prepared with Tetronic 1102, Pluronic L92, and Span 60 blended with Tween 61. Adding electrolyte increases zeta potential in the case of Span 60, as expected for an electrostatically stabilized latex; however, adding electrolyte decreases the zeta potential of latex prepared with Tetronic 1102. Similarly, using persulfate initiator raises

TABLE 6.3

Electrokinetic Measurements

Desig-nation	Variables	Electro-phoretic Mobility $cm^2/volt \cdot sec$	Specific Conductance[1] mho/cm $x10^{-7}$	Ions ℓ_2 n^2 $x10^{20}$	Zeta Potential mV	Debye Length $1/k^3$ nm	Smolukowski Time[4] $t^{1/2}$ msec	Diffusion Coeffi-cient[5] D $x10^{-11}$
A	4% Tetronic 1102	0.10	1.2	1.2	52.6	3.9	0.049	1.63
B	12% Tetronic 1102	0.21	1.2	0.94	114.0	4.8	0.026	2.05
C	4% Span 60	0.005	1.1		2.63	4.9	0.065	2.36
D	12% Span 60	0.005	1.1		2.63	4.2	4.63	1.70
E	4% Pouronic L92	0.16	1.2	1.2	84.2	4.0	0.039	1.65
F	12% Pluronic L92	0.056	1.2	1.0	29.5	4.2	0.045	1.89
G	3/1 Span 60/ Tween 61	0.10			52.6		0.066	1.58
H	1/1 OLOA 340D/ Emid 6545	0.05			26.3		0.28	1.50
I	12% Span 60/Na_2SO_4	0.08	2.9	2.7	42.1	2.6	0.49	1.71
J	12% Tetronic 1102/ Na_2SO_4	0.04	1.2	0.73	21.1	5.0	0.039	2.63
K	4% Tetronic 1102/ KPS	0.05			26.3		0.15	1.80
L	4% Span 60/KPS	0.01			5.27		0.034	2.94

Table 6.3 (Continued)

[1]The specific conductance of distilled deionized water = 9×10^{-7} mho/cm.

[2]$n = \sigma kT/e^2D$ where σ is the specific conductance of the latex and e is the electronic charge.

[3]$1/K = (\varepsilon_r \varepsilon_o D/2\sigma)^{1/2}$ where ε_r is the dielectric constant of o-xylene and ε_o is the permittivity of free space.

[4]$T_{1/2} = 3\eta/4kT\ v_o$; $v_o = 3\phi/4\pi r_p^2$ where η is the latex viscosity, ϕ is the disperse phase volume, and r_p is the particle radius.

the zeta potential in the case of Span 60 but not in the case of Tetronic 1102. Increasing the concentration of Pluronic L92 lowers the zeta potential of the latex: the significance of this is not clear due to the complex relationship of the zeta potential to the nature of the surfactant and medium (6.9). Perhaps proton transfer from the water to the hydrophile causes dissociation of the hydrophile (6.10). In the case of nonionic surfactants, the double layer may be formed by dissociation due to proton transfer from the water to the hydrophile (6.39). Perhaps, in the Pluronic L92 system, this proton transfer is disfavored by adding more surfactant. The Debye lengths (i.e., the double layer "thickness") averages 4.2 nm, which is roughly 1/10 the diameter of the particles. This length is clearly short enough for electrostatic repulsion to be operative. Adding electrolyte (which is soluble only in the dispersed phase) to latex prepared with Span 60 decreased the Debye length significantly (38%), as expected when the double layer is compressed. However, added electrolyte has no significant effect on the Debye length of latex containing Tetronic 1102.

A notably high concentration of ions per unit volume is found in Span 60 latex with added electrolyte, which is consistent with significant electrostatic repulsion. On the average, the molar concentration of ions in these latexes was 1 mM, which is in the range usually sufficient to stabilize dispersions in aqueous medium.

These electrokinetic measurements indicate that significant electrostatic repulsion can exist between particles in these latexes. The effect of electrolyte on latex electrokinetic properties is characteristic of an electrostatically stabilized latex in the case of Span 60 latex but not in the case of Tetronic 1102 latex. Of course; the presence of significant electrostatic repulsion is not necessarily sufficient for electrostatic stabilization. The correlation between electrokinetic properties and stability against flocculation must be established to identify the mechanism of stabilization. Rheological measurements are also useful in establishing the mechanism because they give information on the state of aggregates in the system.

The settling behavior of latexes was quantified both by comparing the appearance of the fresh latex with that of latex aged one week and by recording the number of weeks required for the latexes to settle sufficiently to form a translucent upper layer (Table 6.4). Distinct differences among latexes can be seen after aging for only one week. All monomer emulsions except those prepared with Tetronic 1102 settled significantly after one week: even the Tetronic 1102 emulsion settled in the presence of electrolyte,perhaps due to increased particle density. The long-term stability of latexes prepared with Tetronic 1102 and Pluronic L92 is dramatically better than with any other surfactant: the latexes prepared with Tetronic 1102 or Pluronic L92 remain stable for over eight months whereas with other surfactants they settle

TABLE 6.4

Settling Behavior

Designation	Variable	Appearance of Fresh Latex	Appearance After 1 Week		Weeks to Settle*
			Monomer Emulsion	Latex	
A	4% Tetronic 1102	No coagulum, v. fluid	No change		30
B	12% Tetronic 1102	" " "	No change		30
C	4% Span 60	Much coagulum, vs. fluid	Complete settling		1
D	12% Span 60	No coagulum, v. viscous	Some settling		3
E	4% Pluronic L92	Tr. coagulum, v. fluid	Some settling	No change	30
F	12% Pluronic L92	No coagulum, vs. fluid	Tr. settling	No change	30
G	3/1 Span 60/ Tween 61	Tr. coagulum, v. viscous	Complete settling		1
H	1/1 OLOA 340D/ Emid 6545	Tr. coagulum, v. viscous	Complete settling		1
I	12% Span 60/ Na_2SO_4	Tr. coagulum, sl viscous	Complete settline	Some settling	3
J	12% Tetronic 1102/ Na_2SO_4	No coagulum, v. fluid	Some settling	No change	30
K	4% Tetronic 1102/ KPS	mod. coagulum, v. fluid	Some settling	No change	12
L	4% Span 60/KPS	Tr. coagulum, v. fluid	Complete settling		1

*Settling time = time required for phase separating resulting in formation of a translucent upper (oil) layer in the latex.

within three weeks.

The viscosity stability was determined by measuring shear stress at shear rates of 8 to 1000 sec^{-1} as the latexes aged. The viscosity at very low shear rates was not measured because very small shear stresses could not be measured reliably. Viscosity profiles are shown in Fig. 6.1-6.9. The Tetronic 1102 and Pluronic L92 surfactant dispersions were Newtonian (Figures 6.2a, 6.3a), while the Span 60 solution is shear-thinning (Figure 6.1a) even at low concentration (4%): this indicates that the Span 60 molecules associate in solution while the Tetronic 1102 and Pluronic L92 block copolymers do not. This is not surprising, since block copolymers do not form molecular solutions. The high viscosity of the Span 60 solution reflects the rigidity of these molecules, which is not unexpected since Span 60 probably forms fibrous structures below the melting point of the stearate groups.

The Span 60 latexes were pseudoplastic (Figure 6.1b) whereas the Tetronic 1102 and Pluronic L92 latexes were Newtonian (Figures 6.2b,6.3b): this indicates that the latex particles in the Span 60 latex are aggregates. The viscosity profile of Tetronic 1102 latexes was strongly affected by the presence of ionic species: addition of electrolyte (Figure 6.8b) and, to a lesser extent, use of KPS initiator (Figure 6.9b) induced pseudoplasticity. This is not a double layer effect, since the molar concentration of ions and the Debye length are only slightly affected by ionic species:

Figure 6.1

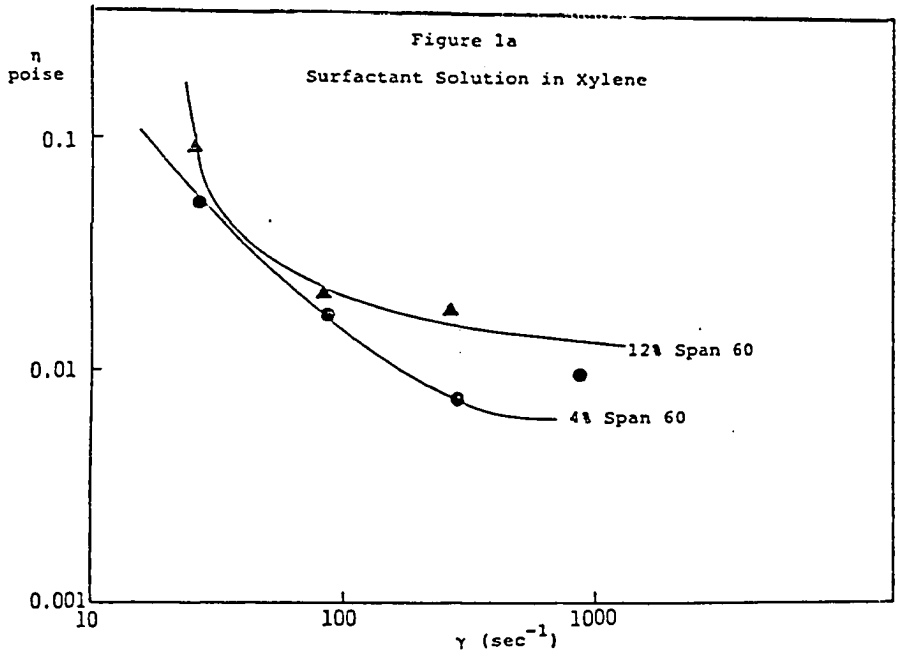

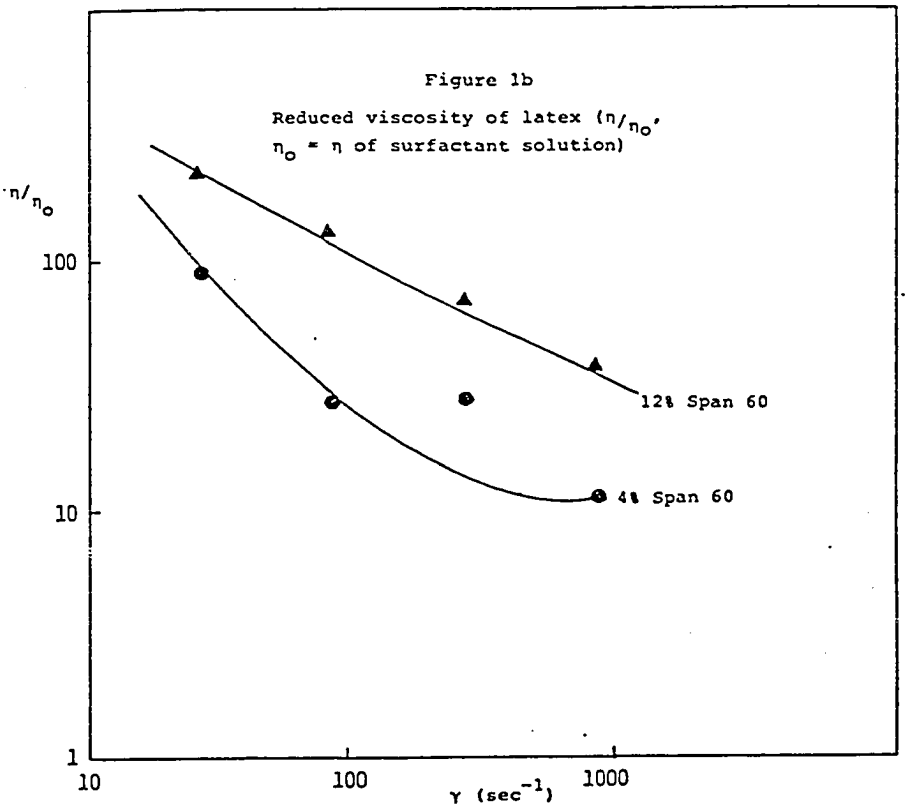

Figure 6.2

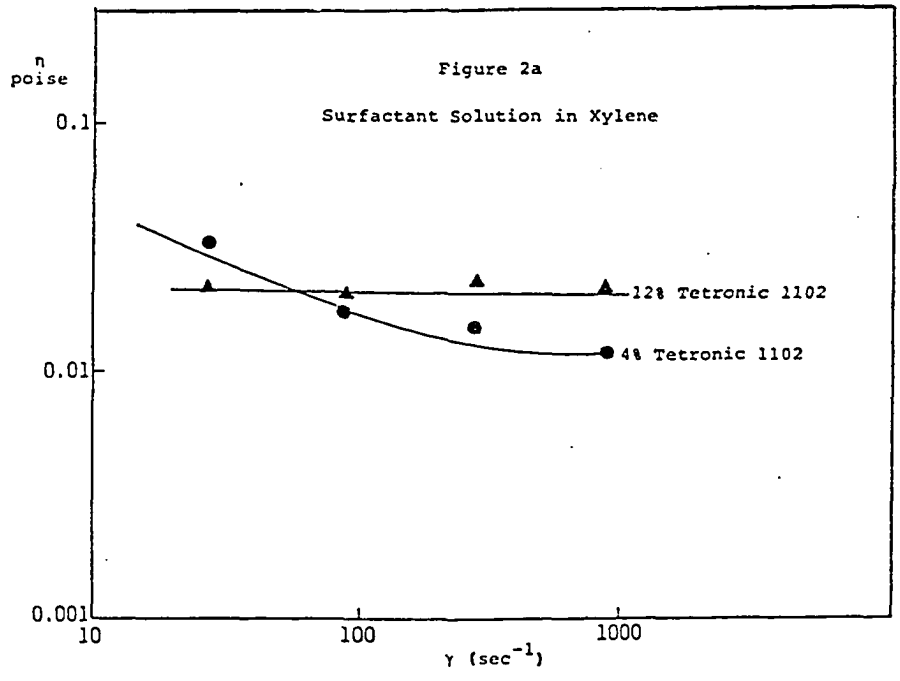

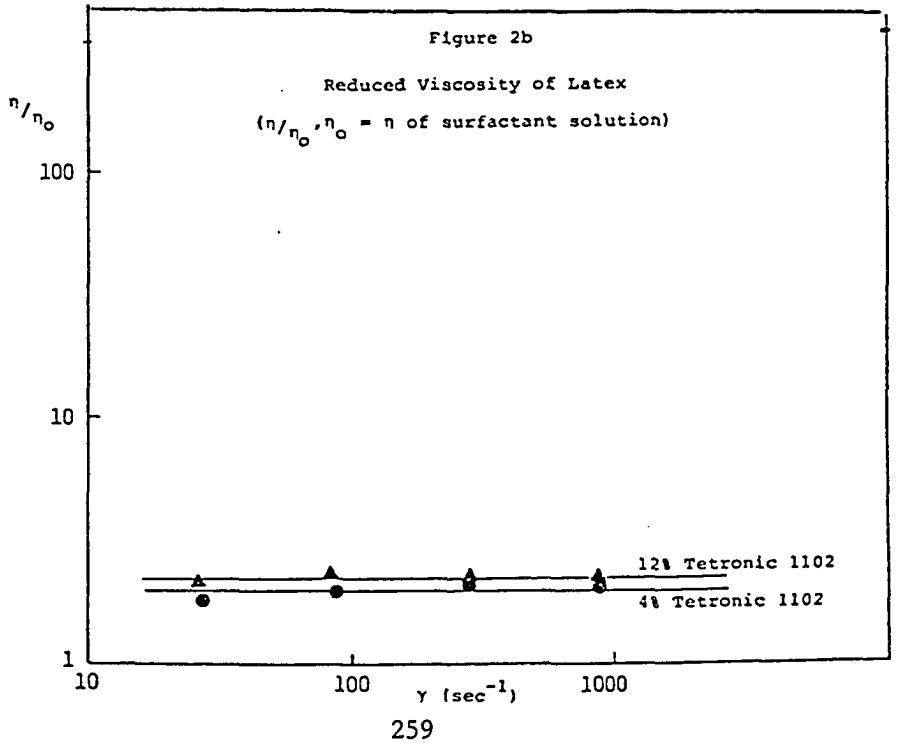

Figures 6.3

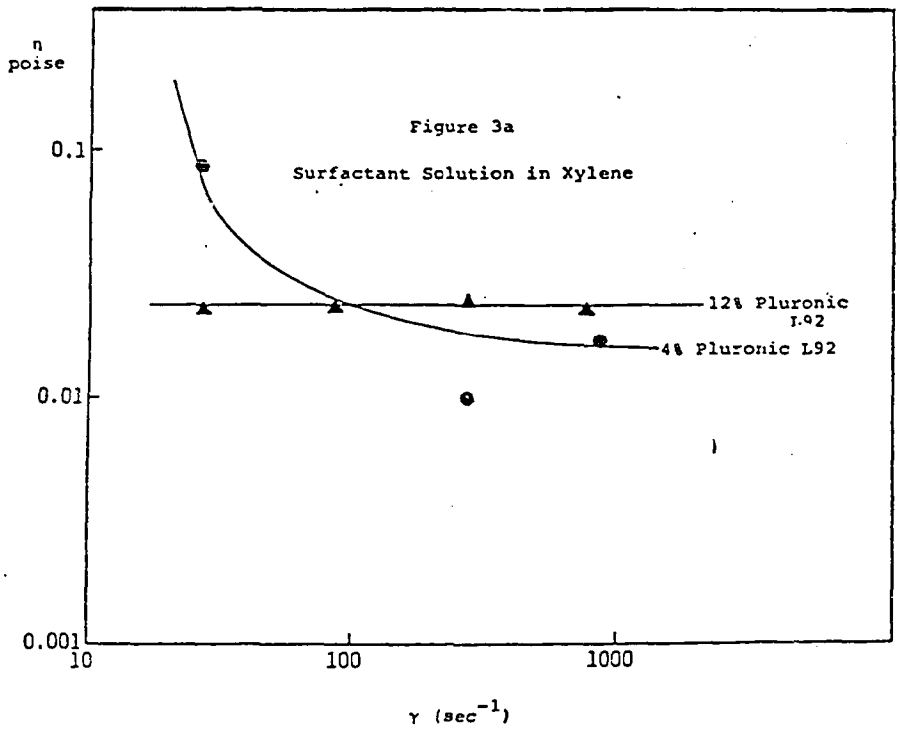

Figure 3a

Surfactant Solution in Xylene

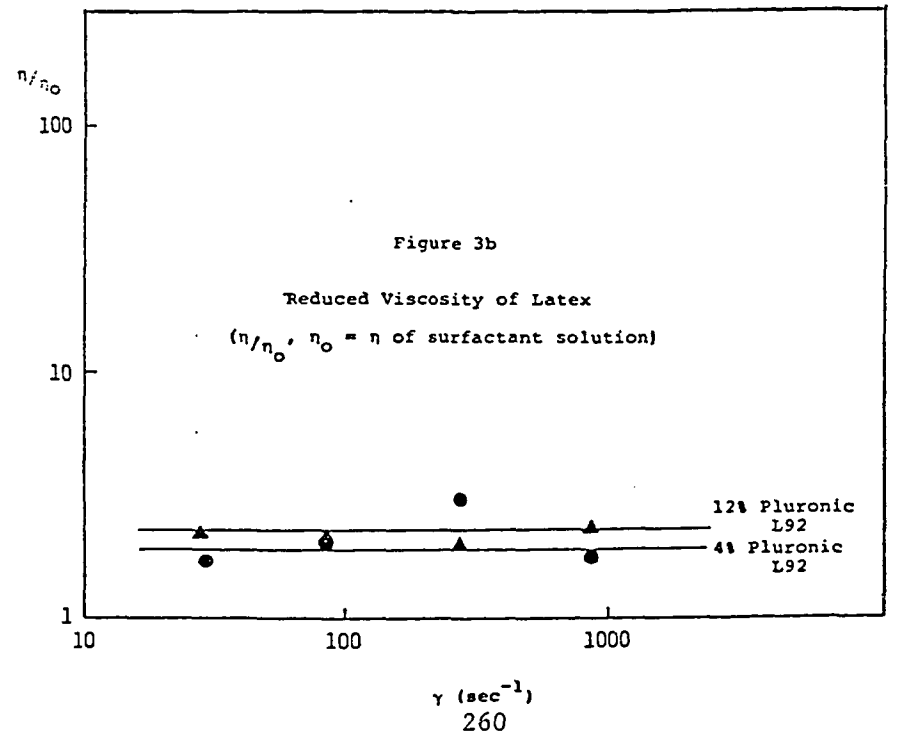

Figure 3b

Reduced Viscosity of Latex

(η/η_o, η_o = η of surfactant solution)

Figures 6.4

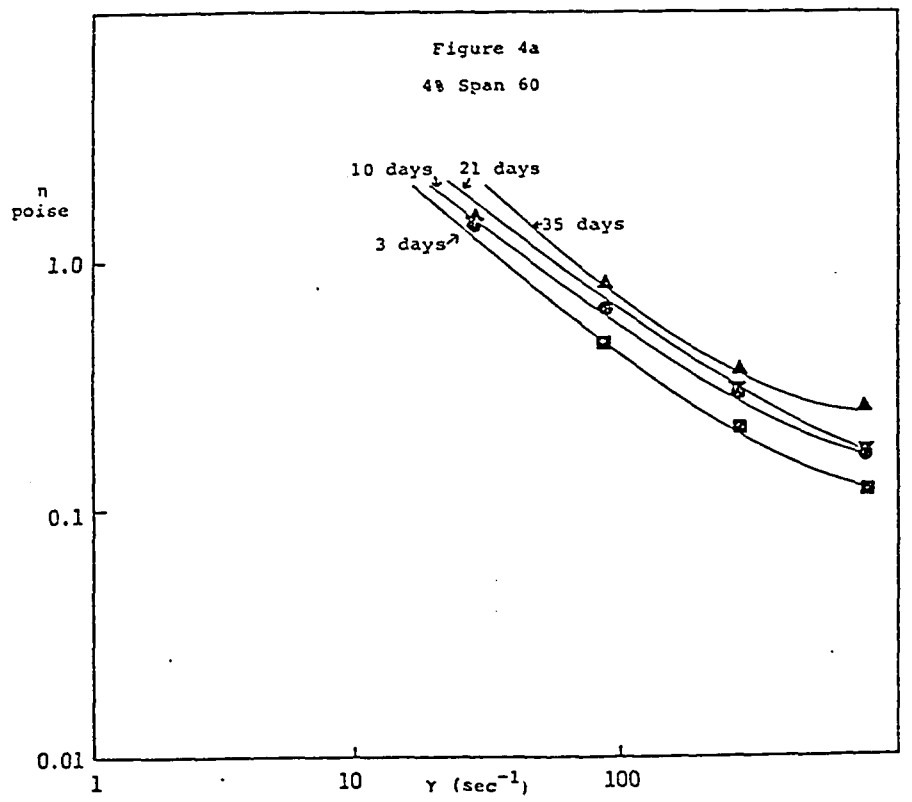

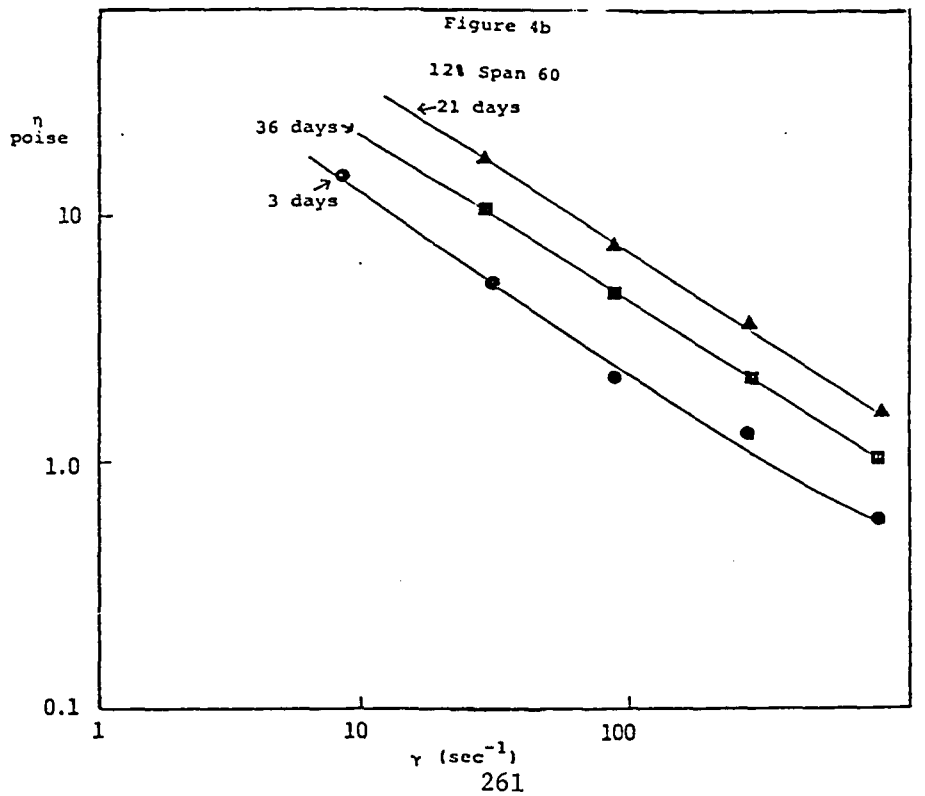

Figures 6.5

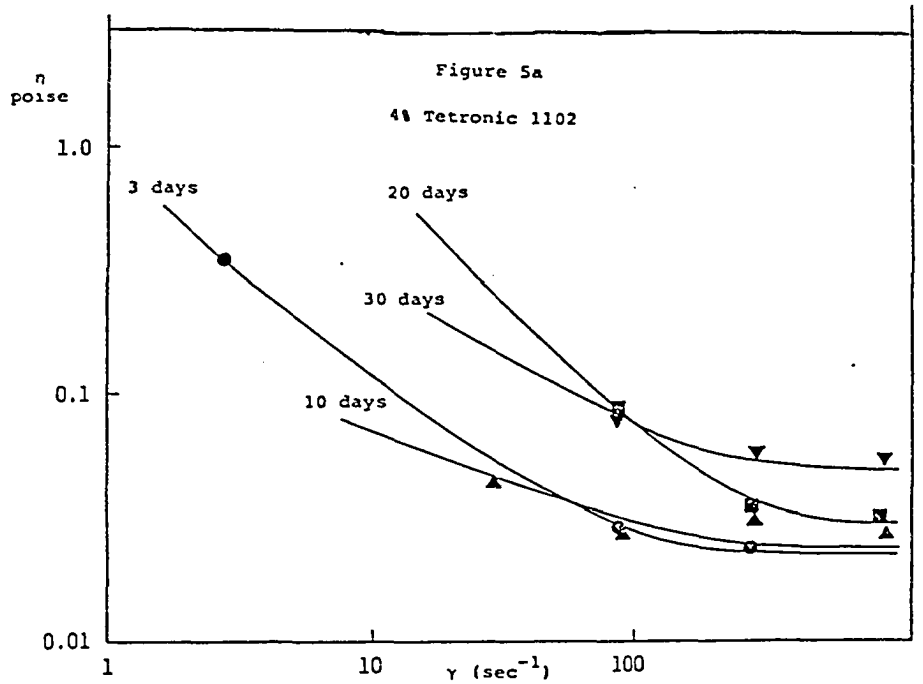

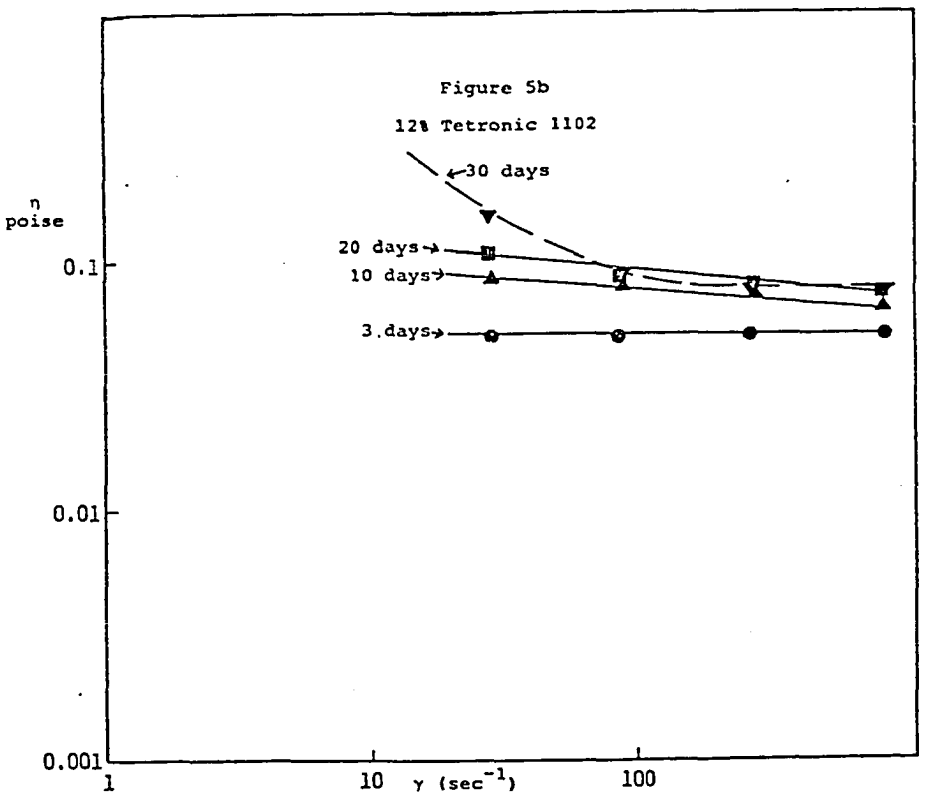

Figures 6.6

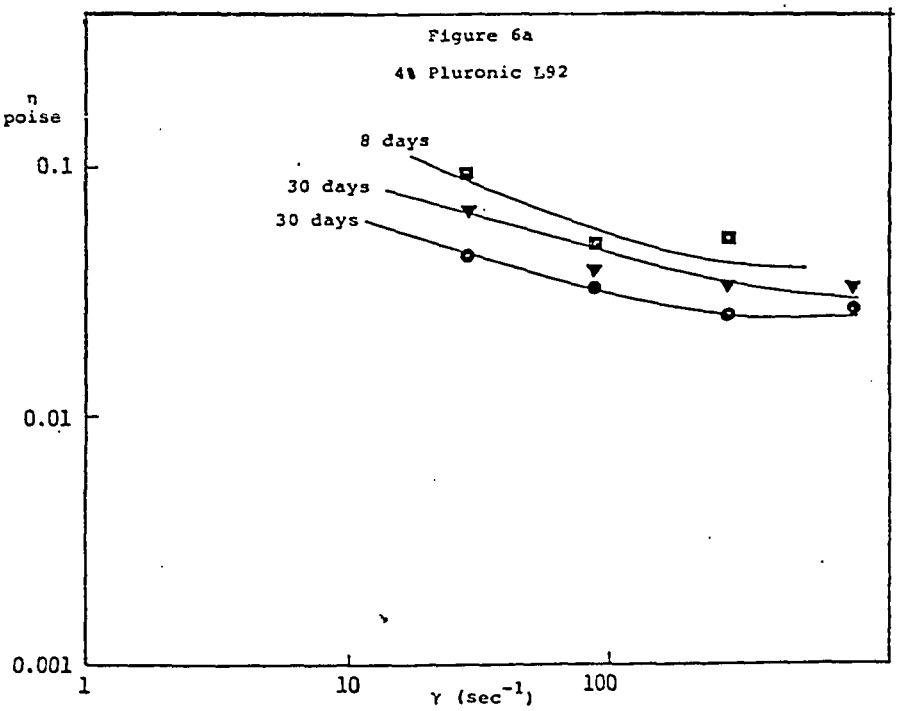

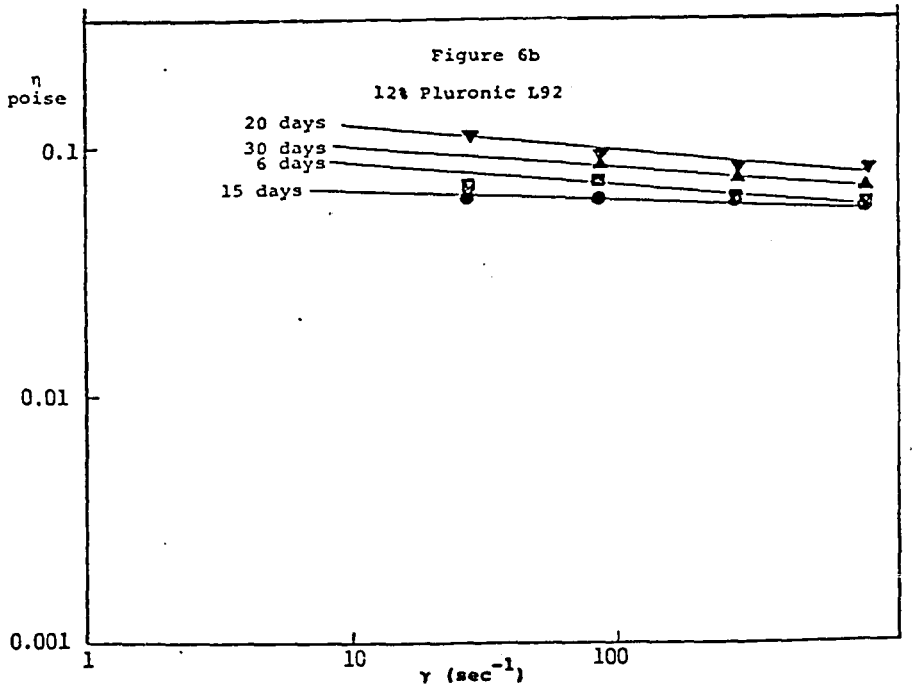

Figures 6.7

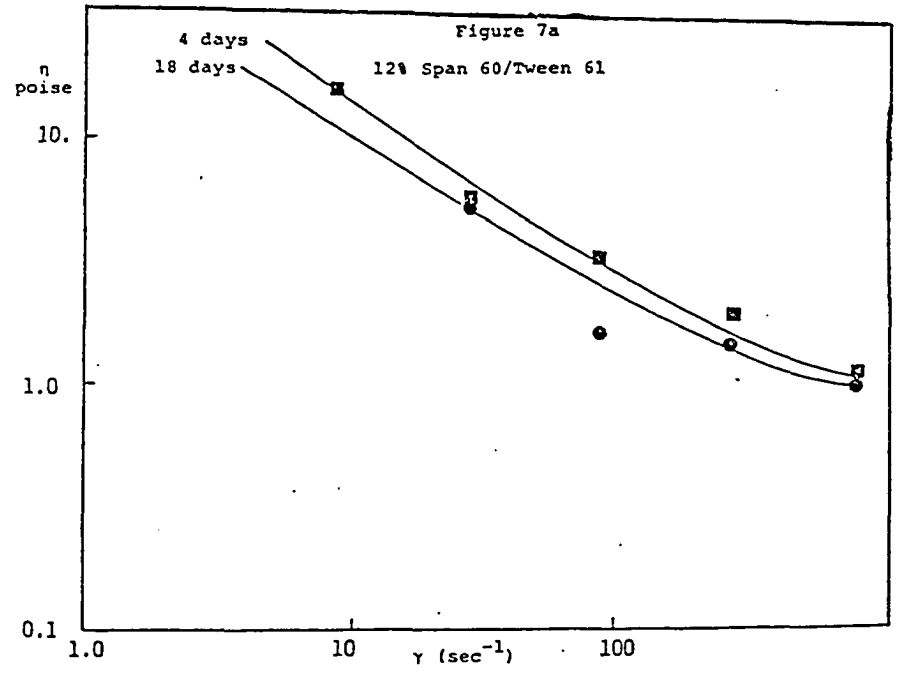

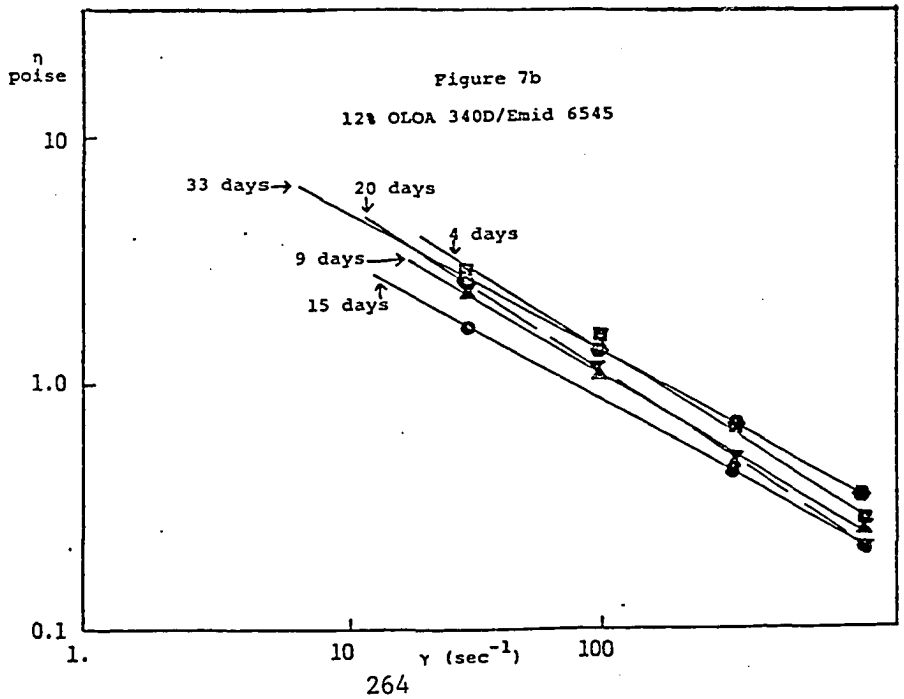

Figures 6.8

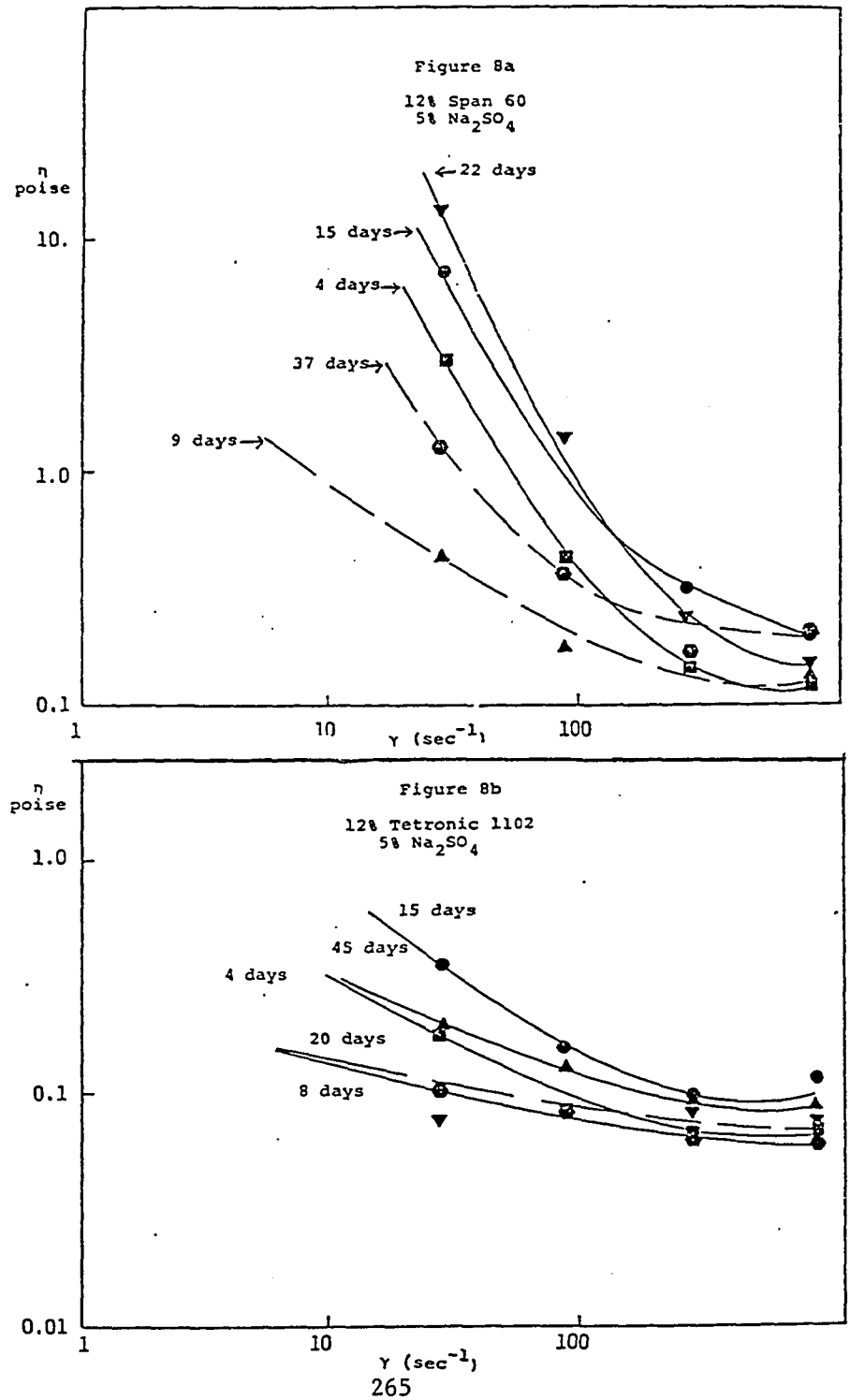

Figures 6.9

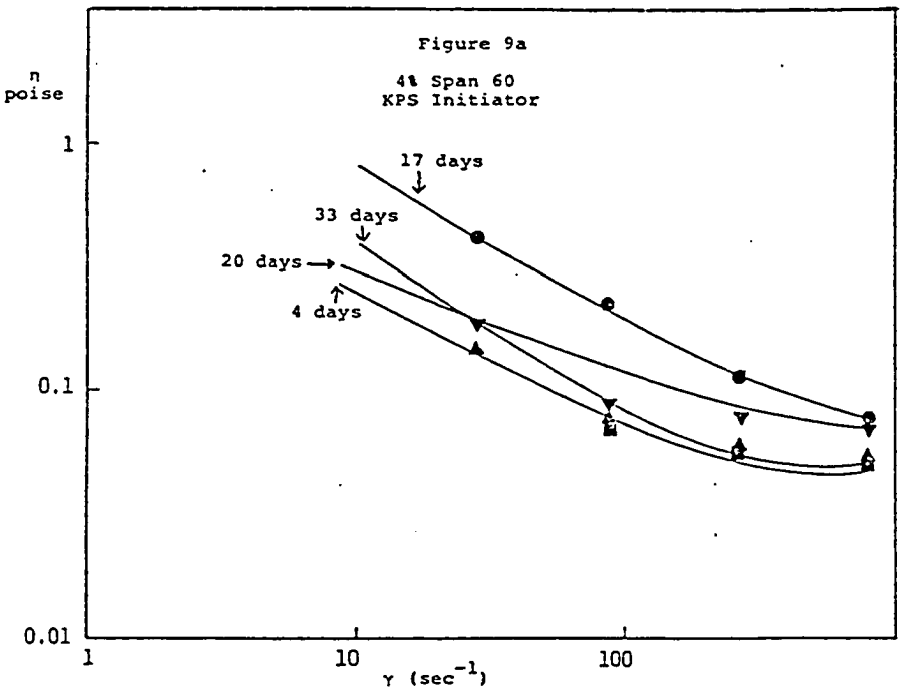

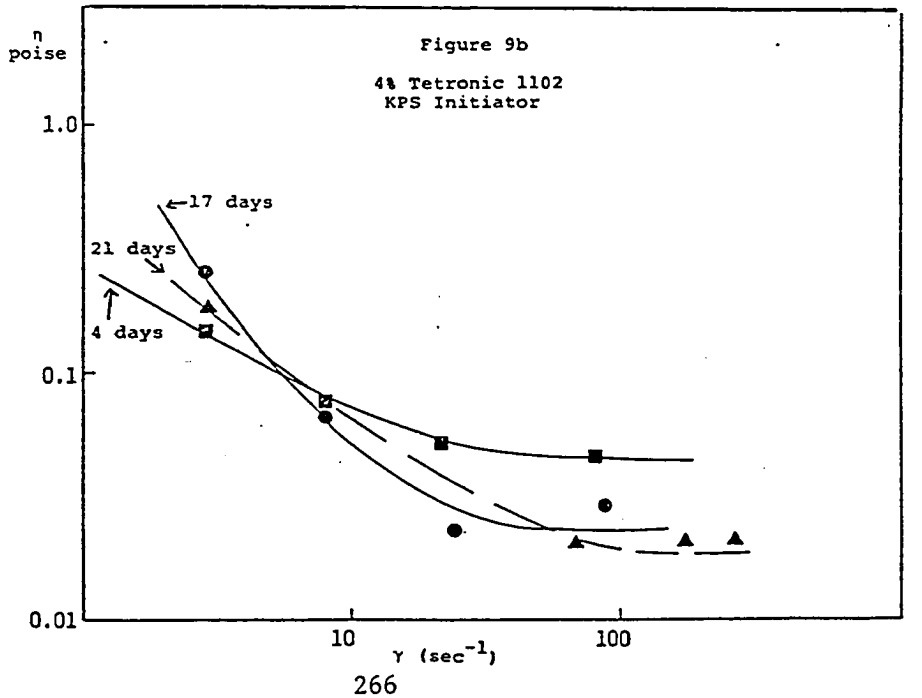

apparently the conformation of the adsorbed surfactant molecules, and perhaps also the intermolecular interactions occurring in the hydrophilic regions incorporating the ions, are greatly affected by the presence of ions. Span 60 latexes were less dramatically affected by electrolyte: the presence of electrolyte (Figure 6.8a) or ionic initiator residues (Figure 6.9a) shifts the viscosity profile toward lower viscosities, but does not significantly alter the shape of the profile. This probably indicates double layer contraction. Increasing the surfactant concentration increased the viscosity of the Tetronic 1102 and Pluronic L92 latexes only very slightly (Figures 6.2b,6.3b), but greatly increased the viscosity of the Span 60 latexes (Figure 6.1b); this indicates rigidity of both solubilized and micellar Span 60 molecules. Both of the surfactant blends studied gave shear-thinning latexes (Figures 6.7a,6.7b).

Upon aging, the viscosities of the Tetronic 1102 and Pluronic L92 latexes generally increased slightly(Figures 6.5a and b, 6.6a and b). The viscosities of the Span 60 latexes also generally increased with time (Figure 6.4a and b), although the data showed much scatter, probably owing to the difficulty in obtaining a representative sample from a severely flocculated latex. At high shear rates, the viscosities are all approximately the same, regardless of the latex's age, indicating that the floc structure can be disrupted by high shear. The degree of non-Newtonian behavior of a latex can be estimated from the ratio of viscosities measured at

high and low shear rates. A plot of this ratio as a function of aging time was independent of aging time for the Tetronic 1102 and Pluronic L92 latexes, whereas it decayed apparently exponentially for the Span 60 latexes (Figure 6.10). This indicates that the soft polyacrylamide particles in an unstable latex aggregate to form larger particles as they age; this continuous aggregation reduces the viscosity at low shear rates as the latex ages, but, since the particle aggregates can be broken up by high shear, the high-shear viscosity is relatively independent of aging.

C. Discussion

The possible explanations for the enhanced stability of latexes prepared with block copolymeric surfactants Tetronic 1102 and Pluronic L92 include reduced sedimentation due to gravitational forces (which is a function of the particle diameter), electrostatic stabilization, and steric stabilization. To evaluate the importance of sedimentation effects, settling time was plotted as a function of particle diameter (Figure 6.11): no correlation was apparent. To evaluate the importance of electrostatic effects, zeta potential is plotted as a function of settling time (Figure 6.12). Independent of the zeta potential, the latexes prepared with Tetronic 1102 and Pluronic L92 surfactants were the most stable. In some cases, latexes with zeta potentials roughly twice as high as the Tetronic 1102 and Pluronic L92 latexes settled much more quickly. This may be due to lower

Figure 6.10

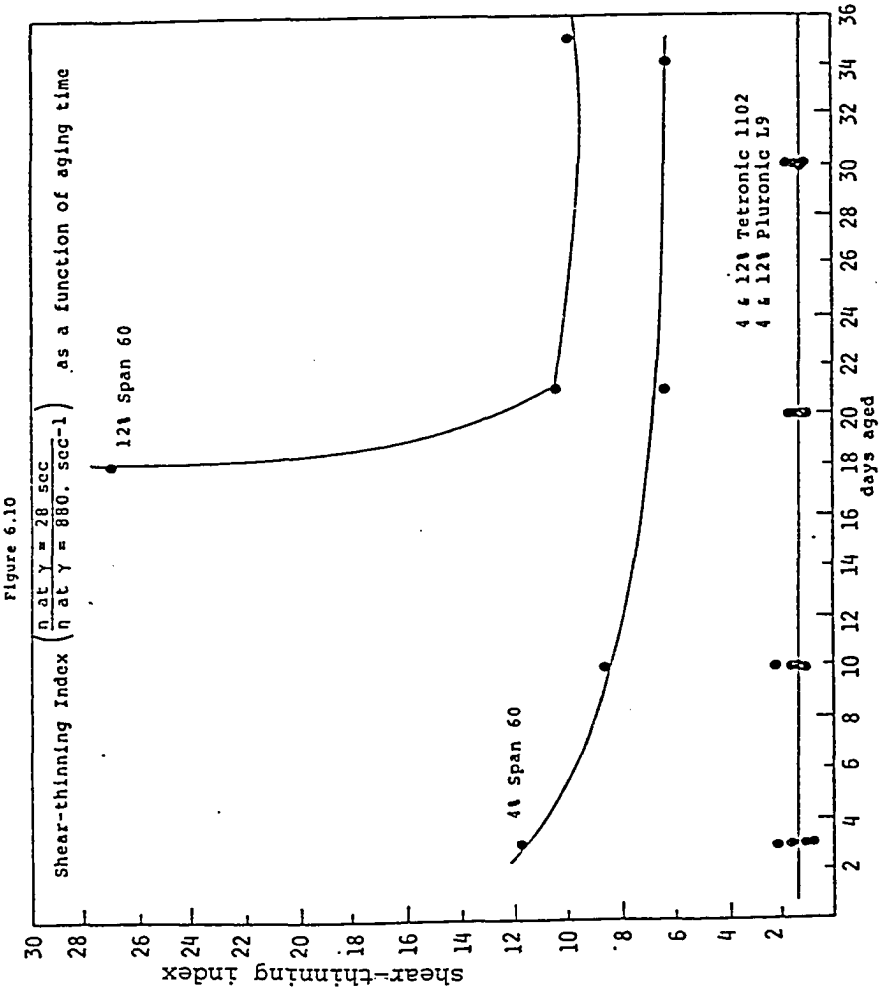

Figure 6.11

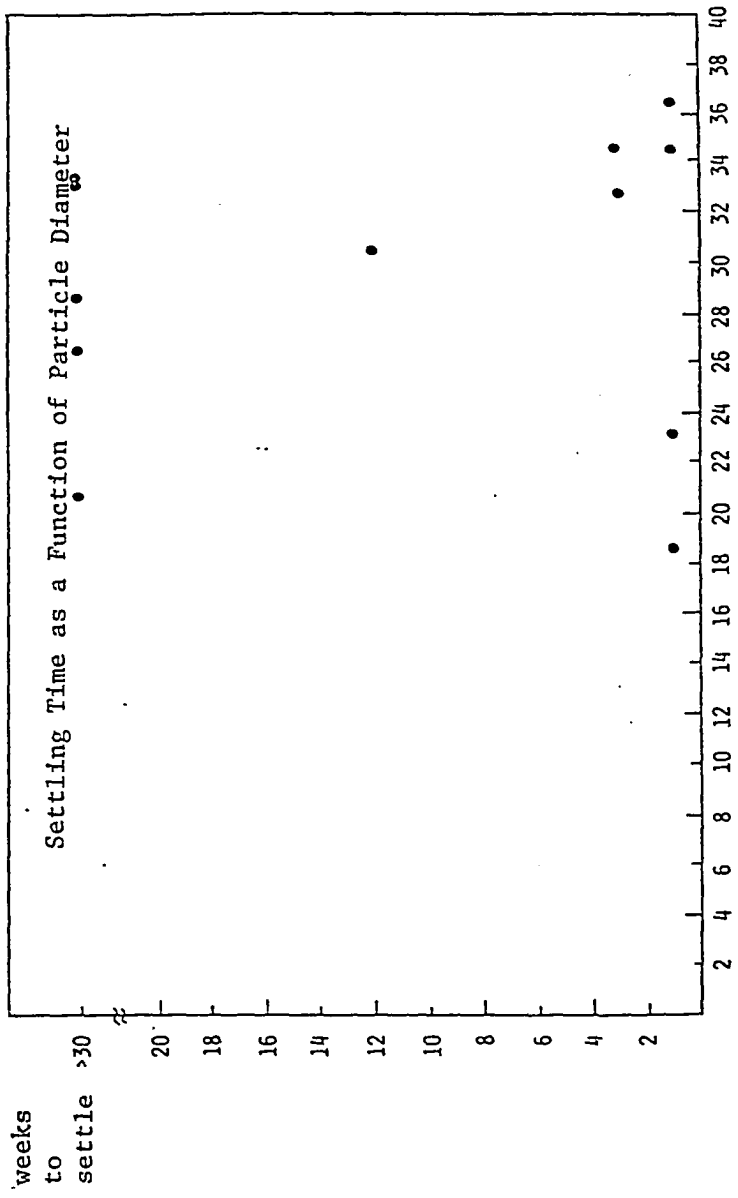

Figure 6.12

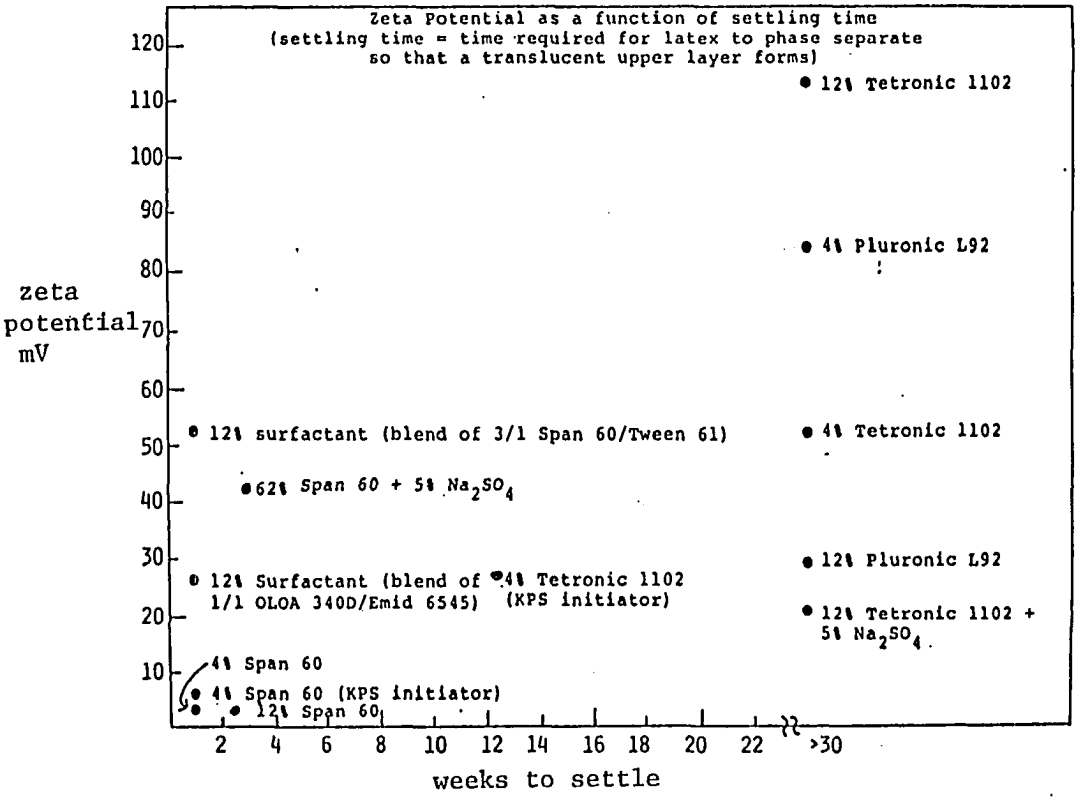

attractive forces in systems containing Tetronic 1102 and Pluronic L92. The hydrophobic portion of both of these molecules is poly(propylene oxide). Since the only interactive forces available in hydrocarbon medium are dispersion forces, the excellent solubility of poly(propylene oxide) in o-xylene indicates that poly(propylene oxide) has nearly the same value for the dispersion force contribution to interfacial tension as o-xylene; hence the effective Hamaker constant is low. Both Tetronic 1102 and Pluronic L92 are oligomeric block copolymers, having molecular weights of 6300 and 3650, respectively: hence they are expected to be able to function better as steric stabilizers compared to the other low-molecular-weight surfactants in this study.

To confirm the effectiveness of Tetronic 1102 as a steric stabilizer, the adsorbed layer thicknesses of both Tetronic 1102 and Span 60 were determined by measuring the viscosity at various particle sizes to determine the hydrodynamic particle diameter (6.42,6.43) and comparing it to the particle diameter measured by TEM. The relationship between viscosity and hydrodynamic particle diameter was calculated using the equation of Krieger et al. for concentrated dispersions (6.53). The results are tabulated in Table 6.5. The adsorbed layer thickness of the Span 60 latex was 3.06 $\pm$ 0.71 nm, independent of the amount of surfactant added in this high-concentration region, as expected for monolayer adsorption of a short-chain surfactant. Since the end-to-end distance of the stearate moiety of Span 60 is 2.16 nm, an adsorbed layer

TABLE 6.5

Adsorbed Layer Thickness:

Latex Viscosity Measured at Limiting Shear Rate

(γ = 880 sec^{-1})

I. Span 60 (10% solids, 33% aqueous volume fraction)

% surfactant on organic phase	$\bar{D}_N$ nm	η poise	Adsorbed Layer Thickness (nm)
4	32.8	0.095	2.35
6	27.9	0.467	3.46
12	23.1	1.47	3.37

II. Tetronic 1102 (10% solids, 33% aqueous volume fraction)

% surfactant on organic phase	$\bar{D}_n$ nm	η poise	Adsorbed Layer Thickness (nm)	$\bar{D}^*_{act}$ nm
4	33.6	0.029	0.283	33.0
8	30.1	0.051	1.43	27.2
12	26.6	0.066	1.61	23.4

III. Pluronic L92 (10% solids, 33% aqueous volume fraction)

% surfactant on organic phase	$\bar{D}_n$ nm	η poise	Adsorbed Layer Thickness (nm)	$\bar{D}_{act}$ nm
4	33.1	0.028	0.281	33.0
12	28.8	0.056	1.40	26.0

*$\bar{D}_{act} = \bar{D}_N$ - (adsorbed layer thickness x 2)

thickness of 3.06 nm is physically reasonable. For the Tetronic 1102 and Pluronic L92 latexes, the adsorbed layer thicknesses were extremely small (0.3-1.6nm), generally an order of magnitude smaller than with the Span 60 latex (2.3-3.4 nm). This result is unexpected for high-molecular-weight molecules, since these usually adsorb in loops and trains. The Tetronic 1102 and Pluronic L92 molecules may be adsorbed flat on the surface rather than in loops and trains, which would lead to small adsorbed layer thickness; however, this seems unlikely in the case of surface-active molecules like Tetronic 1102 and Pluronic L92. It is possible that the poly(ethylene oxide) portions of the Tetronic 1102 and Pluronic L92 molecules lie flat on the particle surface while the poly(propylene oxide) segments remain coiled in the continuous medium. Adding more surfactant increased the adsorbed layer thickness, as expected for multilayer adsorption, but still the adsorbed layer thickness was less than 2 nm. The latex viscosity remained very low, indicating that significant dissolution of the surfactant was not occurring. Hence, the enhanced stability of the latexes prepared with Tetronic 1102 and Pluronic L92 cannot be attributed to classic steric stabilization in which the adsorbed polymer chains form a thick layer of solvated loops and trains and thereby protect the particles from agglomeration upon collision. Formation of a thin adsorbed layer is probably due to the block polymeric structure of the surfactant, which thermodynamically

favors formation of ordered structures in solution. Improved emulsion stability has been attributed to a highly structured interface in a number of studies (6.19,6.27-6.30,6.54,6.55). A highly structured interface would be expected to enhance stability by hindering molecular diffusion in accord with the Higuchi-Misra theory of emulsion stabilization. However, the high molecular weight of the polyacrylamide in these inverse latex particles and the low solubility of polyacrylamide in xylene hinders the ability of the polyacrylamide to diffuse out of the particles, making the Higuchi-Misra mechanism destabilization by molecular diffusion unlikely to be operative in these systems. Formation of a structured interface has been attributed to processes such as: formation of a thick film of surfactant molecules at the interface (6.19,6.30); formation of liquid crystals in the interfacial layer (6.27,6.28, 6.36); and formation of a "solid-like" interfacial film (6.54,6.55), perhaps due to hydrogen bonding between surfactant molecules (6.29). None of the surfactants used in these studies are block copolymers like Tetronic 1102 and Pluronic L92. However, block copolymer molecules have been shown to form ordered structures 6.35). Experimental studies discussed earlier in this dissertation show that Tetronic 1102 forms liquid crystals in emulsion. Hence the formation of a structured interface is not unexpected in emulsions stabilized by block copolymeric surfactants and is supported by the experimentald finding of very low adsorbed layer thickness of particles stabilized with Tetronic

1102 and Pluronic L92.

D. Conclusions

Although significant repulsive electrostatic forces are generated in inverse latexes, these forces are not adequate to provide stability against settling. Excellent stability is obtained by using a block copolymeric surfactant.

Latexes prepared using block copolymeric surfactants show Newtonian viscosity behavior; those prepared with other surfactants show pseudoplastic behavior. The Newtonian behavior indicates that there is very little attraction between the molecules in solution or in micelles.

CHAPTER VII

Claims to Original Research

The objectives of the work described in this dissertation were to study the kinetics of inverse emulsion polymerizations of acrylamide, to propose a polymerization mechanism, and to elucidate the mechanism of latex stabilization. The objectives were fulfilled and resulted in several original findings.

1. Multicelled particles are formed in solution with block copolymeric surfactants such as Tetronic 1102 because of the heterogeneous solubility of this block copolymeric molecule: a true solution cannot be formed in oil because the hydrophilic block is too long. This multicellular structure persists on formations of an emulsion because the crystallizability of the hydrophilic block prevents its chain extension and hence the fold length changes but the overall structure does not.

2. The multicellular structure of the emulsifier used in this system introduces an additional level of complexity into the mechanism: the number of latex particles cannot be determined directly and the activation energy of the polymerization reaction changes above the melting temperature of the surfactant. However, the polymerization mechanism, derived from measurement of kinetic parameters in this system, is remarkably similar to the mechanism proposed by Vanderhoff et al. for the inverse emulsion

polymerization of sodium styrene sulfonate. In both systems, polymerization occurs in monomer droplets and the effects of initiator concentration, emulsifier concentration, and temperature on the number of particles are similar but different from conventional emulsion polymerization in that the degree of subdivision is less important in inverse emulsion polymerization. None of the unusual features of the mechanism proposed in the present work can be attributed to the unusual structure of Tetronic 1102 molecules in solution or emulsion, but rather they must be considered characteristic of the inverse emulsion polymerization process.

3. Latexes prepared with block copolymeric surfactants have excellent storage stability. This excellent stability is not due to classical steric or electrostatic stabilization.

4. Hydrodynamic chromatography has been shown to be suitable as a way of measuring molecular weight of polyacrylamide.

CHAPTER VIII

Conclusions and Recommendations for Future Study

From the studies of the formation and stabilization of inverse emulsion polymers described in this disssertation, the following conclusions can be made:

1. Multicelled particles are formed in solution and in emulsion with Tetronic 1102 surfactant. These particles are reticulated emulsifier particles. Adding an aqueous phase to o-xylene dispersions of these particles fills the particle cells to form water-in-emulsifier-in-oil particles; in addition, the emulsifier phase may be swollen with o-xylene or aqueous phase.

2. The Tetronic 1102 surfactant undergoes liquid crystalline transitions over the temperature range 25-62^{o}C. All liquid crystalling order is destroyed above the melting temperature of the poly(ethylene oxide) segments.

3. In inverse emulsion polymerization using water-soluble initiator, initiation probably occurs by radical transfer to emulsifier, with subsequent diffusion into monomer droplets. Radicals thus enter the particles singly.

4. In inverse emulsion polymerization using oil-soluble initiator, initiation occurs by initiation in the adsorbed layer, owing to preferential solubilization of initiator molecules in the interfacial layer, resulting in generation of pairs of monomer

radicals which initiate polymerization. Some polymerization may also be initiated in the continuous phase.

5. Multicellular morphology of the monomer emulsion cannot survive polymerization if the polymerization temperature is above the surfactant's melting temperature.

6. The mechanistic differences between conventional and inverse emulsion polymerization are likely related to the characteristics of the interacial region. Formation of a stable w/o emulsion usually requires a highly structured interface, while o/w emulsions are usually electrostatically stabilized. Transport and diffusion of monomer and initiator species through a highly structured interface is expected to be a much different processs than through an interface covered with a monolayer of surfactant and having a uniform charge.

7. The the presence of a plateau in the conversion-time curve is correlated with low polymerization rate, indicating that diffusion of monomer through a highly structured interface to the locus of polymerization can be sufficiently slow and so lead to starved conditions.

8. Polymerization rate is generally twice as rapid with persulfate initiator compared to azo initiator on an equimolar basis. This is unexpected, since, at a given temperature, the decomposition rate constant of the persulfate initiator is about 6% lower than the decomposition rate constant of the azo initiator. This indicates

that the efficiency factor for the persulfate initiator is substantially higher than for the azo initiator.

9. Although significant electrostatic repulsive forces are generated in inverse latexes, these forces are not adequate to provide stabilizations against settling.

10. The viscosity profiles of latexes prepared with block copolymeric surfactants are Newtonian, whereas those prepared with conventional surfactants are pseudoplastic. This indicates that there is very little interaction between block copolymer molecules on the particle surface with those in micelles or in the continuous phase.

11. Some surfactants suitable for use in inverse emulsion polymerization (such as polyisobutylene succimimides and amine sulfonates, including some OLOA surfactants and Arnnate 462) can act as chain transfer agents and thereby lower total conversion.

12. Several polymerization systems were identified which produced high molecular weight polyacrylamide at rapid rate with little coagulum. Many fewer systems were found suitable with Isopar M continuous phase than with o-xylene, indicating that surfactant blends may be necessary in aliphatic continuous phases because they are very nonpolar.

As a consequence of the conclusions drawn from this research, several research areas requiring further study are identified:

1. The desorption of oil-soluble radicals was incorporated by

arbitrarily setting the parameter m (which indicates the rate of transfer of radicals out of the particle to termination within the particle) equal to 1. This was necessary because of the uncertainty in measuring the number of particles in a system containing multicelled particles. However, desorption of oil-soluble radicals is characteristic of inverse emulsion polymerization. Hence, applying the theoretical treatment of Ugelstad and Hansen to a system prepared with a conventional soap would allow measurement of $\bar{n}$ from the value of az determined by the relative rates and particle sizes of polymers prepared with both oil-soluble and water-soluble initiators, using the method described in this dissertation. Knowing $\bar{n}$ and the parameter a (which is a function of the rate constants for termination and initiator decomposition, the initiator efficiency factor, the initiator concentration, and the average particle volume), the parameter α can be determined. Since the ratio of α to m is constant for a given $\bar{n}$, the value of the desorption rate constant k_{de} cen be uniquely determined from Ughelstad and Hansen's graphical analysis and the following equation:

$$\alpha/m = \rho_i/k_{de}N$$

where ρ_i is the rate of radical production.

2. The mechanism of initiation in this system using water-soluble initiator appears to be diffusion rather than capture. This could be conclusively proven by assuming that the particle size

distribution of the monomer droplets is the same as that of the initiator droplets and generating the resulting latex particle size distribution by Monte Carlo simulation. If the simulated distribution agrees with the measured distribution capture is indeed the mechanism of initiation.

3. The excellent stability of polyacrylamide latex prepared with Tetronic 1102, and the ease of inverting this latex by adding a small amount of a high HLB surfactant such as Triton X-100, make it a likely candidate for use in a continuous process for industrial application.

4. Use of hydrodynamic chromatography for molecular weight determination can be optimized by using a differential refractometer detector and by optimizing the surfactant concentration of the eluant. The relationship between the polymer's polydispersity and the peak broadness should be elucidated.

5. The relationship between liquid crystalline surfactant structure and latex morphology can be explored by polymerizing at temperature between 20 and 45°C, which is below the surfactant melting temperature and also below the region of liquid crystal existence.

6. The trapping of inclusions of continuous phase into the polyacrylamide particles make latexes prepared with Tetronic 1102 likely to be able to act as hiding pigments if the polymer were cross-linked.

CHAPTER IX

References

1.1 J. W. Vanderhoff, E. B. Bradford, H. L. Tarkowski, J. B. Shaffer, and R. M. Wiley, Adv. Chem. Ser. 34, 32 (1962).

1.2 J. W. Vanderhoff and R. M. Wiley (to the Dow Chemical Co.), US3,284,393, Nov. 8, 1966.

1.3 J. Ugelstad, M. S. El-Aasser, and J. W. Vanderhoff, J. Polym. Sci. Polym. Lett. 11, 503 (1973).

1.4 V. F. Kurenkov, T. M. Osipova, E. V. Kuznetsov and V. A. Myagchenov, Vysokomol. Soedin. Ser. B20, 647 (1978); CA 89: 198089q.

1.5 Ibid.

1.6 List compiled by J. W. Vanderhoff, Advances in Emulsion Polymerization and Latex Technology (15th Annual Short Course Notes), Lehigh University, 1984.

1.7 U.S. Department of Energy/BETC/560305 (1979).

1.8 D. C. MacWilliams, Functional Monomers, Vol. 1 (R. H. Yocum and E. B. Nyquist, eds.), New York: Marcel Dekker 1973, p. 1.

1.9 W. Albers and J. Th. G. Overbeek, J. Coll. Sci. 14, 501, 510 (1959); 15, 489 (1960).

1.10 E. L. Carpenter and H. S. Davis, J. Appl. Chem. 7, 671 (1957).

1.11 N. M. Bikales, Water Soluble Polymers (N. M. Bikales, ed.) New York: Plenum Press 1973, p. 213.

1.12 R. Schulz, G. Renner, A. Henglein, and W. Kern, Makromol. Chem. 12, 20 (1954).

1.13 E. H. Gleason, M. L. Miller, and G. F. Sheats, J. Polym. Sci. 38, 133 (1959).

1.14 R. M. Joshi, J. Polym. Sci. 56, 313 (1962).

1.15 E. A. S. Cavell, Makromol. Chem. 54, 70 (1962).

1.16 J. P. Riggs and F. Rodriguez, J. Polym. Sci. 5A1, 3151 (1967).

1.17 T. Ishige and A. E. Hamielec, J. Appl. Polym. Sci. 17, 1479 (1973).

1.18 J. P. Riggs and F. Rodriguez, J. Polym. Sci., 5A1, 3167 (1967).

1.19 E. Collinson, F. S. Dainton, and G. S. McNaughton, Trans. Faraday Soc. 53, 489 (1957); E. Collinson, F. S. Dainton, D. R. Smith, G. J. Trudie, and S. Tazuke, Disc. Faraday Soc. 29, 188 (1960).

1.20 E. Collinson, F. S. Dainton, and G. S. McNaughton, Trans. Faraday Soc. 53, 476 (1957).

1.21 F. S. Dainton and M. Tordorff, Trans. Faraday Soc. 53, 499 and 666 (1957).

1.22 T. J. Suen, Y. Jen, and J. V. Lockwood, J. Polym. Sci. 31, 481 (1958).

1.23 J. P. Friend and A. E. Alexander, J. Polym. Sci. 6A1, 1833 (1968).

1.24 S. N. Trubitsyna, I. Ismailov, and M. A. Askanov, Polymer Sci. USSR 20, 2926 (1979).

1.25 F. V. DiStefano, M. S. Report, Lehigh University, 1981.

1.26 J. W. Vanderhoff in Vinyl Polymerization (G. E. Ham, ed.), 1(2), 1 (1969).

2.1 W. H. Beattie and C. Booth, J. Phys. Chem. 64, 696 (1960).

2.2 J. L. Cayias, R. H. Schechter, and W. H. Wade, ACS Symp. Ser. 8 (K. L. Mittal, ed.), 234 (1975).

2.3 A. L. Van Geet, Anal. Chem. 40, 2227 (1968).

2.4 G. E. P. Box, W. G. Hunter, and J. S. Hunter, Statistics for Experimenters, New York: John Wiley and Sons, 1978.

2.5 K. C. Peng, The Design and Analysis of Scientific Experiments, Reading, Massachusetts: Addison-Wesley 1967.

2.6 National Bureau of Standards Applied Mathematics Series 78 (1957).

2.7 G. M. Saidel and S. Katz, J. Polym. Sci. 7C(27), 149 (1969).

2.8 F. W. Billmeyer and L. R. Siebert, in Adv. Chem. Ser. 125 (M. Ezrin, ed.), p. 9 (1973).

2.9 D. K. Carpenter and L. Westerman, in Polymer Molecular Weights, Vol. II (P. E. Slade, ed.), New York: Marcel Dekker (1975), p. 379.

2.10 E. A. Collins, J. Bares, and F. W. Billmeyer, Experiments in Polymer Science, New York: John Wiley and Sons, 1973, p. 405.

2.11 A. C. Ouano, E. M. Barrall, and J. F. Johnson, in Polymer Molecular Weights, Vol. II (P. E. Slade, ed.), New York: Marcel Dekker (1975), p. 287.

2.12 T. D. Swartz, D. D. Bly, and A. S. Edwards, J. Appl. Polym. Sci. 16, 3353 (1972).

2.13 M. J. R. Cantow, R. S. Porter, and J. F. Johnson, J. Polym. Sci. 5A1, 1391 (1967).

2.14 A. H. Abdel-Alim and A. E. Hamielec, J. Appl. Polym. Sci. 18, 297 (1974).

2.15 A. E. Hamielec and S. N. E. Omorodion, in ACS Symposium Series 138 (T. Provder, ed.), p. 183 (1980).

2.16 Application Note LS-5, Chromatix, Inc., Sunnyvale, CA (1978).

2.17 R. C. Jordan, J. Liq. Chrom., 3, 439 (1980).

2.18 C. J. Kim, A. E. Hamielec, and A. Benedek, J. Liq. Chrom. 5, 1277 (1982).

2.19 R. K. Prud'homme, G. Froman, and D. A. Hoagland, Carbohydrate Res. 106, 225 (1982).

2.20 R. K. Prud'homme and D. A. Hoagland, Sep. Sci. Tech. 18, 121 (1983).

2.21 A. H. Abdel-Alim and A. E. Hamielec, J. Appl. Polym. Sci. 17, 3769 (1973).

2.22 S. M. Shawki and A. E. Hamielec, J. Appl. Polym. Sci. 23, 3323 (1979).

2.23 J. Klein and A. Westerkamp, J. Polym. Sci.:Polym. Chem. 19, 707 (1981).

2.24 C. M. Tseng, Lehigh University Emulsion Polymers Institute Graduate Research Progress Reports 19, 148 (January 1983).

2.25 D. J. Nagy, PhD Thesis, Lehigh University, 1979.

3.1 F. V. DiStefano, M.S. Report, Lehigh University, 1981.

3.2 Private communication, BASF Wyandotte Co.

4.1 Ch. Sadron, Angew Chem. Intl. Ed. 2, 248 (1963).

4.2 J. A. Manson and L. H. Sperling, Polymer Blends and Composites, New York: Plenum Press 1976.

4.3 Z. Tuzar and P. Kratchovil, Adv. Coll. Int. Sci. 6, 201 (1976).

4.4 K. N. Prasad, T. T. Luong, A. T. Florence, J. Paris, C. Vaution, M. Seiller, and F. Puisieux, J. Coll. Int. Sci. 69, 225 (1979).

4.5 W. Mandema, H. Zeldenrust, and C. Emeis, Makromol. Chem. 180, 1521 (1979).

4.6 P. Marie, R. Duplessix, Y. Gallot, and C. Picot, Macromolecules 12, 1180 (1979).

4.7 M. Ikemi, N. Odagiri, S. Tanaka, I. Shinohara, and A. Chiba, Macromolecules 14, 34 (1981); 15, 281 (1982).

4.8 J. V. Dawkins and G. Taylor, Makromol. Chem. 180, 1737 (1979).

4.9 T. Kotaka, T. Tanaka, M. Hattori, and H. Inagaki, Macromolecules 11, 138 (1978).

4.10 G. E. Molau and W. M. Wittbrodt, Macromolecules 1, 260 (1968).

4.11 Y. Ikada, F. Horii, and I. Sakurada, J. Polym. Sci.: Polym. Chem. 11, 27 (1973).

4.12 Z. Tuzar, P. Bahadur, and P. Kratochvil, Makromol. Chem. 182, 1751 (1981).

4.13 P. Marie and Y. Gallot, Makromol. Chem. 180, 1611 (1979).

4.14 J. B. Kayes and D. A. Rawlins, Coll. Polym. Sci. 257, 622 (1979).

4.15 B. R. M. Gallot, Adv. Polym. Sci. 29, 85 (1978).

4.16. A. Douy and B. R. Gallot, Mol. Cryst. Liq. Cryst. 14, 191 (1971); Makromol. Chem. 156, 81 (1972).

4.17 Ch. Sadron and B. Gallot, Makromol. Chem. 164, 301 (1973).

4.18. M. Gervais and B. Gallot, Makromol. Chem. 171, 157 (1973); 174, 193 (1973), 178, 1577 and 2071 (1977).

4.19 R. Vitali and E. Montani, Polymer 21, 1220 (1980).

4.20 J. S. Trent, J. I. Scheinbeim, and P. R. Couchman, J. Polym. Sci: Polym Lett. 19, 315 (1981); Macromolecules 16, 589 (1983).

4.21 P. A. Winsor, Trans. Faraday Soc. 44, 376, 382, 387, 390 (1948).

4.22 G. Friedel, Ann. Phys. 18, 273 (1922); cited by E. B. Priestly, Introduction to Liquid Crystals (E. B. Priestly, P. J. Wojtowicz, and P. Sheng, eds.), New York: Plenum Press 1975, p. 4.

4.23 A. DeVries, Liquid Crystals (F. D. Saeva, ed.), New York: Marcel Dekker 1979, p. 15.

4.24 J. H. Wendorff, Liquid Crystalline Order in Polymers (A. Blumstein, ed.), New York: Academic Press 1978, p. 1.

4.25 T. J. Flautt and K. D. Lawson, Adv. Chem. Ser. 63, 26 (1967); Molec. Cryst. 1, 241 (1966).

4.26 C. L. Khetrapal, A. C. Kunwar, A. S. Tracey, and P. Diehl, NMR: Basic Principles and Progress 9, 3 (1975).

4.27 L. C. Pizzini and J. T. Patton, in Encyclopedia of Polymer Science and Technology 6, 120-145 (1967).

4.28 S. Friberg, I. Bieraczewska, and J. C. Raney, in Micellization, Solubilization, and Microemulsion (K. Mittal, ed.),

4.29 S. Matsumoto, Y. Kita, and D. Yonezawa, J. Coll. Int. Sci. 57, 353 (1976); 62, 87 (1977).

4.30 S. S. Davis and A. S. Burbage, J. Coll. Int. Sci. 62, 361 (1977).

4.31 C. J. Panchal, J. E. Zajec, and D. F. Gerson, J. Coll. Int. Sci. 68, 295 (1979).

4.32 M. Hashida, T. Yoshioka, S. Maranishi, and H. Sezak, Chem. Pharm. Bull. 28, 1009 (1980).

4.33 A. T. Florence and D. Whitehill, J. Coll. Int. Sci. 79, 243 (1981).

4.34 S. M. Ng and S. G. Frank, J. Disp. Sci. Tech. 3, 217 (1982).

4.35 C. D. Lack, M.S. Report, Lehigh University, 1983.

5.1 F. V. DiStefano, M.S. Report, Lehigh University, 1981.

5.2 G. Licht, R. G. Gilbert, and D. H. Napper, J. Polym. Sci. 15, 1957 (1977); 21, 269 (1983).

5.3 "Vazo Polymerization Initiators," E. I. DuPont de Nemours Co., 1979.

5.4 E. L. Carpenter and H. S. Davis, J. Appl. Chem. 7, 671 (1957).

5.5. I. M. Kolthoff and J. K. Miller, J. Am. Chem. Soc. 73, 3055 (1961).

5.6 W. H. Stockmayer, J. Polym. Sci. 24, 314 (1957).

5.7 J. T. O'Toole, J. Appl. Polym. Sci. 9, 1291 (1965).

5.8 B. M. E. van der Hoff, J. Polym. Sci. 33, 487 (1958).

5.9 G. W. Poehlein,"Advances in Emulsion Polymerization and Latex Technology," 12th Annual Short Course Notes, 1(3), 29, Lehigh University, 1981.

5.10 W. V. Smith and R. H. Ewart, J. Chem. Phys. 16, 592 (1948); W. V. Smith, JACS 70, 3695 (1948) and 71, 4077 (1949).

5.11 J. W. Vanderhoff, E. B. Bradford, H. L. Tarkowski, J. B. Shaffer, and R. M. Wiley, Adv. Chem. Ser. 34, 32 (1962).

5.12 J. Ugelstad, P. C. Mork, and J. O. Aasen, J. Polym. Sci. 5A1, 2281 (1967).

5.13 J. W. Vanderhoff, E. B. Bradford, H. L. Tarkowski, and B. W. Wilkinson, J. Polymer Sci. 50, 265 (1961).

5.14 J. W. Vanderhoff, in Vinyl Polymerization (G. E. Ham, ed.) 1(2), 1 (1969).

5.15 F. DeSchrijver and G. Smets, J. Polym. Sic. 4A1, 2201 (1966).

5.16 B. M. E. Van der Hoff, Adv. Chem. Ser 34, 6 (1962).

5.17 R. M. Joshi, J. Polym. Sci. 56, 313 (1962).

6.1 E. J. W. Verwey and J. Th. G. Overbeek, Theory of the Stability of Lypophobic Colloids, Amsterdam: Elsevier, (1948).

6.2 D. W. J. Osmond and F. A. Waite, in Dispersion Polymerization in Organic Media (K. E. J. Barret, ed.), New York: John Wiley and Sons 1975, pp. 9-45.

6.3 J. L. van der Minne and P. H. J. Hermanie, J. Coll. Sci. 7, 600 (1952); 8, 38 (1953).

6.4 J. Lyklema, Adv. Coll. Int. Sci. 2, 67 (1968).

6.5 D. N. L. McGown, G. D. Parfitt, and E. Willis, J. Colloid. Sci. 20, 650 (1965).

6.6 L. A. Romo, J. Phys. Chem. 67, 386 (1963).

6.7 F. J. Micale, Y. K. Lui, and A. C. Zettlemoyer, Disc. Faraday Soc. 42, 238 (1966).

6.8 L. A. Romo, Disc. Faraday Soc. 42, 232 (1966).

6.9 G. D. Parfitt and J. Peacock, Surf. and Coll. Sci. (E. Matijevic, ed.) 10, 163 (1978).

6.10 I. D. Chapman, J. Phys. Chem. 75, 537 (1971).

6.11 A. Kitahara, Prog. Org. Coat. 2, 81 (1973); quoted in (6.9).

6.12 W. D. Cooper and P. Wright, J. Coll. Int. Sci. 54, 28 (1976).

6.13 F. M. Fowkes, H. Jinnai, M. A. Mostafa, F. W. Anderson, and R. J. Moore, ACS Symposium Ser. 200 (M. Hair and M. D. Croucher, eds.), 307 (1982).

6.14 P. C. Hiemenz, Principles of Colloid and Surface Chemistry, New York: Marcel Dekker, 1977, p. 369.

6.15 D. W. J. Osmond, Disc. Faraday Soc. 42, 247 (1966).

6.16 B. Deryagin, Disc. Faraday Soc. 42, 318 (1966).

6.17 G. D. Parfitt, J. A. Wood, and R. T. Ball, J. Chem. Soc. Faraday Trans. I 69, 1908 (1973).

6.18 R. M. Wiley, J. Coll. Sci. 9, 427 (1954).

6.19 W. Albers and J. Th. G. Overbeek, J. Coll. Sci. 14, 501 (1959).

6.20 P. C. Hiemenz, Principles of Colloid and Surface Chemistry, New York: Marcel Dekker, 1977, p. 424.

6.21 T. Gillespie and R. M. Wiley, J. Phys. Chem. 66, 1077 (1962).

6.22 R. Evans and D. H. Napper, J. Coll. Int. Sci. 45, 138 (1973).

6.23 M. J. Vold, J. Coll. Sci. 16, 1 (1961); D. W. J. Osmond, B. Vincent, and F. A. Waite, J. Coll. Int. Sci. 42, 262 (1973): B. Vincent, J. Coll. Int. Sci. 42, 270 (1973).

6.24 G. R. Feat and S. Levine, J. Coll. Int. Sci. 54, 34 (1976).

6.25 H. Koelmans and J. Th. G. Overbeek, Disc. Faraday Soc. 18, 52 (1954).

6.26 D. N. L. McGown and G. D. Parfitt, Disc. Faraday Soc. 42, 225 (1966); D. N. L. McGown, G. D. Parfitt, and E. Willis, J. Coll. Sci. 20, 650 (1965).

6.27 G. D. Parfitt and E. Willis, J. Coll. Int. Sci. 22, 100 (1966).

6.28 E. A. Nieuwenhuis and A. Vrij, J. Coll. Int. Sci. 72, 321 (1979).

6.29 R. E. Ford and C. G. L. Furmidge, J. Coll. Int. Sci. 22, 331 (1966).

6.30 W. Albers and J. Th. G. Overbeek, J. Coll. Sci. 15, 489 (1960).

6.31 W. I. Higuchi and J. Misra, J. Pharm. Sci. 51, 459 (1962); W. I. Higuchi, J. Pharm. Sci. 53, 405 (1964).

6.32 G. W. Hallworth and J. E. Carless, J. Pharm. Pha. 24, P71 (1972).

6.33 G. W. Hallworth and J. E. Carless, J. Pharm. Pha. 25, P87 (1973).

6.34 D. J. Walbridge, in Dispersion Polymerization in Organic Media (K. E. J. Barrett, ed.), New York: John Wiley and Sons 1975, pp. 45-110.

6.35 Z. Tuzar and P. Kratochvil, Adv. Coll. Int. Sci. 6, 201 (1976).

6.36 S. Friberg, L. Mandell, and M. Larsson, J. Coll. Int. Sci. 29, 155 (1969).

6.37 S. Friberg and K. Larsson, in Advances in Liquid Crystals (G. H. Brown, ed.) 2, 173 (1976).

6.38 W. Albers and J. Th. G. Overbeek, J. Coll. Sci. 14, 510 (1959).

6.39 A. K. Van Helden, J. W. Jansen, and A. Vrij, J. Coll. Int. Sci. 81, 354 (1981).

6.40 A. Einstein, Ann. Phys. 17, 459 (1905); cited by D. W. J. Osmond and I. Wagstaff, in Dispersion Polymerization in Organic Media (K. E. J. Barrett, ed.), New York: John Wiley and Sons 1975, p. 243.

6.41 D. G. Thomas, J. Coll. Sci. 20, 267 (1965).

6.42 P. H. Johnson and R. H. Kelsey, Rubber World 138, 877 (1958).

6.43 D. J. Walbridge and J. A. Waters, Disc. Faraday Soc. 42, 294 (1966).

6.44 S. J. Barsted, L. J. Nowakowska, I. Wagstaff, and D. J. Walbridge, Trans. Faraday Soc. 67, 3598 (1971).

6.45 Doroszkowski and Lambourne, J. Polym. Sci. 34C, 253 (1971).

6.46 T. Gillespie, J. Coll. Sci. 15, 219 (1960).

6.47 I. M. Krieger and T. J. Dougherty, Trans. Soc. Rheol. 3, 137 (1959).

6.48 W. R. Schowalter, C. E. Chaffey, and H. Brenner, J. Coll. Int. Sci. 26, 152 (1968); Y. S. Papir and I. M. Krieger, J. Coll. Int. Sci. 34, 126 (1970).

6.49 T. Gillespie and R. M. Wiley, J. Phys. Chem. 66, 1077 (1962); A. Doroszkowski and R. Lambourne, J. Coll. Int. Sci. 26, 128 (1968).

6.50 M. J. Vold, J. Coll. Sci. 18, 684 (1963).

6.51 B. A. Firth, Rheol. Acta. 19, 716 (1980).

6.52 P. Sherman, J. Phys. Chem. 67, 2531 (1963); J. Coll. Int. Sci. 24, 67 and 107 (1967).

6.53 M. E. Woods and I. M. Krieger, J. Coll. Int. Sci. 34, 91 (1970); I. M. Krieger and T. J. Dougherty, Trans. Soc. Rheol. 3, 137 (1959).

6.54 J. H. Schulman and E. G. Cockbain, Trans. Faraday Soc. 36, 651 and 661 (1940).

6.55 P. Sherman, J. Coll. Sci. 8, 35 (1953).

6.56 M. S. El-Aasser, Advances in Emulsion Polymerization and Latex Technology (Short Course Notes), 1981.

6.57 E. G. Cockbain and T. S. McRoberts, J. Coll. Sci. 8, 440 (1953).

6.58 D. N. L. McGown and G. D. Parfitt, Kolloid Z. Z19, 48 (1967).

APPENDIX A

GRAPHICAL ANALYSIS OF THE KINETICS OF INVERSE EMULSION POLYMERIZATION

Figure A.1

Polymerization Rate as a Function of Initiator Concentration

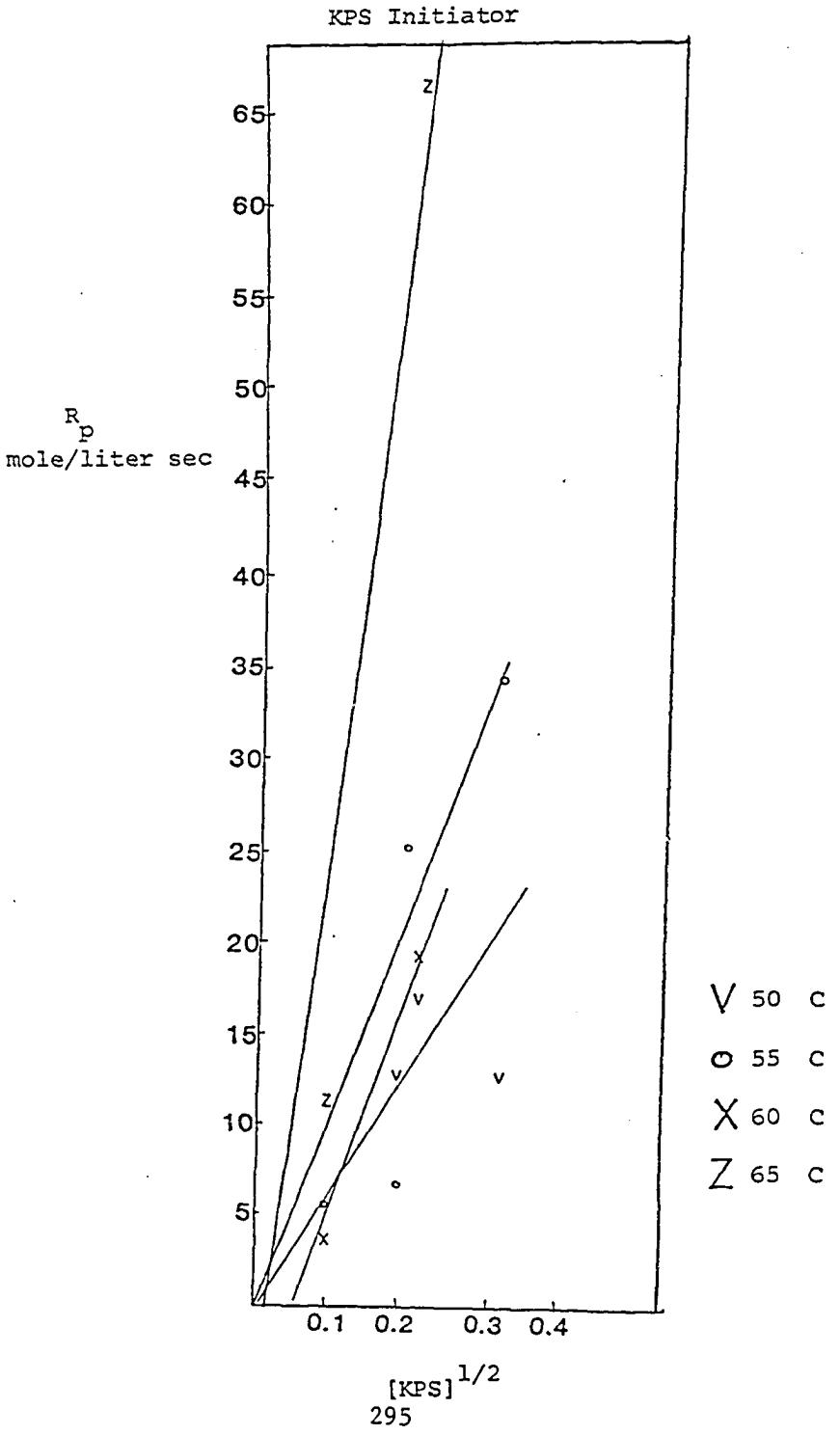

Figure A.2

Polymerization Rate as a Function of
Polymerization Temperature

KPS Initiator

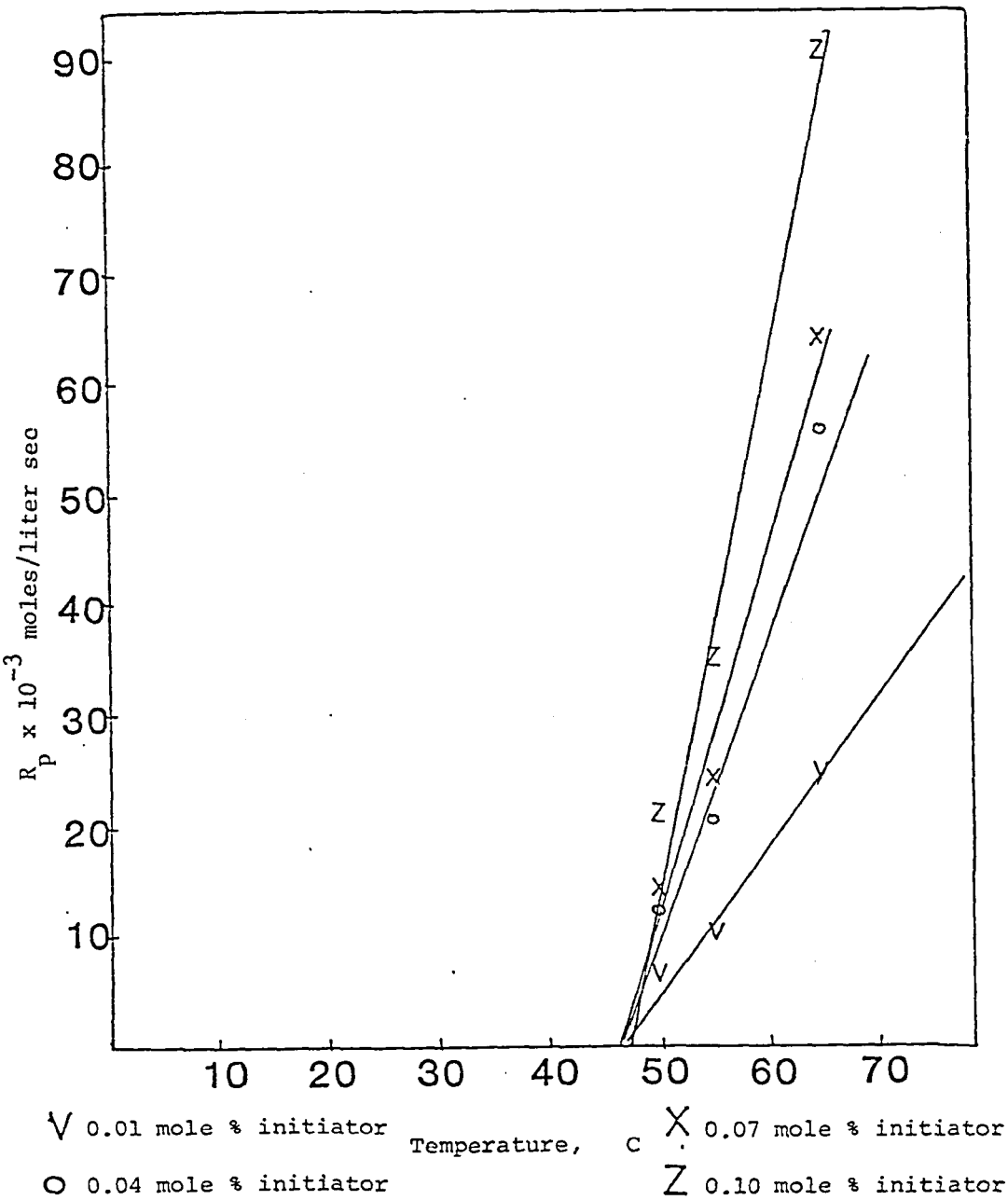

Figure A.3

Polymerization Rate as a Function of
Initiator Concentration
KPS Initiator

Polymerization Temperature= 50° C

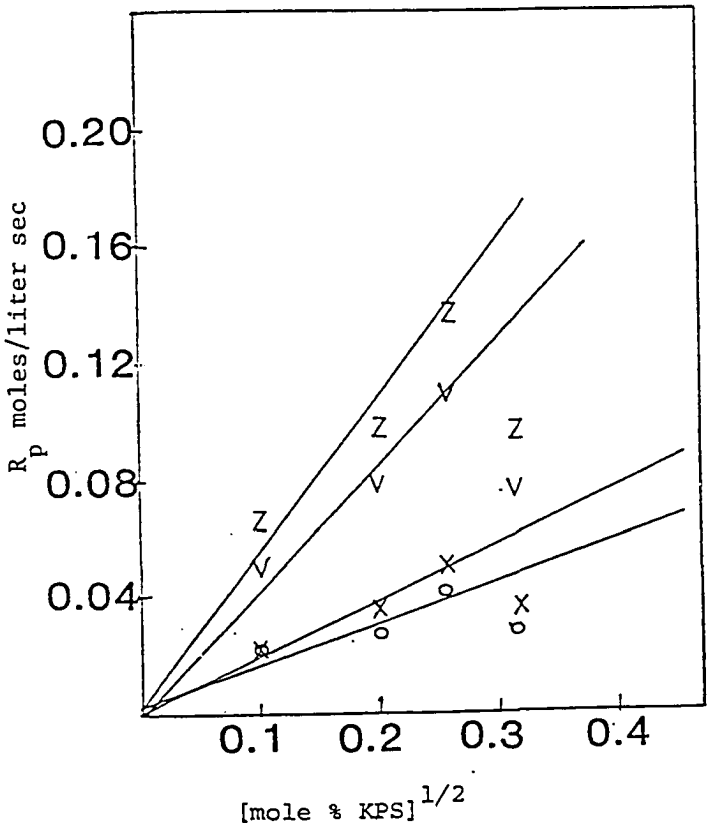

V 3% Tetronic 1102

O 6% Tetronic 1102

X 9% Tetronic 1102

Z 12% Tetronic 1102

Figure A.4

Polymerization Rate as a Function of
Initiator Concentration
KPS Initiator
Polymerization Temperature= 55° C

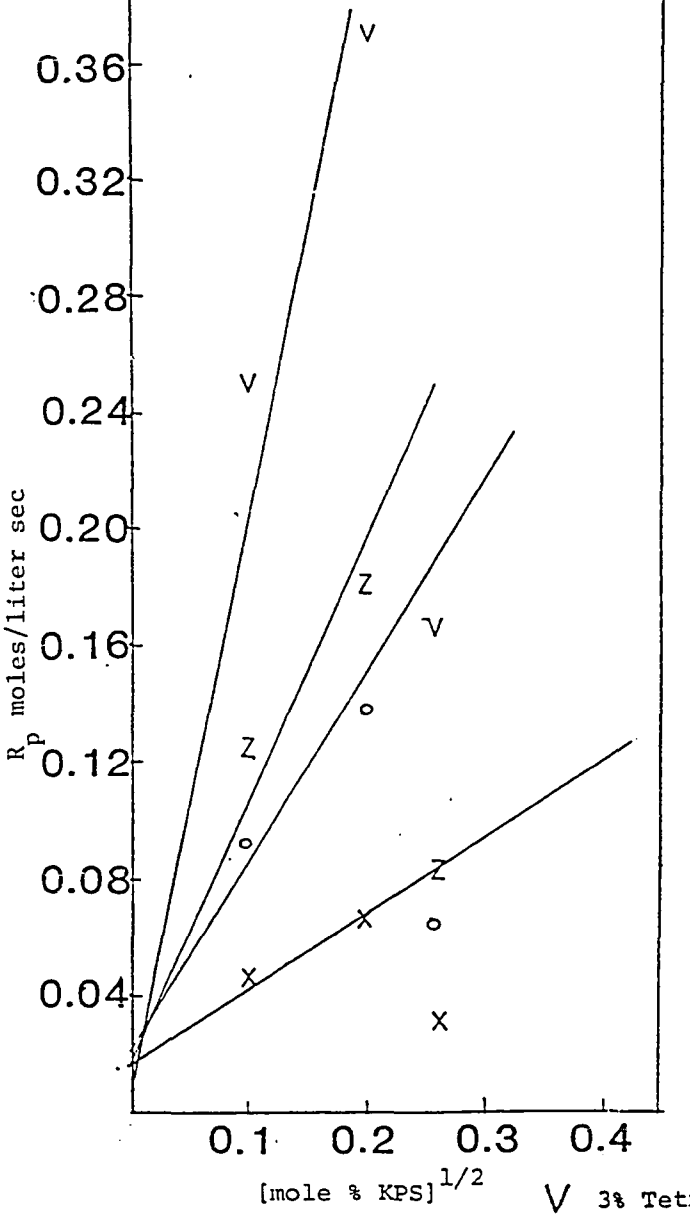

Polymerization Rate as a Function of Initiator Concentration

KPS Initiator

Figure A.5

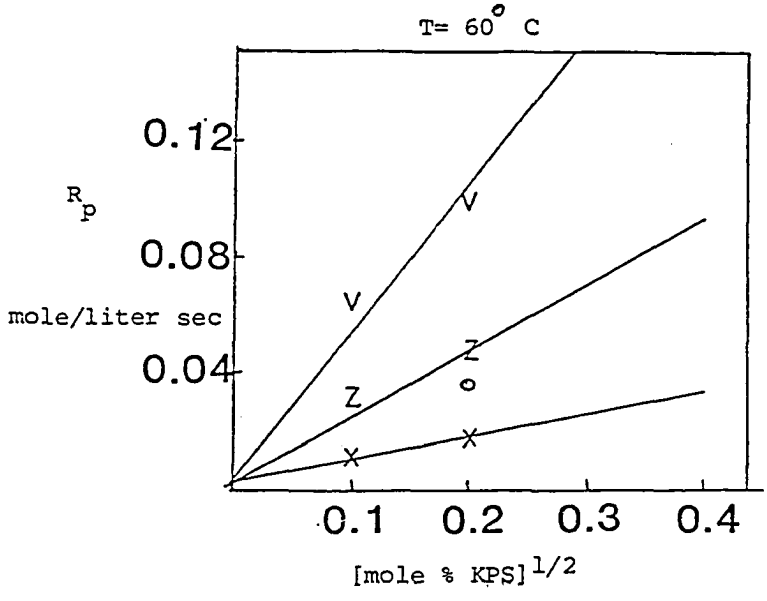

Figure A.6

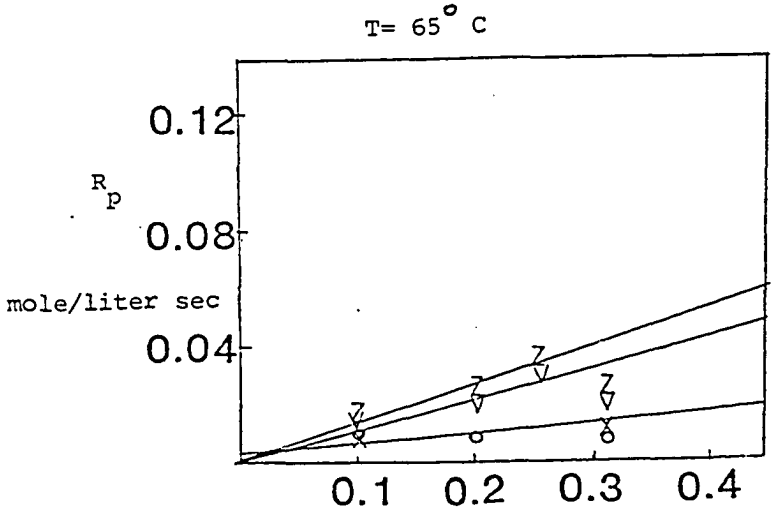

V 3% Tetronic 1102

O 6% Tetronic 1102

X 9% Tetronic 1102

Z 12% Tetronic 1102

Figure A.7

Correlation Between Polymerization Rate and a KPS Initiator

Polymerization Temperature= 50° C

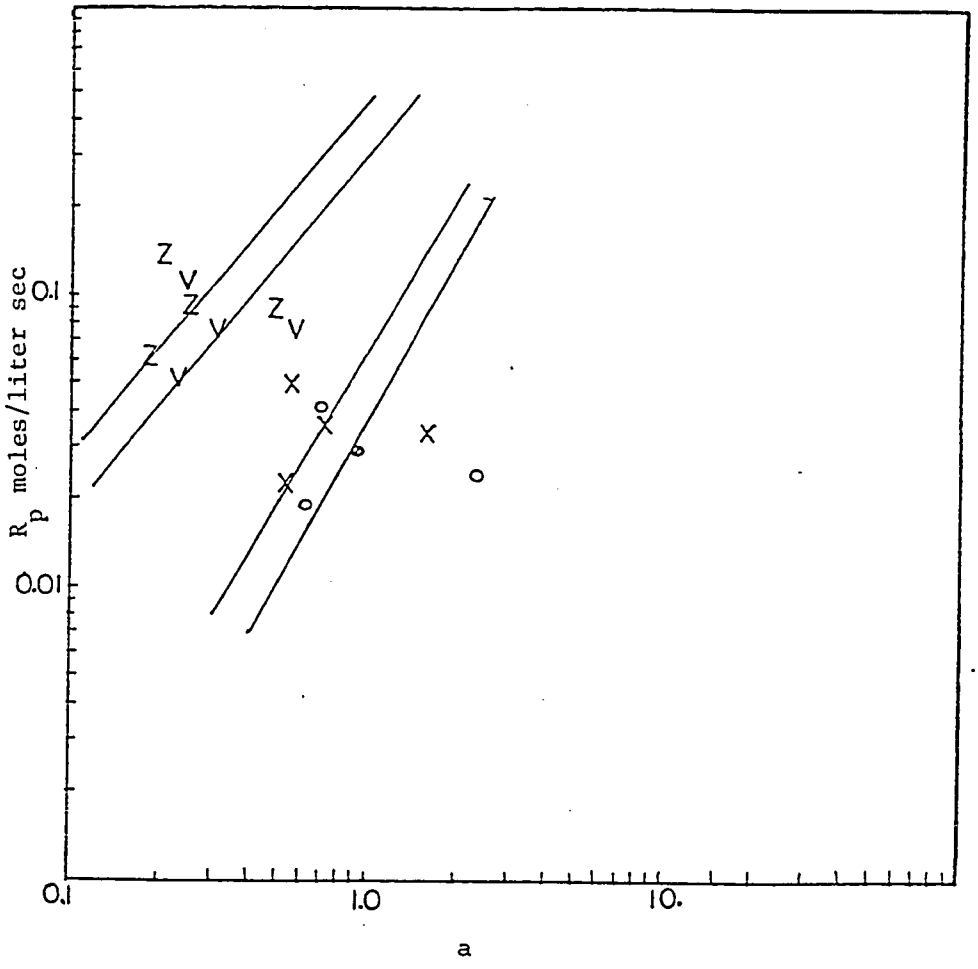

V 0.01 mole % initiator

O 0.04 mole % initiator

X 0.07 mole % initiator

Z 0.10 mole % initiator

Figure A.8

Correlation Between Polymerization Rate and a

KPS Initiator

Polymerization Temperature= 50° C

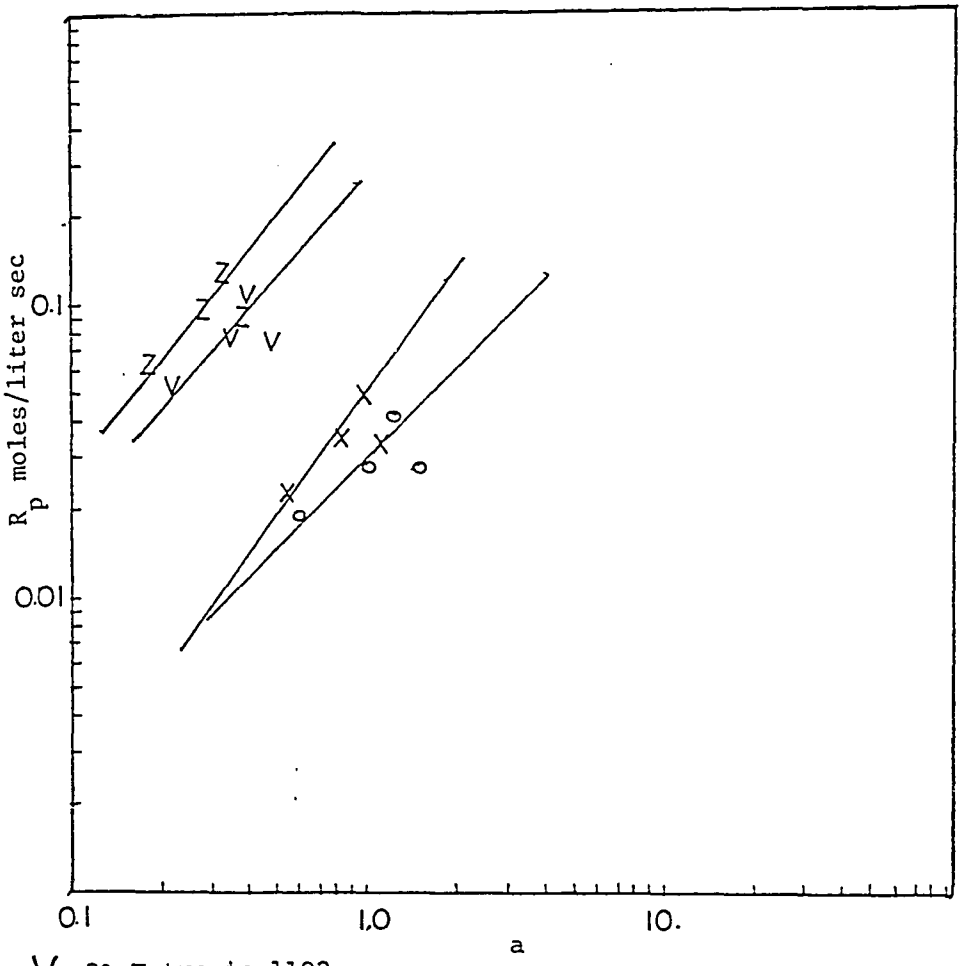

V 3% Tetronic 1102

o 6% Tetronic 1102

X 9% Tetronic 1102

Z 12% Tetronic 1102

Figure A.9

Correlation Between Polymerization Rate and a

KPS Initiator

Polymerization Temperature= 55° C

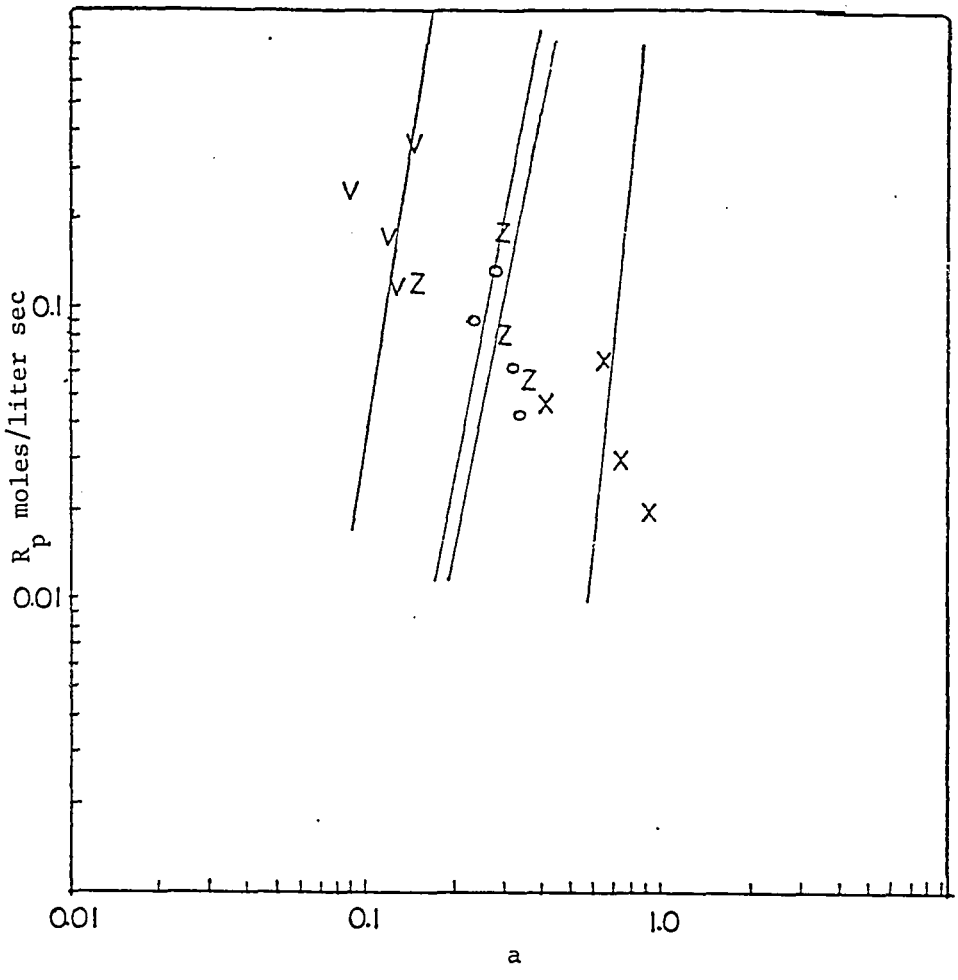

V 0.01 mole % initiator

O 0.04 mole % initiator

X 0.07 mole % initiator

Z 0.10 mole % initiator

Figure A.10

Correlation Between Polymerization Rate and a KPS Initiator

Polymerization Temperature= 55° C

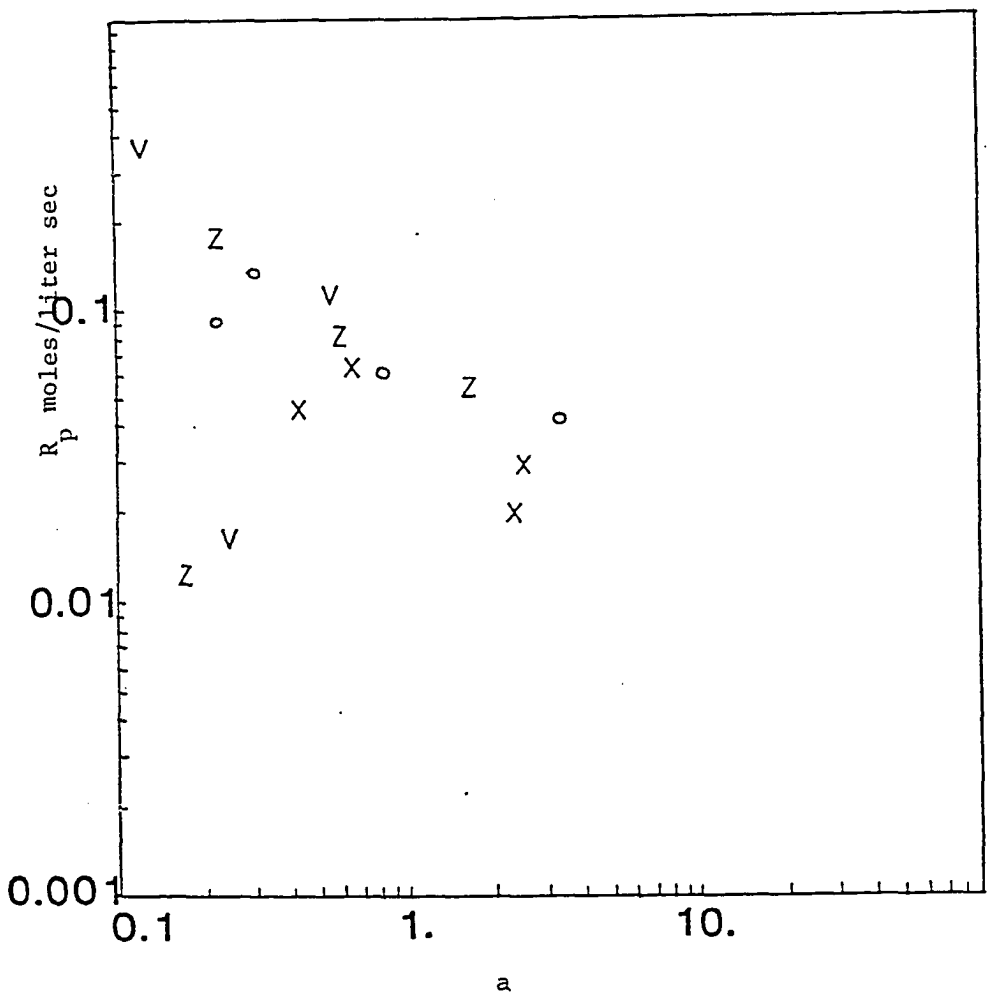

V 3% Tetronic 1102

o 6% Tetronic 1102

X 9% Tetronic 1102

Z 12% Tetronic 1102

Figure A.11

Correlation Between Polymerization Rate and a KPS Initiator

Polymerization Temperature= 60° C

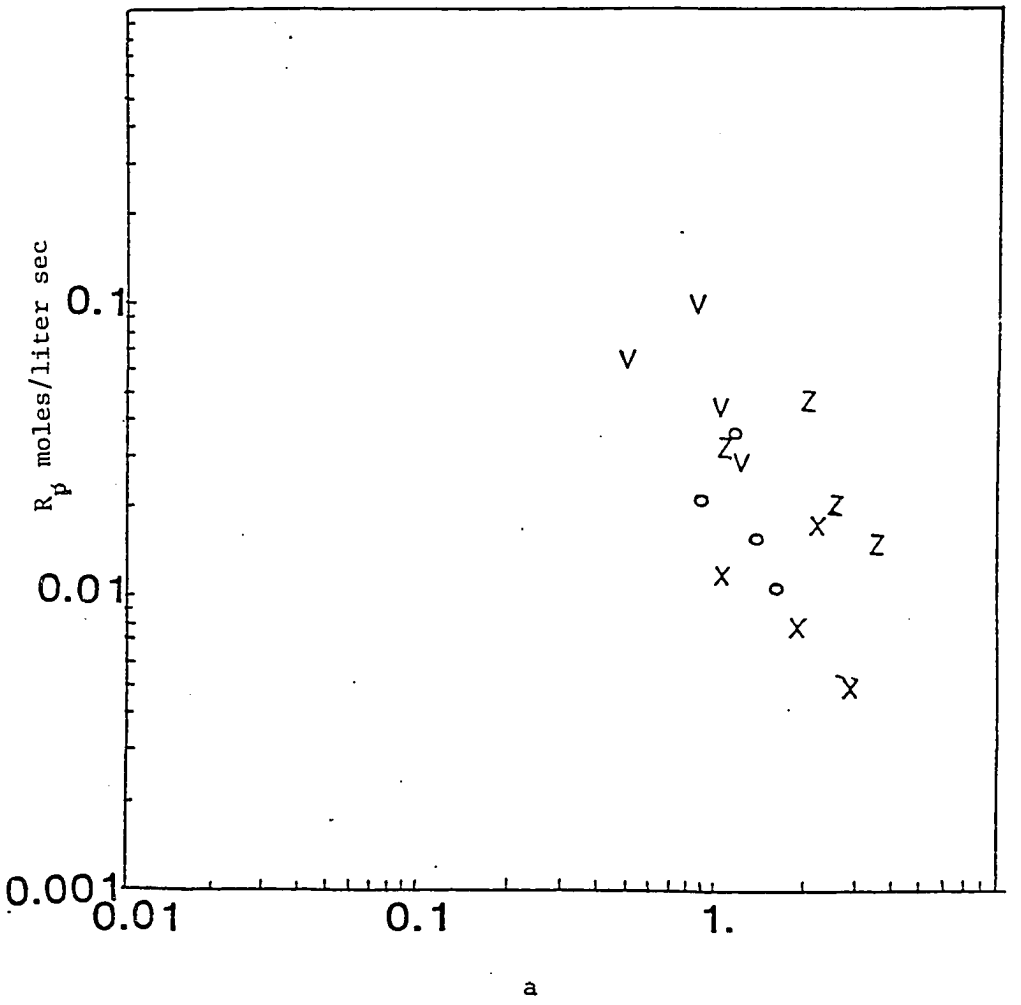

V 3% Tetronic 1102

o 6% Tetronic 1102

X 9% Tetronic 1102

Z 12% Tetronic 1102

Figure A.12

Correlation Between Polymerization Rate and a

KPS Initiator

Polymerization Temperature= 65° C

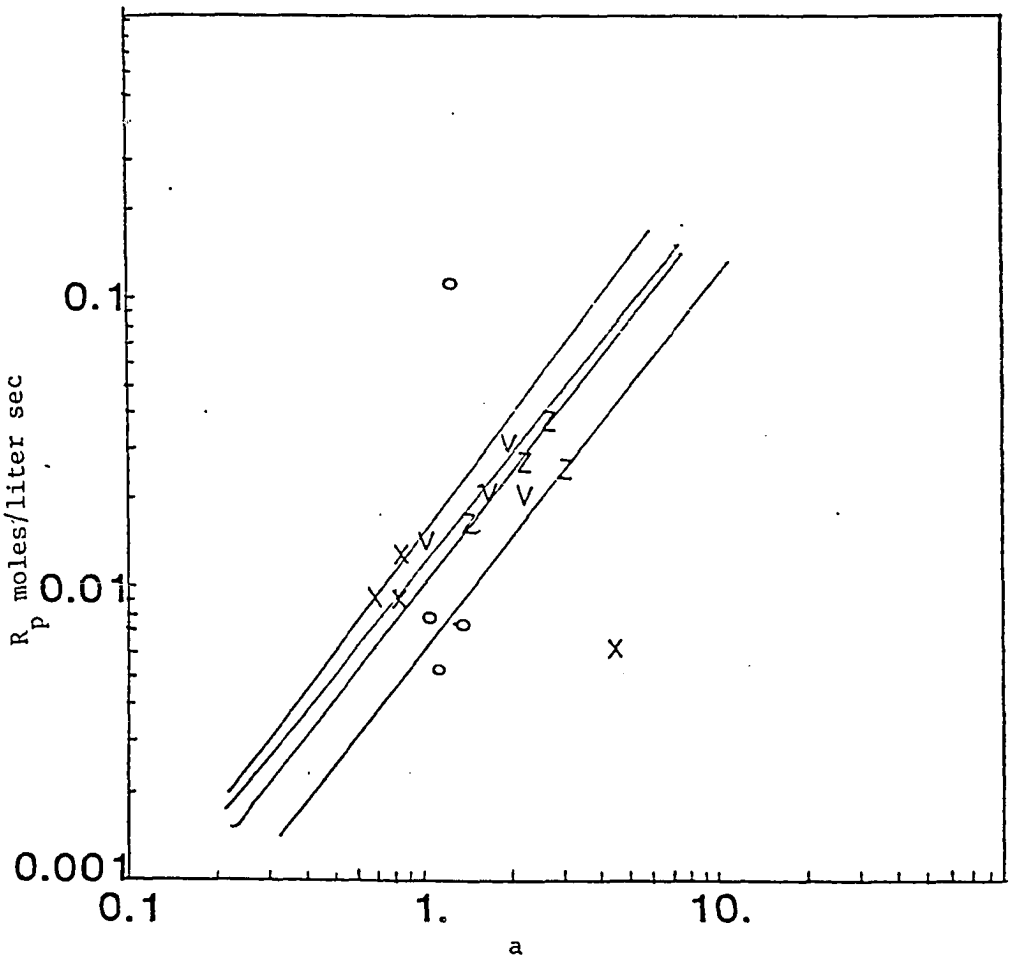

V 3% Tetronic 1102

o 6% Tetronic 1102

X 9% Tetronic 1102

Z 12% Tetronic 1102

Figure A.13

Correlation Between Polymerization Rate and Particle Volume

KPS Initiator

Polymerization Temperature= 50° C

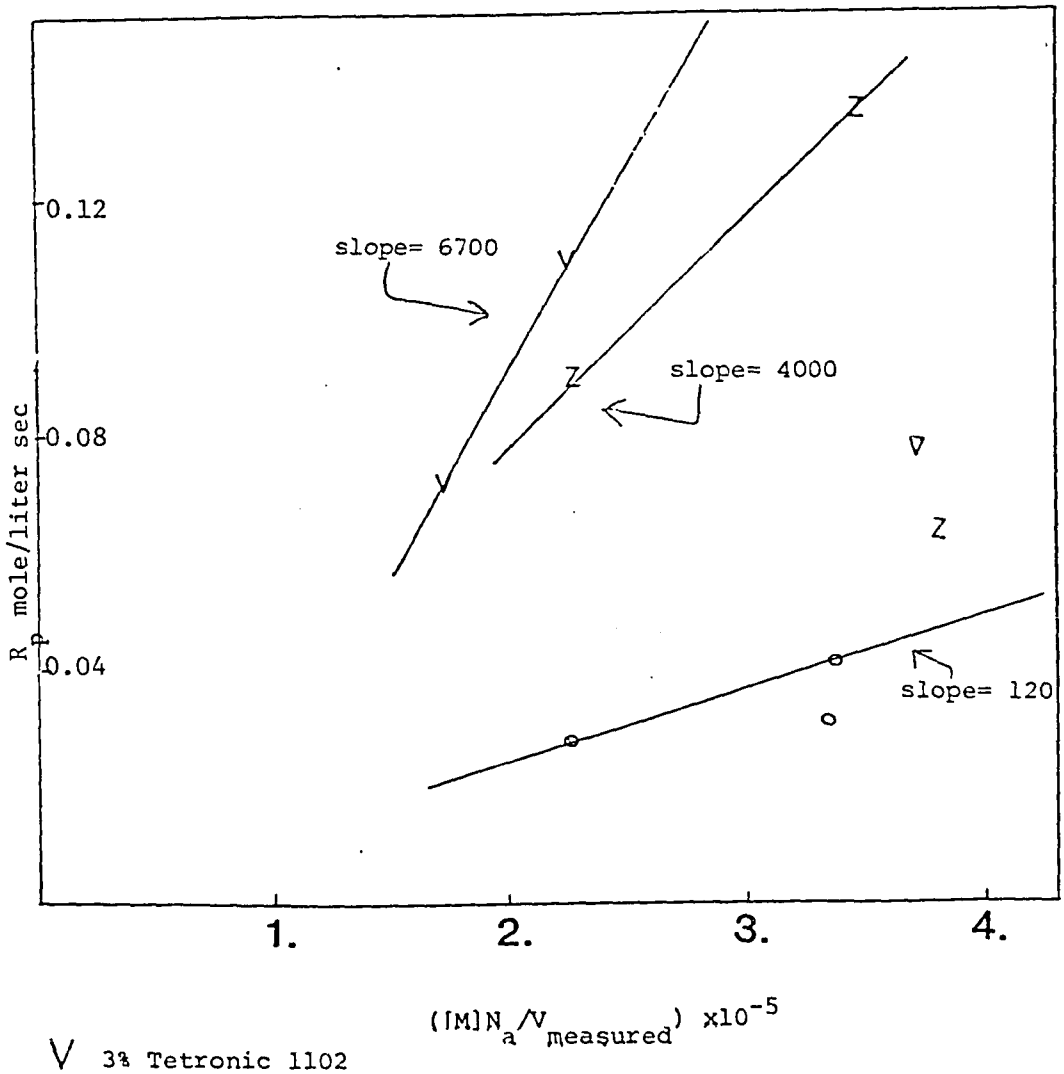

V 3% Tetronic 1102

O 6% Tetronic 1102

X 9% Tetronic 1102

Z 12% Tetronic 1102

Figure A.14

Correlation Between Polymerization Rate and Particle Volume

KPS Initiator

Polymerization Temperature= 55° C

Corr.

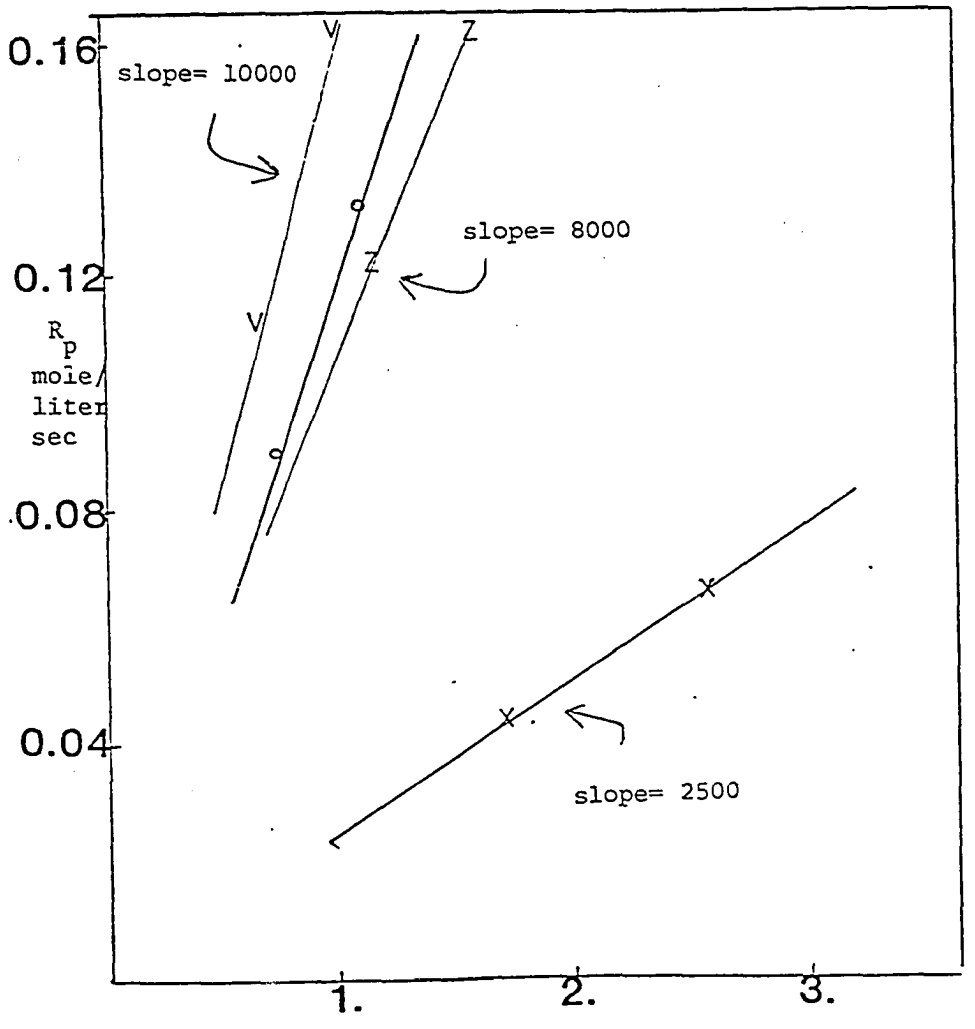

V 3% Tetronic 1102

o 6% Tetronic 1102

X 9% Tetronic 1102

Z 12% Tetronic 1102

$([M]N_a/V_{measured}) \times 10^{-5}$

Figure A.15

Correlation Between Polymerization Rate and Particle Volume

KPS Initiator

Polymerization Temperature= 60° C

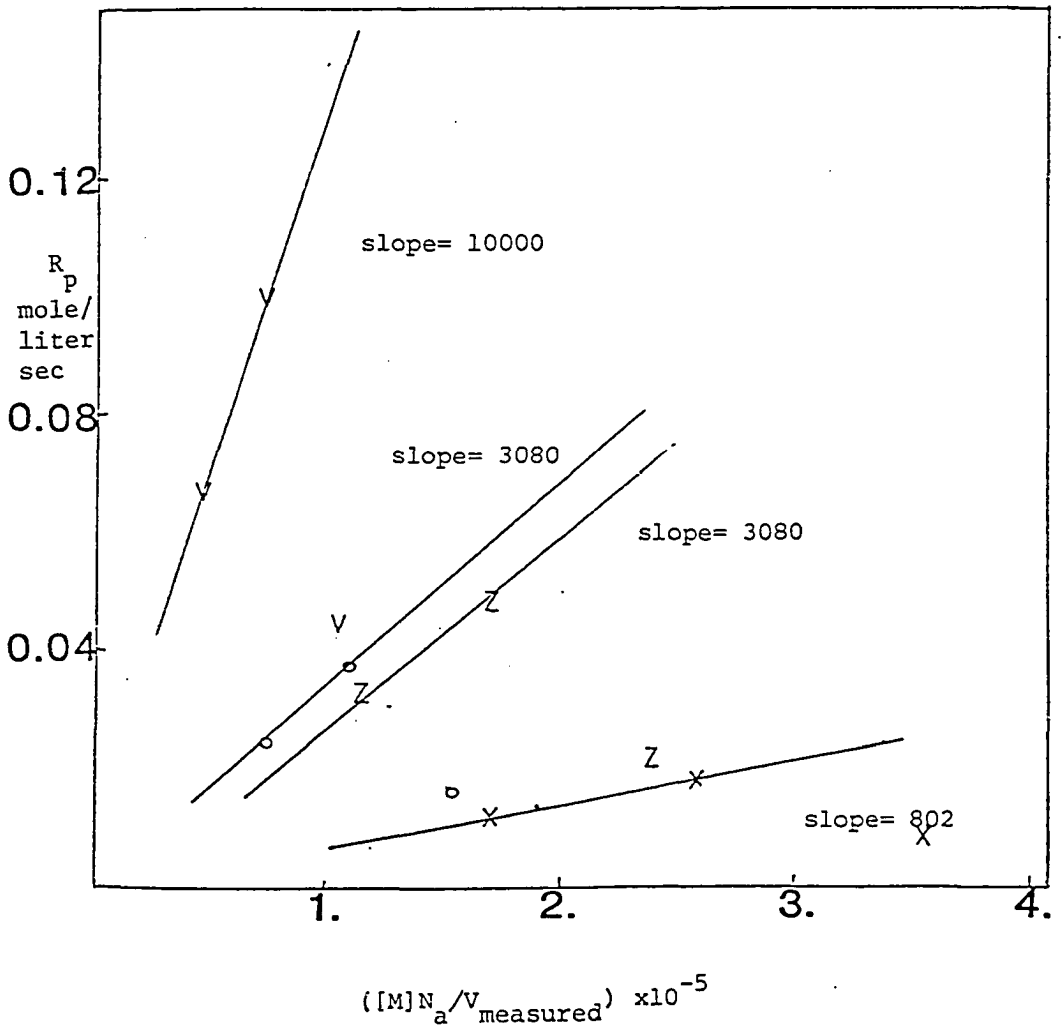

V 3% Tetronic 1102

o 6% Tetronic 1102

X 9% Tetronic 1102

Z 12% Tetronic 1102

Figure A.16

Correlation Between Polymerization Rate and Particle Volume

KPS Initiator

Polymerization Temperature = 65° C

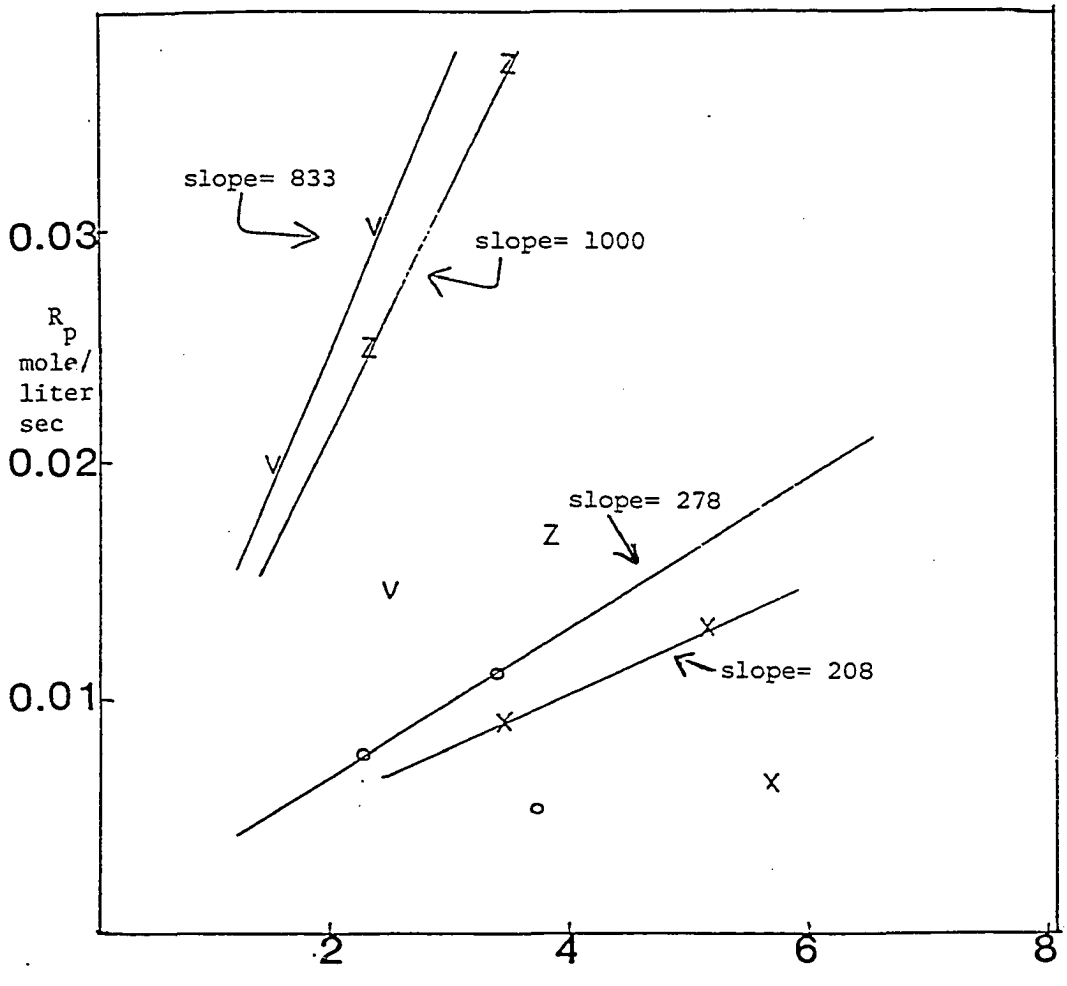

V 3% Tetronic 1102

o 6% Tetronic 1102

X 9% Tetronic 1102

Z 12% Tetronic 1102

Figure A.17

Rate per Particle as a function of Average Particle Volume

KPS Initiator

Polymerization Temperature= 50 ^{o} C

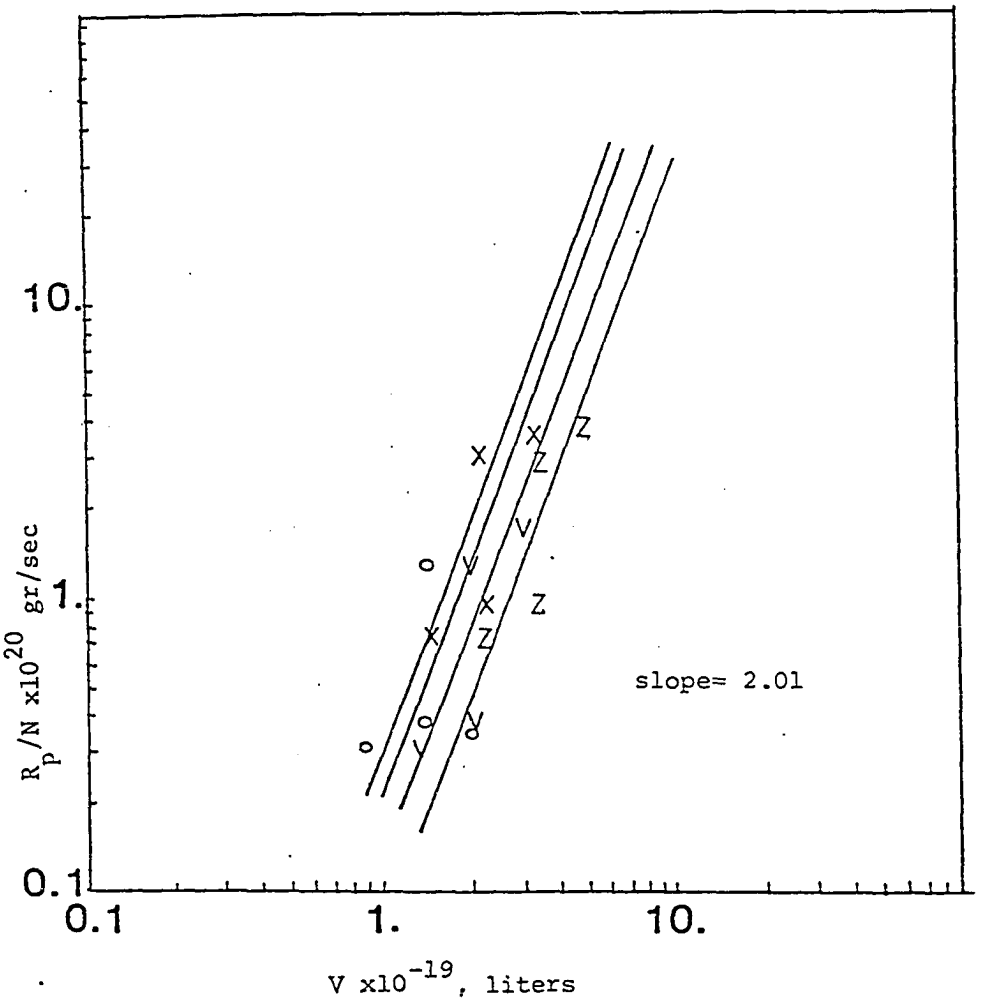

V 0.01 mole % initiator

O 0.04 mole % initiator

X 0.07 mole % initiator

Z 0.10 mole % initiator

Figure A.18

Rate per Particle as a Function of Average Particle Volume

KPS Initiator

Polymerization Temperature= 50° C

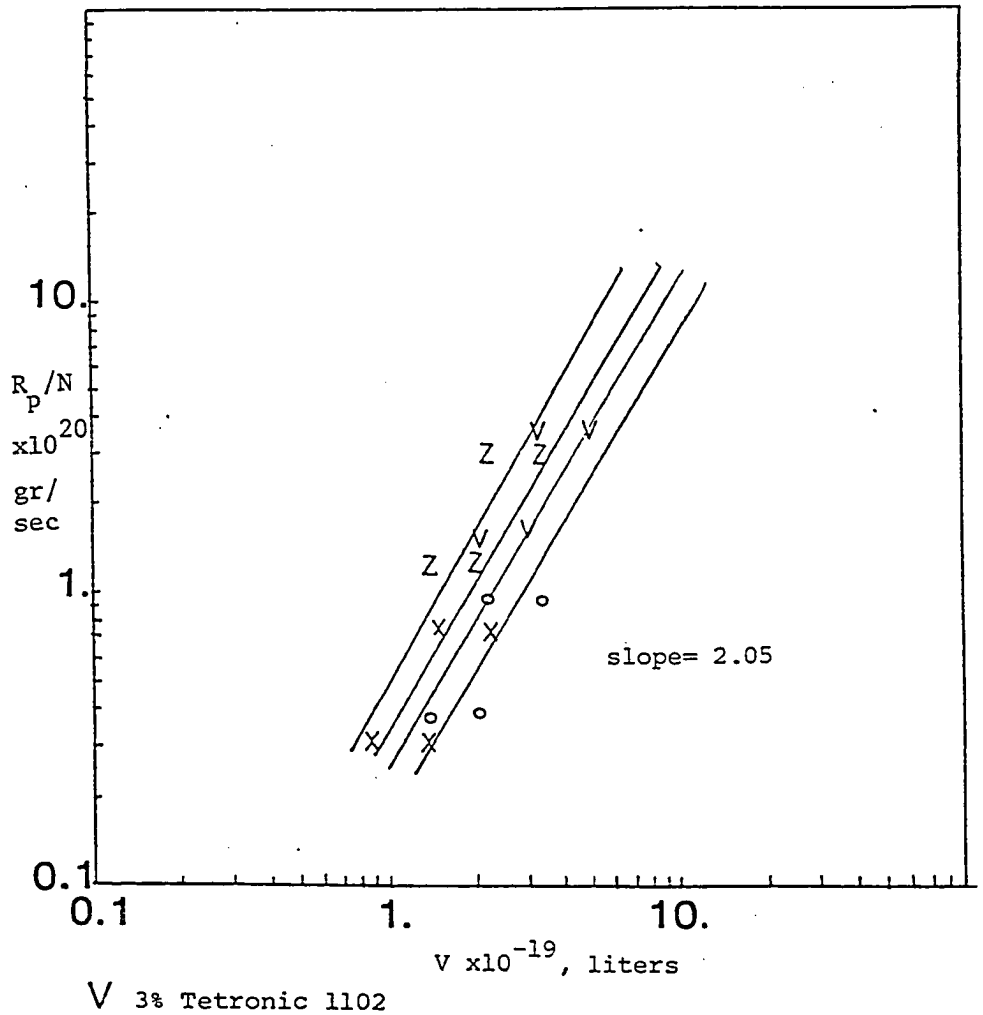

V 3% Tetronic 1102

o 6% Tetronic 1102

X 9% Tetronic 1102

Z 12% Tetronic 1102

Figure A.19

Rate per Particle as a Function of Average Particle Volume

KPS Initiator

Polymerization Temperature= 55 °C

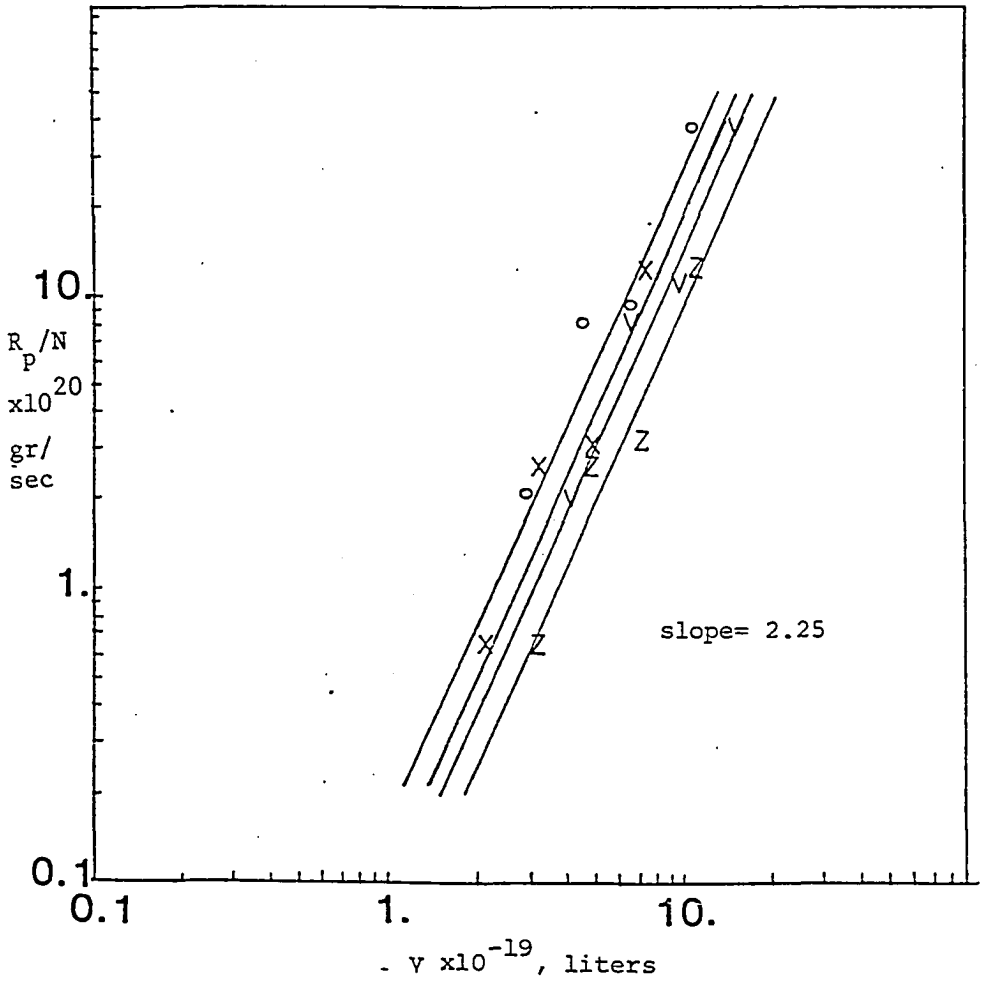

V 0.01 mole % initiator

O 0.04 mole % initiator

X 0.07 mole % initiator

Z 0.10 mole % initiator

Figure A.20

Rate per Particle as a Function of Average Particle Volume

KPS Initiator

Polymerization Temperature= 60° C

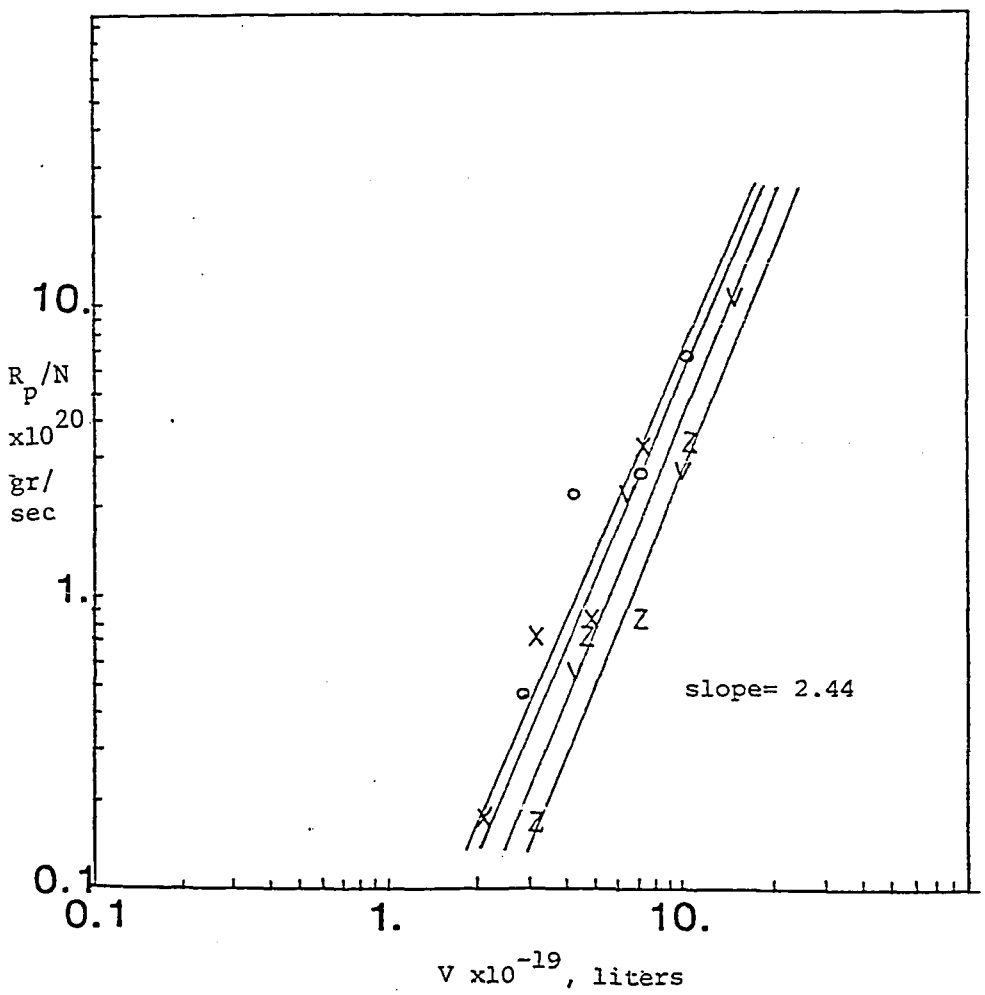

V 0.01 mole % initiator

o 0.04 mole % initiator

X 0.07 mole % initiator

Z 0.10 mole % initiator

Figure A.21

Rate per Particle as a Function of Average Particle Volume

KPS Initiator

Polymerization Temperature= 65° C

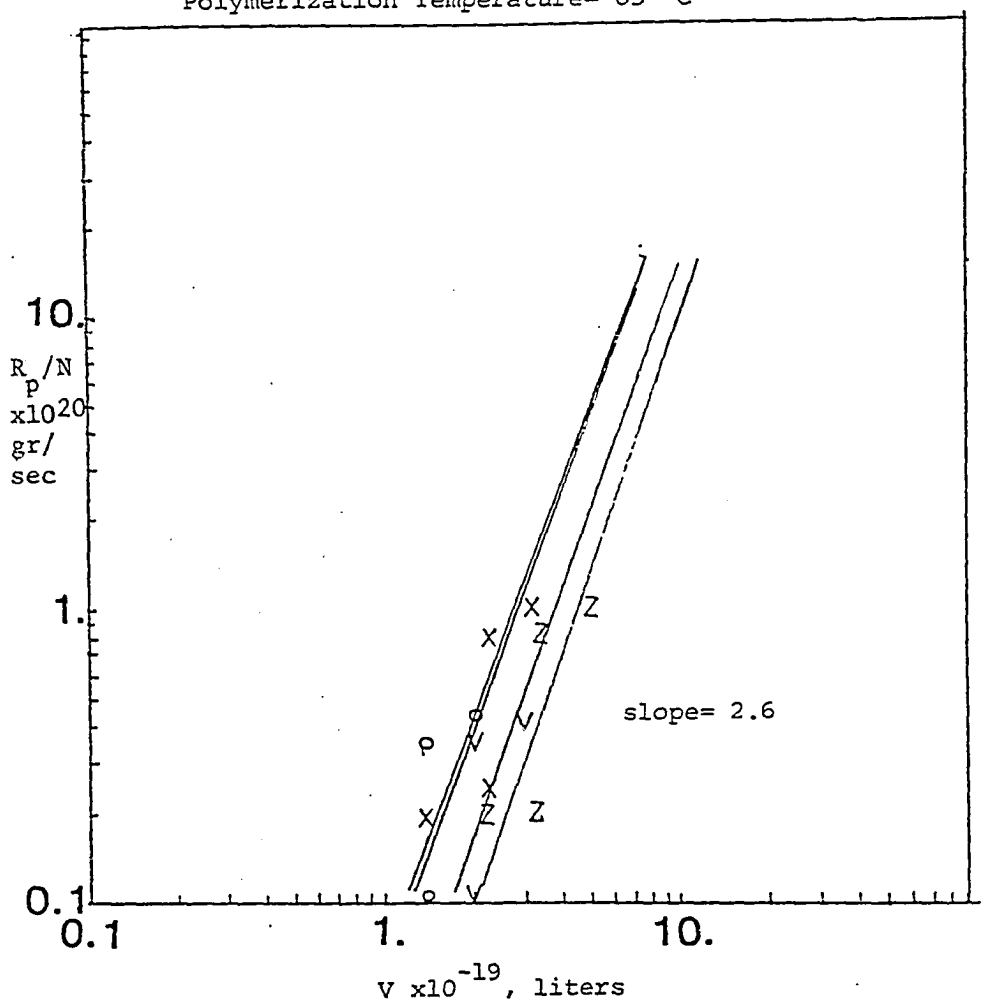

V 0.01 mole % initiator

O 0.04 mole % initiator

X 0.07 mole % initiator

Z 0.10 mole % initiator

Figure A.22

Rate per Particle as a Function of Average Particle Volume

KPS Initiator

0.07% KPS

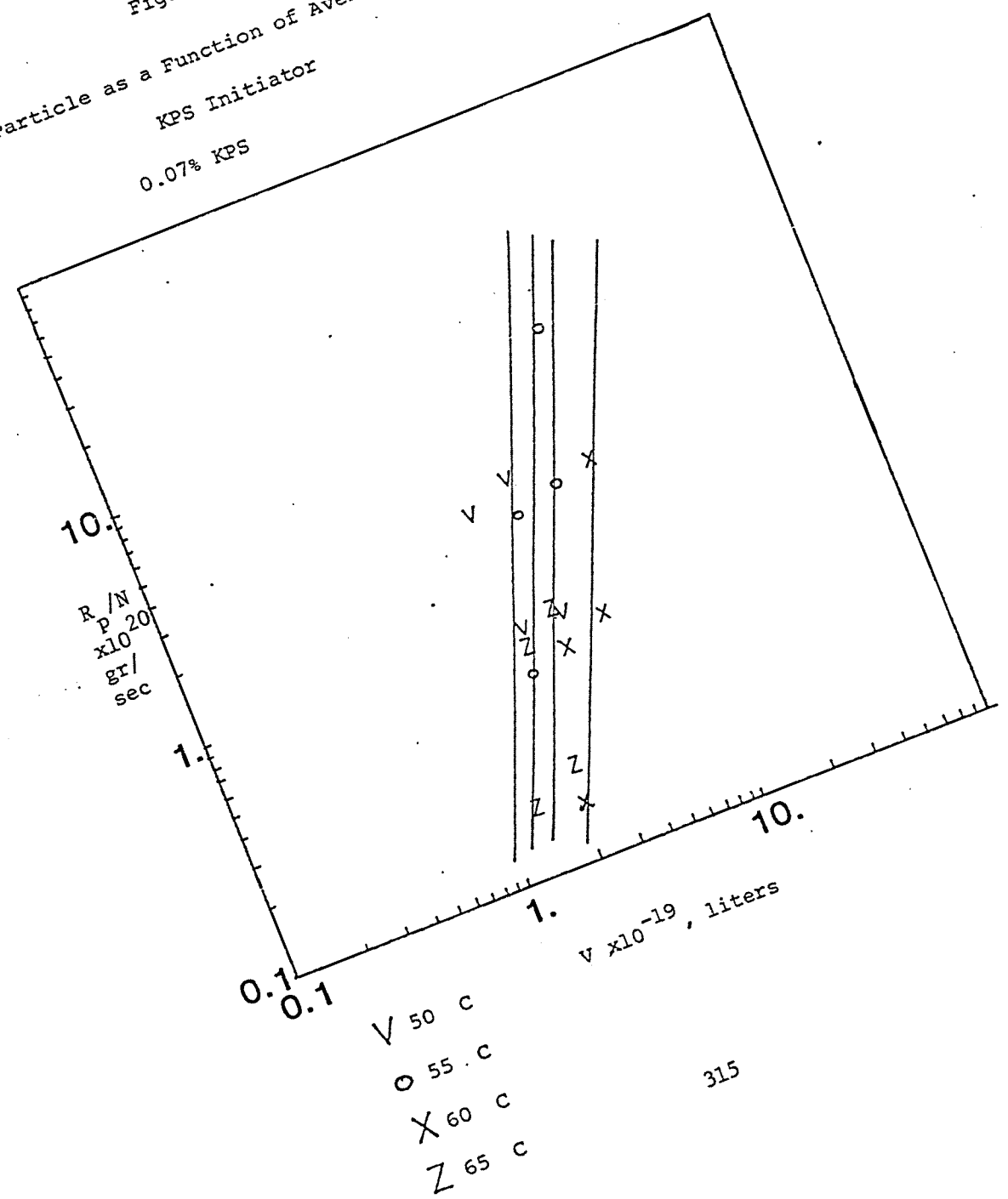

Figure A.23

Correlation Between Polymerization Rate
and Polymer Molecular Weight
KPS Initiator
Polymerization Temperature= 50 °C

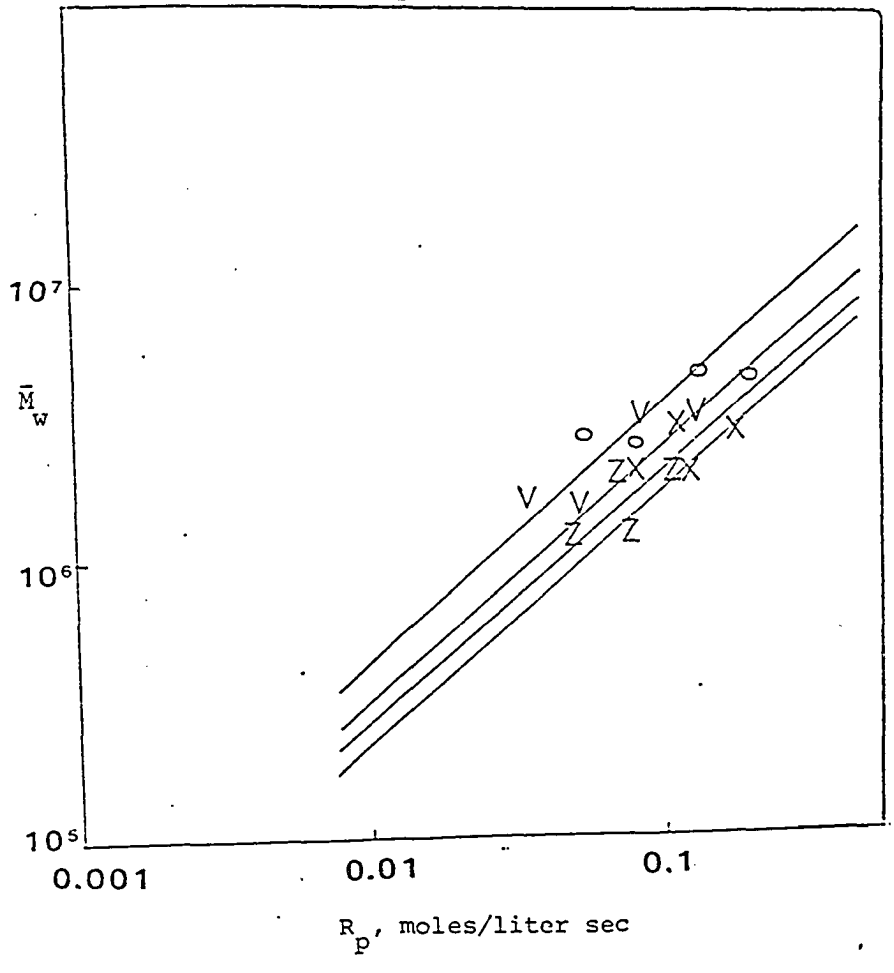

V 0.01 mole % initiator
O 0.04 mole % initiator
X 0.07 mole % initiator
Z 0.10 mole % initiator

Figure A.24

Correlation Between Polymerization Rate
and Polymer Molecular Weight
KPS Initiator

Polymerization Temperature= 55 C

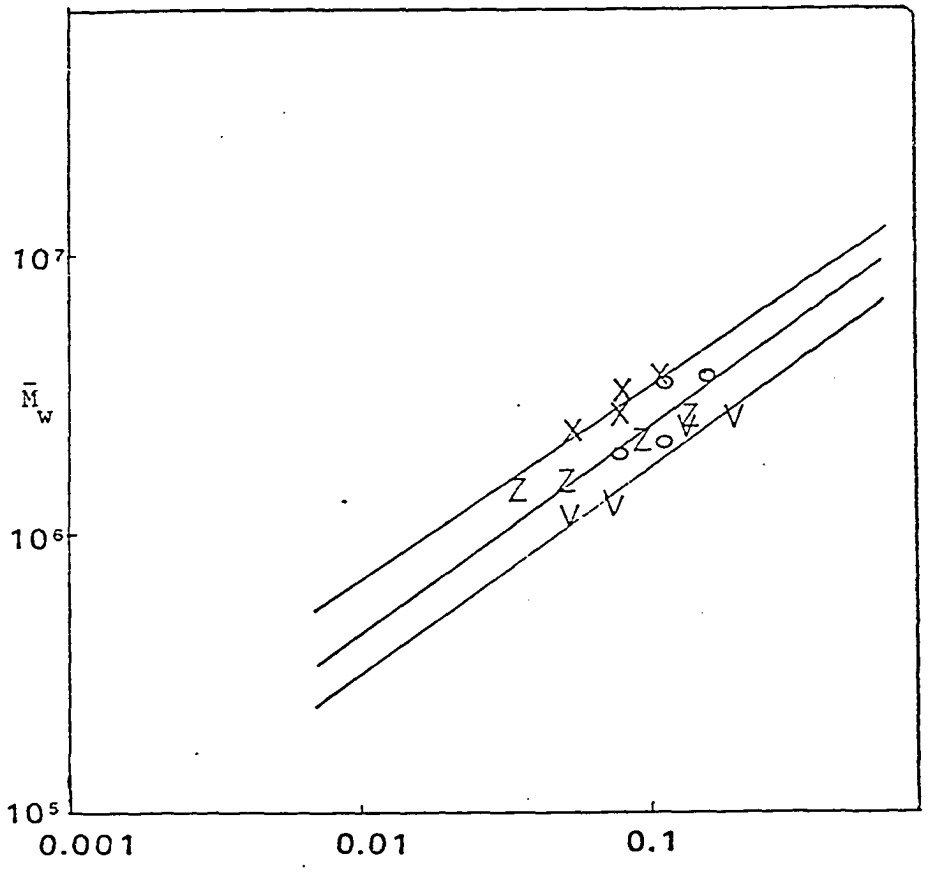

V 0.01 mole % initiator

O 0.04 mole % initiator

X 0.07 mole % initiator

Z 0.1. mole % initiator

Figure A.25

Correlation Between Polymerization Rate
and Polymer Molecular Weight

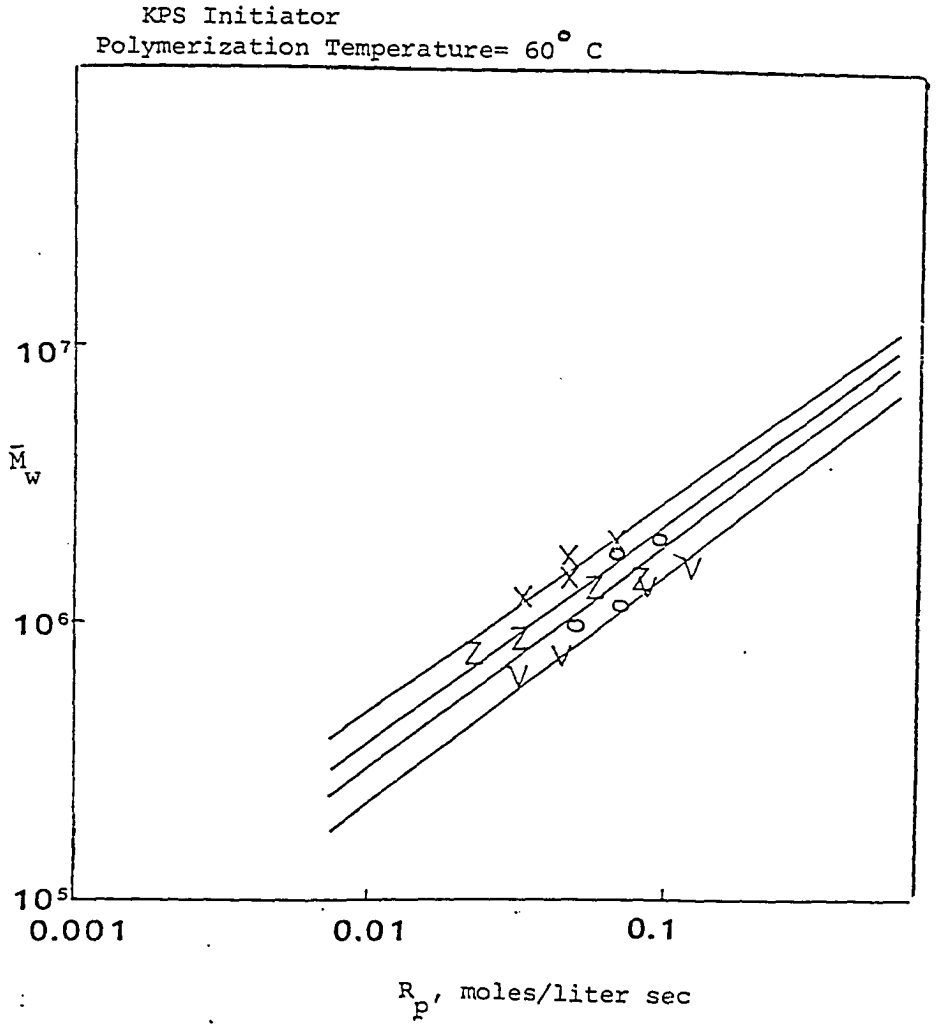

V 0.01 mole % initiator

O 0.04 mole % initiator

X 0.07 mole % initiator

Z 0.10 mole % initiator

Figure A.26

Correlation Between Polymerization Rate
and Polymer Molecular Weight

KPS Initiator

Polymerization Temperature= 65° C

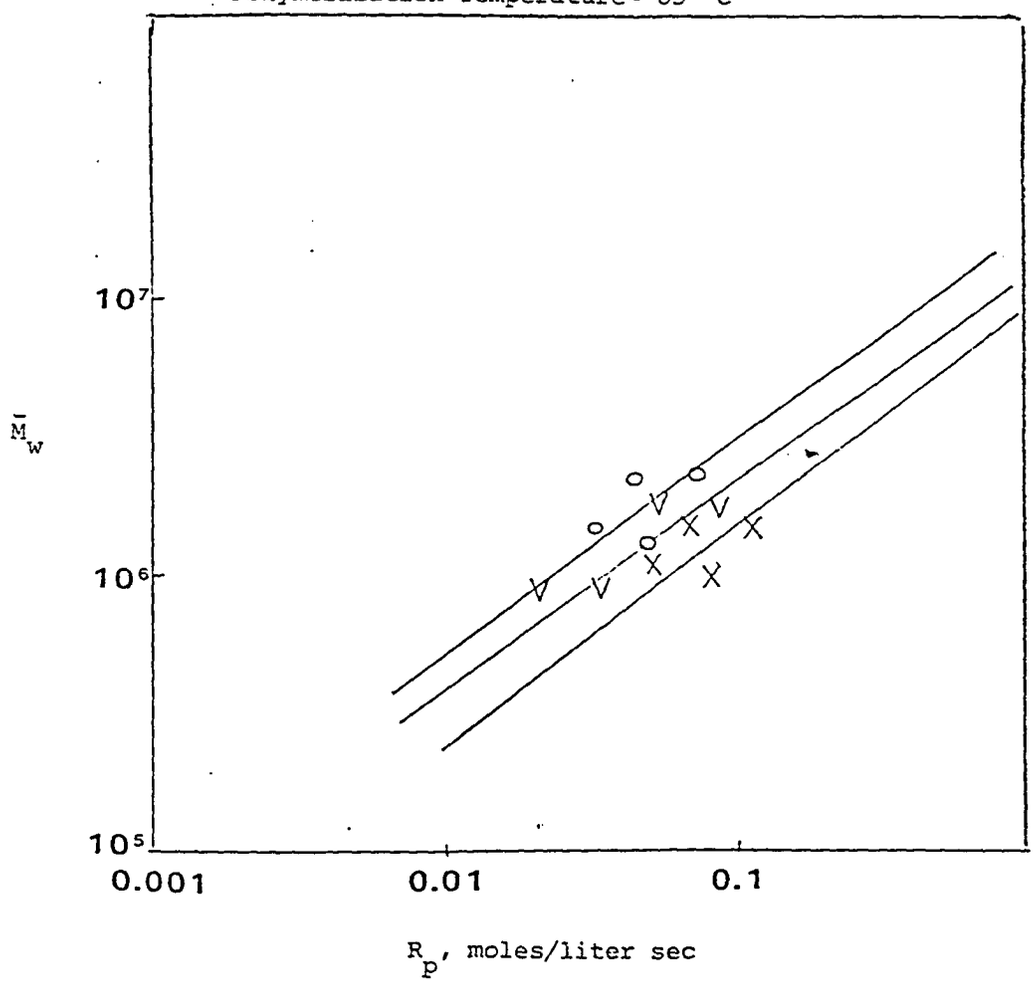

V 0.01 mole % initiator

O 0.04 mole % initiator

X 0.07 mole % initiator

Z 0.10 mole % initiator

Figure A.27

Correlation Between Polymerization Rate and a

ADVN Initiator

Polymerization Temperature= 50° C

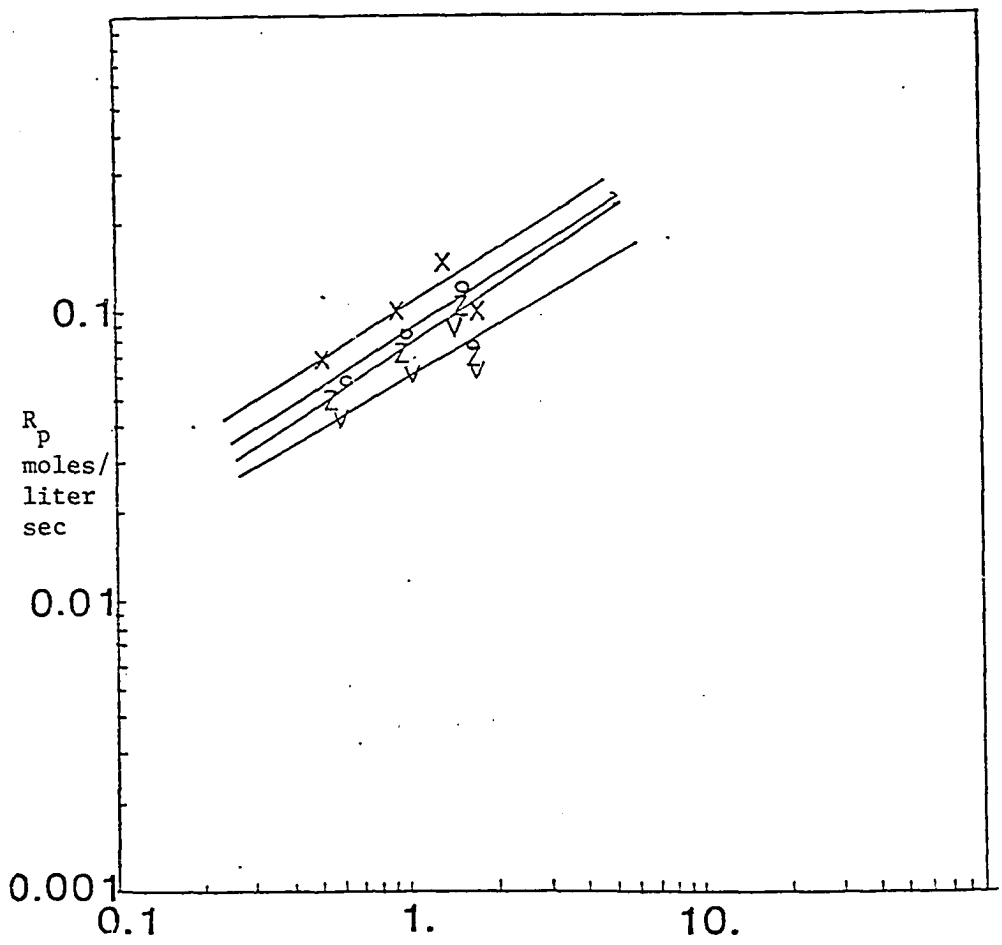

V 3% Tetronic 1102

O 6% Tetronic 1102

X 9% Tetronic 1102

Z 12% Tetronic 1102

Figure A.28

Correlation Between Polymerization Rate and a

ADVN Initiator

Polymerization Temperature= 50° C

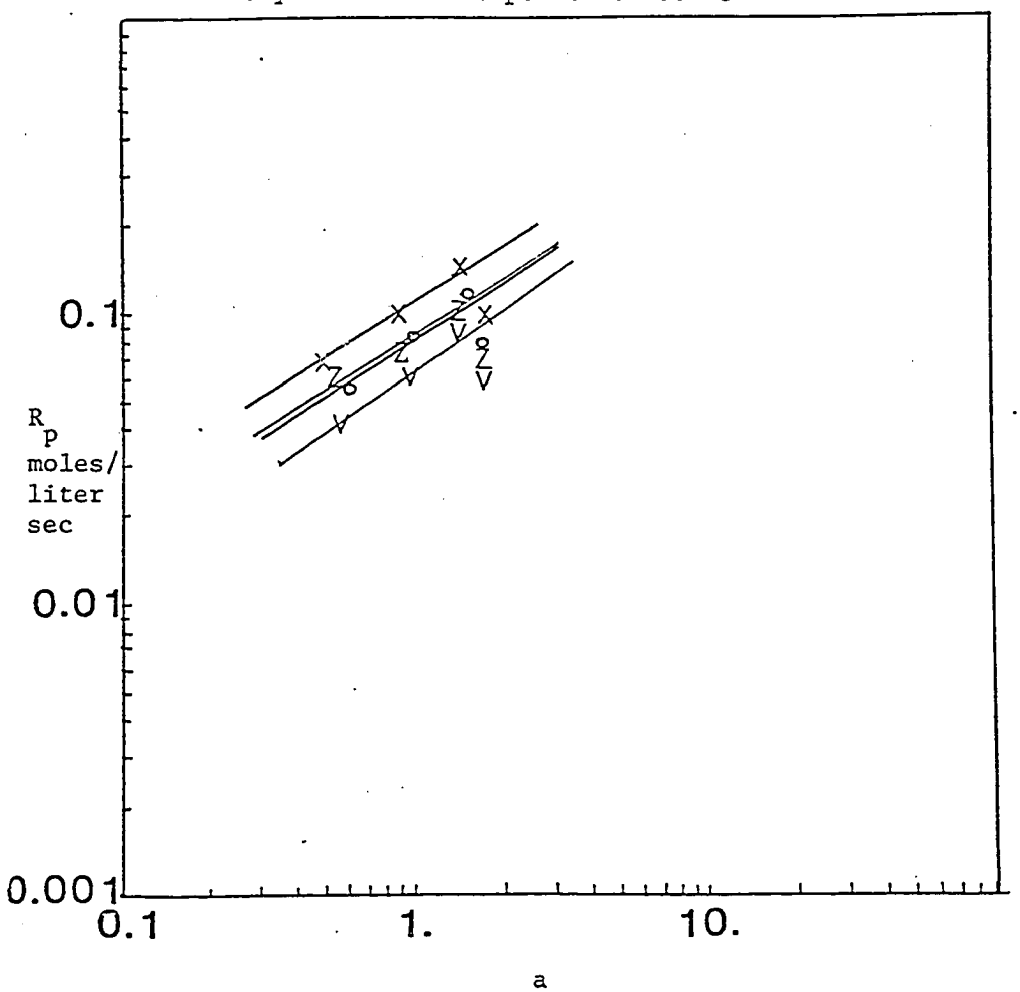

V 3% Tetronic 1102

o 6% Tetronic 1102

X 9% Tetronic 1102

Z 12% Tetronic 1102

Figure A.29

Correlation Between Polymerization Rate and a

ADVN Initiator

Polymerization Temperature= 55° C

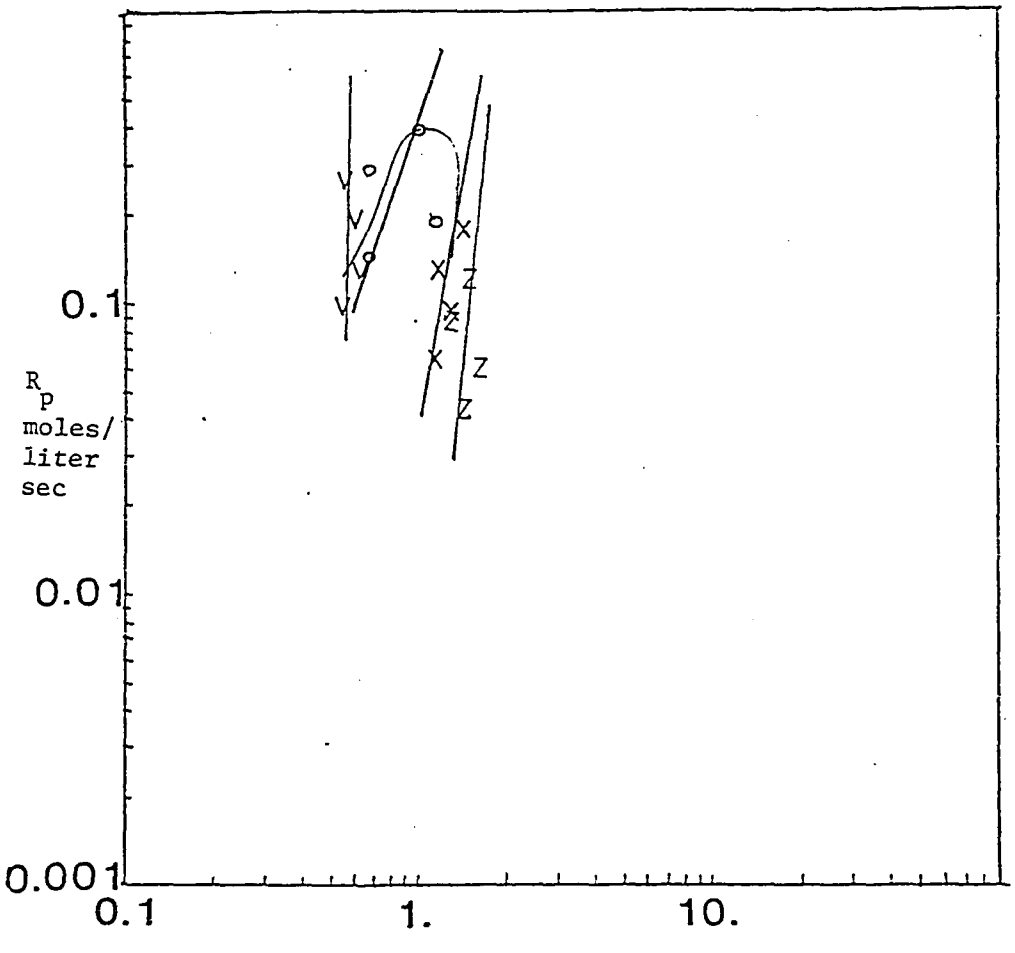

V 0.01 mole % initiator

O 0.04 mole % initiator

X 0.07 mole % initiator

Z 0.10 mole % initiator

Figure A.30

Correlation Between Polymerization Rate and a

ADVN Initiator

Polymerization Temperature= 55° C

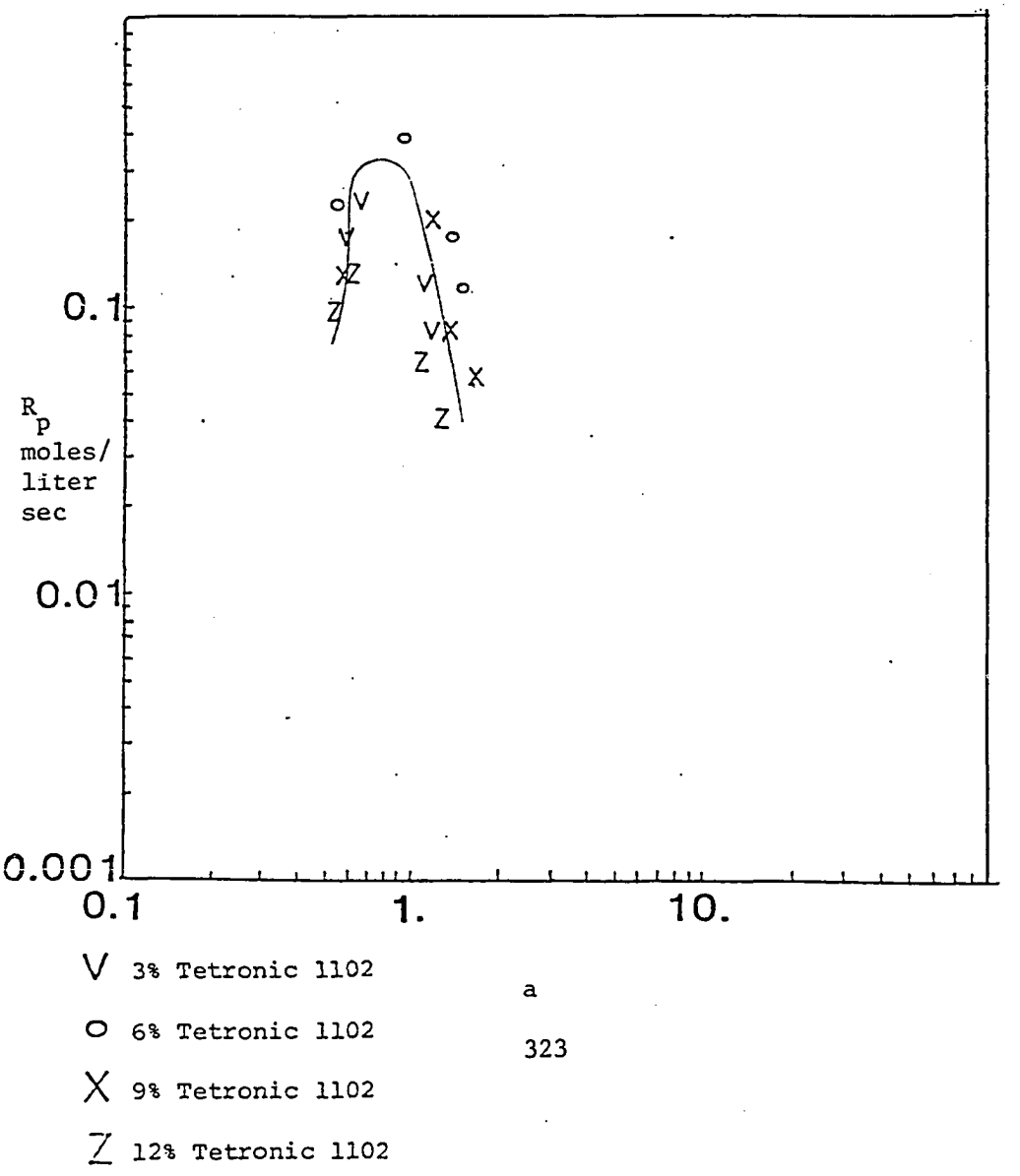

Figure A.31

Correlation Between Polymerization Rate and a

ADVN Initiator

Polymerization Temperature= 60° C

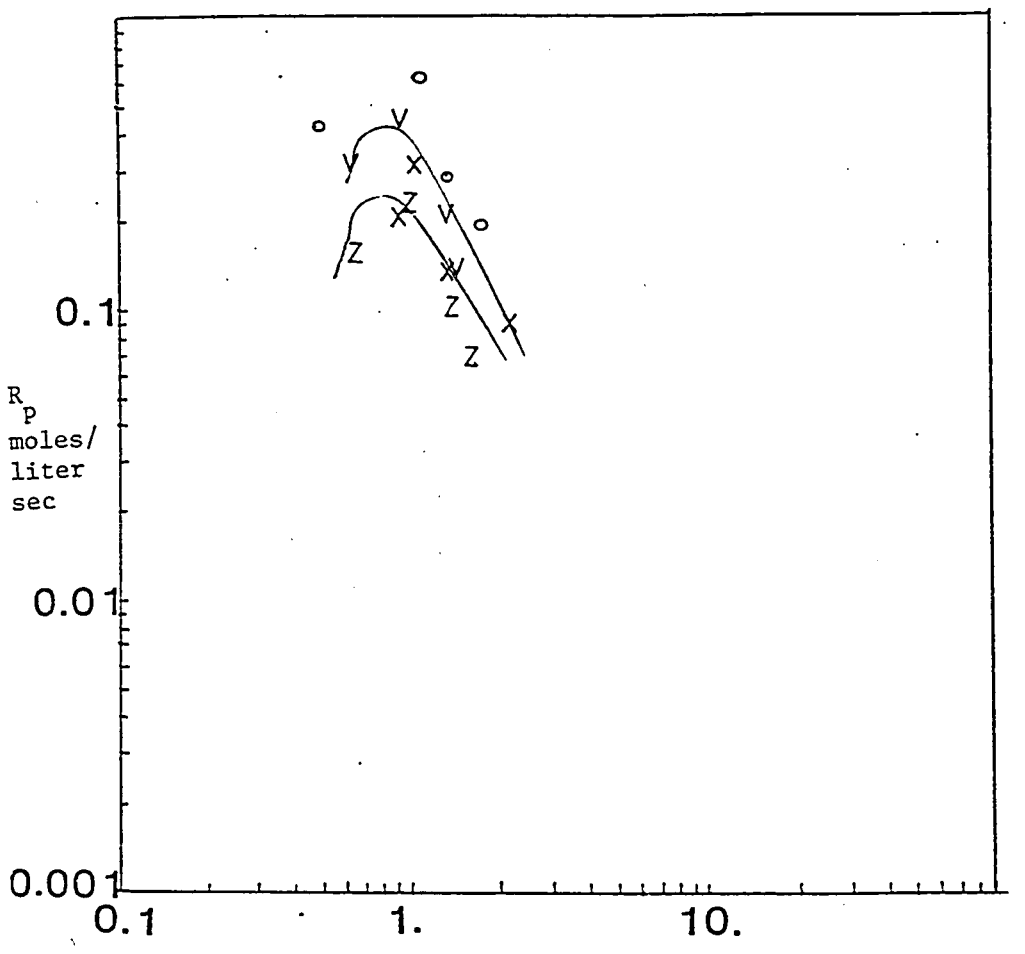

V 3% Tetronic 1102

O 6% Tetronic 1102

X 9% Tetronic 1102

Z 12% Tetronic 1102

Figure A.32

Correlation Between Polymerization Rate and a

ADVN Initiator

Polymerization Temperature= 60 °C

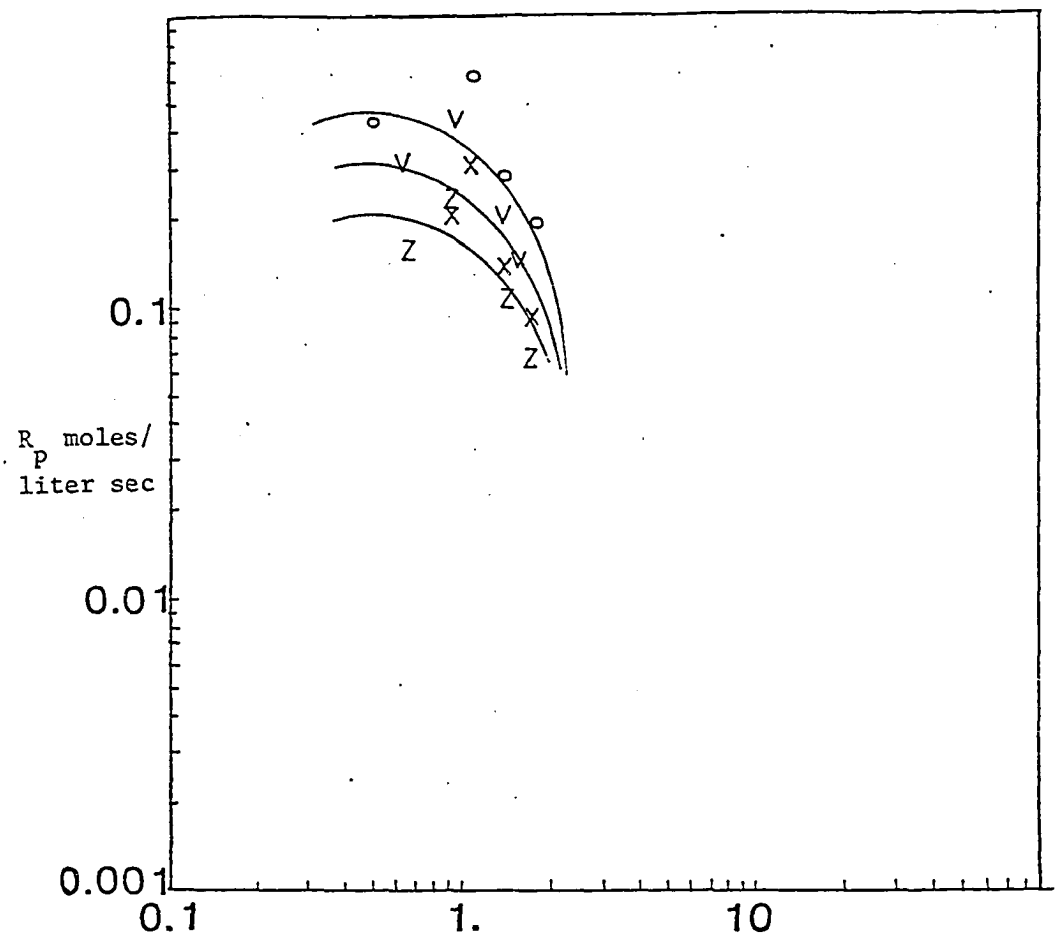

V 3% Tetronic 1102

O 6% Tetronic 1102

X 9% Tetronic 1102

Z 12% Tetronic 1102

Figure A.33

Correlation Between Polymerization Rate and Average Particle Volume

ADVN Initiator

Polymerization Temperature = 50° C

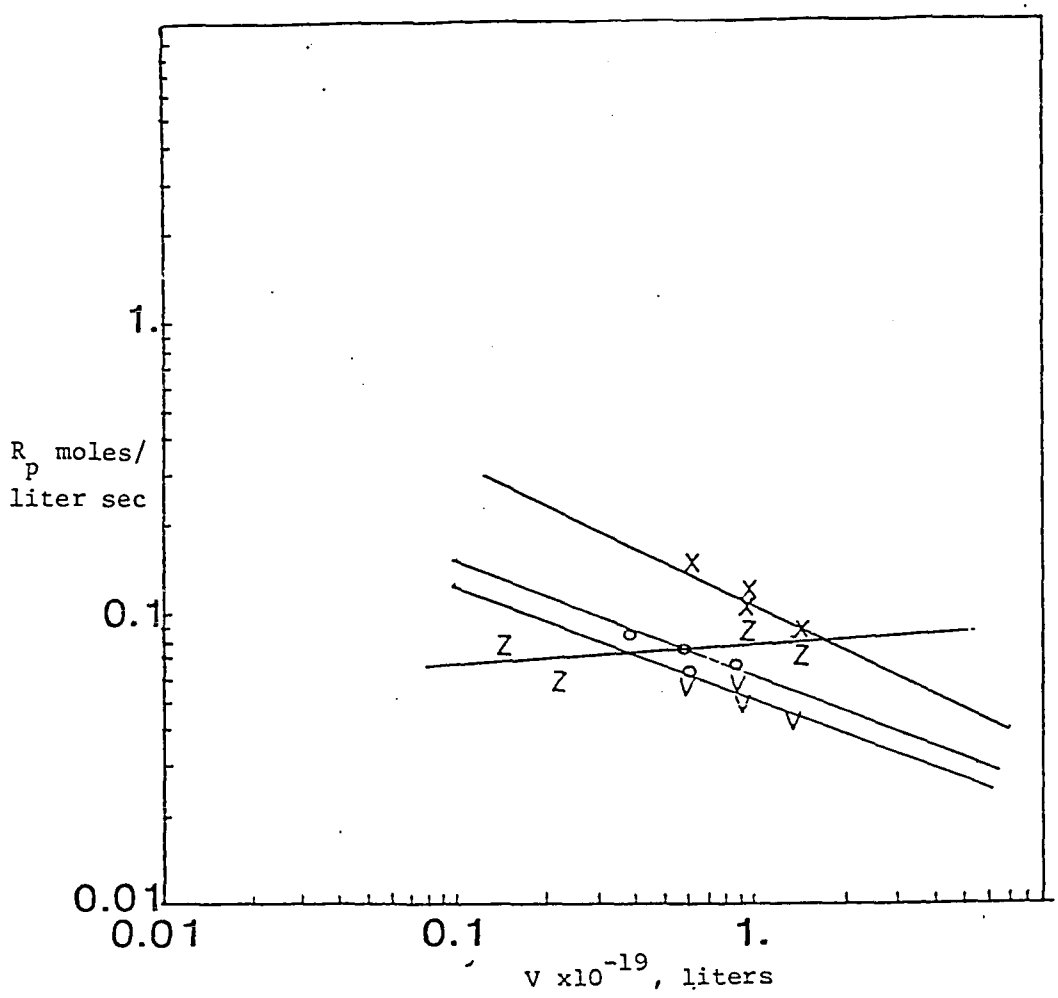

V 0.01 mole % initiator

O 0.04 mole % initiator

X 0.07 mole % initiator

Z 0.10 mole % initiator

Figure A.34

Correlation Between Polymerization Rate and Average Particle Volume

ADVN Initiator

Polymerization Temperature = 55°C

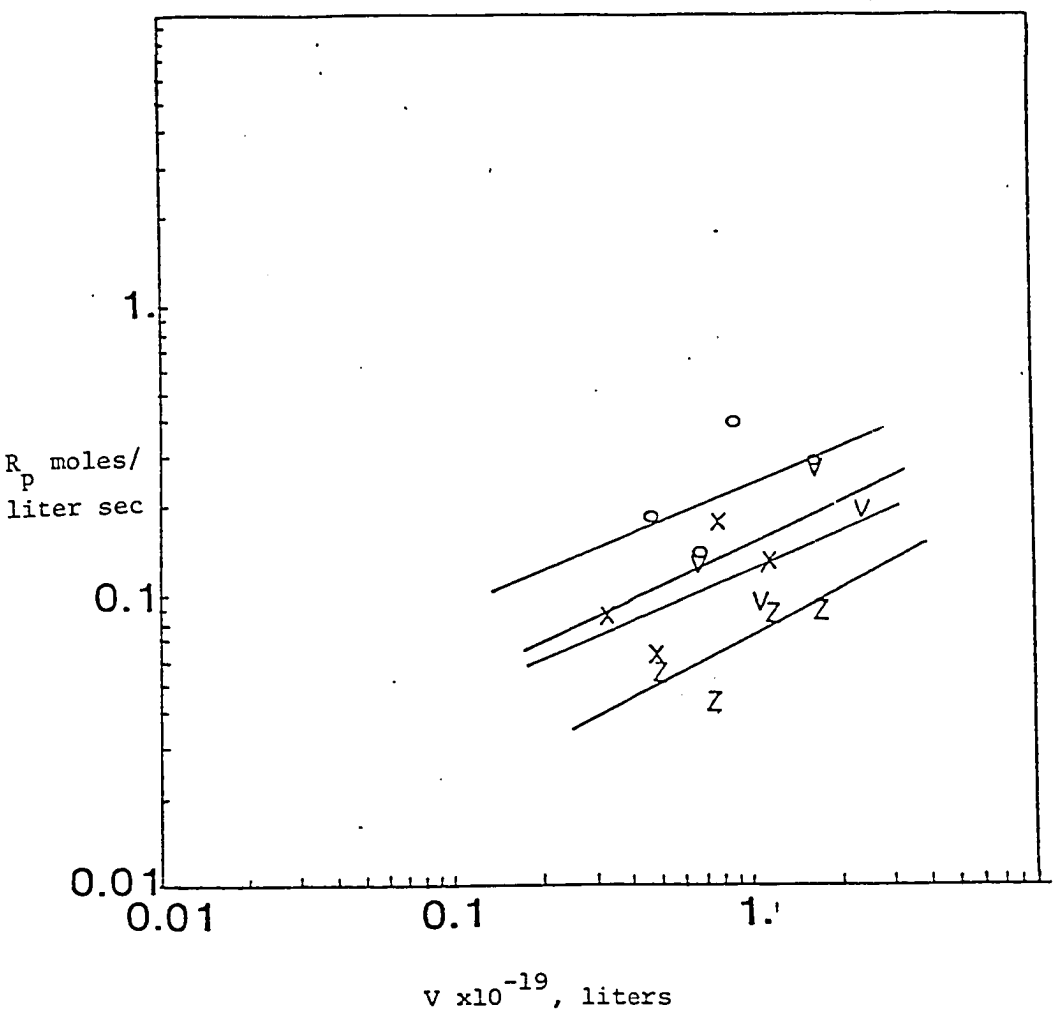

V 0.01 mole % initiator

o 0.04 mole % initiator

X 0.07 mole % initiator

Z 0.10 mole % initiator

Figure A.35

Correlation Between Polymerization Rate and Average Particle Volume

ADVN Initiator

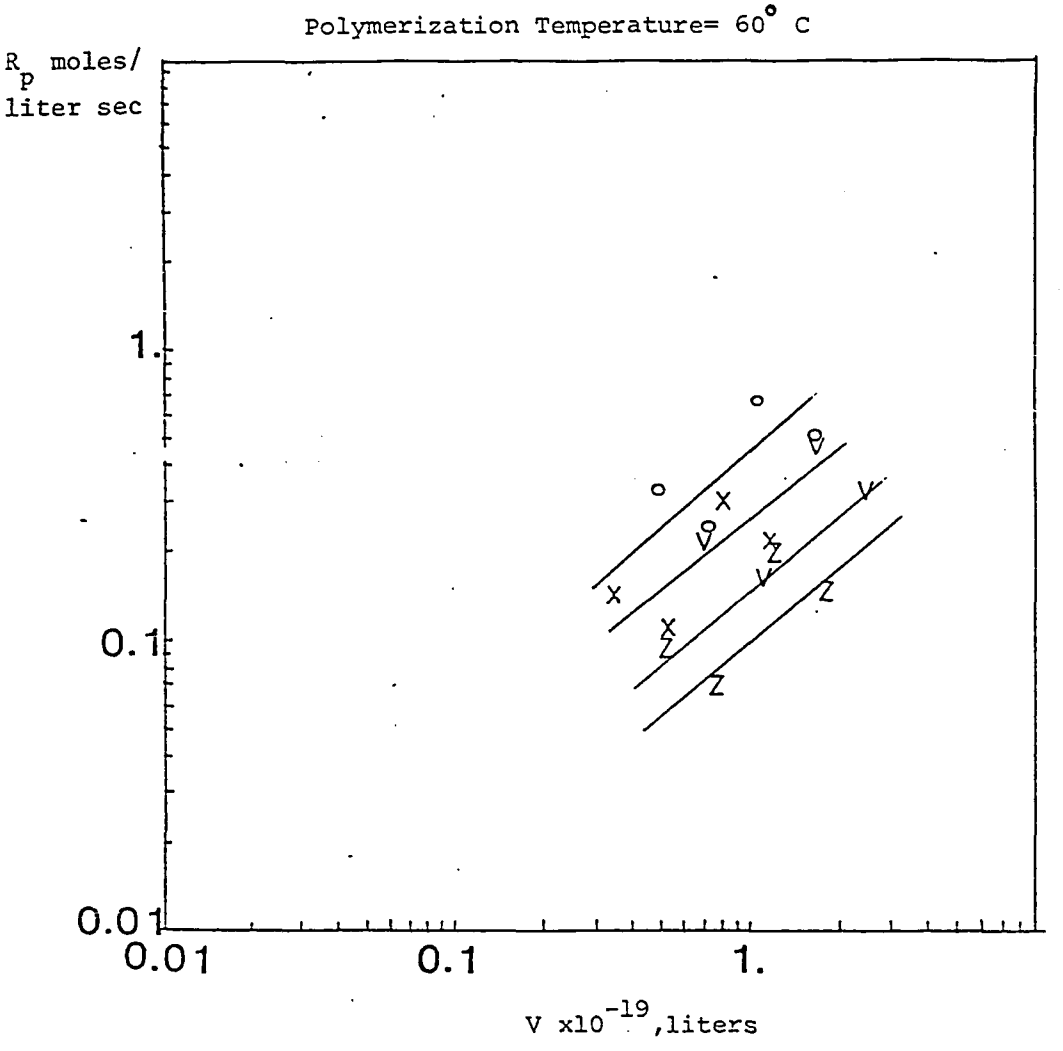

V 0.01 mole % initiator

O 0.04 mole % initiator

X 0.07 mole % ini iator

Z 0.10 mole % initiator

Figure A.36

Rate per Particle as a Function of Average Particle Volume

ADVN Initiator

Polymerization Temperature= 50° C

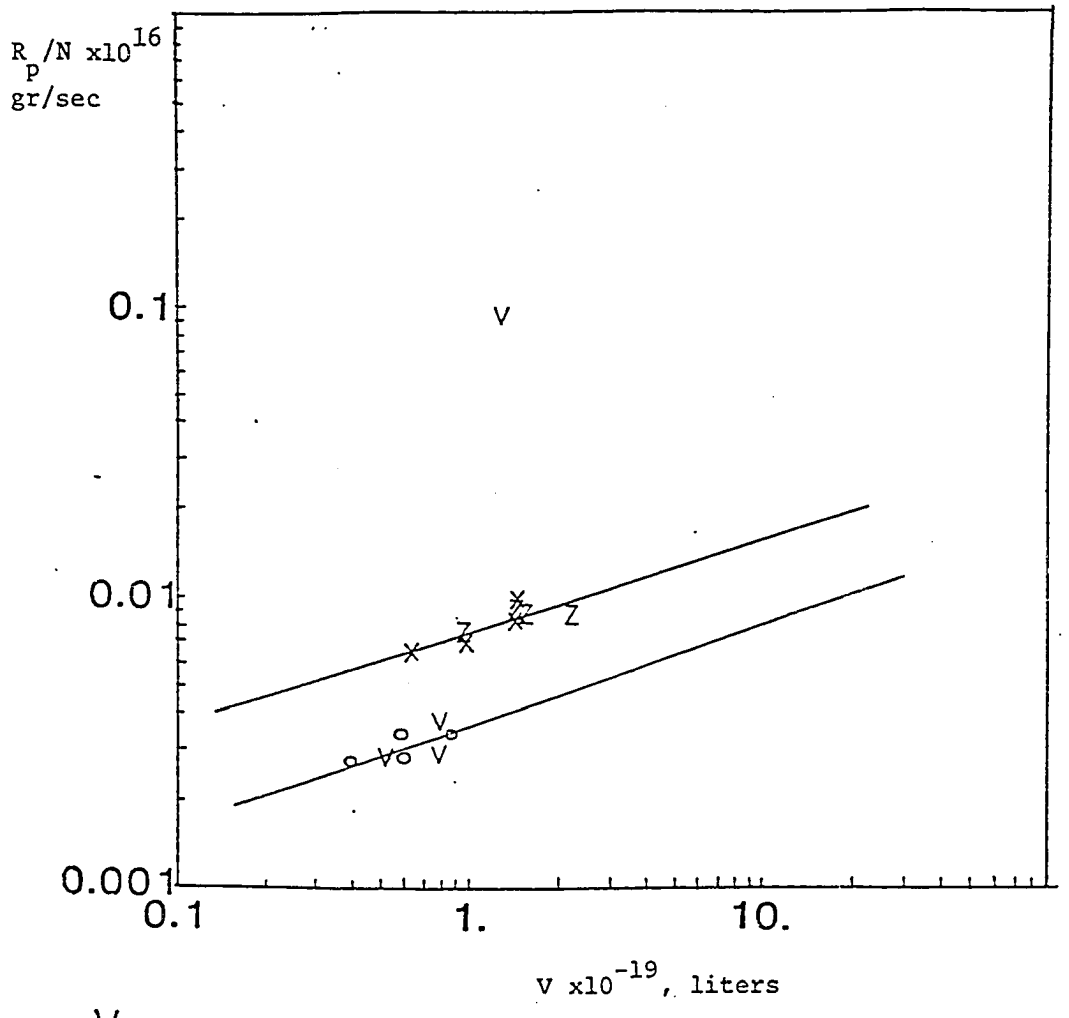

V 0.01 mole % initiatc:

o 0.04 mole % initiator

X 0.07 mole % initiator

Z 0.10 mole % initiator

Figure A.37

Rate per Particle as a Function of Average Particle Volume

ADVN Initiator

Polymerization Temperature= 50° C

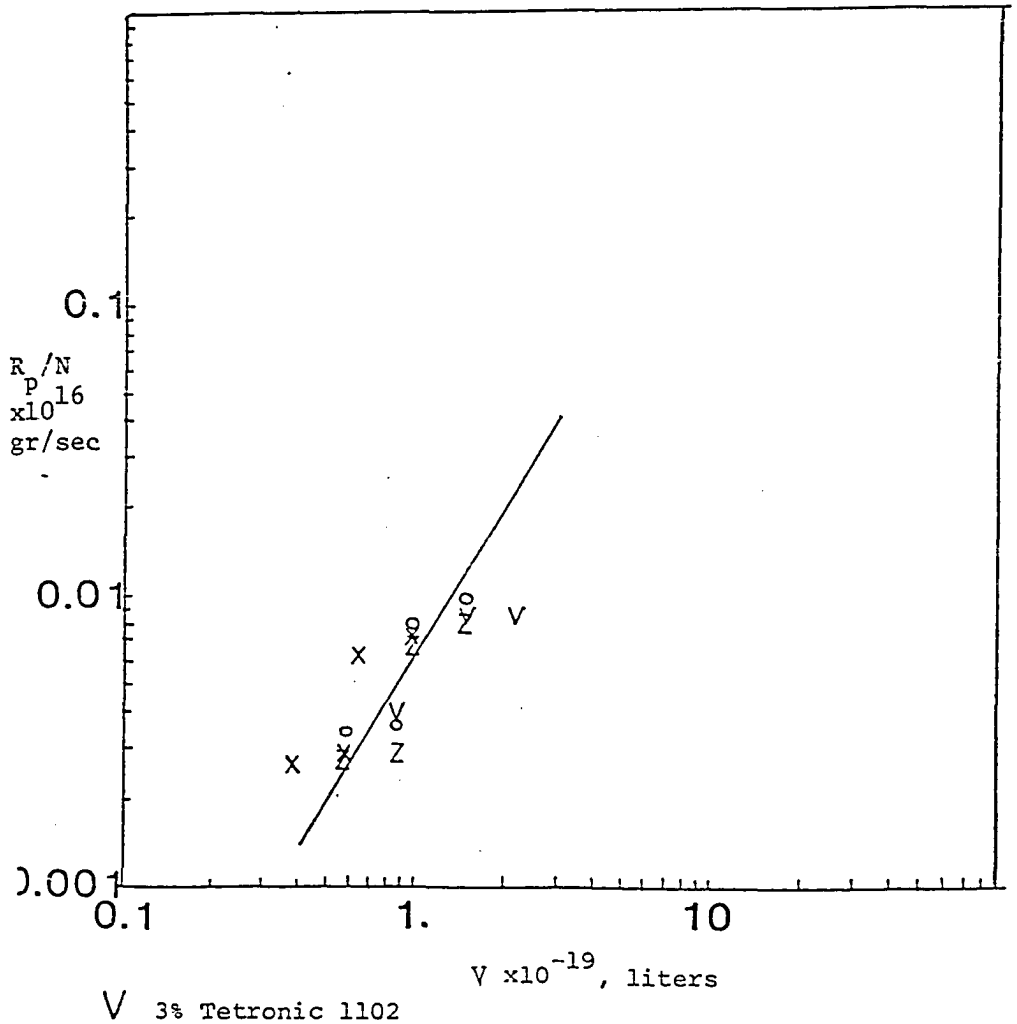

V 3% Tetronic 1102

o 6% Tetronic 1102

X 9% Tetronic 1102

Z 12% Tetronic 1102

Figure A.38

Rate per Particle as a Function of Average Particle Volume

ADVN Initiator

Polymerization Temperature= 55° C

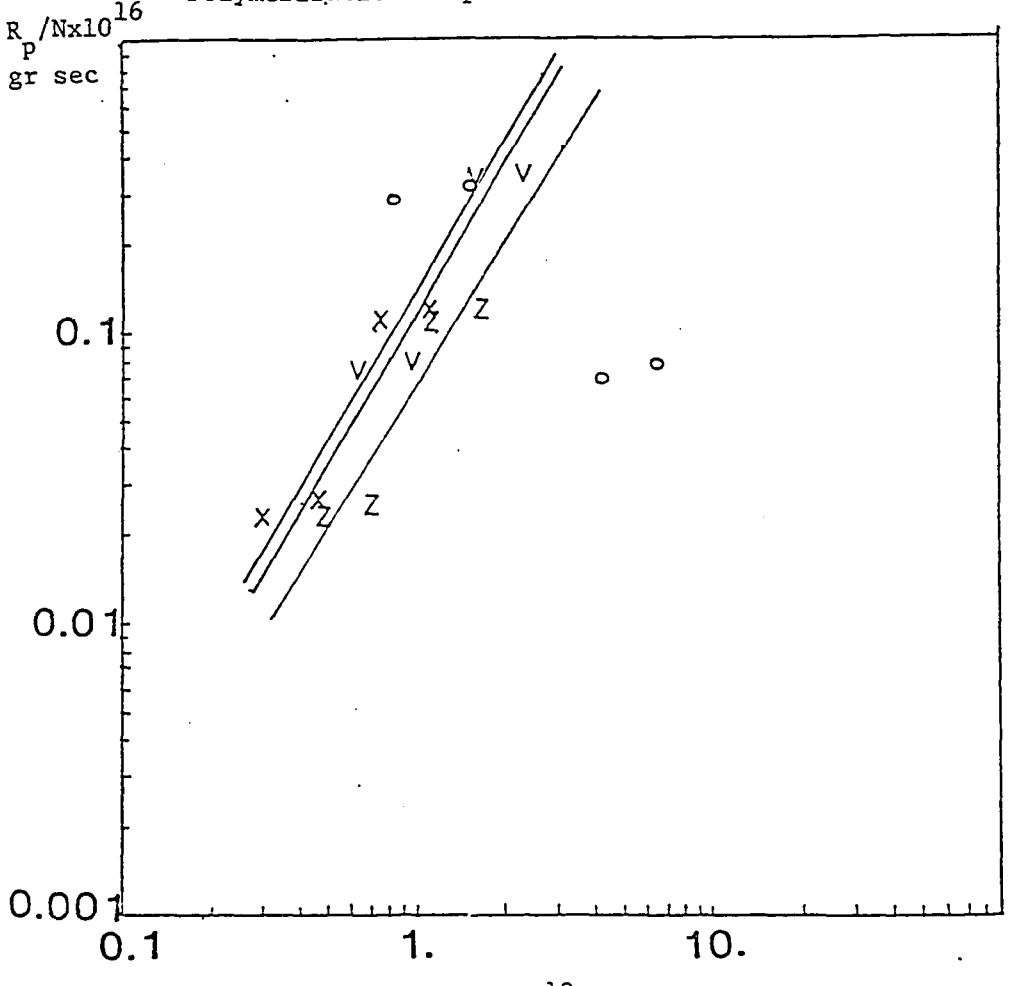

V 0.01 mole % initiator

O 0.04 mole % initiator

X 0.07 mole % initiator

Z 0.10 mole % initiator

Figure A.39

Rate per Particle as a Function of Average Particle Volume

ADVN Initiator

Polymerization Temperature= 55° C

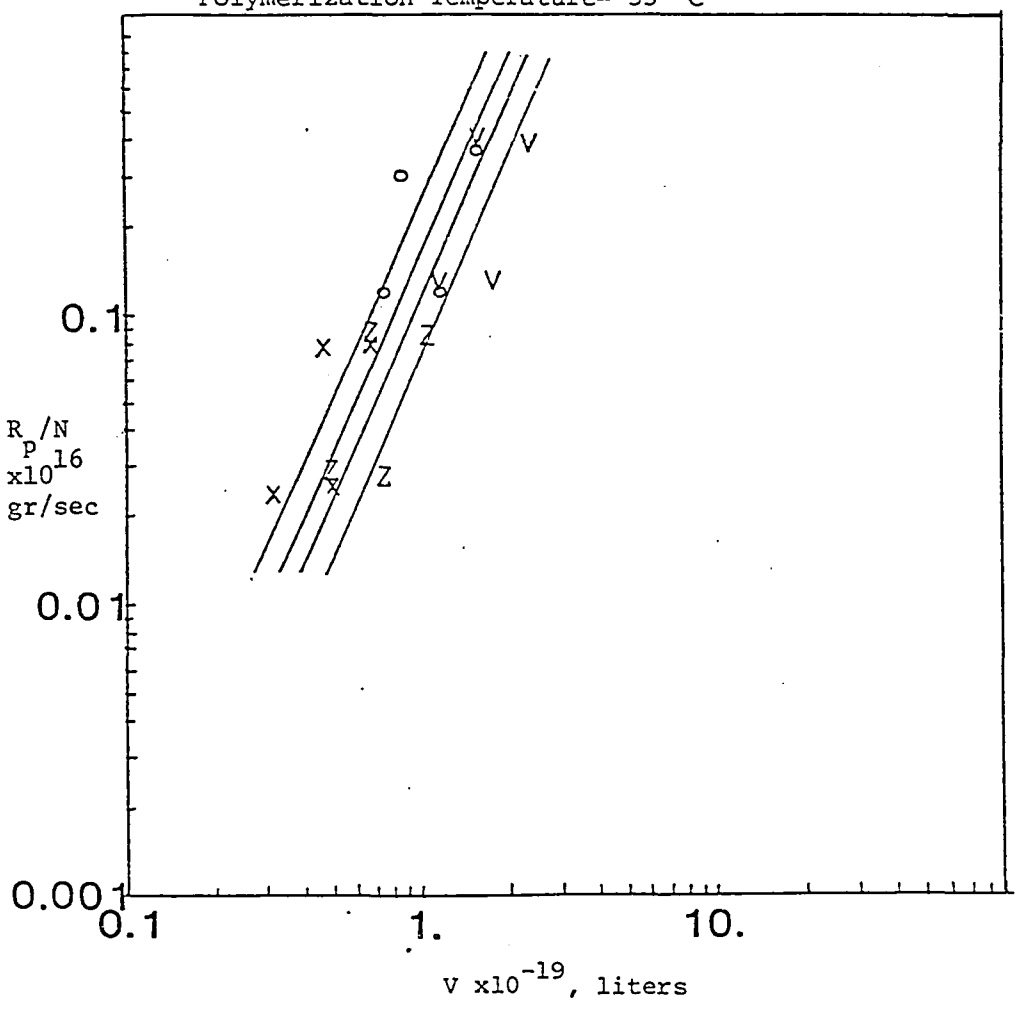

V 3% Tetronic 1102

o 6% Tetronic 1102

X 9% Tetronic 1102

Z 12% Tetronic 1102

Figure A.40

Rate per Particle as a Function of Average Particle Volume

ADVN Initiator

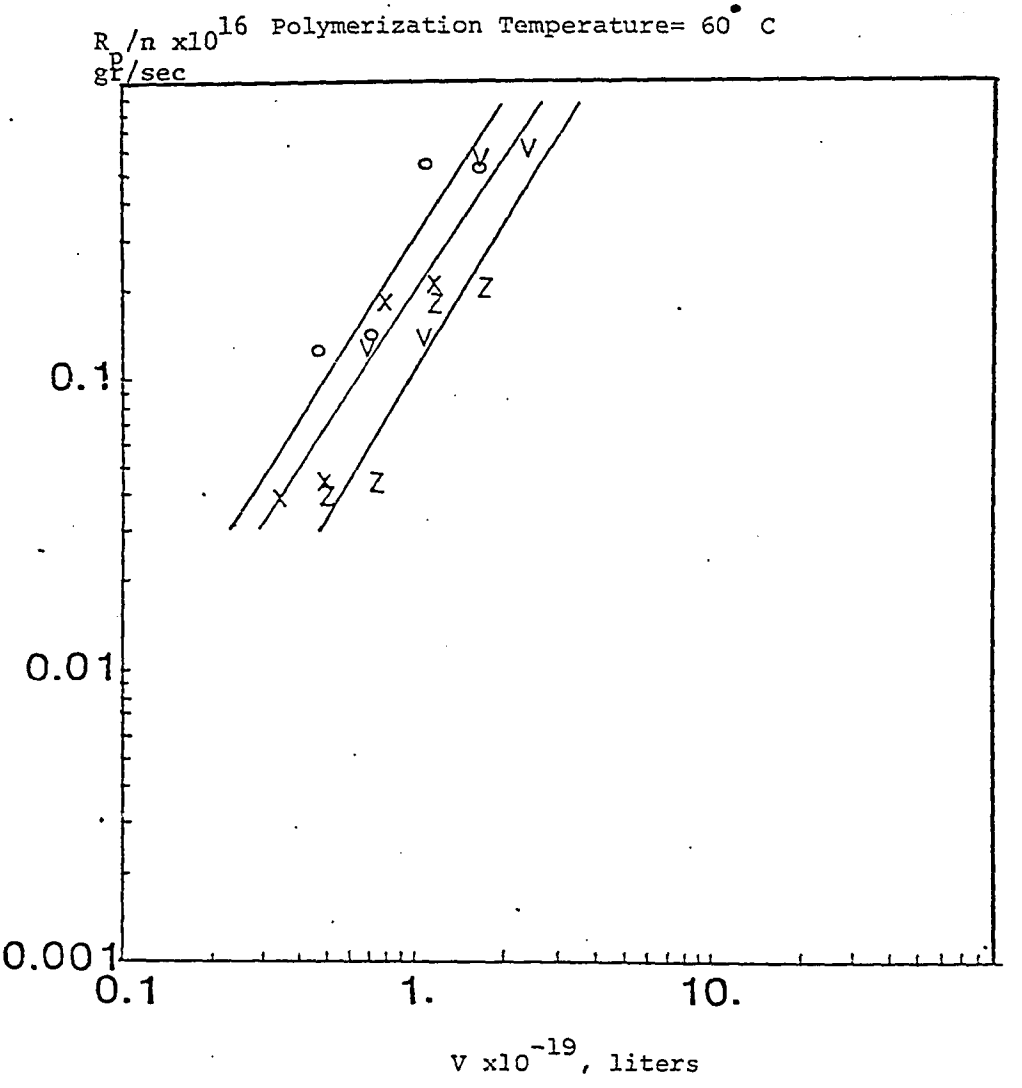

V 0.01 mole % initiator

O 0.04 mole % initiator

X 0.07 mole % initiator

Z 0.1. mole % initiator

Figure A.41

Rate per Particle as a Function of Average Particle Volume

ADVN Initiator

Polymerization Temperature= 60° C

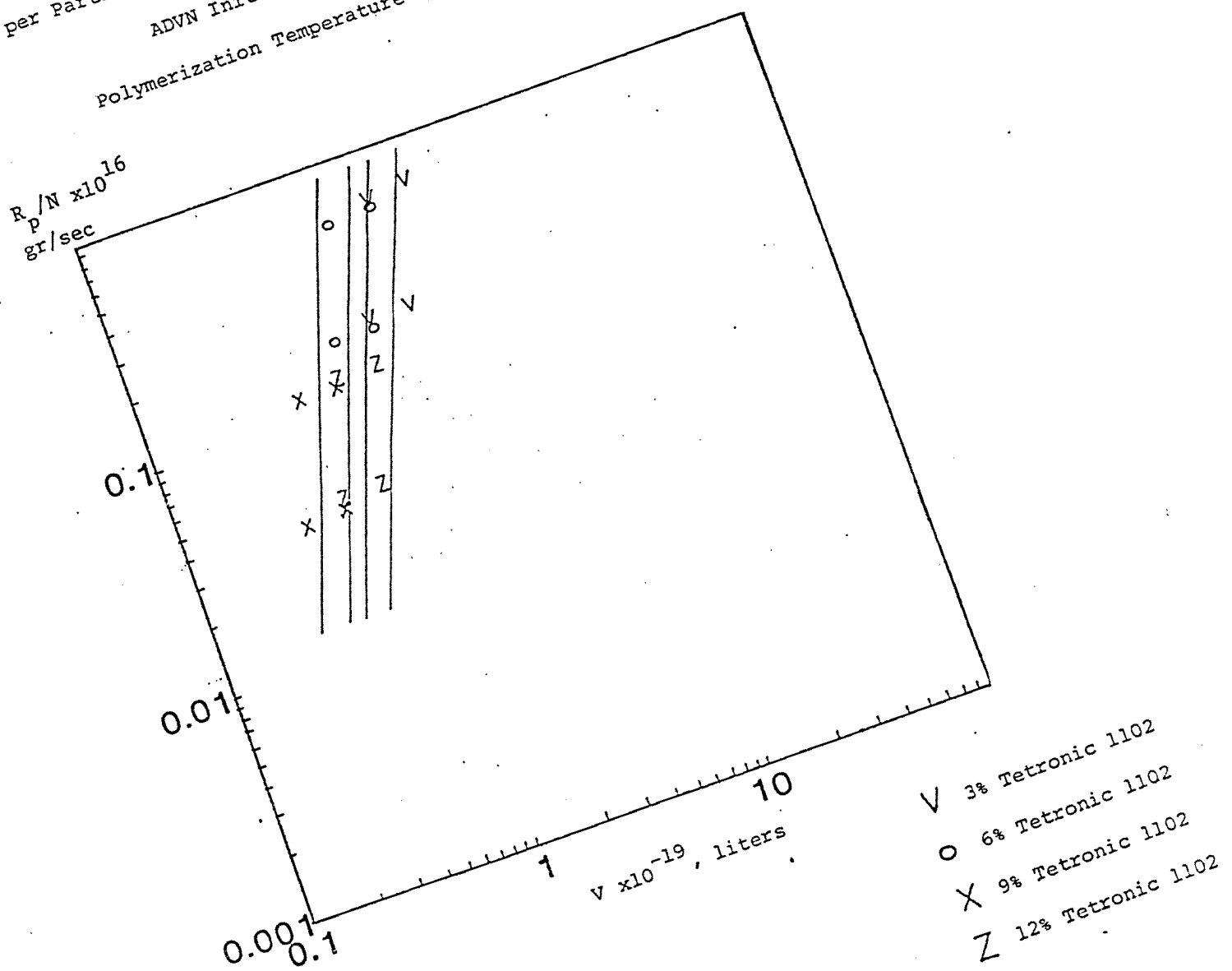

Figure A.42

Calculation of Number of Particles at Polymerization Temperature = 65°C

ADVN Initiator

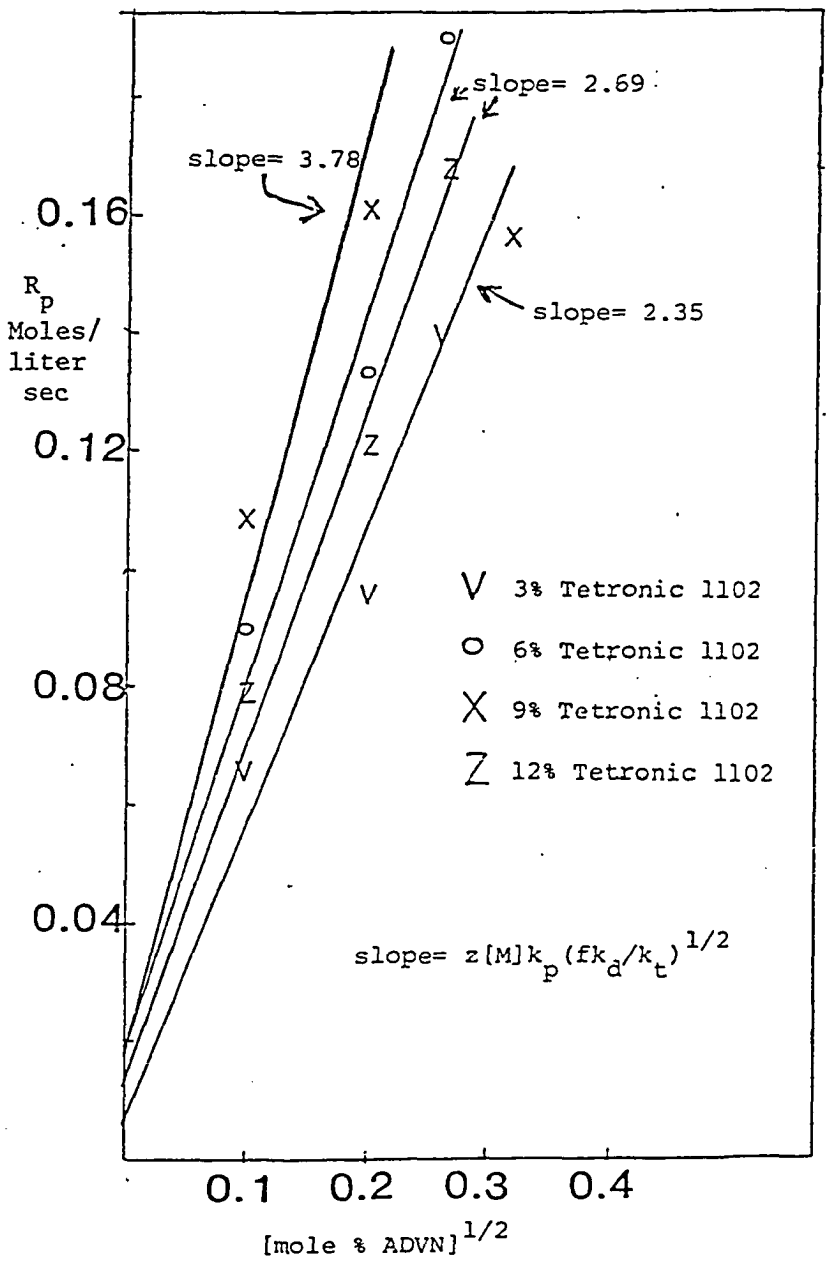

Figure A.43

Correlation Between Polymerization Rate and Polymer Molecular Weight

ADVN Initiator

Polymerization Temperature= 50° C

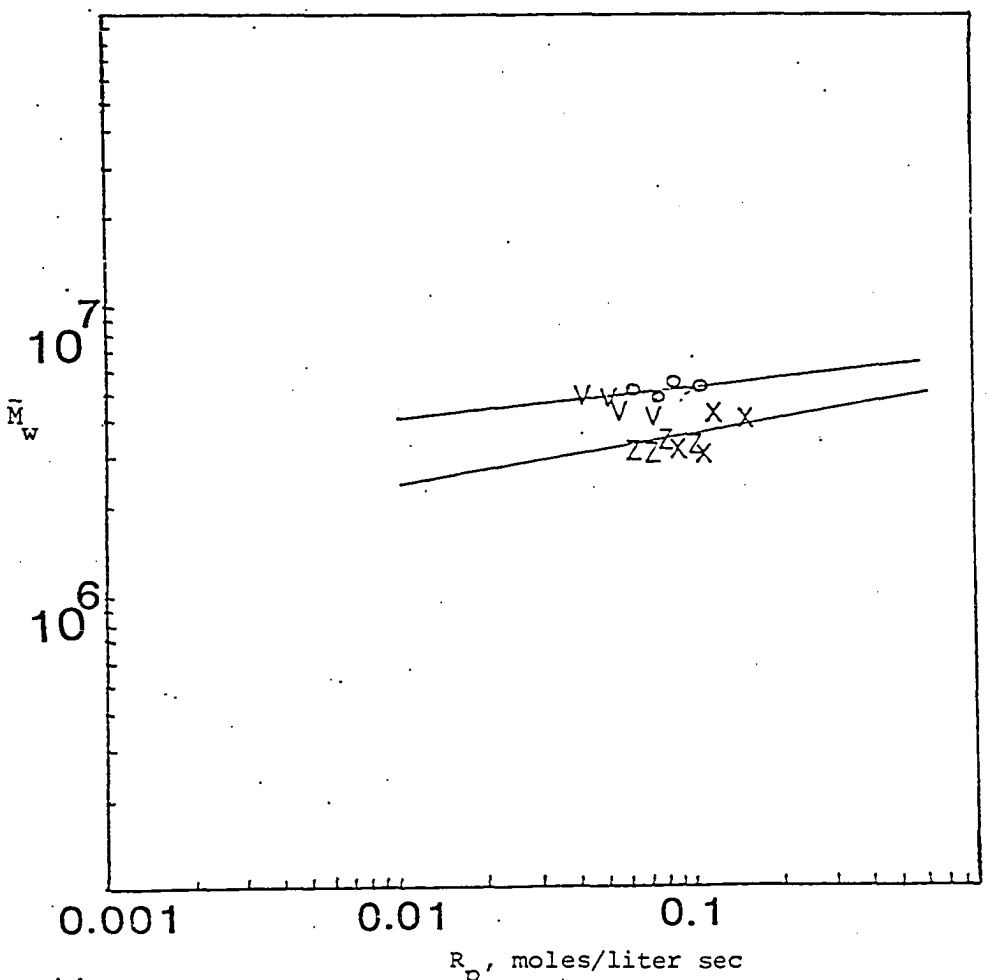

V 0.01 mole % initiator

O 0.04 mole % initiator

X 0.07 mole % initiator

Z 0.10 mole % initiator

Figure A.44

Correlation Between Polymerization Rate and Polymer Molecular Weight

ADVN Initiator

Polymerization Temperature= 55° C

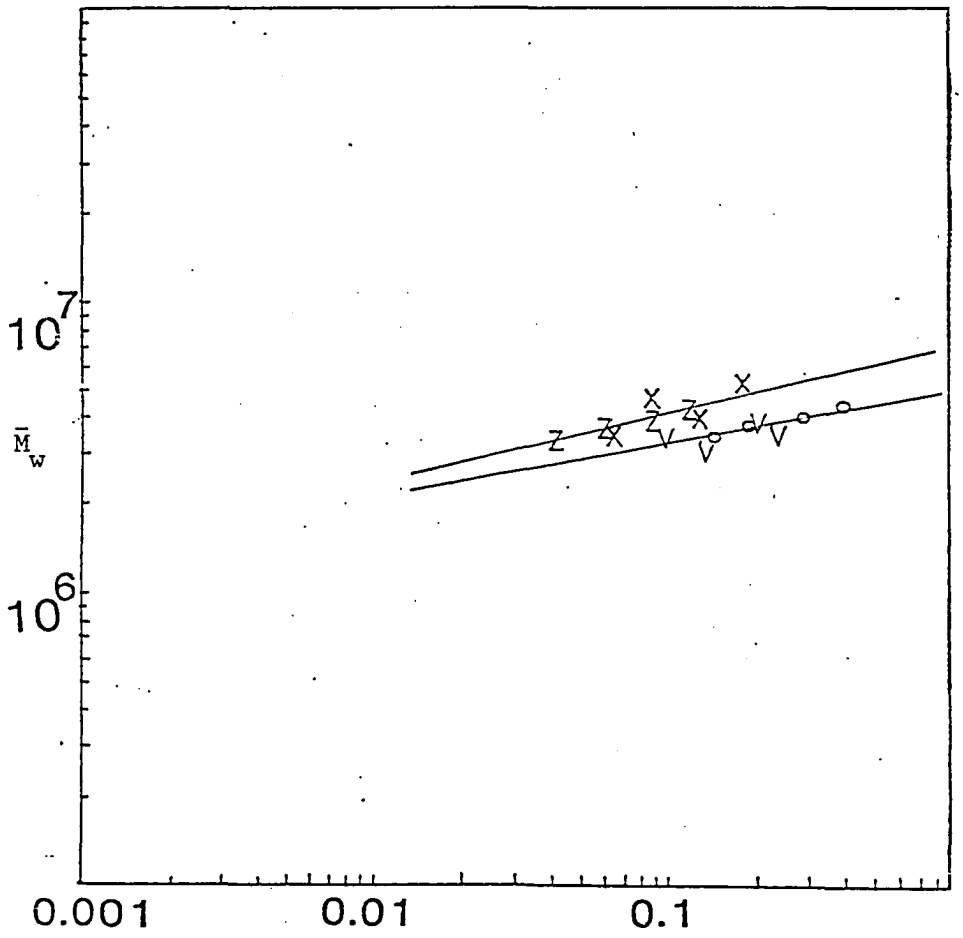

V 0.01 mole % initiator

O 0.04 mole % initiator

X 0.07 mole % initiator

Z 0.10 mole % initiator

Figure A.45

Correlation Between Polymerization Rate and Polymer Molecular Weight

ADVN Initiator

Polymerization Temperature= 60° C

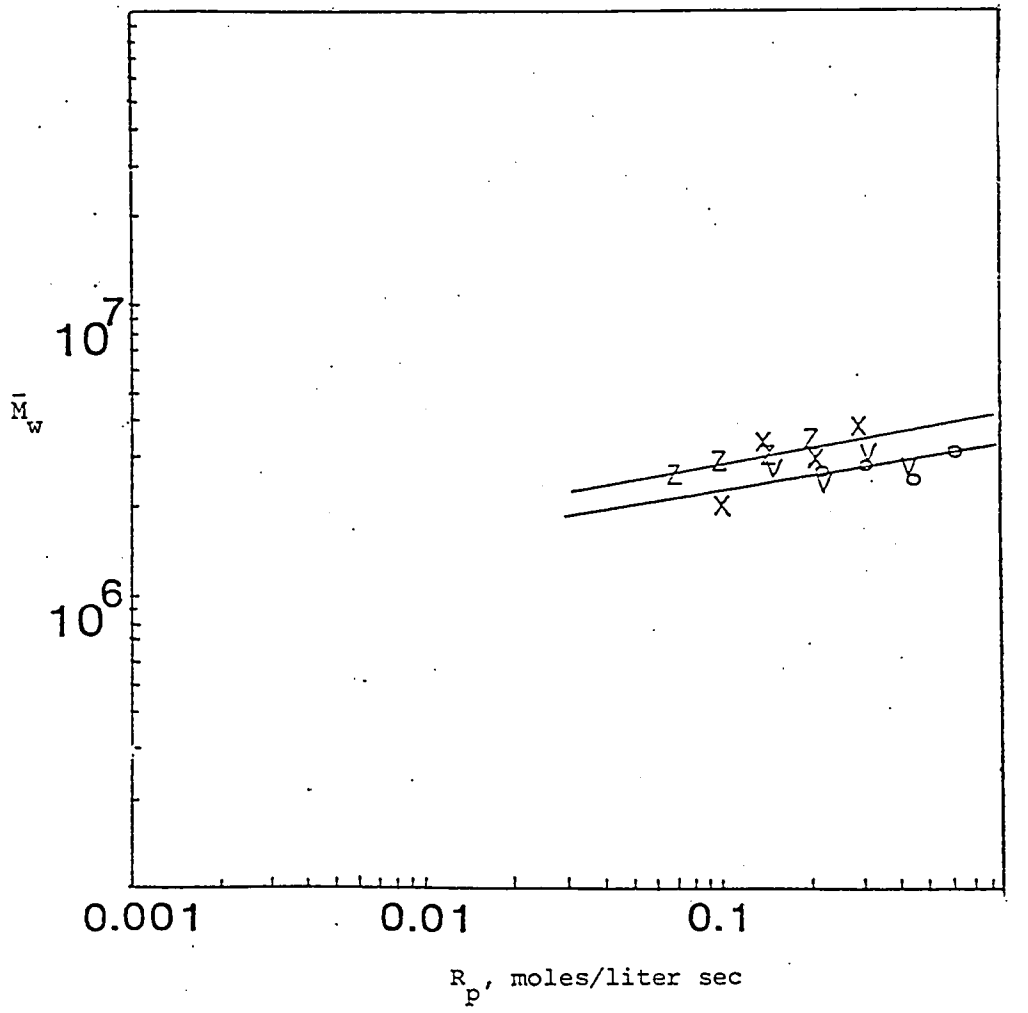

V 0.01 mole % initiator

O 0.04 mole % initiator

X 0.07 mole % initiator

Z 0.10 mole % initiator

Figure A.46

Correlation Between Polymerization Rate and Polymer Molecular Weight

ADVN Initiator

Polymerization Temperature= 65° C

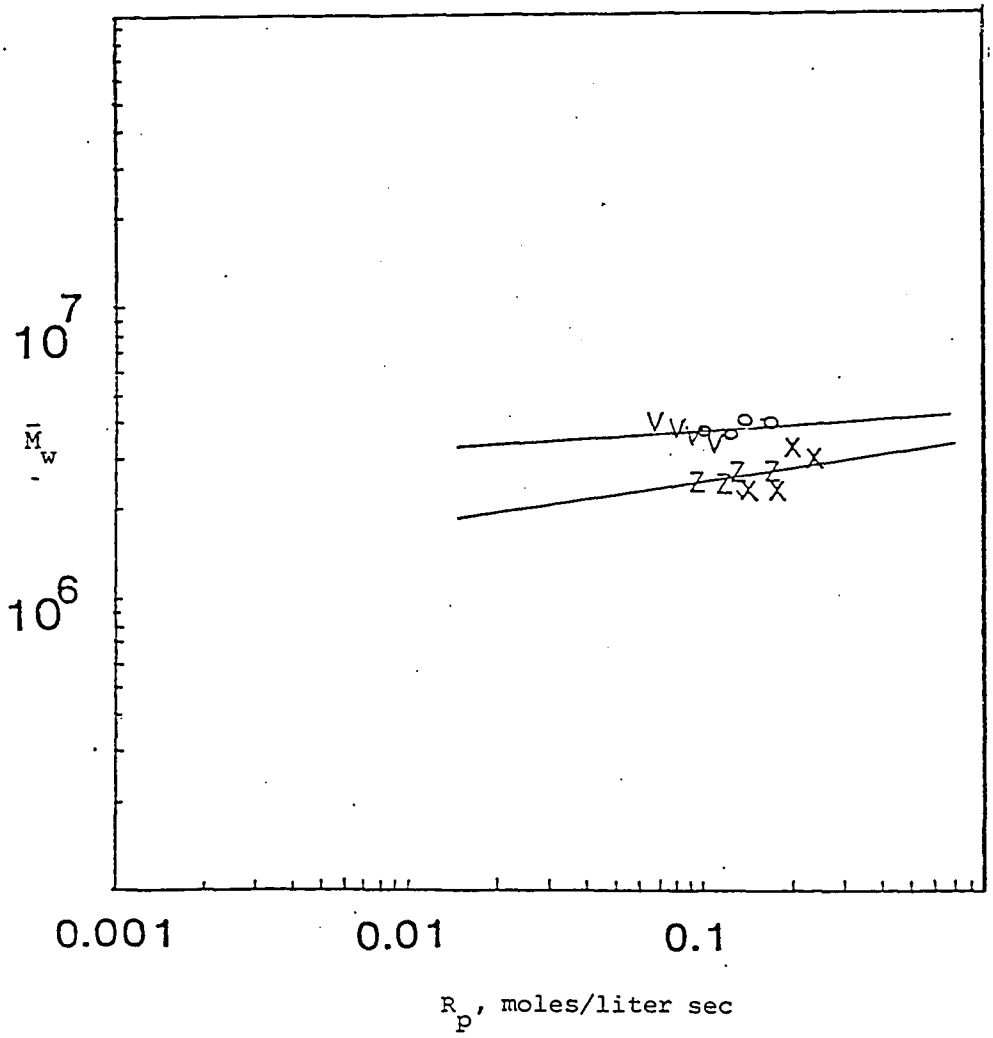

V 0.01 mole % initiator

O 0.04 mole % initiator

X 0.07 mole % initiator

Z 0.10 mole % initiator

APPENDIX B

AVERAGE LATEX PARTICLE SIZE AS A FUNCTION OF RECIPE VARIABLES

1. Measured Overall Average Latex Particle Diameter, nm

Experiment	T, °C	Initiator	% Tetronic 1102	D_n	D_w	D_v
1	55	0.04% ADVN	6	93.4	234.4	131.0
2	55	0.07% KPS	6			
3	55	0.04% KPS	12	58.8	90.8	68.5
4	55	0.07% KPS	12	66.9	112.9	81.9
5	55	0.01% ADVN	3	73.3	96.9	81.2
8	55	0.10% ADVN	9	48.1	73.6	56.3
10	60	0.04% ADVN	9	54.3	97.4	64.3
11	60	0.07% ADVN	3	59.1	91.1	70.4
13	60	0.10% KPS	12	34.3	49.6	39.3
14	60	0.01% ADVN	12	85.2	122.0	94.7
15	60	0.10% ADVN	6	49.2	74.6	57.8
17	65	0.10% ADVN	3	73.3	140.1	89.3
18	65	0.01% KPS	3	97.9	136.9	110.8
19	65	0.10% KPS	9	59.5	72.0	63.7
22	65	0.04% KPS	6	49.0	70.5	56.5
23	65	0.07% KPS	12	45.2	71.2	54.4
24	65	0.04% ADVN	12	82.9	107.1	91.1
25	50	0.01% KPS	12	43.4	60.6	49.3
27	50	0.01% ADVN	6	69.1	95.0	76.1
28	50	0.10% KPS	6	56.1	73.0	61.7
29	50	0.04% KPS	9	61.0	76.6	66.0
30	50	0.07% ADVN	9	133.9	285.6	182.4
32	50	0.07% KPS	3	48.5	63.4	53.4

2.
Average Overall Latex Particle Diameter Calculated by Regression Analysis, nm

T	Initiator	% Initiator	% Tetronic 1102	D_v
50	ADVN	0.01	3	92.1
50	ADVN	0.04	3	99.7
50	ADVN	0.07	3	111.6
50	ADVN	0.10	3	91.9
50	ADVN	0.01	6	68.2
50	ADVN	0.04	6	82.8
50	ADVN	0.07	6	92.6
50	ADVN	0.10	6	76.3
50	ADVN	0.01	9	59.5
50	ADVN	0.04	9	72.2
50	ADVN	0.07	9	80.8
50	ADVN	0.10	9	66.6
50	ADVN	0.01	12	71.6
50	ADVN	0.04	12	87.0
50	ADVN	0.07	12	97.4
50	ADVN	0.10	12	80.2
55	ADVN	0.01	3	112.4
55	ADVN	0.04	3	136.5
55	ADVN	0.07	3	125.1
55	ADVN	0.10	3	103.0
55	ADVN	0.01	6	93.3
55	ADVN	0.04	6	113.3
55	ADVN	0.07	6	103.8
55	ADVN	0.10	6	85.5
55	ADVN	0.01	9	71.1
55	ADVN	0.04	9	86.3
55	ADVN	0.07	9	79.0
55	ADVN	0.10	9	65.1
55	ADVN	0.01	12	85.6
55	ADVN	0.04	12	104.0
55	ADVN	0.07	12	95.3
55	ADVN	0.10	12	78.4
60	ADVN	0.01	3	112.5
60	ADVN	0.04	3	80.3
60	ADVN	0.07	3	73.5
60	ADVN	0.10	3	103.1
60	ADVN	0.01	6	105.9
60	ADVN	0.04	6	75.6
60	ADVN	0.07	6	69.3
60	ADVN	0.10	6	97.1
60	ADVN	0.01	9	80.7

T	Initiator	% Initiator	% Tetronic 1102	D_v
60	ADVN	0.04	9	57.6
60	ADVN	0.07	9	52.7
60	ADVN	0.10	9	73.9
60	ADVN	0.01	12	85.7
60	ADVN	0.04	12	61.1
60	ADVN	0.07	12	56.0
60	ADVN	0.10	12	78.5
65	ADVN	0.01	3	82.2
65	ADVN	0.04	3	58.6
65	ADVN	0.07	3	65.6
65	ADVN	0.10	3	92.0
65	ADVN	0.01	6	77.4
65	ADVN	0.04	6	55.2
65	ADVN	0.07	6	61.8
65	ADVN	0.10	6	86.6
65	ADVN	0.01	9	67.5
65	ADVN	0.04	9	48.2
65	ADVN	0.07	9	53.9
65	ADVN	0.10	9	75.6
65	ADVN	0.01	12	71.7
65	ADVN	0.04	12	51.2
65	ADVN	0.07	12	57.3
65	ADVN	0.10	12	80.3
50	KPS	0.01	3	80.0
50	KPS	0.04	3	97.2
50	KPS	0.07	3	108.7
50	KPS	0.10	3	89.6
50	KPS	0.01	6	66.4
50	KPS	0.04	6	80.6
50	KPS	0.07	6	90.2
50	KPS	0.10	6	74.3
50	KPS	0.01	9	57.9
50	KPS	0.04	9	70.4
50	KPS	0.07	9	78.7
50	KPS	0.10	9	64.8
50	KPS	0.01	12	69.8
50	KPS	0.04	12	84.8
50	KPS	0.07	12	94.9
50	KPS	0.10	12	78.1
55	KPS	0.01	3	109.5
55	KPS	0.04	3	133.0
55	KPS	0.07	3	121.8
55	KPS	0.10	3	100.4
55	KPS	0.01	6	90.9
55	KPS	0.04	6	110.4

T	Initiator	% Initiator	% Tetronic 1102	D_v
55	KPS	0.07	6	101.1
55	KPS	0.10	6	83.3
55	KPS	0.01	9	69.2
55	KPS	0.04	9	84.0
55	KPS	0.07	9	77.0
55	KPS	0.10	9	63.4
55	KPS	0.01	12	83.4
55	KPS	0.04	12	101.3
55	KPS	0.07	12	92.8
55	KPS	0.10	12	76.4
60	KPS	0.01	3	54.9
60	KPS	0.04	3	39.2
60	KPS	0.07	3	35.9
60	KPS	0.10	3	50.3
60	KPS	0.01	6	51.7
60	KPS	0.04	6	36.9
60	KPS	0.07	6	33.8
60	KPS	0.10	6	47.3
60	KPS	0.01	9	39.3
60	KPS	0.04	9	28.1
60	KPS	0.07	9	25.7
60	KPS	0.10	9	38.3
60	KPS	0.01	12	41.8
60	KPS	0.04	12	29.8
60	KPS	0.07	12	27.4
60	KPS	0.10	12	36.9
65	KPS	0.01	3	40.1
65	KPS	0.04	3	28.6
65	KPS	0.07	3	32.0
65	KPS	0.10	3	44.9
65	KPS	0.01	6	37.8
65	KPS	0.04	6	26.9
65	KPS	0.07	6	30.2
65	KPS	0.10	6	42.3
65	KPS	0.01	9	32.9
65	KPS	0.04	9	23.5
65	KPS	0.07	9	26.3
65	KPS	0.10	9	36.9
65	KPS	0.01	12	35.0
65	KPS	0.04	12	25.0
65	KPS	0.07	12	27.9
65	KPS	0.10	12	39.2

APPENDIX C

CONVERSION-TIME CURVES FROM THE STATISTICALLY DESIGNED EXPERIMENTAL STUDY OF INVERSE EMULSION POLYMERIZATION

Experiment #1

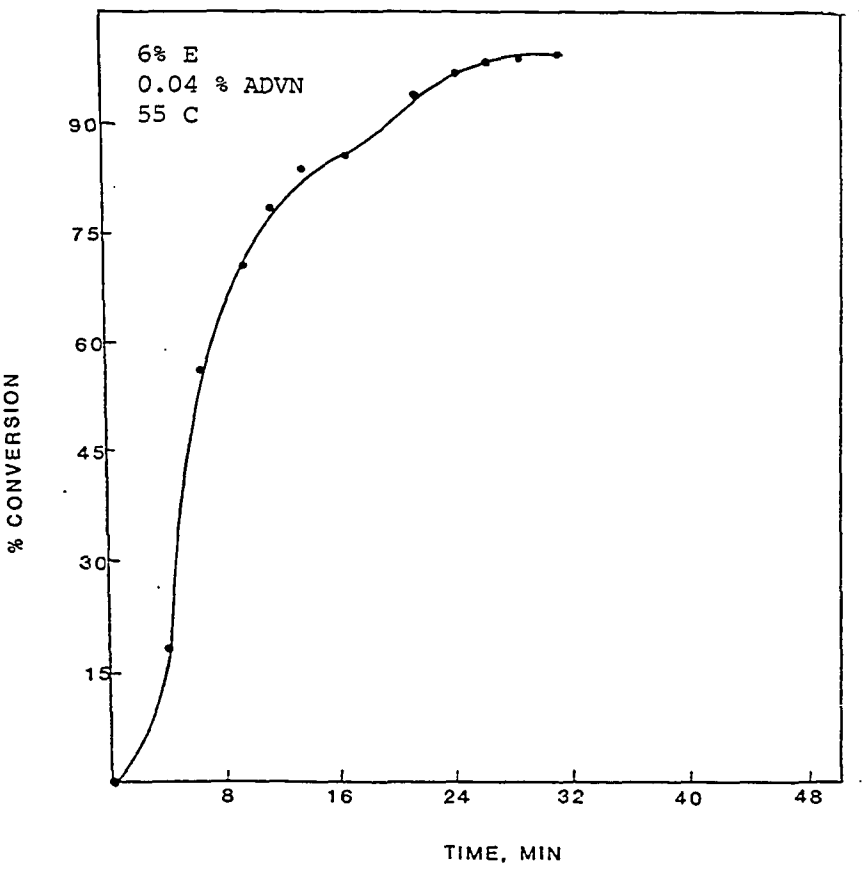

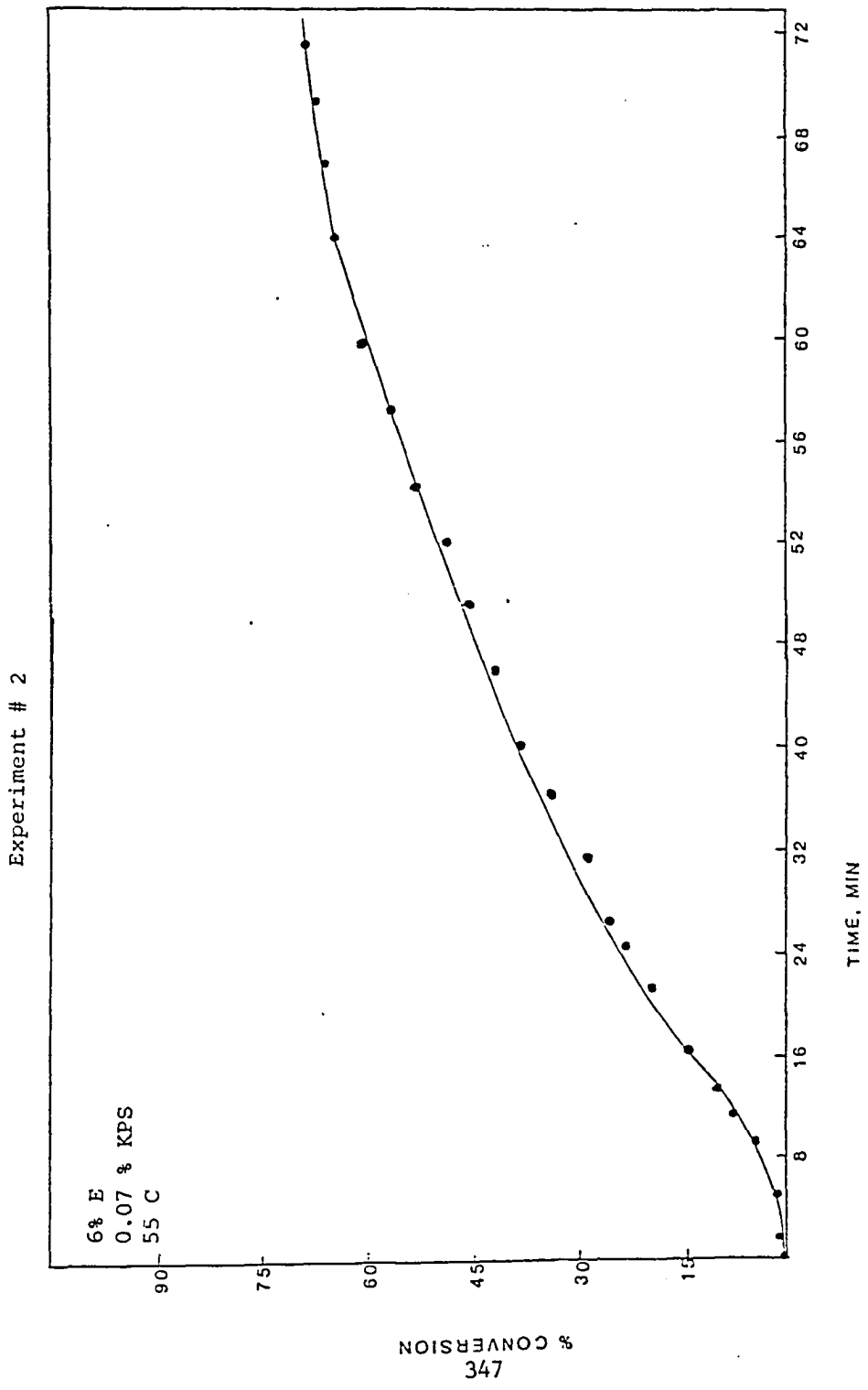

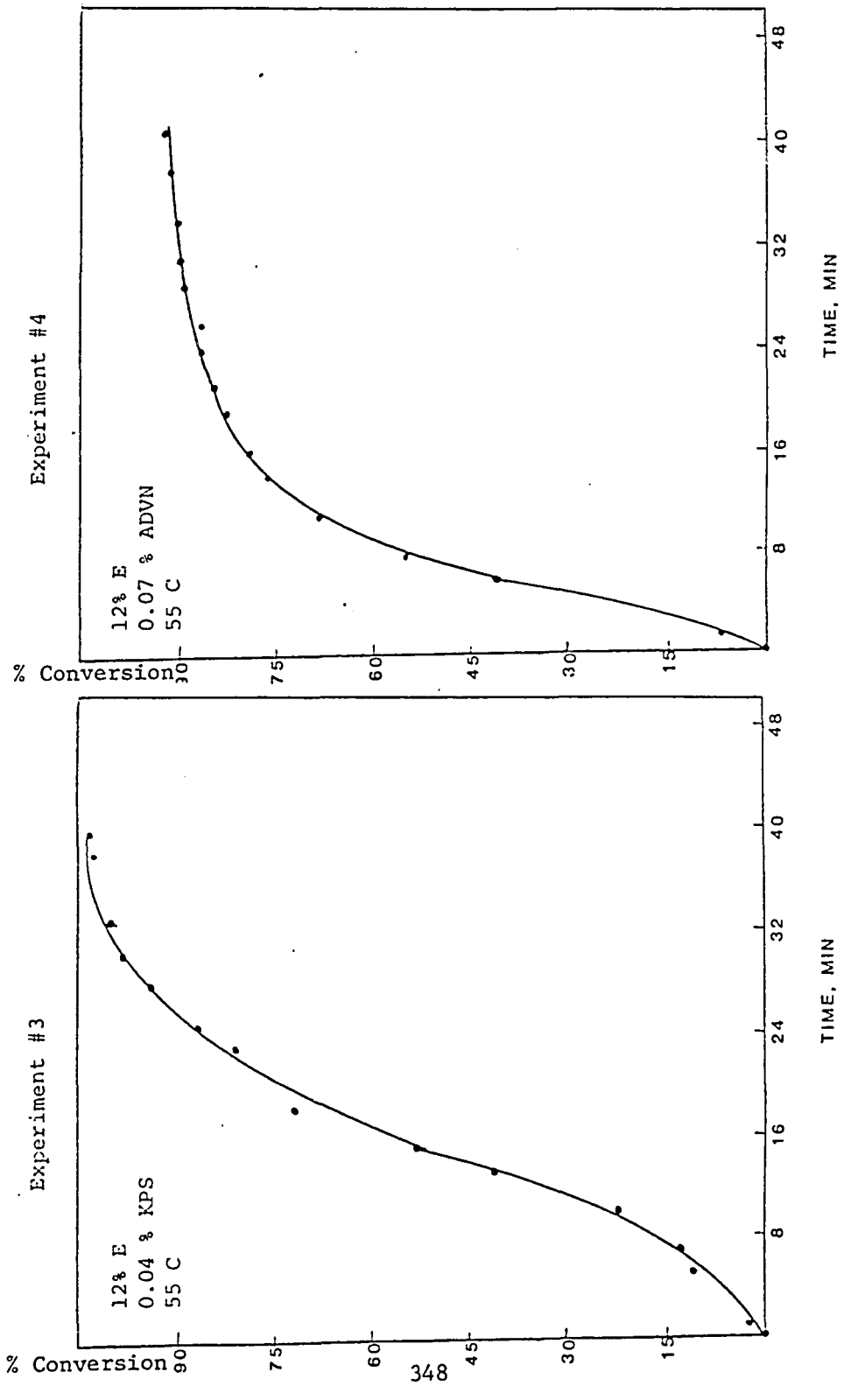

Experiment #5

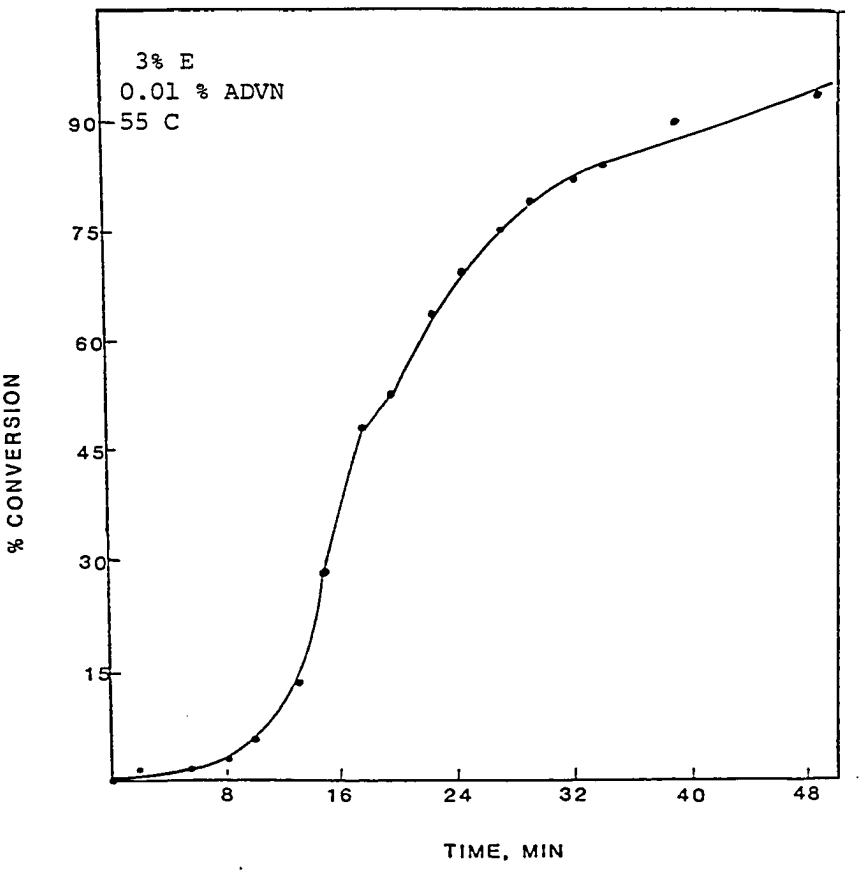

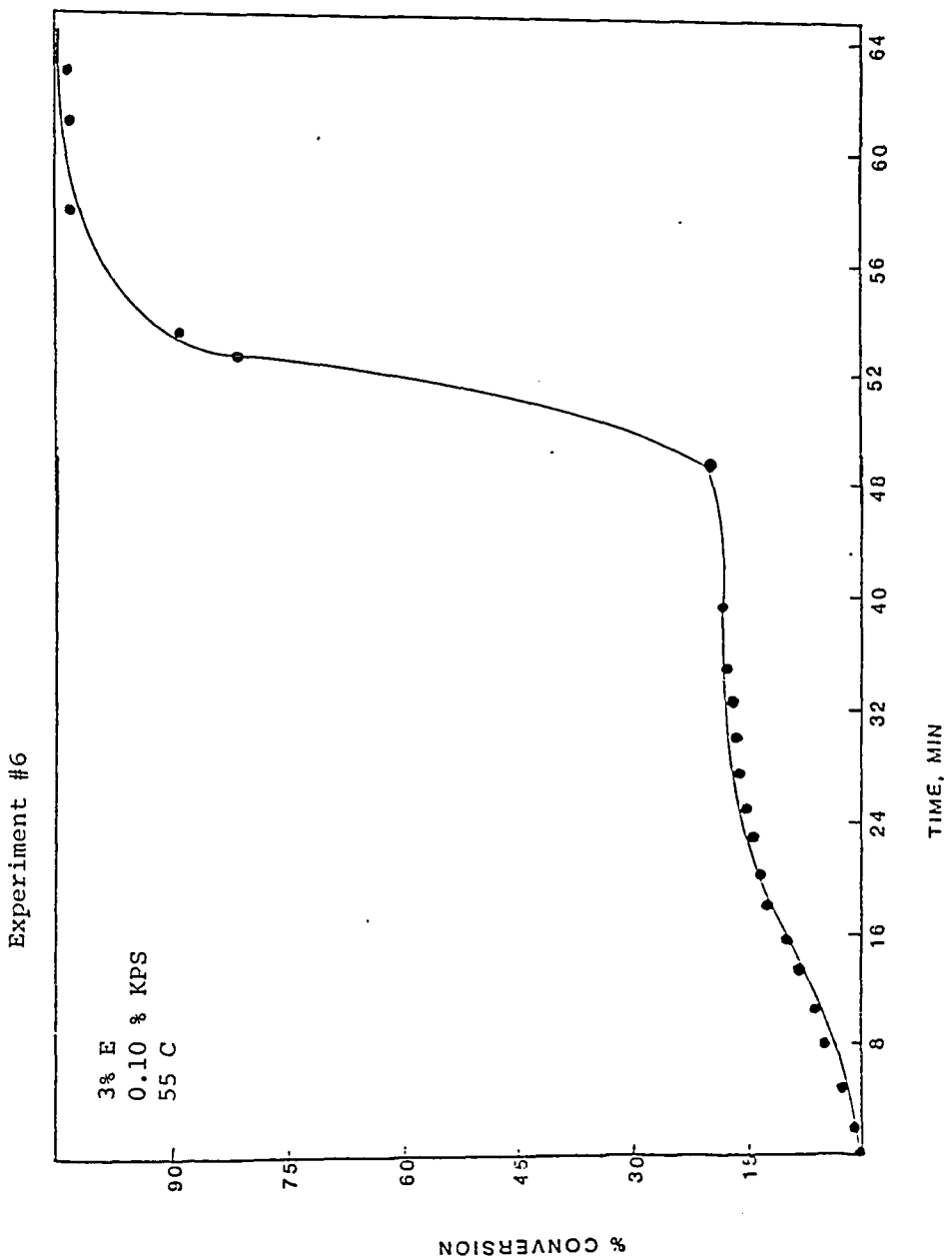

350

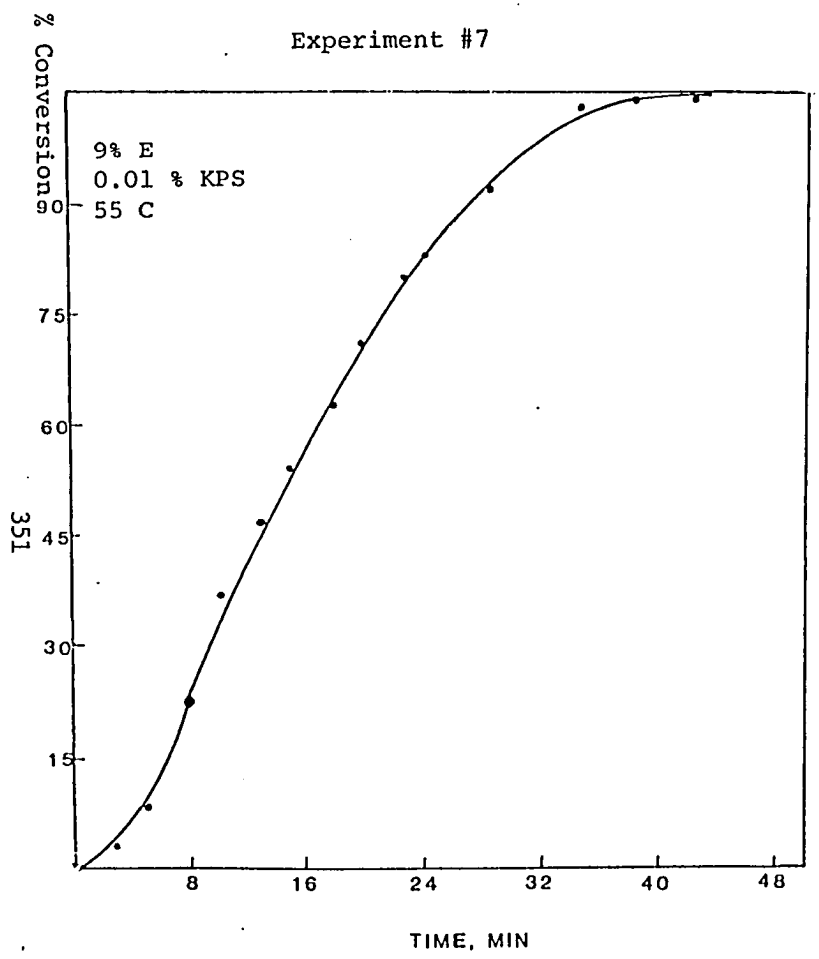

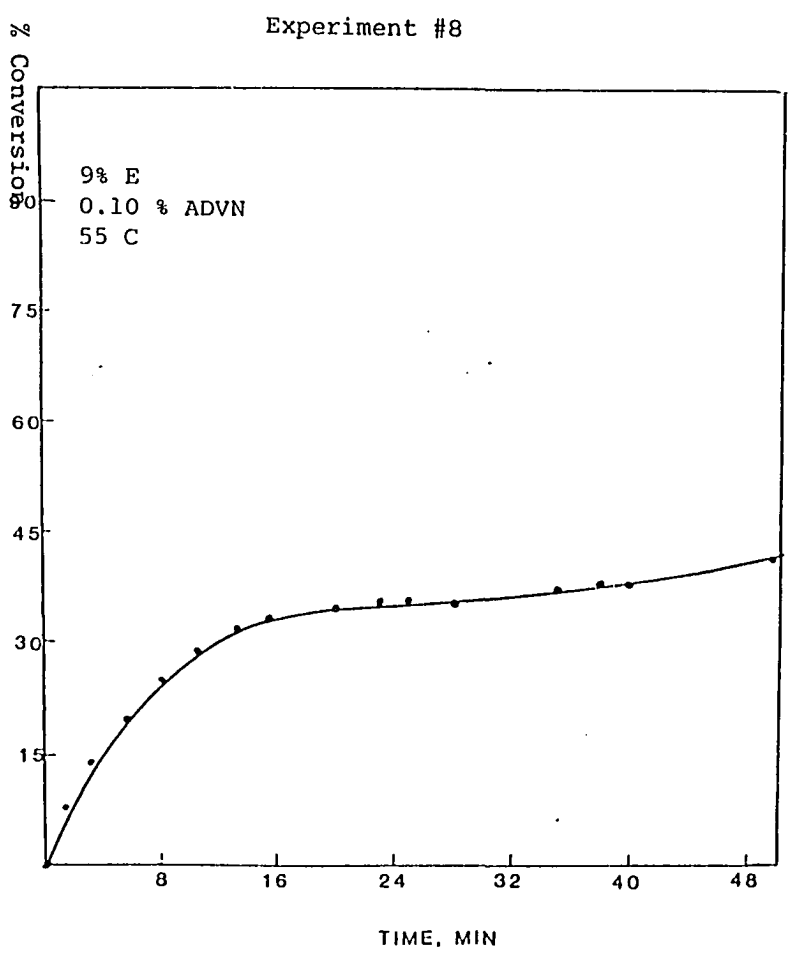

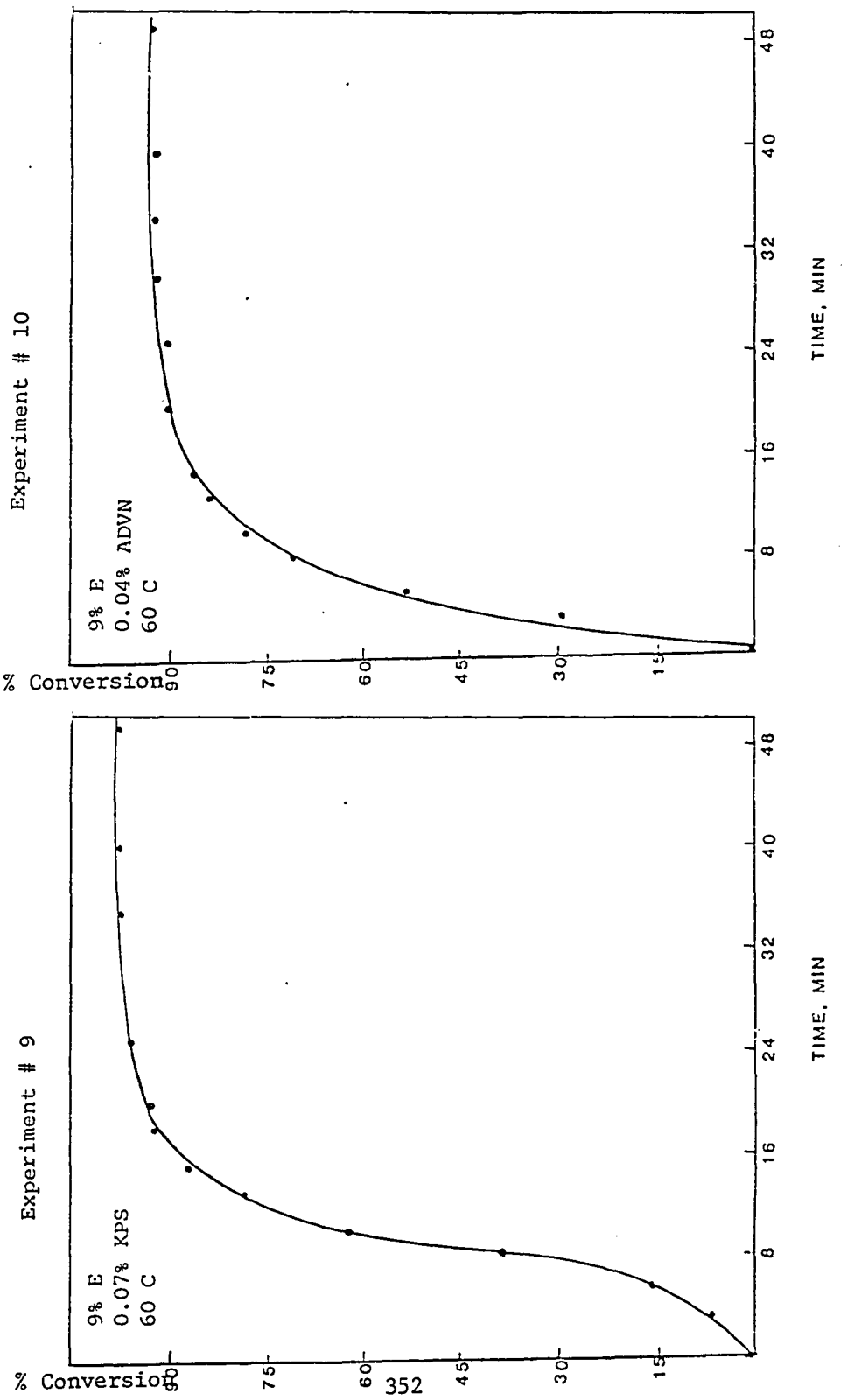

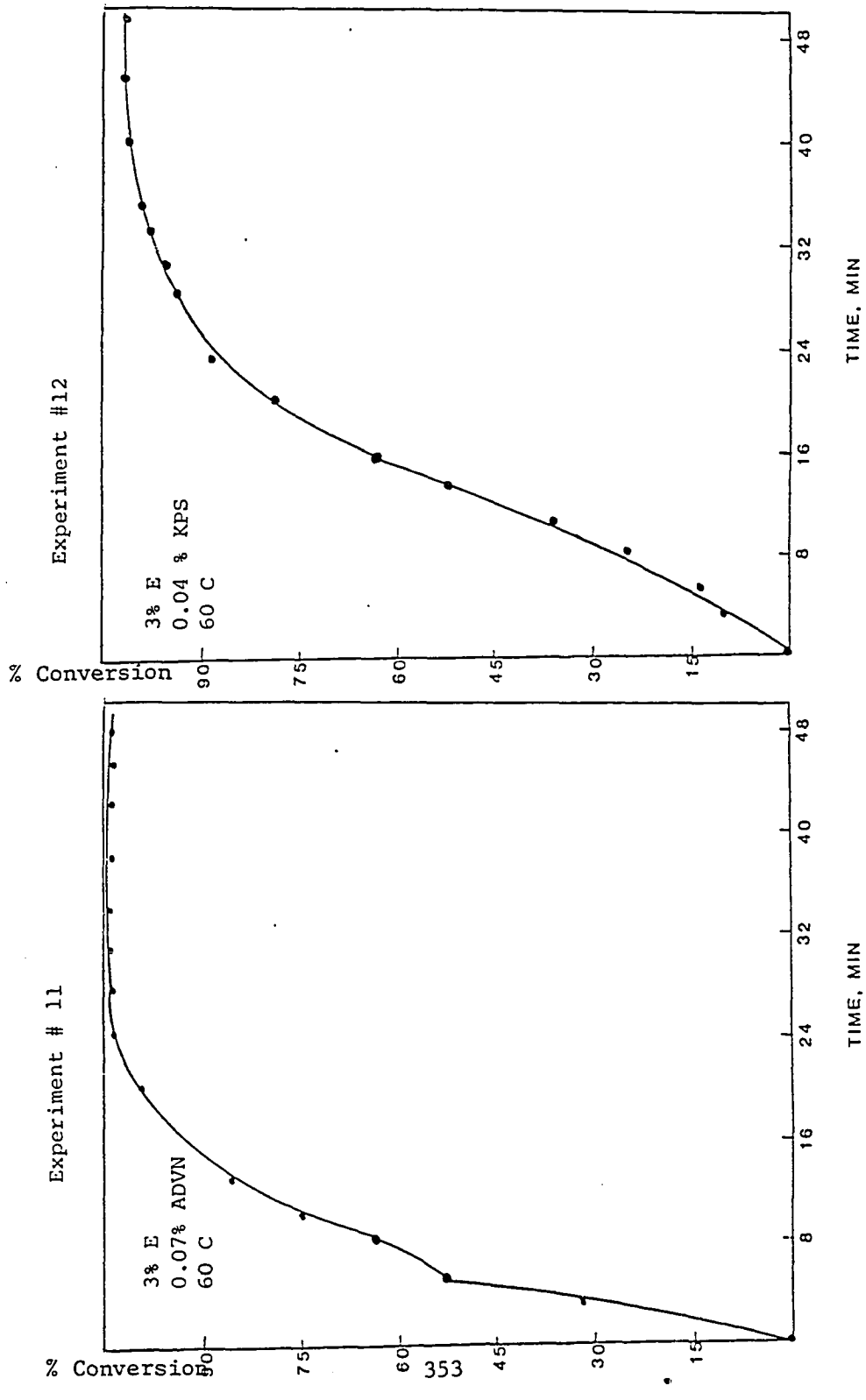

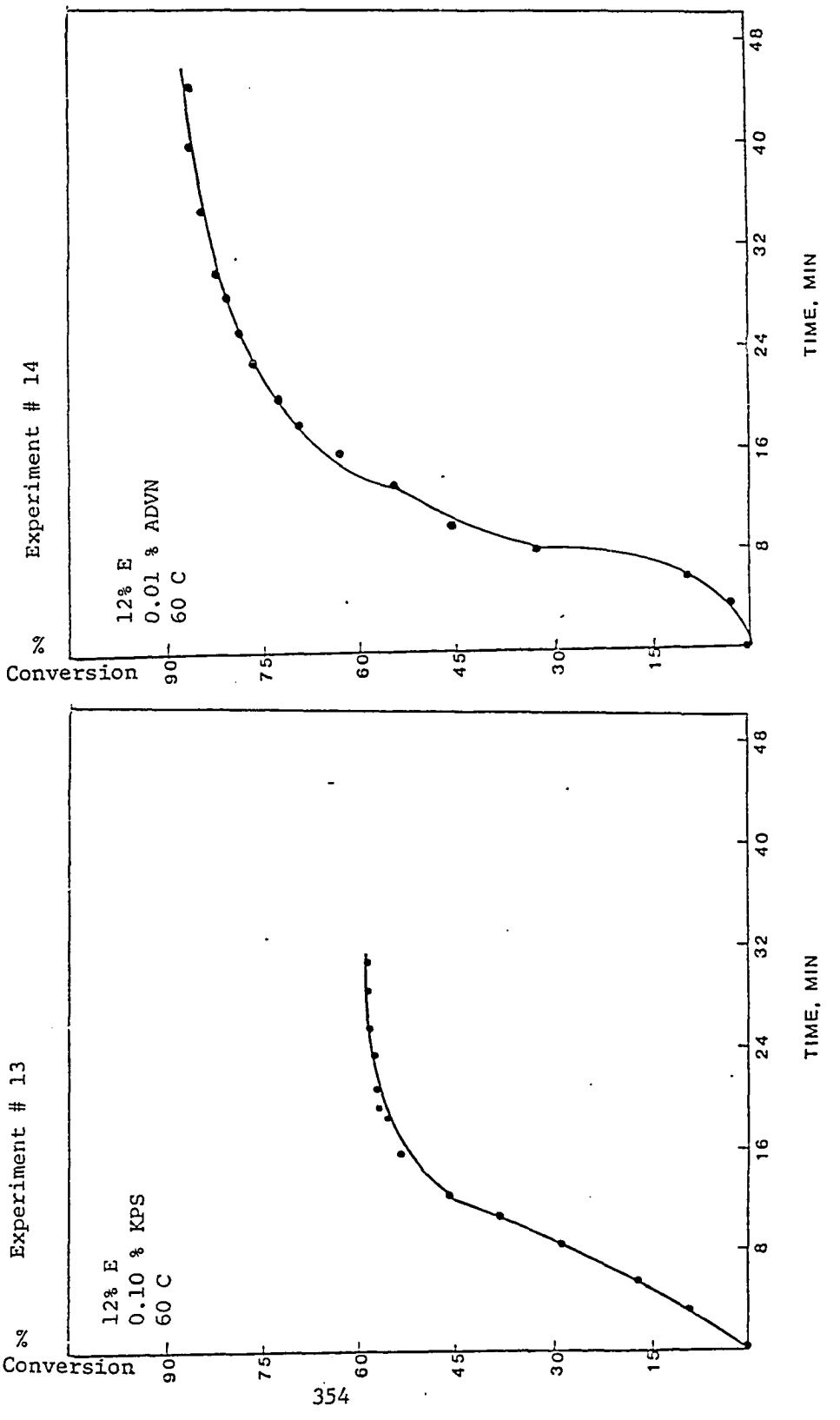

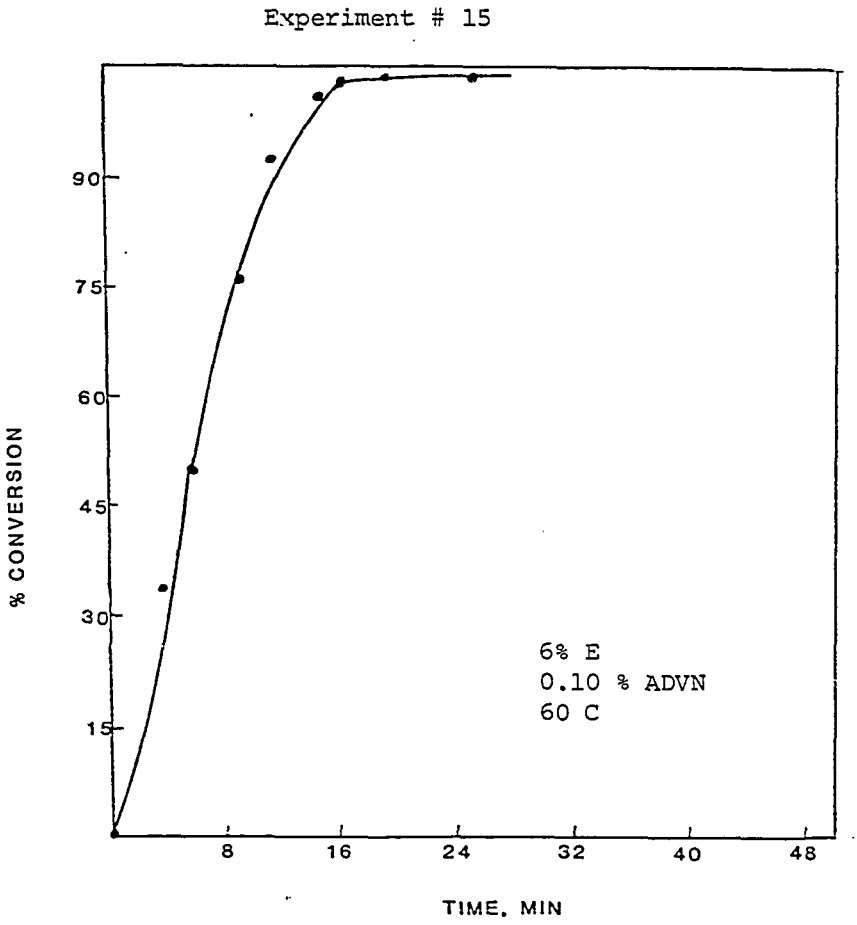

Experiment # 16

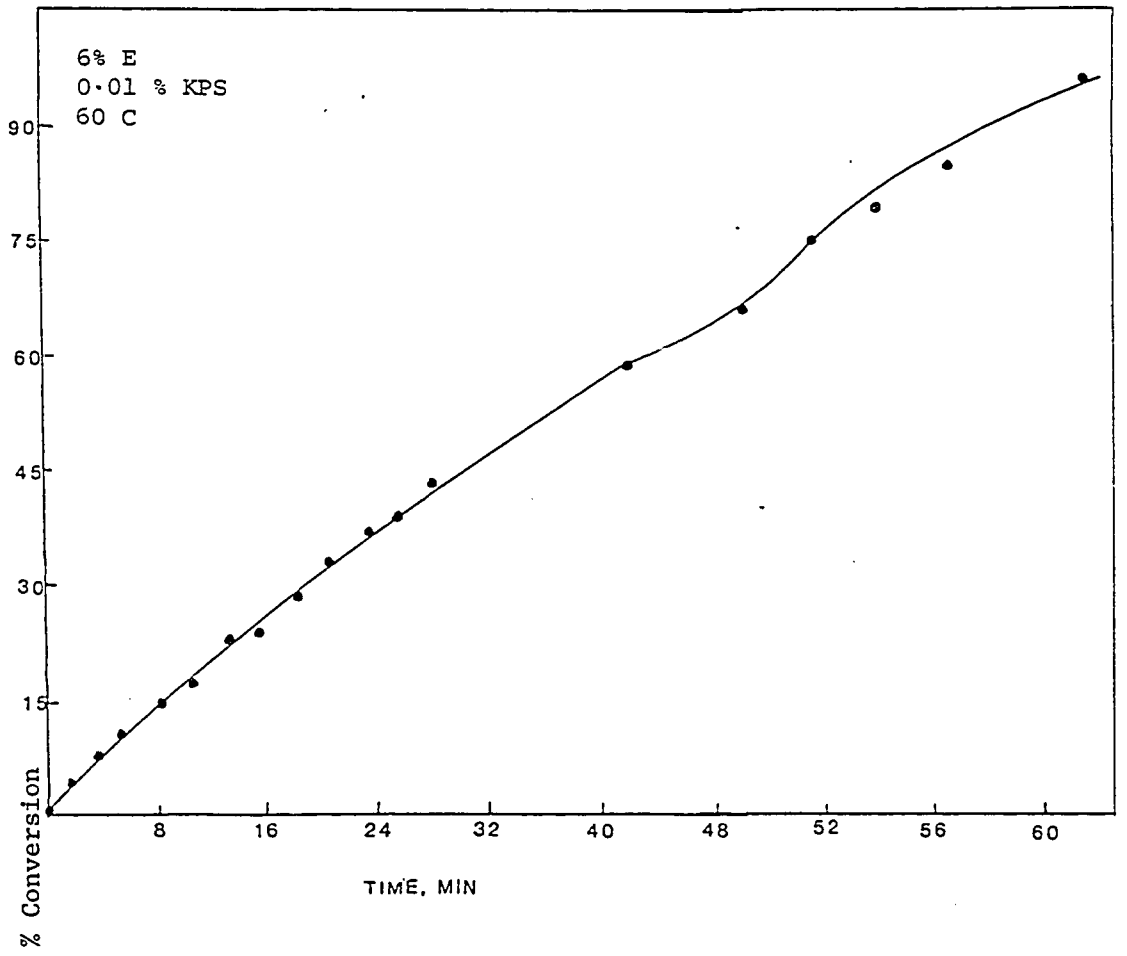

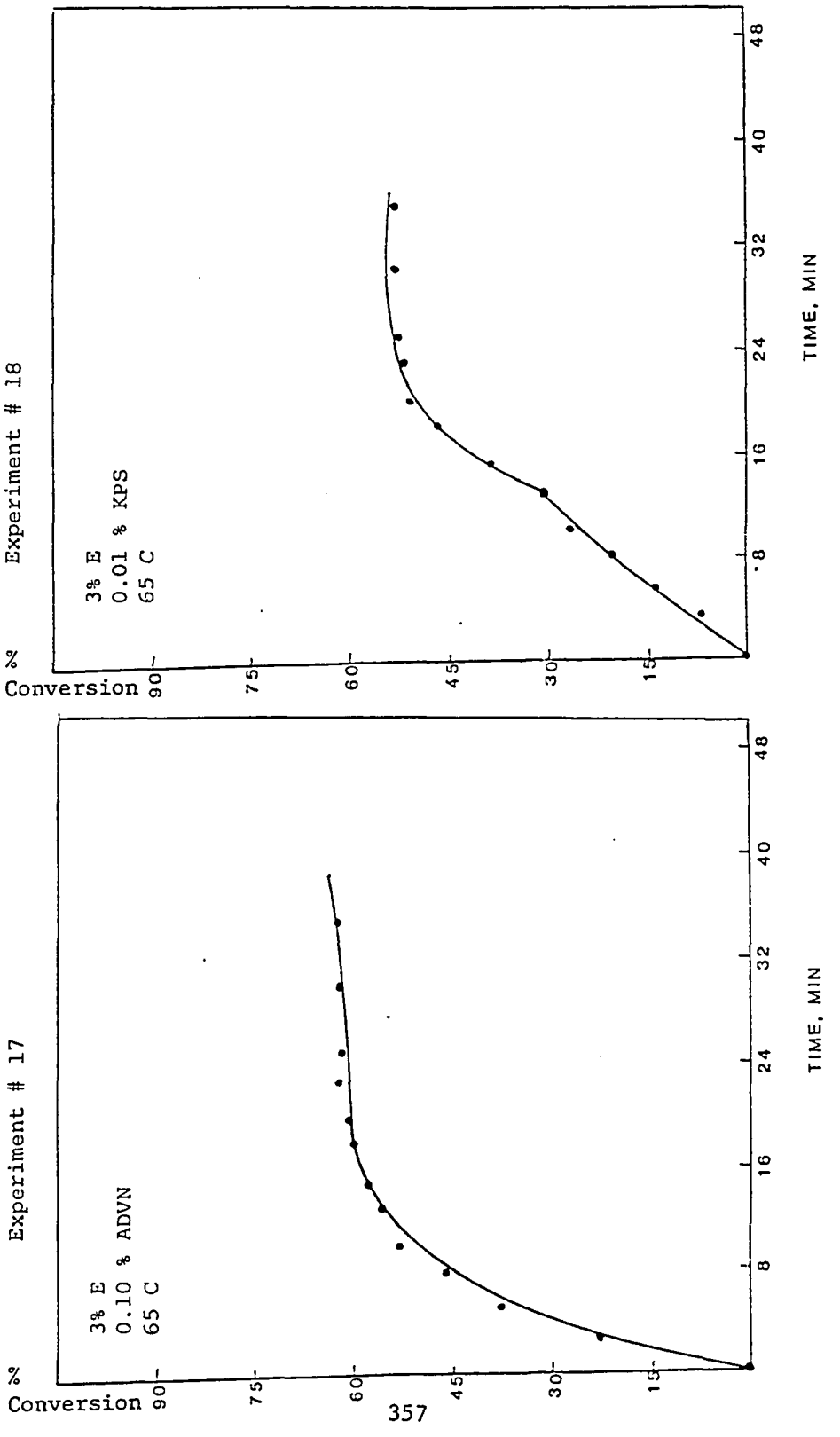

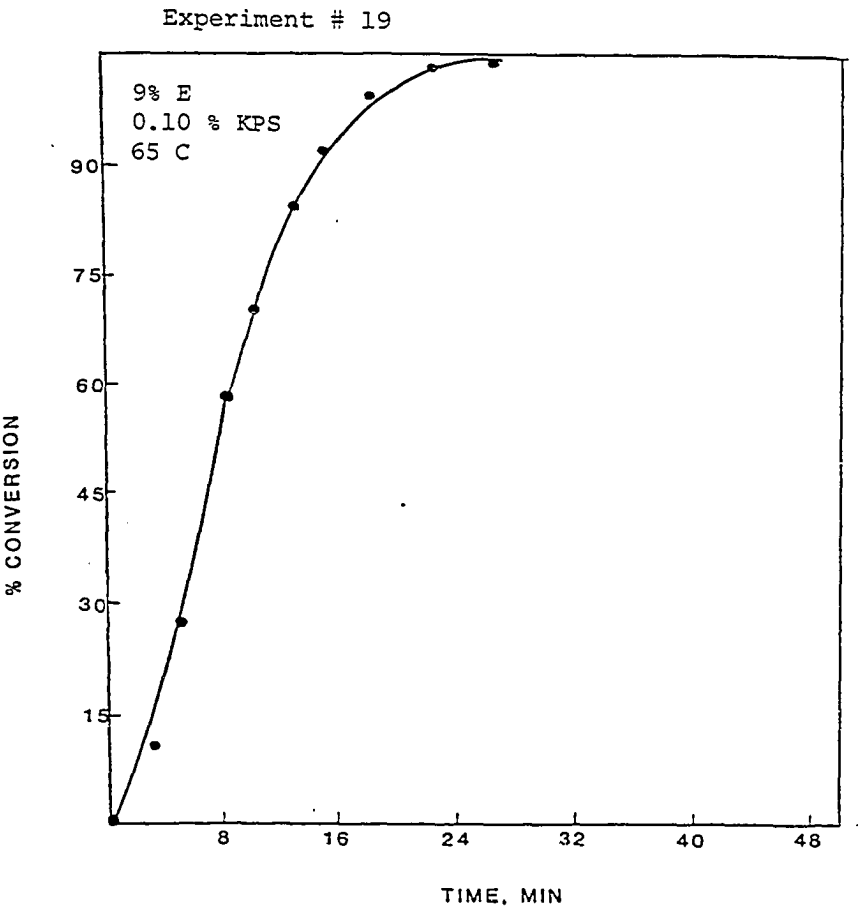

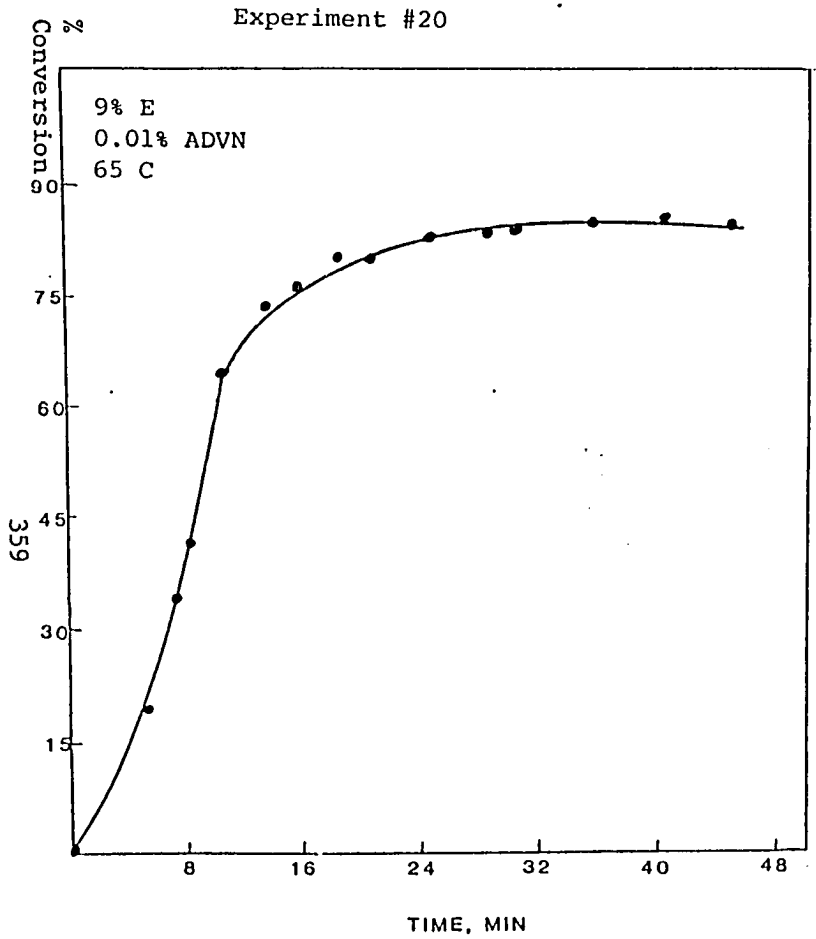

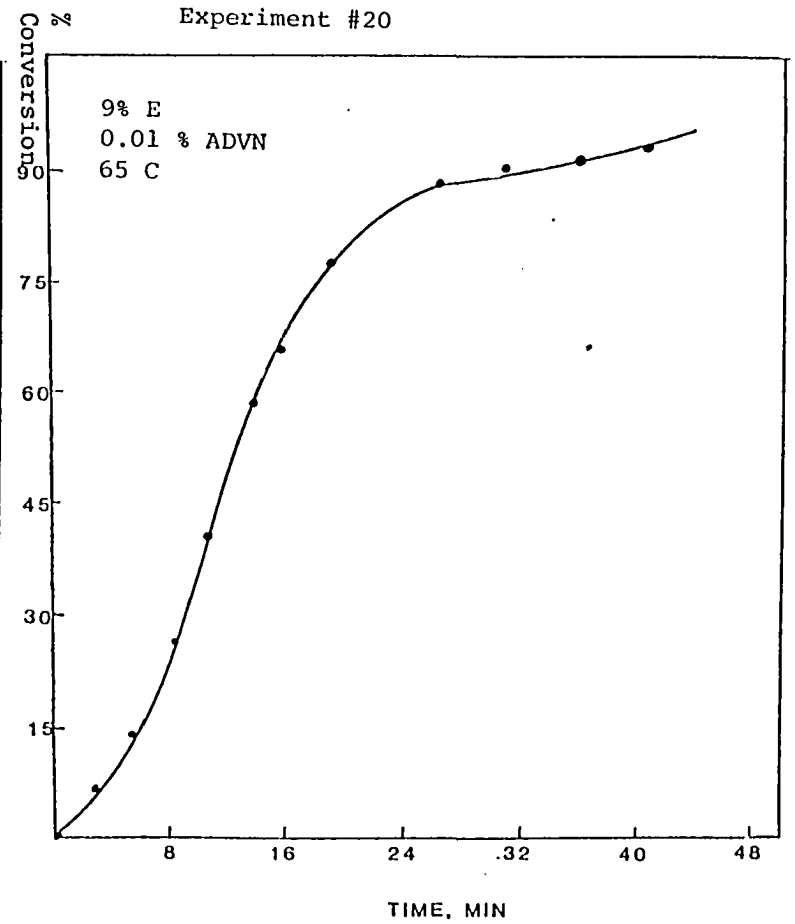

*Experiment duplicated to estimate reproducibility

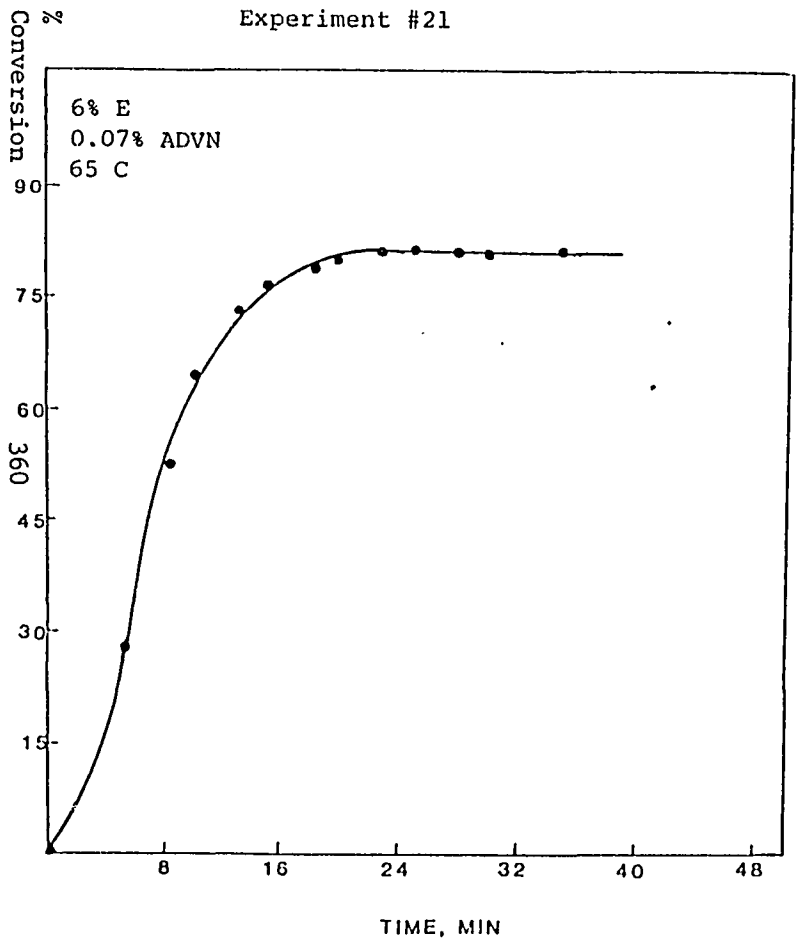

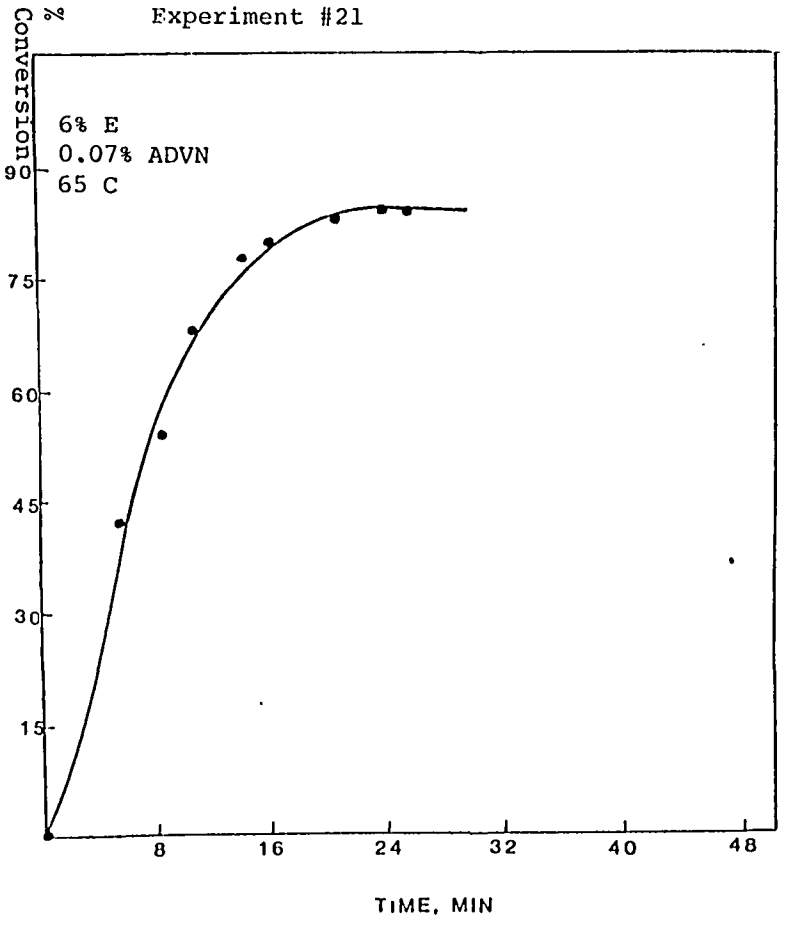

360

*Experiment duplicated to estimate reproducibility

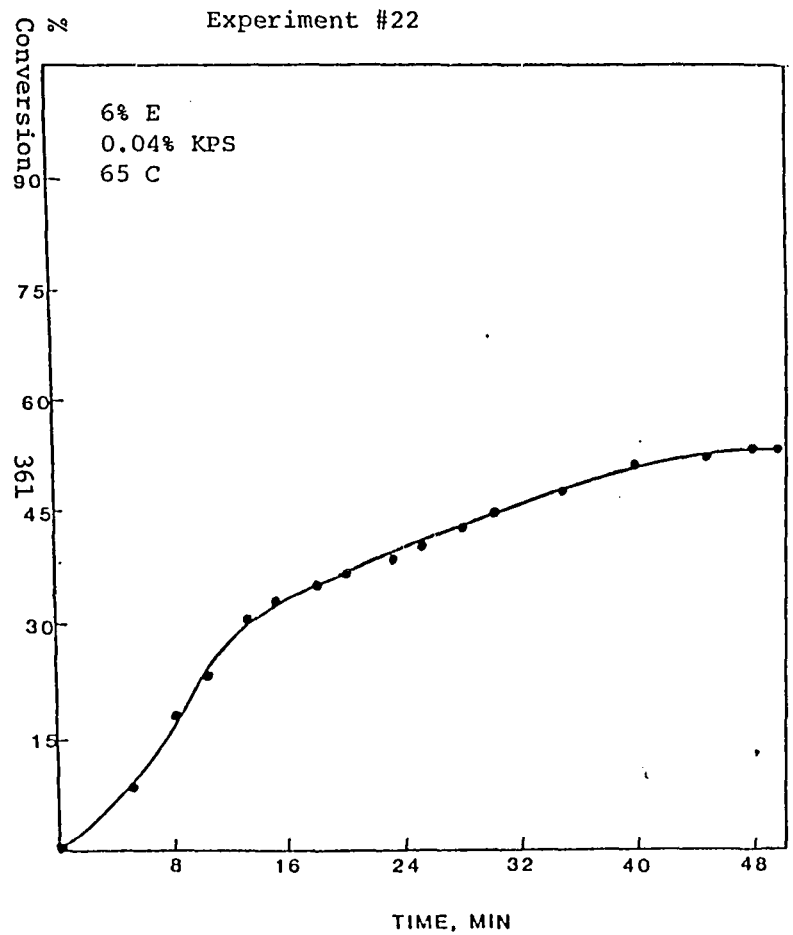

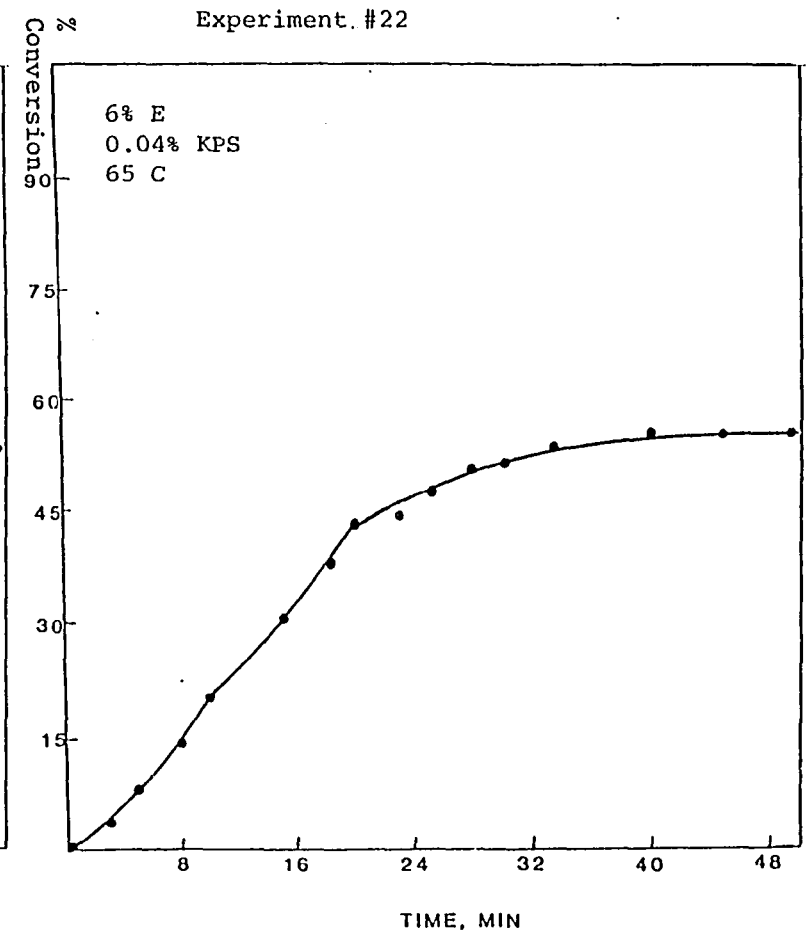

* Experiment duplicated to estimate reproducibility

Experiment #23

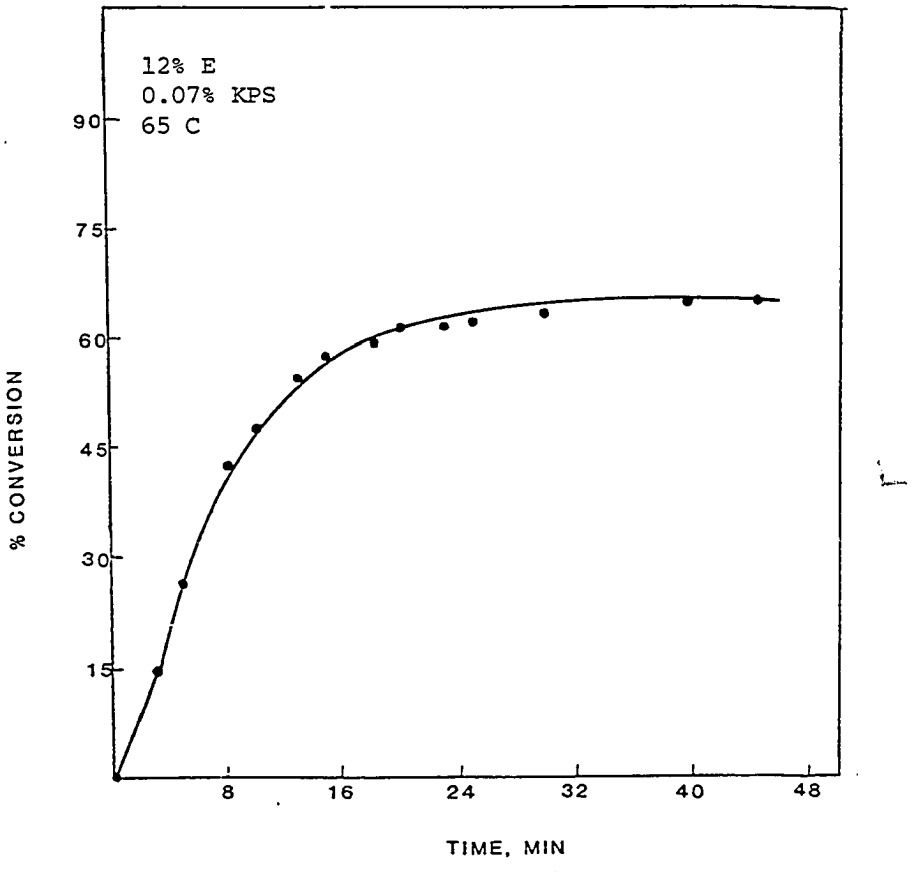

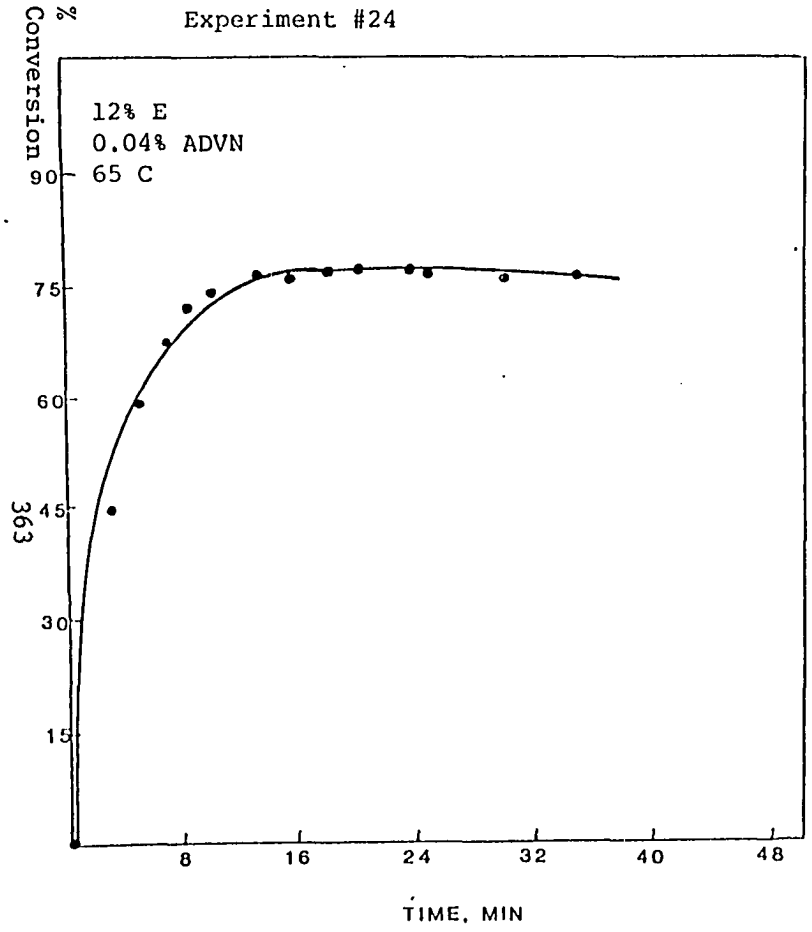

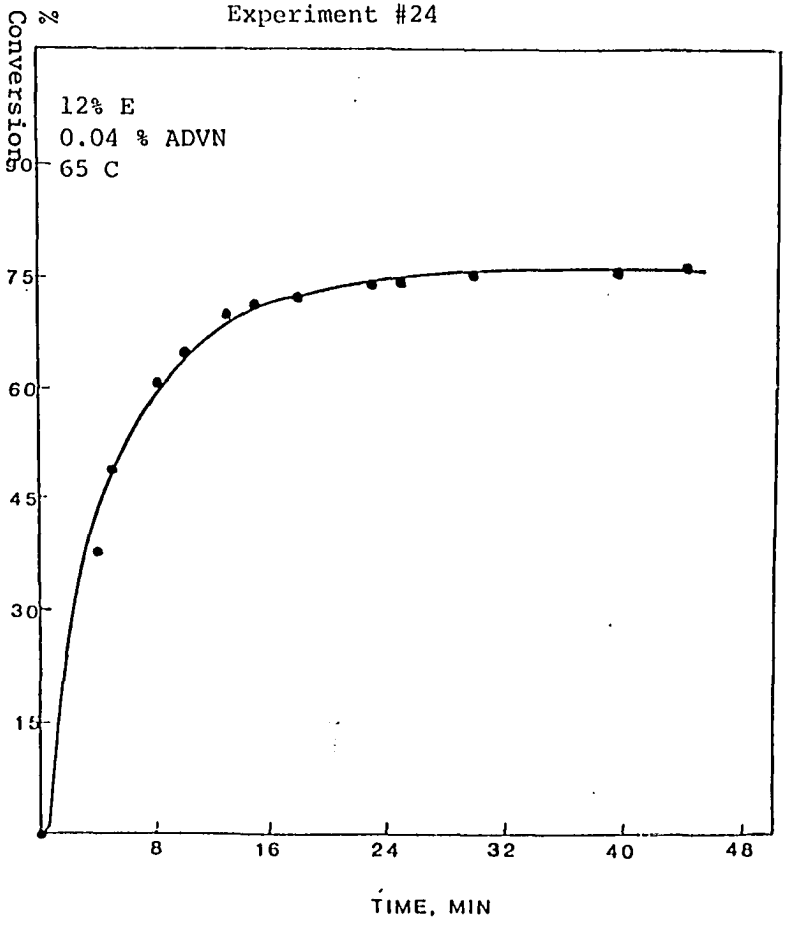

* Experiment duplicated to estimate reproducibility

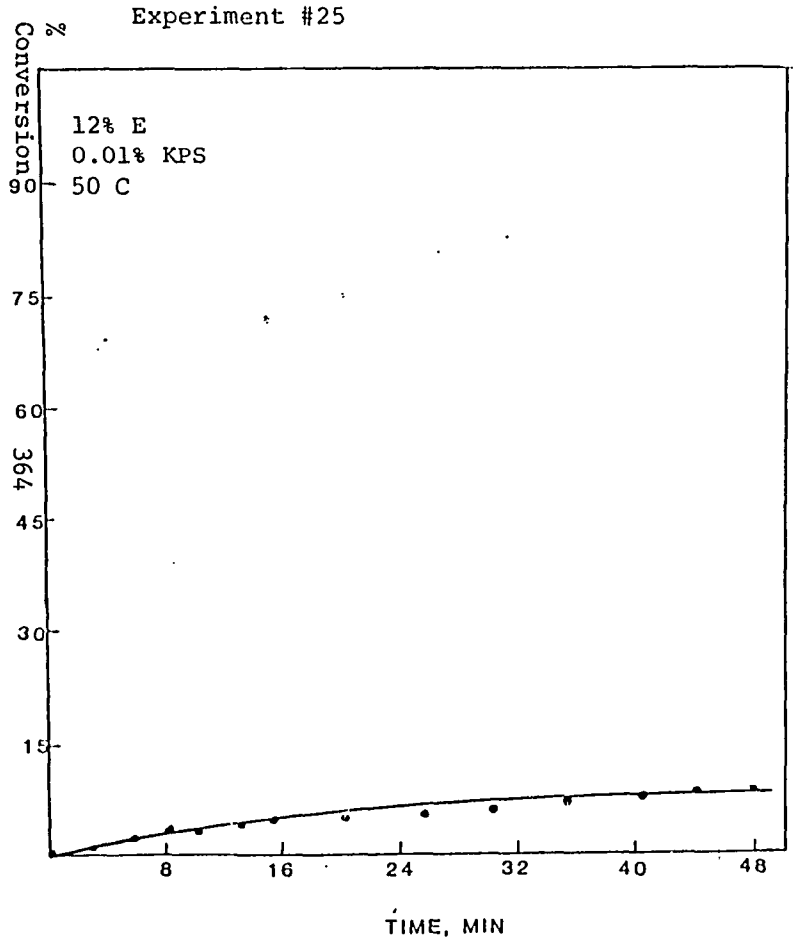

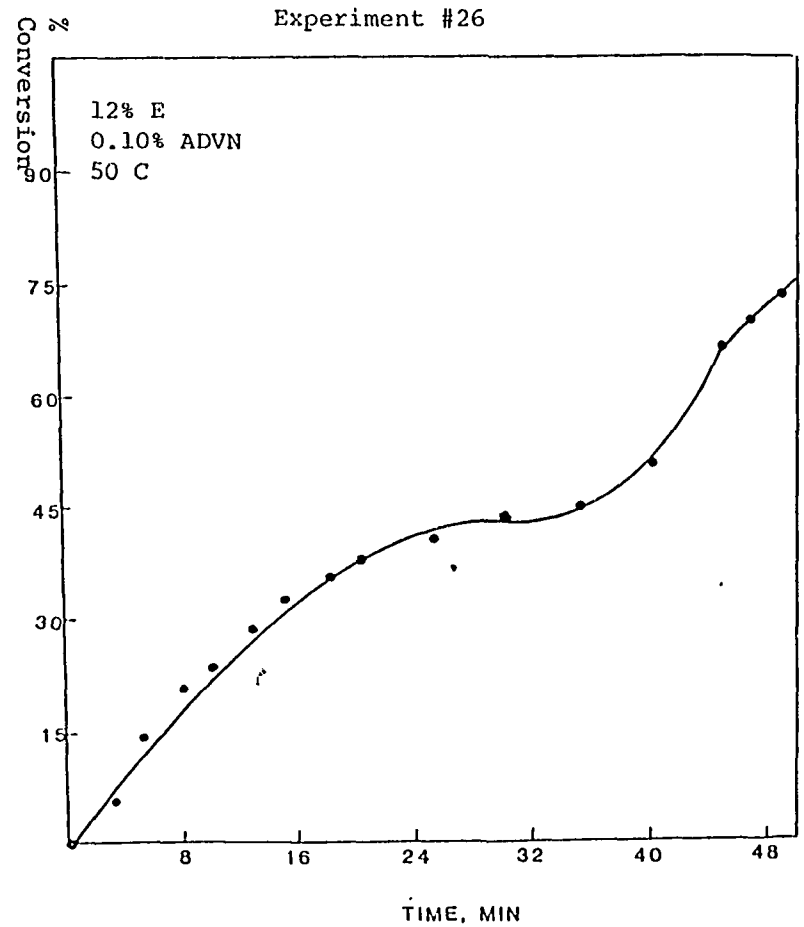

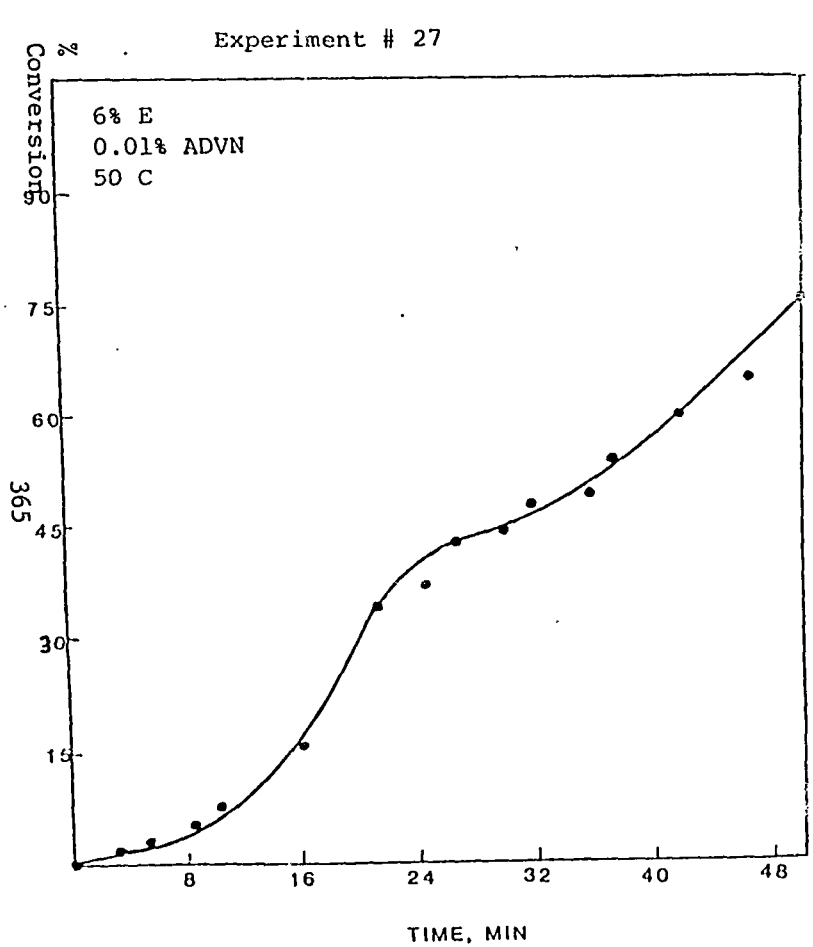

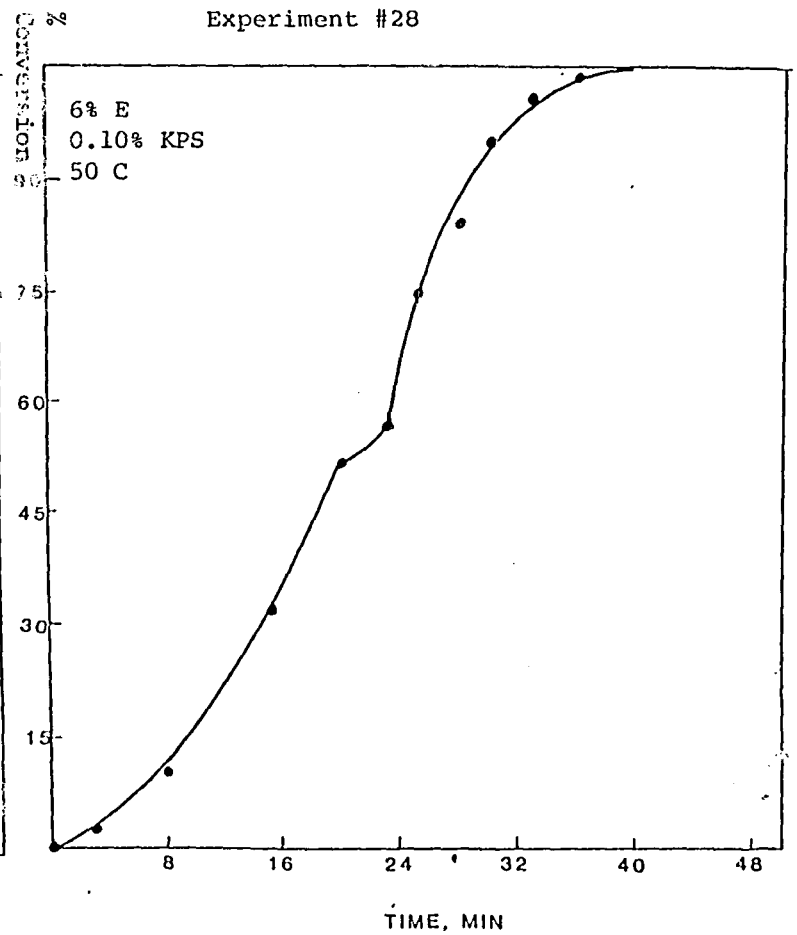

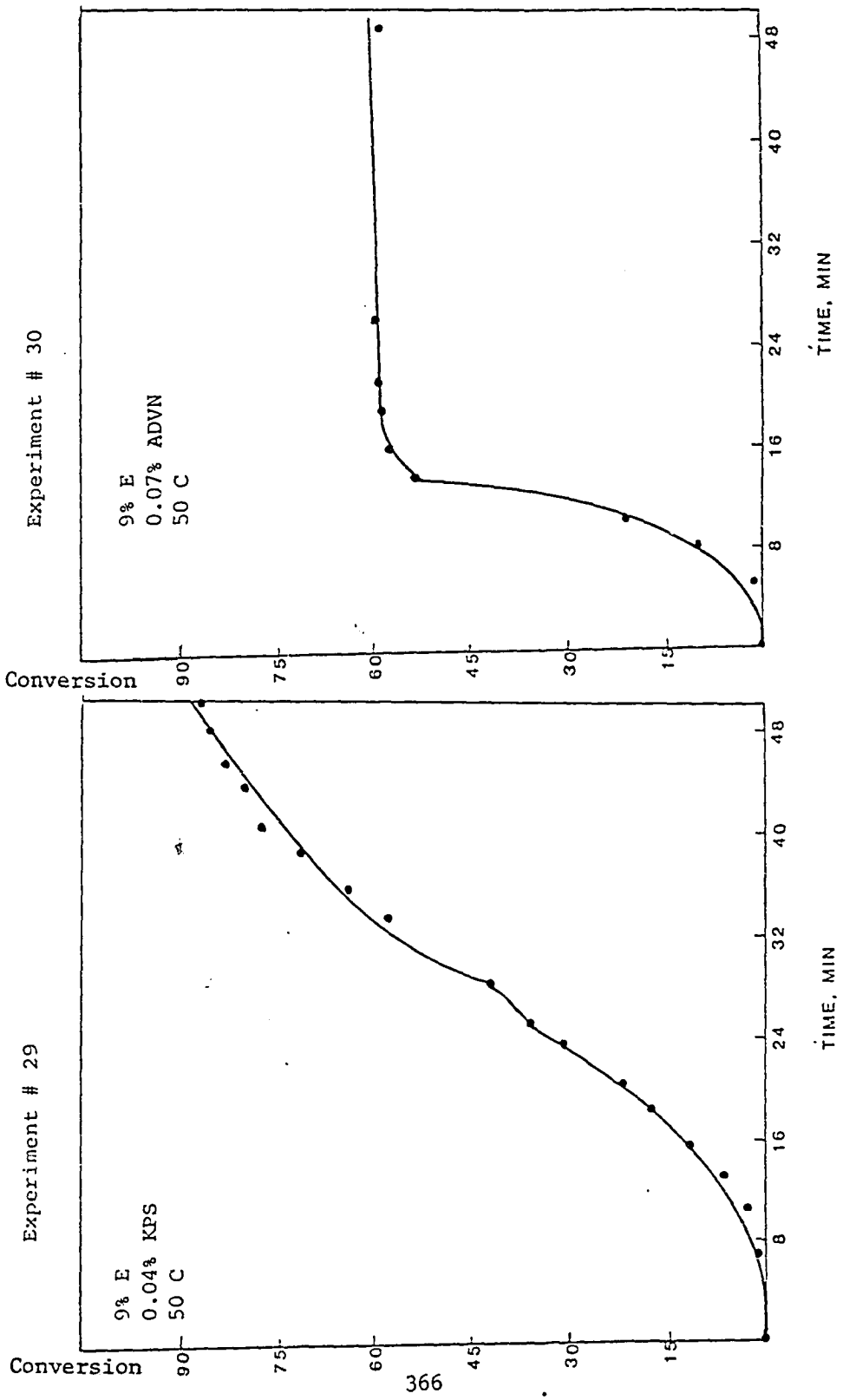

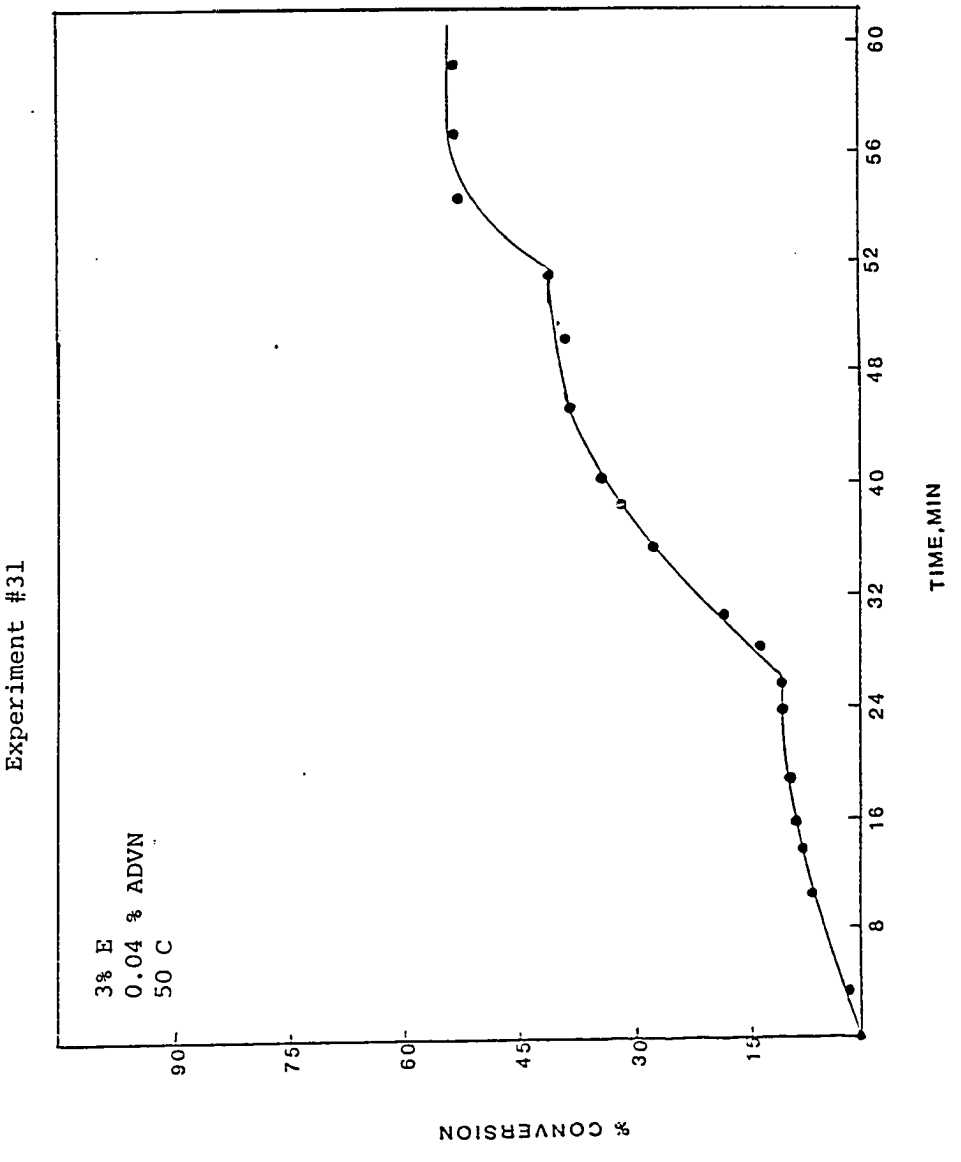

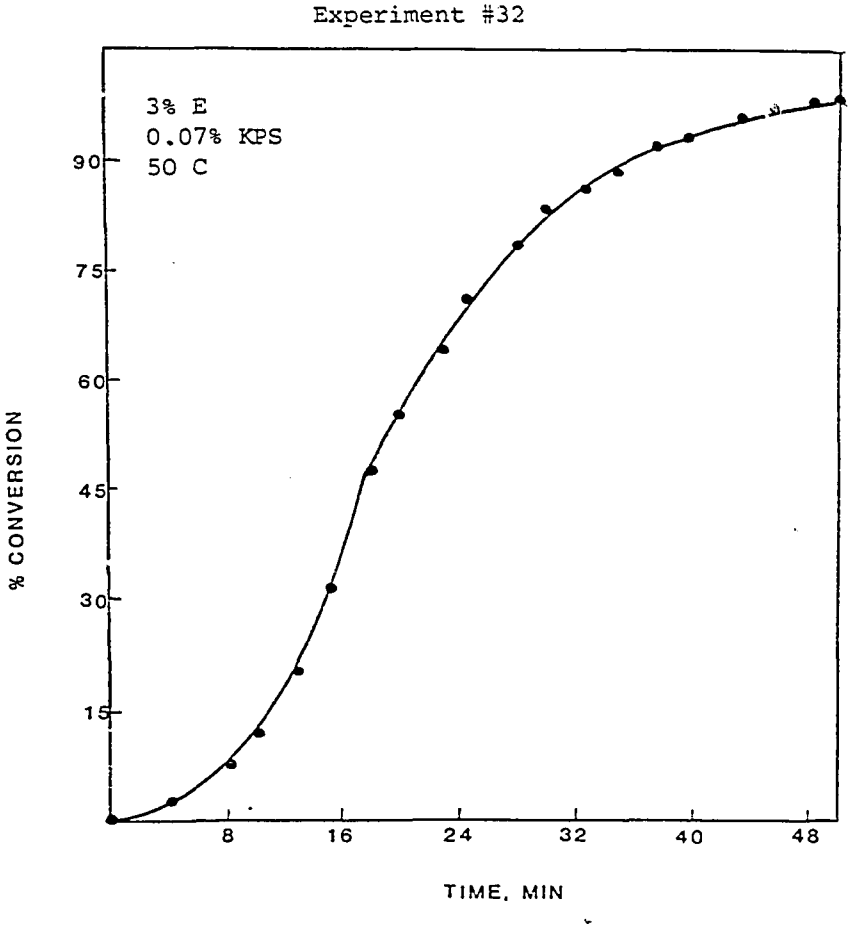

APPENDIX D

CONVERSION-TIME CURVES FROM THE SOLUTION POLYMERIZATION OF ACRYLAMIDE

50°C

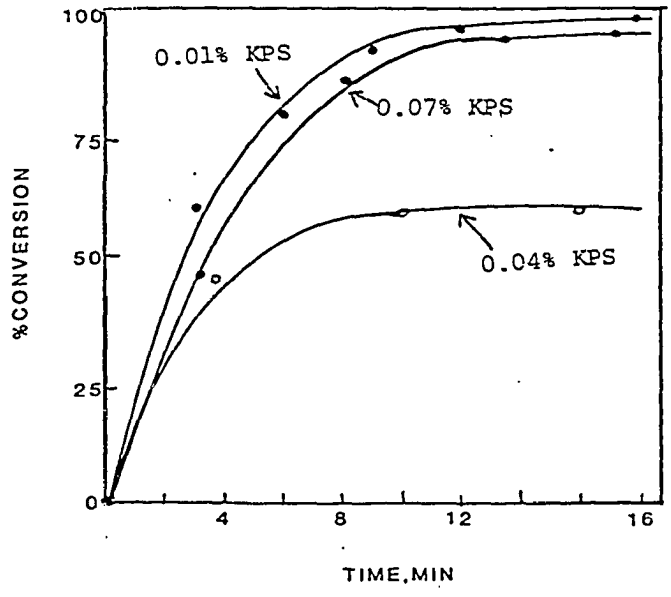

55°C

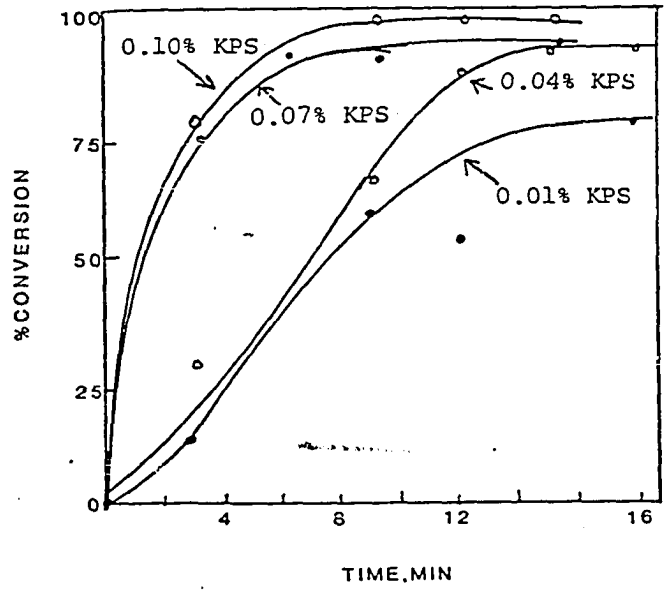

60° C

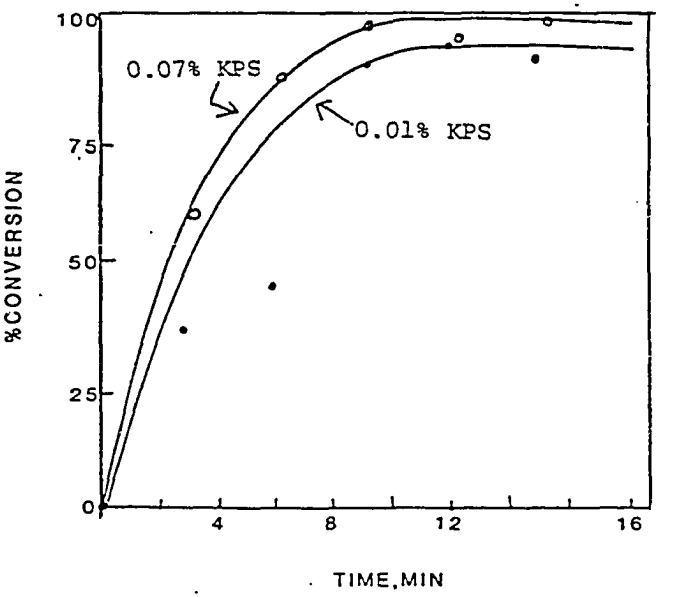

65° C

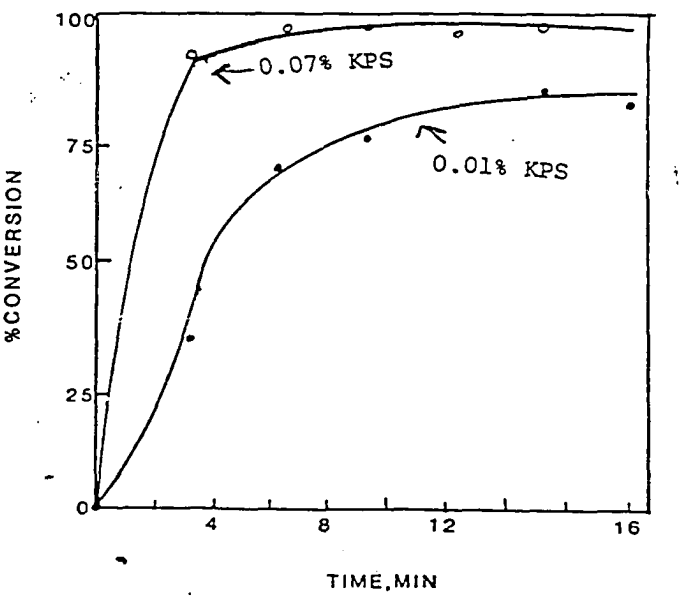

VITA

Donna Lynn Visioli was born July 1, 1955, in Denville, New Jersey, daughter of Marion J. and the late Emilio J. Visioli. She received her elementary education in New Jersey and Pennsylvania and was graduated in 1973 from Archbishop Carroll High School, Radnor, PA.

Ms. Visioli received her undergraduate education at Villanova University, Villanova, PA. She was elected to membership in Who's Who in American Colleges and Universities in 1976 and received the Merck Award for academic achievement in 1977. She was graduated from Villanova University with a B.S. in Chemistry in 1977. That same year Ms. Visioli joined the Research Division of Rohm and Haas Company as a research chemist. She received a Rohm and Haas Research Division Award for Exceptional Progress in Research in 1981. She remained with the Rohm and Haas Company until 1982.

Ms. Visioli began graduate studies at Lehigh University part-time in 1980, and joined Lehigh University's Emulsion Polymers Institute as a research assistant in 1982. She pursued graduate studies in the Polymer Science and Engineering curriculum. Upon graduation from Lehigh University, Ms. Visioli has accepted a position as a research scientist with E. I. DuPont de Nemours and Company.